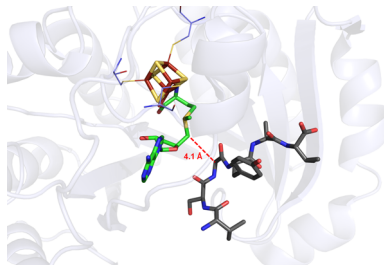


## Radical S-Adenosylmethionine Enzymes

Joan B. Broderick,\* Benjamin R. Duffus, Kaitlin S. Duschene, and Eric M. Shepard

Department of Chemistry and Biochemistry, Montana State University, Bozeman, Montana 59717, United States



### CONTENTS

1. Introduction	4231	4.1.2. The Iron–Sulfur Clusters of Biotin Synthase	4250
2. Unifying Structural and Mechanistic Features of the Radical SAM Enzymes	4231	4.1.3. X-ray Crystal Structure of Biotin Synthase	4251
2.1. The Iron–Sulfur Cluster and Its Interaction with SAM	4231	4.1.4. Source of the Sulfur in Biotin Biosynthesis	4252
2.2. A 5'-Deoxyadenosyl Radical Intermediate	4232	4.1.5. Biotin Synthase Mechanism	4252
2.3. A Framework Mechanism	4233	4.2. Lipoyl Synthase	4253
2.4. Energetic Considerations in the Mechanism	4234	4.2.1. Octanoic Acid as a Precursor for Lipoic Acid	4253
2.5. SAM: Mechanisms and Regioselectivity of S–C Bond Cleavage and Inner-Sphere Electron Transfer	4235	4.2.2. Similarity to Biotin Synthase	4253
2.6. A Common Protein Architecture for Radical SAM Catalysis	4236	4.2.3. In Vitro Activity Requires an Iron–Sulfur Cluster, SAM, and Preattachment of the Octanoyl Substrate	4253
2.7. [4Fe–4S]/SAM and Adenosylcobalamin: Parallels and Departures	4237	4.2.4. A Mechanism for LipA Involving Two [4Fe–4S] Clusters	4254
3. Glycyl Radical Enzyme Activating Enzymes	4239	5. Radical SAM Mutases	4254
3.1. Pyruvate Formate-Lyase Activating Enzyme	4239	5.1. Lysine 2,3-Aminomutase	4254
3.1.1. Early Studies on Pyruvate Formate-Lyase and Its Activation	4239	5.1.1. Early Characterization of a $B_{12}$ -Independent Aminomutase	4254
3.1.2. The Iron–Sulfur Cluster of PFL-AE and Its Role in Catalysis	4239	5.1.2. SAM as a dAdo $\bullet$ Precursor in LAM	4255
3.1.3. Defining the Unique SAM–Cluster Interaction in Radical SAM Enzymes	4244	5.1.3. The Role of PLP in LAM	4255
3.1.4. X-ray Crystal Structure of PFL-AE	4246	5.1.4. The Iron–Sulfur Cluster in LAM and Its Interaction with SAM	4255
3.1.5. PFL-AE Mechanism and the Interaction with PFL	4247	5.1.5. The Structure of LAM	4255
3.2. The Anaerobic Ribonucleotide Reductase Activating Enzyme	4247	5.1.6. The Mechanism of LAM	4255
3.2.1. Identification of an Anaerobic Ribonucleotide Reductase Containing a Glycyl Radical	4248	5.1.7. LAM and LAM-like Enzymes from Other Organisms	4256
3.2.2. A [4Fe–4S] Cluster in the Activating Enzyme for the aRNR	4248	5.2. Pyrrolysine Biosynthesis: Carbon Backbone Rearrangement Catalyzed by the Lysine Mutase PylB	4257
3.3. The $B_{12}$ -Independent Glycerol Dehydratase Activating Enzyme	4249	6. Enzymes Catalyzing Complex Rearrangements and Cyclizations	4258
3.4. Other Glycyl Radical Enzyme Activating Enzymes	4249	6.1. MoaA	4258
4. Enzymes Catalyzing Sulfur Insertion	4249	6.1.1. Molybdopterin Cofactor Biosynthesis	4258
4.1. Biotin Synthase	4250	6.1.2. Identification of Two [4Fe–4S] Clusters in MoaA	4258
4.1.1. Initial Identification of Fe–S Cluster and SAM Dependence	4250	6.1.3. The X-ray Crystal Structure of MoaA	4259
		6.1.4. A Role for the C-Terminal Cluster in MoaA	4259
		6.1.5. Mechanism of a Complex Rearrangement Initiated by H-Atom Abstraction	4260
		6.2. ThiC	4260
		6.2.1. Radical SAM Chemistry in the Synthesis of Thiamine Pyrophosphate	4260
		6.2.2. Conversion of 4-Aminoimidazole Ribonucleotide (AIR) to HMP-P by ThiC	4260

**Special Issue:** 2014 Bioinorganic Enzymology

**Received:** August 25, 2013

**Published:** January 29, 2014

6.2.3. Mechanistic Insight into the Complex Rearrangement Catalyzed by ThiC	4261	10.2.1. Identification of SPL as a Radical SAM Enzyme	4283
6.2.4. The Structure of ThiC	4261	10.2.2. The Iron–Sulfur Cluster of Spore Photoprotein Lyase and Its Interaction with SAM	4283
6.2.5. Pathways Utilizing Multiple Radical SAM Enzymes	4262	10.2.3. Defining the Substrate for Spore Photoprotein Lyase	4283
6.3. Synthesis of Pyrrolopyrimidines: QueE and ToyC	4262	10.2.4. SAM: Substrate or Cofactor in the SPL-Catalyzed Reaction?	4284
6.4. Biosynthesis of the F <sub>420</sub> Cofactor: FbiC/CofH and CofG	4263	10.2.5. Structural Characterization of SPL	4285
6.5. Synthesis of Menaquinone: MqnC and MqnE	4264	10.2.6. Mechanism of Repair of SP by SPL	4285
6.6. Synthesis of Modified Side Chain Rings of Thiopeptides: NosL or NocL	4266	10.3. DeslI and the Synthesis of D-Desosamine	4286
7. Enzymes Catalyzing Methylation and Methylthiolation Reactions	4267	10.4. PhnJ: Catalysis of C–P Bond Cleavage	4288
7.1. Class A Radical SAM Methyltransferases Methylate the 23S rRNA at A2503	4267	10.5. Elp3: Demethylation by the Elongation Complex	4288
7.1.1. A Novel rRNA Methylation	4267	10.6. Decarboxylation during Blasticidin S Biosynthesis Catalyzed by BlsE	4290
7.1.2. Mechanistic Studies	4268	11. Radical SAM Enzymes in the Synthesis of Modified Tetrapyrroles	4290
7.1.3. Insights from the Structure of RlmN	4269	11.1. HemN: An Oxygen-Independent Coproporphyrinogen Oxidase	4291
7.2. Class B RSMTs: Cobalamin–Radical SAM Partnership	4269	11.1.1. The Iron–Sulfur Cluster of HemN	4291
7.3. Class C Radical SAM Methyltransferases: Similar to HemN	4271	11.1.2. Structural Characterization of HemN	4291
7.3.1. NocN: Methyltransferase in Nosiheptide and Nocathiacin Biosynthesis	4271	11.1.3. Insight into the HemN Mechanism	4291
7.3.2. Methylation during the Synthesis of the Natural Product Yatakemycin: YtkT	4272	11.2. NirJ and Related Enzymes in the Synthesis of Heme d <sup>1</sup>	4292
7.4. Radical SAM Methylthiotransferases	4272	11.3. BchE in Chlorophyll and Bacteriochlorophyll Biosynthesis	4293
7.4.1. Modification of tRNA <sup>Phe</sup> A-37 by MiaB	4272	11.4. BchQ/BchR: Methyl Transfer in Chlorophyll Biosynthesis	4294
7.4.2. Methylthiolation of Ribosomal Protein S12	4273	12. Synthesis of Complex Metal Clusters	4295
7.4.3. Classification of MTTases	4274	12.1. NifB and the Biosynthesis of the FeMoCo of Nitrogenase	4295
8. Dehydrogenation Reactions by Radical SAM Enzymes	4274	12.1.1. Nitrogenase and the FeMoCo	4295
8.1. Formylglycine Generation during Sulfatase Maturation: The anSMEs	4275	12.1.2. Biogenesis of the FeMoCo and Nitrogenase Maturation	4295
8.1.1. AnSMEs as Radical SAM Enzymes	4275	12.1.3. Radical SAM Chemistry and the Insertion of the Interstitial Carbide	4297
8.1.2. The Fe–S Clusters and Enzymatic Activities of AnSMEs	4275	12.2. Biosynthesis of the H-Cluster of the [FeFe]-Hydrogenase	4297
8.1.3. Mechanistic Studies of AnSMEs	4275	12.2.1. H-Cluster Maturation Machinery	4298
8.1.4. Structure of anSME and Clarification of the Role of the Auxiliary Clusters	4276	12.2.2. HydA Expressed in the Absence of HydE, HydF, and HydG Contains a [4Fe–4S] Cluster	4298
8.2. Dehydrogenation in Antibiotic Synthesis: BtrN and the Synthesis of Butirosin	4277	12.2.3. HydF as an Assembly Scaffold or Carrier Protein for Radical SAM Chemistry	4298
9. Formation of New C–C, C–N, and C–S Bonds	4278	12.2.4. Radical SAM Chemistry and the Synthesis of Diatomic Ligands	4299
9.1. The Synthesis of Pyrroloquinoline Quinone: PqqE	4278	12.2.5. Radical SAM Chemistry and the Synthesis of the Bridging Dithiolate	4301
9.2. Modification of tRNA at G37 To Generate Wybutosine: TYW1	4278	13. Radical SAM Enzymes of Unknown Function	4303
9.3. Catalysis of Thioether Cross-Link Formation in Antimicrobial Peptides	4280	13.1. Radical SAM Chemistry in the Antiviral Response: Viperin	4303
9.3.1. AlbA and the Synthesis of Subtilosin A	4280	13.2. Radical SAM Chemistry in the Synthesis of the Iron-Guanylpyridinol Cofactor in [Fe]-Hydrogenase?	4303
9.3.2. Biosynthesis of Thuricin CD	4280	13.3. A Radical SAM Epimerase? AviX12 in Avilamycin A Biosynthesis	4304
9.3.3. Biosynthesis of Thurincin H	4280	14. Radical SAM Chemistry Outside the Superfamily: Dph2	4305
9.3.4. SkfB and the Maturation of Sporulation Killing Factor	4281	15. Concluding Remarks	4306
10. Using Radical SAM Chemistry To Cleave C–X (X = C, N, P) Bonds	4282	Author Information	4306
10.1. Cleavage of the α–β Bond of Amino Acids: ThiH	4282		
10.2. Repair of Thymine Dimers in DNA: Spore Photoprotein Lyase	4282		

Corresponding Author	4306
Notes	4306
Biographies	4306
Acknowledgments	4307
Abbreviations	4307
References	4308
Note Added after ASAP Publication	4317

## 1. INTRODUCTION

It was once widely held that nearly all reactions in biology were catalyzed via mechanisms involving paired electron species. Beginning approximately 40 years ago, this paradigm was repeatedly challenged as examples of enzymatic reactions involving organic radical intermediates began to emerge, and it is now well accepted that biochemical reactions often involve organic radicals. Indeed, some of the most intensely studied metalloenzymes, including cytochrome P450, methane monooxygenase, ribonucleotide reductase, and the adenosylcobalamin ( $B_{12}$ ) enzymes, catalyze reactions employing organic radical intermediates. As a general rule, enzymes utilizing radical mechanisms catalyze reactions that would be difficult or impossible to catalyze by polar mechanisms, most often involving H-atom abstraction from an unactivated C–H bond.

Among the more recent additions to the enzymes that catalyze radical reactions are the radical S-adenosylmethionine (radical SAM) enzymes, which were first classified as a superfamily in 2001.<sup>1</sup> These enzymes utilize a [4Fe–4S] cluster and SAM to initiate a diverse set of radical reactions, in most or all cases via generation of a 5'-deoxyadenosyl radical (dAdo<sup>•</sup>) intermediate. Although 2001 marked the identification of this superfamily largely through bioinformatics, the discovery of iron metalloenzymes utilizing SAM to initiate radical reactions precedes this date by more than a decade. For example, early studies on the activation of pyruvate formate-lyase showed that it involved the generation of a stable protein radical,<sup>2</sup> and was stimulated by the presence of iron, SAM, and an “activating component” from the cell extract now known to be the pyruvate-formate lyase activating enzyme (PFL-AE).<sup>3</sup> The radical on PFL was ultimately shown to be located on a specific glycine residue,<sup>4</sup> and was one of the first stable protein radicals characterized. PFL-AE was ultimately shown to contain a catalytically essential iron–sulfur cluster,<sup>5</sup> and to use SAM as an essential component of PFL activation.<sup>6</sup> The anaerobic ribonucleotide reductase, similar to PFL, contains a stable glycol radical that was shown in early work to require an iron–sulfur cluster and SAM for activation.<sup>7</sup> Likewise, preliminary investigations on lysine 2,3-aminomutase (LAM) published in 1970 demonstrated activation by ferrous ion and a strict requirement for SAM.<sup>8</sup> Like PFL-AE, LAM was ultimately found to contain a catalytically essential iron–sulfur cluster.<sup>9</sup> Work in Perry Frey's lab showed that LAM used the adenosyl moiety of SAM to mediate hydrogen transfer in a manner similar to adenosylcobalamin-dependent rearrangements, implicating radical intermediates.<sup>10</sup> Biotin synthase was first reported to require iron and SAM in 1995,<sup>11</sup> and was subsequently shown to contain iron–sulfur clusters and to catalyze a radical reaction.<sup>12</sup>

These four enzyme systems (PFL/PFL-AE, aRNR, LAM, and biotin synthase) provided early indications of a new type of biological cofactor consisting of an iron–sulfur cluster and SAM, which initiate radical reactions using a fundamental new mechanism of catalysis.<sup>13</sup> What none of us in the field in the

early days probably anticipated, however, was just how ubiquitous these enzymes would turn out to be. The initial report of the superfamily by Sofia et al. identified ~600 members;<sup>1</sup> however, now that number is ~48 100 members.<sup>14</sup> These enzymes are found across the phylogenetic kingdom and catalyze an amazingly diverse set of reactions, the vast majority of which have yet to be characterized.

This Review will begin by summarizing unifying features of radical SAM enzymes, and in subsequent sections delve further into the biochemical, spectroscopic, structural, and mechanistic details for those enzymes that have been characterized. In most cases, these enzymes are grouped by reaction type; however, in two cases (syntheses of modified tetrapyrroles and complex metal cluster cofactors), we have chosen to group together several radical SAM enzymes that catalyze different reaction types but which act together in the same or related metabolic pathways.

## 2. UNIFYING STRUCTURAL AND MECHANISTIC FEATURES OF THE RADICAL SAM ENZYMES

### 2.1. The Iron–Sulfur Cluster and Its Interaction with SAM

The members of the radical SAM superfamily exhibit only limited sequence homology. The most characteristic sequence feature is a CX<sub>3</sub>CX<sub>2</sub>C motif that is present in most of the superfamily members, although a number have variations in this motif. The three cysteine residues coordinate three of the four irons of a [4Fe–4S] cluster at the active site of the enzyme (Figure 1). The remaining ligand to the fourth iron in the

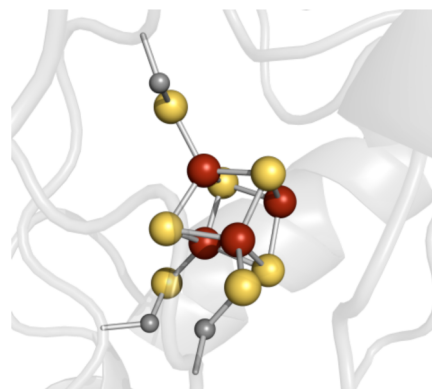


**Figure 1.** The site-differentiated [4Fe–4S] cluster coordinated by the CX<sub>3</sub>CX<sub>2</sub>C radical SAM motif (PDB ID 3IIZ).

absence of SAM is not known; spectroscopic evidence is ambiguous, although small-molecule thiols from the buffer likely coordinate in some cases.<sup>15</sup> The lack of a protein ligand on this fourth iron of the cluster renders it labile, and explains why in many cases these proteins are found to contain [3Fe–4S]<sup>+</sup> clusters in their as-isolated or air-exposed states. Upon reduction with a mild reducing agent such as dithiothreitol (DTT), the [3Fe–4S]<sup>+</sup> clusters in these enzymes can generally be converted to the [4Fe–4S]<sup>2+</sup> clusters, by scavenging of adventitious iron or by cannibalization of a fraction of the clusters. Upon treatment with a stronger reducing agent such as dithionite or photoreduced 5-deazariboflavin, the clusters can generally be reduced to the catalytically active [4Fe–4S]<sup>+</sup> state. In almost all cases, the iron–sulfur clusters of the radical SAM enzymes are air sensitive, requiring anaerobic conditions for isolation and handling of the enzyme. Brief exposure to oxygen

can result in significant degradation of the [4Fe–4S] clusters to the [3Fe–4S] state, and prolonged exposure generally leads to further cluster destruction. Because of the difficulties with air sensitivity and cluster lability, radical SAM enzymes are often isolated as apo-enzymes, under aerobic or anaerobic conditions, and subsequently chemically reconstituted *in vitro* with iron and sulfide under anaerobic conditions to generate the active enzymes.

In the enzyme–SAM complex, the unique iron of the [4Fe–4S] cluster is coordinated by the amino and carboxylate moieties of SAM, forming a classical five-member chelate ring (Figure 2).<sup>16</sup> While it is well-known that amino acids can

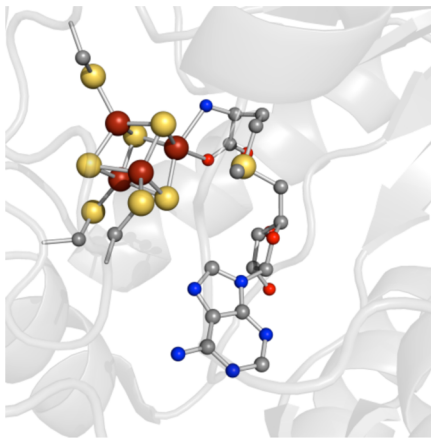


**Figure 2.** The bidentate coordination of *S*-adenosylmethionine to the unique iron site of the [4Fe–4S] cluster in radical SAM enzymes (PDB ID 3IIZ).

chelate metal ions, the [4Fe–4S]–SAM complex was a novel structure in biology when it was first determined. The identification of this novel structure was first made by detailed ENDOR and Mössbauer spectroscopic studies of PFL-AE, which will be described in detail in a later section of this Review (section 3.1.3).<sup>16a,17</sup> This unique structural feature has since been found in every radical SAM enzyme examined using X-ray crystallographic or ENDOR spectroscopic methods. The SAM–[4Fe–4S] cluster coordination complex therefore appears to be a unifying structural and catalytic feature of radical SAM enzymes.

## 2.2. A 5'-Deoxyadenosyl Radical Intermediate

It was determined from early studies that radical SAM enzymes cleaved SAM generating methionine and 5'-deoxyadenosine (dAdoH). Further, in some cases, use of isotopically labeled substrate provided evidence for H-atom transfer from substrate to dAdoH during catalysis. These observations, together with the recognition that both LAM and the anaerobic RNR catalyzed reactions that were directly analogous to adenosylcobalamin (AdoCbl)-dependent reactions, led to the hypothesis that the radical SAM enzymes generated the same intermediate, the 5'-deoxyadenosyl radical (dAdo<sup>•</sup>), which AdoCbl enzymes generated (Figure 3).<sup>18</sup> While the dAdo<sup>•</sup> intermediate has not yet been directly observed for any radical SAM or AdoCbl enzyme, a stabilized allylic analogue of this radical has been observed and characterized for both an AdoCbl and a radical SAM enzyme. 3',4'-Anhydroadenosylcobalamin was synthesized by Magnusson and Frey and shown to give rise to the relatively stable allylic radical species, 5'-deoxy-3',4'-anhydroadenosine-5'-yl (anAdo<sup>•</sup>), upon reaction with the enzyme diol

dehydrolase.<sup>19</sup> Work in the same lab resulted in the synthesis of S-3',4'-anhydroadenosyl-L-methionine (anSAM), which upon reaction with reduced LAM and substrate gave rise to the same allylic radical species anAdo<sup>•</sup> (Figure 4).<sup>20</sup> Together, these results support the involvement of SAM as a precursor of a dAdo<sup>•</sup> in the radical SAM enzymes, with the dAdo<sup>•</sup> abstracting a H-atom from substrate during catalysis.

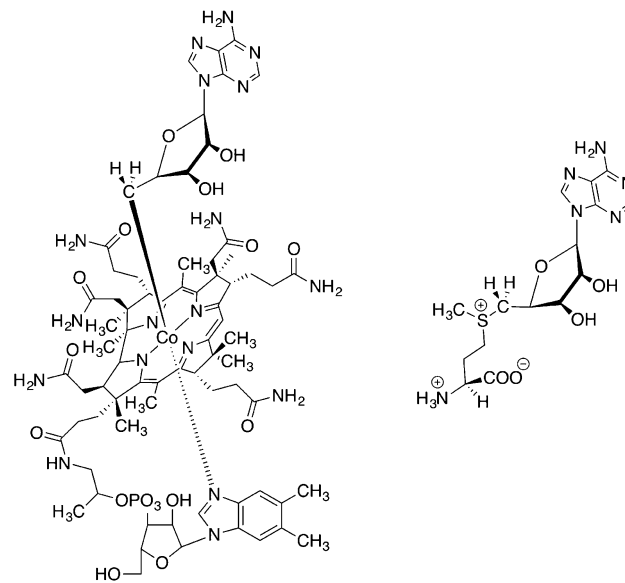


**Figure 3.** Structures of AdoCbl (left) and SAM (right).

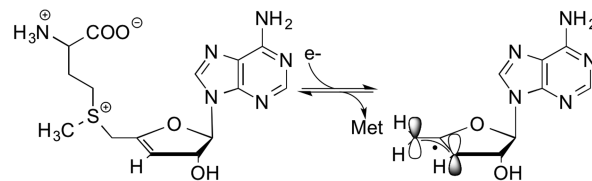


**Figure 4.** Reductive cleavage of S-3',4'-anhydroadenosyl-L-methionine (anSAM) results in generation of the stable allylic radical species 5'-deoxy-3',4'-anhydroadenosine-5'-yl (anAdo<sup>•</sup>).

The reductive cleavage of SAM to generate dAdo<sup>•</sup> and methionine requires the input of one electron, now known to come from the reduced site-differentiated [4Fe–4S] cluster (Figure 5). The [4Fe–4S]<sup>+</sup> state is the catalytically active oxidation state for the iron–sulfur cluster in the radical SAM enzymes. This was unequivocally demonstrated for PFL-AE by controlled generation of defined quantities of the [4Fe–4S]<sup>+</sup> state, followed by the addition of the substrate PFL and the observation using EPR that the quantity of glycyl radical generated on PFL was equivalent to the quantity of [4Fe–4S]<sup>+</sup> originally on the PFL-AE (Figure 6).<sup>21</sup> Further, it was shown that upon generation of the glycyl radical, the [4Fe–4S]<sup>+</sup> state was oxidized to the EPR-silent [4Fe–4S]<sup>2+</sup> state, indicating that the [4Fe–4S]<sup>+</sup> cluster provides the electron required for the reductive cleavage of SAM. Concurrently, it was shown for LAM that the [4Fe–4S]<sup>+</sup> state was the active state by correlating the quantity of [4Fe–4S]<sup>+</sup> signal with the activity, although direct stoichiometric conversion of reduced cluster to product could not be shown because LAM utilizes SAM as a cofactor and therefore the iron–sulfur cluster is rereduced after each catalytic cycle.<sup>22</sup> These observations for PFL-AE and LAM, together with the requirement of a strong reducing agent

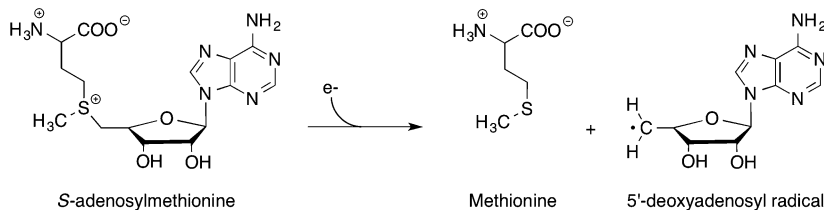


**Figure 5.** The cleavage of SAM to generate methionine and the  $dAdo^\bullet$  is a reductive cleavage event, requiring the input of one electron.

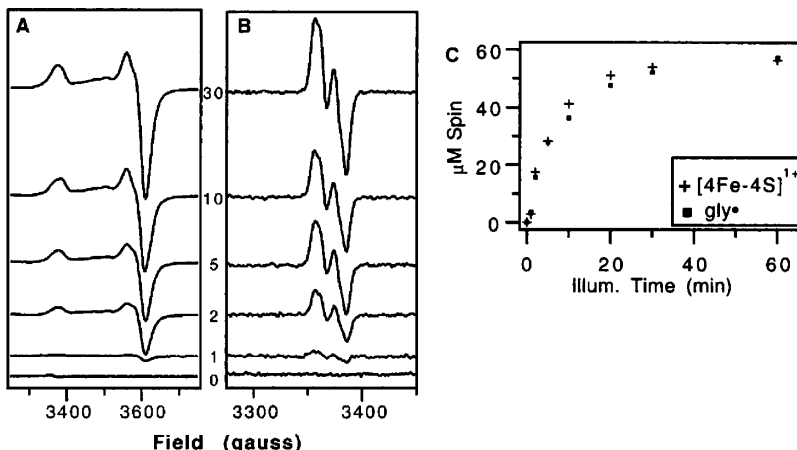


**Figure 6.** X-band EPR spectra of photoreduced PFL-AE before (A) and after addition of PFL (B), photoreduction time indicated in minutes. (C) Spin quantitation of the EPR spectra in (A) for the amount of the  $[4Fe-4S]^{1+}$  cluster (+) and EPR spectra in (B) for the amount of glycyl radical (■) as a function of illumination time. Reprinted with permission from ref 21. Copyright 2000 American Chemical Society.

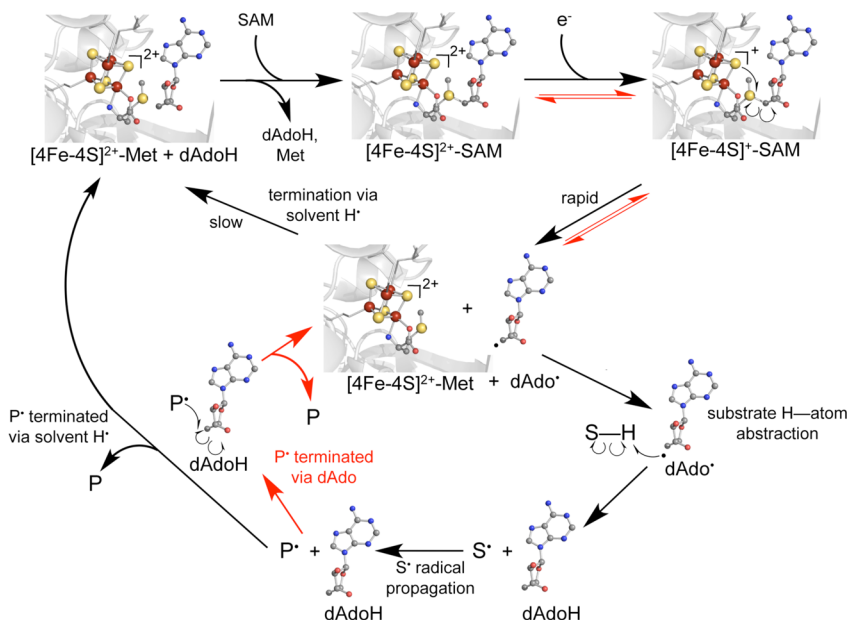


**Figure 7.** Framework mechanism for radical SAM cleavage (PDB ID 3IIZ).

in all radical SAM enzyme activity assays, have led to the general acceptance of the  $[4Fe-4S]^{1+}$  state being the catalytically active oxidation state for these enzymes.

### 2.3. A Framework Mechanism

Given the clues provided in the preceding paragraphs, a framework mechanism for the radical SAM enzymes has been proposed (Figure 7). This unifying preliminary mechanism involves a site-differentiated  $[4Fe-4S]^{2+}$  cluster with SAM chelating the unique iron. The cluster is reduced by one

electron to the  $[4Fe-4S]^{1+}$  state; *in vivo* the reducing system requires flavodoxin or other single electron donors, while *in vitro* strong reductants such as dithionite or photoreduced 5-deazariboflavin are employed. The reduced  $[4Fe-4S]^{1+}$  cluster can transfer one electron to SAM to homolytically cleave the S-C(S') bond, generating methionine (still bound to the unique iron) and a  $dAdo^\bullet$ . This reductive cleavage of SAM occurs in most radical SAM enzymes *in vitro* even in the absence of substrate, producing as products methionine and  $dAdoH$ , with the  $dAdoH$  presumably resulting from quenching

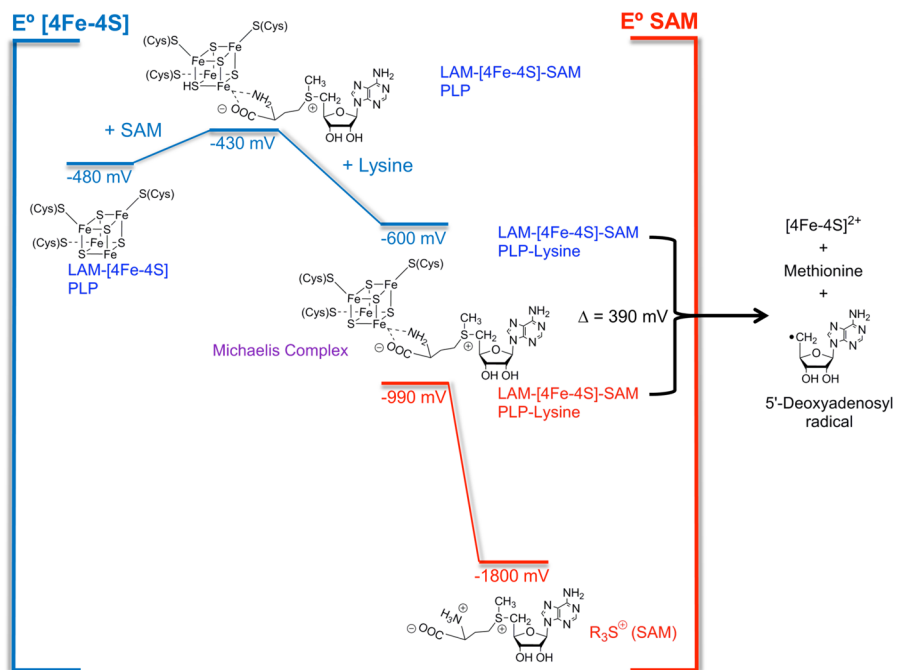


**Figure 8.** Reduction potentials for SAM and the  $[4\text{Fe}-4\text{S}]$  cluster based on experimental measurements for LAM.

of the dAdo<sup>•</sup> with solvent or a protein moiety. In the presence of substrate, however, the rate of the reductive cleavage reaction is generally considerably enhanced; this rate enhancement in fact has been used multiple times to identify unknown substrates of radical SAM enzymes, as will be detailed further in later sections of this Review. The dAdo<sup>•</sup> produced by reductive cleavage in the presence of substrate abstracts a H-atom from substrate in a regio- and stereospecific manner to generate a substrate radical. In some cases, this substrate radical is the end product of the reaction, such as in the case of PFL-AE where the end product is the glycyl radical on PFL. In most cases, however, the substrate radical is an intermediate, and undergoes simple or complex transformations and may react with additional substrates prior to product formation. In most radical SAM enzymes characterized to date, methionine and dAdoH are produced in a 1:1:1 stoichiometry with product, indicating that SAM is being used as a cosubstrate and is consumed during catalysis. Several characterized radical SAM enzymes, however, use SAM catalytically; in these cases, rearrangement of a substrate radical intermediate produces a product radical intermediate, and this latter species abstracts a H-atom from dAdoH to regenerate dAdo<sup>•</sup>, which recombines with methionine to regenerate SAM.

#### 2.4. Energetic Considerations in the Mechanism

Longstanding questions in the radical SAM mechanisms revolve around the topic of energetics. For the unified mechanism described in the previous section, a  $[4\text{Fe}-4\text{S}]^+$  cluster must reduce SAM. While the reduction potential of SAM itself is not known, other trialkylsulfonium compounds have been shown to have extremely negative reduction potentials that approximate  $-1.8 \text{ V}$ .<sup>23</sup> The  $2+/+$  redox couple for biological  $[4\text{Fe}-4\text{S}]$  clusters is rarely more negative than  $-500$  to  $-600 \text{ mV}$ , with specific potentials measured for LAM, BioB, and MiaB ranging from  $-479$  to  $-505 \text{ mV}$ .<sup>15,24</sup> Examining these potentials leads to the conclusion that the cluster to SAM electron transfer depicted in Figure 7 is, at face value, energetically very unfavorable (Figure 8). Despite the

mismatch in potentials, the facile cleavage of sulfonium containing compounds by synthetic site-differentiated  $[4\text{Fe}-4\text{S}]$  clusters has been demonstrated.<sup>25</sup> While these synthetic clusters have reduction potentials more negative ( $\sim -1 \text{ V}$ ) than those found in proteins, the energetic barrier is still large, and yet the reactions occur. The reactions of the model compounds differ from the enzyme-based chemistry in that the models generally react in a 2-electron process with electrophilic attack of the sulfonium on the coordinating thiolates; however, evidence for some reductive cleavage of SAM was also provided, indicating the general feasibility despite the mismatch in redox potentials.<sup>25</sup>

Given the demonstration that SAM binds in proximity to, and even coordinates, the  $[4\text{Fe}-4\text{S}]$  clusters of radical SAM enzymes, it is clear that the redox potentials of the iron–sulfur cluster and of SAM cannot be considered in isolation. Indeed, it is expected that the close proximity of the positively charged sulfonium group, as well as the coordination of one iron of the cluster by the hard, charged atoms of the methionine moiety, would have significant effects on the cluster reduction potential. Likewise, positioning SAM in close proximity to the charged iron–sulfur cluster would be expected to alter the SAM reduction potential. Perry Frey and co-workers have explored these issues using the radical SAM enzyme LAM (Figure 8). The reduction potential for the  $[4\text{Fe}-4\text{S}]^{2+/+}$  cluster in reconstituted LAM is  $-479 \text{ mV}$ ; addition of SAM shifts the potential  $+49 \text{ mV}$ .<sup>15</sup> On the basis of measured reduction potentials for the active site of LAM in the presence of SAM and alanine, *S*-adenosyl-*L*-homocysteine (SAH) and alanine, and SAH and lysine, the reduction potential of the cluster is estimated to drop to  $\sim -600 \text{ mV}$  in the Michaelis complex (SAM and lysine bound).<sup>26</sup> Conversely, the extremely negative potential of free SAM (estimated to be  $-1800 \text{ mV}$ ) is elevated to a value of  $-990 \text{ mV}$  upon its bidentate coordination to the  $[4\text{Fe}-4\text{S}]^+$  cluster in the Michaelis complex.<sup>26</sup> While these measurements reveal how interactions in the active site decrease the barrier for SAM cleavage by  $1.4 \text{ V}$ , the reduction of SAM by the  $[4\text{Fe}-4\text{S}]$  cluster is still energetically

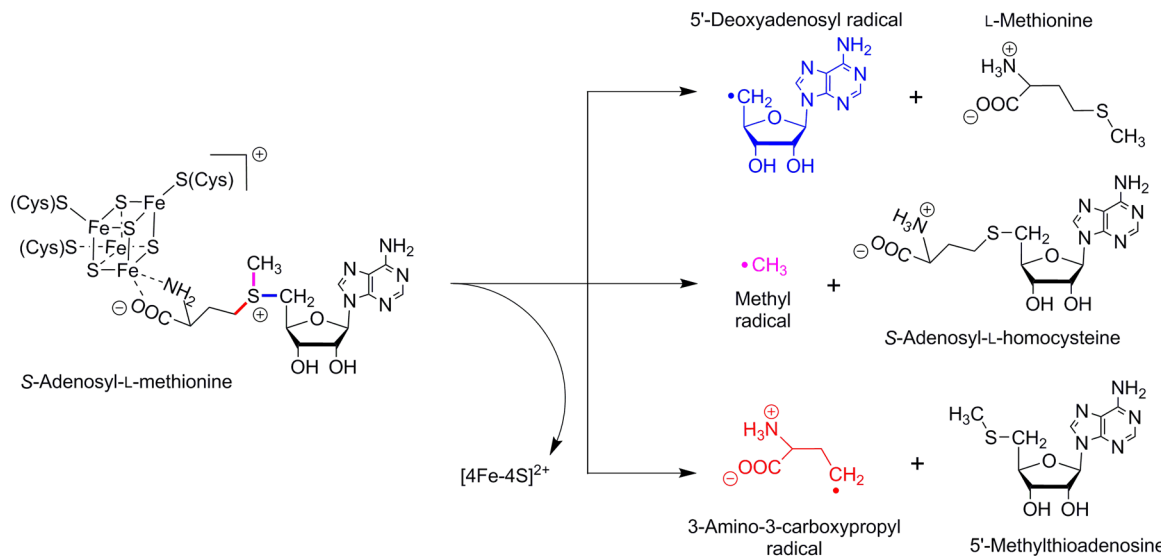


**Figure 9.** Regioselective cleavage of the S–C bonds of SAM. Bonds that may undergo enzymatic-based homolytic cleavage are demarcated in varying colors with S–C(5') in blue, S–C( $\gamma$ ) in red, and the S–C(methyl) in magenta.

unfavorable by  $\sim 390$  mV. One factor that may contribute to further closing the gap is that the unique Fe ion is pentacoordinate in the SAM bound state, but following cleavage is hexacoordinate with methionine bound;<sup>26</sup> an inner-sphere mechanism leading to Fe–S coordination to methionine was originally published in 2003.<sup>16b</sup> It should be stated that the tight binding of methionine in radical SAM enzymes appears to be favored only when SAM is utilized as a cofactor;<sup>27</sup> enzymes that consume SAM can be expected to bind methionine with less affinity, possibly indicating that the hexacoordinate geometry of the unique iron does not occur as readily in these cases (or more readily exchanges with another molecule of SAM).

Recent findings have indicated that the polarity of the active site environment plays a significant role in tuning the barrier for SAM cleavage; the reaction barrier is observed to increase with rising polarity.<sup>28</sup> Importantly, the crystallographic work with LAM supports this observation as the presence of lysine in the active site would likely limit solvent exposure and thus decrease the activation barrier, a result borne out by the midpoint potential solution studies.<sup>26</sup> Similarly, the structure of PFL-AE with SAM bound shows that the active site cavity, including the sulfonium group, is exposed to solvent, but following binding of the polypeptide substrate the active site is shielded from solvent.<sup>28,29</sup> These important observations suggest that the lowering of the dielectric medium in the vicinity of the iron sulfur cluster upon substrate binding could act to generally trigger SAM cleavage in these enzymes by significantly lowering thermodynamic barriers of the catalytic reaction.<sup>28</sup>

## 2.5. SAM: Mechanisms and Regioselectivity of S–C Bond Cleavage and Inner-Sphere Electron Transfer

Long before the acceptance of SAM as a common precursor of 5'-deoxyadenosyl radicals in biology, it was known as a common methyl donor in numerous biochemical reactions. In its typical role as a methyl donor, the bond between the sulfonium sulfur and the methyl carbon is cleaved heterolytically via a nucleophilic mechanism, such that the transferred unit is effectively  $\text{CH}_3^+$ .<sup>30</sup> The other two S–C bonds of the SAM sulfonium group can also undergo heterolytic cleavage in biochemical reactions, although this is less common.<sup>30</sup> In the

radical reactions of SAM, it is primarily the S–C(5') bond that is cleaved to generate methionine and a dAdo<sup>•</sup> (Figure 9). In only one characterized radical SAM enzyme, the  $\text{B}_{12}^-$ -independent glycerol dehydratase activating enzyme, is an alternate S–C bond (S–C( $\gamma$ )) cleaved.<sup>31</sup> Dph2, an enzyme not in the radical SAM superfamily, uses SAM in radical chemistry and also cleaves the S–C( $\gamma$ ) bond.<sup>32</sup> It is perhaps easy to rationalize why no radical SAM enzymes have been found that cleave the S–C(methyl) bond, because the resulting methyl radical species would be of very high energy and lacking a distal handle by which the active site of the enzyme can direct the radical. The discrimination between cleaving the S–C(5') and the S–C( $\gamma$ ) bonds is more subtle, however, as both of these S–C bonds have comparable bond energies and yield product radicals of comparable stability. The most reasonable explanation as to why the vast majority of radical SAM enzymes appear to catalyze S–C(5') rather than S–C( $\gamma$ ) bond cleavage seems to lie in the details of the cluster–SAM interaction.<sup>33</sup> The electron required for reductive cleavage of SAM arises from the reduced [4Fe–4S]<sup>+</sup> cluster, and spectroscopic studies have provided evidence for direct orbital overlap between the sulfonium sulfur and the iron–sulfur cluster.<sup>5,17</sup> Together, these findings suggest that an electron transfers from the iron–sulfur cluster directly into an antibonding orbital involving the sulfonium sulfur; whether the antibonding orbital receiving the electron is S–C(5') or S–C( $\gamma$ ) in nature determines the bond cleaved. This analysis would suggest that the S–C bond that is oriented trans to the sulfonium S–cluster interaction, and thus the S–C bond whose antibonding orbital has a lobe positioned to accept an electron from the Fe–S cluster, is the bond that will undergo homolytic cleavage.<sup>33</sup> Consistent with this idea, most structurally characterized radical SAM enzymes appear to bind SAM such that the S–C(5') bond is in the trans position.<sup>34</sup> Because there are currently no structures available in the SAM-bound state S–C( $\gamma$ ) bond-cleaving enzymes, it remains to be determined whether these enzymes will exhibit an alternate configuration of SAM relative to the cluster.

The intimate nature of SAM coordination to the [4Fe–4S]<sup>2+/+</sup> cluster and positioning within the active site clearly

underscores the role of both the coordination chemistry and the protein environment in dictating cleavage of the S–C(5') bond and in controlling the reactivity of the dAdo<sup>•</sup> toward product. This chemistry is initiated by the bidentate coordination of SAM to the unique Fe ion, which causes electronic perturbations in the [4Fe–4S] cluster and the antibonding S–C(5') orbital that are crucial to lowering the activation barrier for bond cleavage; many of these effects have only recently been observed. For example, spectroscopic evidence examining the effect of SAM binding to the [4Fe–4S]<sup>2+/+</sup> cluster in SPL indicates that cofactor binding induces elongation of the Fe…Fe distances both within the ferromagnetically coupled,  $6M_S = +9/2$  [2Fe–2S] rhomb of which the site-differentiated iron ion resides and between the two antiferromagnetically coupled [2Fe–2S] rhomb pairs.<sup>35</sup> Analysis of X-ray structures of radical SAM enzymes with SAM coordinated in the active site (discussed in greater detail in the following section) shows that the distance between the SAM sulfonium ion and the unique Fe ion is slightly shorter than the distance from the closest cluster sulfide to the sulfonium by ~0.3–0.7 Å for all available structures. In the case of HydE, for which structures exist of the enzyme in both SAM-bound and dAdoH/methionine-bound states, greater distortion of the Fe–S cluster is observed in the latter case due to the pseudo-octahedral coordination of methionine to the unique iron ion.<sup>27a</sup>

Computational studies based on the HydE structures predict a large energy barrier of 54 kJ/mol for SAM cleavage and provide a picture of the transition state (TS) structure, which shows that the main contributions to the TS HOMO are derived from the carbon-based radical of dAdo<sup>•</sup>, the methionine-based  $S\delta$ , and the site-differentiated iron.<sup>27a</sup> Calculations using an active site model suggest that inner-sphere electron transfer to the CS' group of SAM involves a direct path between the unique iron ion of the cluster and the p orbitals of the sulfonium group (Figure 10).<sup>27a</sup> The bidentate

this superfamily. Along these lines, XAS studies with PFL-AE show that upon SAM binding, an increase in S K-edge intensity is observed that derives from a backbonding interaction between the [4Fe–4S] cluster and the antibonding S–C(5') orbital; these results also indicate that the electron transfer pathway involves the unique Fe ion of the cluster.<sup>28</sup> However, the role of iron in the inner-sphere mechanism is not conclusive, as recent computational studies with BioB suggest that the electron transfer step from the [4Fe–4S]<sup>+</sup> cluster into the antibonding S–C orbital likely occurs via a sulfide–sulfonium interaction; the cluster sulfide nearest to the SAM sulfonium contributes to the LUMO of the transition state complex, providing a direct pathway for the reductive cleavage event.<sup>37</sup>

Upon reductive cleavage and generation of the dAdo<sup>•</sup> intermediate, the critical question becomes how the reactivity of this species is controlled within the active site environment. ENDOR studies probing intermediate catalytic states of LAM from the Frey and Hoffman laboratories have provided insight into this question. Initial measurements with LAM and different isotopically labeled SAM (<sup>15</sup>N, <sup>17</sup>O, <sup>13</sup>C, and <sup>2</sup>H) probing coordination between the [4Fe–4S] cluster and the cofactor set the groundwork for subsequent spectroscopic studies using both SAM and lysine analogues that formed stabilized radicals upon reduction.<sup>16b,38</sup> Use of S-3',4'-anhydroadenosyl-L-methionine (anSAM) in the presence of <sup>13</sup>C and <sup>2</sup>H labeled lysine (at the  $\beta$  position) demonstrated that the distance between anAdo<sup>•</sup> and the lysine  $\beta$ -carbon is essentially identical to that from the S'C of SAM and the substrate in the crystal structure, showing that no structural perturbations accompanied the reductive cleavage event.<sup>38</sup> Experiments using two different lysine analogues that formed stable L- $\alpha$ -lysine radicals following H-atom abstraction by dAdo<sup>•</sup> provided the first pictures of the substrate radical catalytic intermediate species (discussed in greater detail in section 5.1.6). Importantly, these results revealed a direct orbital overlap between the substrate radical and the methyl group of dAdoH, indicating these two species were in direct van der Waals contact (Figure 11).<sup>38</sup> Comparison to the crystal structure suggests that the distance between lysine and the 5'-carbon of dAdoH has decreased by ~0.5–1 Å during the transition from the resting state to the trapped substrate radical state;<sup>38,39</sup> the structural movement does not appear to accompany SAM cleavage but instead seems to be associated with the H-atom transfer step. The structural rearrangement resulting in van der Waals contact between the reacting partners that facilitates H-atom transfer is believed to persist throughout the isomerization mechanism of LAM and act to minimize the potential for undesired radical reactions.

## 2.6. A Common Protein Architecture for Radical SAM Catalysis

As of this writing, 14 radical SAM enzymes have been structurally characterized by X-ray crystallography. All of these enzymes exhibit a common fold composed of a full or partial triose phosphate isomerase (TIM) barrel. A full TIM barrel consists of eight alpha helices alternating with eight beta strands, which form a barrel-like structure with the beta strands on the interior and the alpha helices surrounding them on the protein surface. Biotin synthase (BioB),<sup>40</sup> thiamine pyrimidine biosynthetic enzyme ThiC,<sup>41</sup> the hydrogenase biosynthetic enzyme HydE,<sup>27a,42</sup> and most recently PylB<sup>43</sup> have crystal structures solved with complete  $(\beta\alpha)_8$  TIM barrels. The remaining structurally characterized radical SAM enzymes

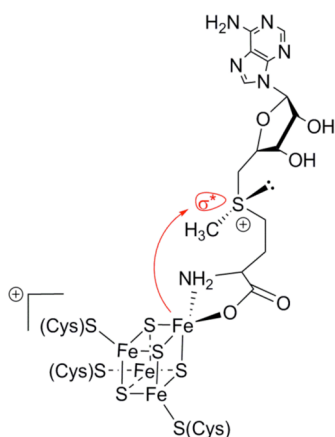


**Figure 10.** The reductive cleavage of SAM occurs through an inner-sphere mechanism involving a direct path between the unique iron ion of the cluster and the sulfonium group antibonding S–C(5') orbital.

coordination of SAM coupled with the close proximity of the sulfonium moiety to the iron sulfur cluster causes a perturbation in the electronic distribution of the cluster away from the standard sulfur-centered<sup>36</sup> to more iron-centered redox chemistry.<sup>27a</sup> The high similarity in SAM orientation for known structures of radical SAM enzymes suggests this cleavage mechanism may operate generally for all members of

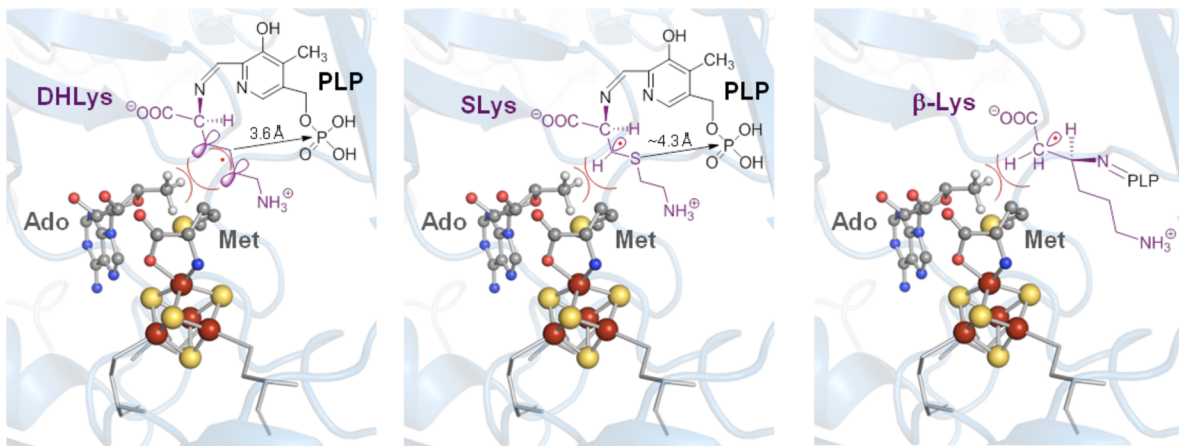


**Figure 11.** Illustration of the results of the LAM ENDOR studies using stabilized substrate and product radical analogue intermediates (PDB ID 2ASH). In all cases, van der Waals contacts are maintained between the 5'-methyl of dAdoH (carbons shown in gray) and the substrate/product radicals. Illustrations for the substrate radicals generated upon reaction with *trans*-4,5-dehydro-*L*-lysine (DHLys, left), 4-thia-*L*-lysine (SLys, middle), and the product radical generated upon equilibration of the reduced state of the enzyme with SAM and *L*- $\alpha$ -lysine (right). Adapted with permission from ref 38. Copyright 2006 American Chemical Society.

contain partial  $(\beta\alpha)_6$  TIM barrels. The smallest known radical SAM enzyme, the activating component of the anaerobic ribonucleotide reductase (aRNR-AE), is predicted to have a  $(\beta\alpha)_4$  partial TIM barrel, although it has yet to be structurally characterized. Half  $(\beta\alpha)_4$  barrel structures have been demonstrated to exist as soluble monomers in solution, suggesting that formation of the hydrophobic core is the driving force for the appearance of a stable structure and that primitive  $(\beta\alpha)_8$  barrels could have evolved through the tandem duplication of a  $(\beta\alpha)_4$  barrel.<sup>44</sup> The most primitive members of the radical SAM family are PFL-AE and aRNR-AE, comprised of  $(\beta\alpha)_6$  and  $(\beta\alpha)_4$  folds, respectively, possibly indicating the evolution of this subunit fold from  $(\beta\alpha)_2$  precursor units.<sup>45</sup>

The TIM barrels can vary from closed barrel structures to open, splayed barrels. In general, the openness of the barrel positively correlates with the size of the substrate; that is, radical SAM enzymes with larger macromolecular substrates exhibit more open barrel structures.<sup>34,45b</sup> The openness of the partial barrel results in exposure of one face of the  $\beta$  sheet known as the lateral opening, which houses the active site located near the top of the barrel. The conserved cluster binding CX<sub>3</sub>CX<sub>2</sub>C motif is found on the loop that follows the first  $\beta$  strand, and the [4Fe–4S] cluster itself is located 7–10 Å from the closest protein surface (Figure 12). The positioning of the cluster is such that it is buried by loop regions at the top of the barrel, and additional protein elements and SAM act to sufficiently shield the cluster and active site environment from bulk solvent. SAM coordination to the cluster positions the molecule across the top of the barrel, forming contacts with residues originating from each of the core  $\beta$  strands. A conserved “GGE” motif forms H-bonds to the amino portion of the methionyl group of SAM, acting to further position this group for coordination to the unique iron of the cluster. Amino acids that interact with the carboxylate functionality are more assorted, with H-bonding interactions among the different structures originating from either arginine, lysine, histidine, or serine and threonine. H-bonding interactions with the ribose hydroxyl groups are accomplished by charged or polar residues that originate mainly from strands  $\beta 4$  and  $\beta 5$ , while the adenine moiety forms a multitude of interactions that are hydrophobic, H-bonding, and  $\pi$ -stacking in nature. Importantly, mutational

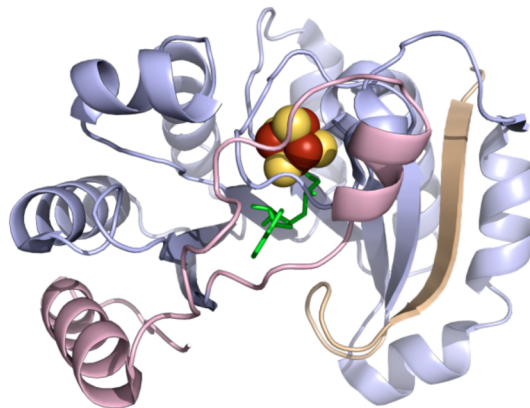


**Figure 12.** Example of a radical SAM partial TIM barrel structure (PDB ID 3CB8 for PFL-AE). N-terminal domain colored in wheat, radical SAM domain in light blue, C-terminal domain in light pink, [4Fe–4S] cluster in yellow and rust spheres, and SAM in green sticks.

studies on the two  $\beta 4$  strand residues N153 and D155 in BioB have implicated these amino acids as playing critical roles in the binding and cleavage of SAM and positioning of the dAdo $^\bullet$  for reaction with substrate.<sup>46</sup> Several of the radical SAM enzymes exhibit additional C-terminal associated structural features outside the core TIM barrel that may confer substrate specificity. Because of the vast disparity in radical SAM enzyme substrates, no common substrate binding motifs exist. That said, substrates are consistently observed to bind within the TIM barrel, representing how these enzymes utilize this tertiary fold to help minimize the deleterious effects on radical chemistry of incidental exposure to other cellular components.

## 2.7. [4Fe–4S]/SAM and Adenosylcobalamin: Parallels and Departures

The parallels between radical SAM enzymes and those utilizing adenosylcobalamin (AdoCbl or B<sub>12</sub>) to catalyze radical reactions are striking and have long been recognized. This was first brought to light more than 40 years ago with the discovery by Barker of lysine 2,3-aminomutase, an enzyme that catalyzes a novel interconversion of *L*- $\alpha$ -lysine and *L*- $\beta$ -lysine.<sup>8</sup> This reaction was recognized as being analogous to B<sub>12</sub>-dependent rearrangement reactions, and yet it was shown to

not require  $B_{12}$  for activity. Instead, activity was shown to be dependent on iron, PLP, SAM, and anaerobic conditions. Perry Frey and co-workers subsequently used 5'-tritium labeled SAM to provide evidence for the adenosyl moiety of SAM being directly involved in hydrogen transfer, in much the same way as the adenosyl moiety of AdoCbl is involved in  $B_{12}$ -dependent rearrangement reactions.<sup>10</sup> The parallels in reactivity for these two disparate cofactors were intriguing, and led to the labeling of SAM as "a poor man's adenosylcobalamin".<sup>18a,47</sup> Indeed, at the time,  $B_{12}$  was the classic example of a cofactor used for H-atom abstraction in enzyme reactions, and SAM was the simpler, less understood cousin. As of this writing, however, it is quite clear that the use of SAM as a radical precursor in the radical SAM reactions is much more widespread than that of  $B_{12}$ : there are currently 48 100 radical SAM superfamily members that span the entire phylogenetic kingdom and catalyze diverse reactions as detailed elsewhere in this Review, while the number of identified  $B_{12}$  enzymes stands at only 12,<sup>48</sup> and these are primarily bacterial in origin. The recognition of the amazing breadth of radical SAM reactions led Frey to propose an alternate adage, calling SAM "a rich man's adenosylcobalamin".<sup>49</sup>

Prior to the discovery of radical SAM enzymes,  $B_{12}$  was considered nature's "reversible free radical carrier",<sup>50</sup> involved in a variety of enzymatic reactions.<sup>51</sup> Considerable evidence available at the time supported the intermediacy of a dAdo<sup>•</sup> intermediate that abstracted an H-atom directly from substrate, and then redelivered an H-atom to the product radical after rearrangement. The dAdo<sup>•</sup> intermediate resulted from homolytic cleavage of the Co-C bond of  $B_{12}$  (adenosylcobalamin, Figures 3 and 13). Such a reaction was predicted to

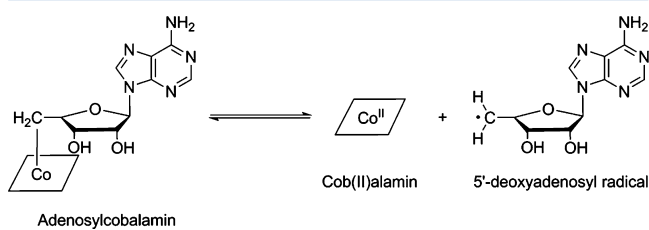


**Figure 13.** Homolytic cleavage of the Co-C bond to generate cob(II)alamin and the 5'- deoxyadenosyl radical.

require a weak Co-C bond, and Halpern provided the first determination of this bond energy in  $B_{12}$  as a relatively weak 26 kcal/mol.<sup>52</sup> It was proposed on the basis of model compound studies that enzyme binding factors such as steric strain would sufficiently weaken the Co-C bond so that homolysis would be a plausible step in  $B_{12}$  enzymatic reactions.<sup>50</sup> With the weak Co-C bond of  $B_{12}$  a central feature of its role as a reversible radical carrier, the observation that SAM seemed to be playing an analogous role in certain enzymes was intriguing.  $B_{12}$  and SAM both contain adenosyl moieties but have nothing else in common. Further, SAM does not have a relatively weak Co-C bond linking the adenosyl moiety to the rest of the cofactor, but rather a considerably stronger S-C bond. The developing realization that iron-sulfur clusters were involved in the SAM-dependent radical enzymes led to speculation about a new type of organometallic cofactor in biology, involving a cluster-adenosyl species with an Fe-C bond;<sup>53</sup> although no such species has yet been observed, the possibility cannot be entirely ruled out. What is clear at this stage for radical SAM enzymatic reactions is that SAM binds to the unique iron of the [4Fe-4S]

cluster via a classical chelate formation using the amino and carboxylate moieties;<sup>16a</sup> in this bound state, the sulfonium of SAM is in close proximity to the cluster, with evidence for direct orbital overlap between the two.<sup>17</sup> Inner-sphere electron transfer from the cluster to SAM initiates S-C bond cleavage to generate the dAdo<sup>•</sup> intermediate also found in  $B_{12}$  radical reactions. As with the  $B_{12}$  radical reactions, radical SAM reactions appear to be guided and tuned by a variety of enzyme binding effects that alter the energetics of individual steps.

As Halpern has pointed out, the reversible Co-C bond cleavage in  $B_{12}$ -dependent reactions (Figure 13) is formally an inner-sphere redox process analogous to reactions of reversible dioxygen carriers such as hemoglobin and myoglobin.<sup>50</sup> We can now add radical SAM-based radical generation to this model, with the inner-sphere electron transfer occurring from the site-differentiated [4Fe-4S] cluster to SAM coupled to S-C bond cleavage to generate the dAdo<sup>•</sup> as shown in Figure 7. As with the  $B_{12}$  enzymes, this reaction in radical SAM enzymes can be reversible, with the dAdo<sup>•</sup> regenerated after each reaction and ultimately regenerating SAM; in these cases, SAM, like  $B_{12}$ , is nature's "reversible free radical carrier". Unlike the  $B_{12}$  enzymes, however, many of the radical SAM enzymes carry out this inner-sphere electron transfer process as irreversible, where SAM is consumed as a cosubstrate and the dAdoH is a product. In these latter cases, SAM is acting as a radical carrier; however, the radical is ultimately an oxidant that is consumed, rather than simply a mediator of rearrangement reactions that is ultimately regenerated. In many ways, then, the radical SAM enzymes complete the analogy originally drawn by Halpern in 1985: the "reversible free radical carrier" role for adenosylcobalamin in  $B_{12}$  enzymes, and for SAM in some of the radical SAM enzymes, is analogous to reversible O<sub>2</sub> binding in proteins such as hemoglobin and myoglobin, while the "radical as oxidant" role for SAM in many of the radical SAM enzymes is analogous to iron enzymes that utilize O<sub>2</sub> as an oxidant. Such an oxidant role for the dAdo<sup>•</sup> derived from  $B_{12}$  is not observed in biology, perhaps because the biosynthetic complexity of  $B_{12}$  renders it evolutionarily disadvantageous to use as a consumed cosubstrate rather than a catalytic cofactor.

With the remarkable similarities in biochemical reactions mediated by such radically different cofactors as  $B_{12}$  and SAM, it is of interest to compare the protein context in which these two reactions are carried out. As discussed in section 2.6, most radical SAM enzymes possess a full or partial TIM barrel fold housing both the substrate binding site and the radical SAM [4Fe-4S] cluster. The radical chemistry thus occurs within this barrel's microenvironment, largely protected from the surroundings by the barrel and often the bound substrate itself. Structurally characterized  $B_{12}$  enzymes also contain a TIM barrel that harbors the substrate binding site; however, the  $B_{12}$  cofactor that serves as the radical precursor is bound not to this barrel but to a separate domain. Thus in the  $B_{12}$  enzymes, the two domains must come together for catalysis to occur. Ultimately, the use of the TIM barrel fold by  $B_{12}$  and radical SAM systems speaks toward the evolutionary development of these enzymes and the requirement for a protein architecture that was inherently not complex and in regards to radical SAM proteins allowed for the diversification of chemical reactions through the acquisition of additional modular protein domains.<sup>54</sup> Early suspicions indicated that radical SAM enzymes may have predicated AdoCbl enzymes in view of the simpler structure and biosynthesis of SAM relative to  $B_{12}$ .<sup>55</sup> Given the utilization of an ancient, highly conserved protein

fold and the presence of a CX<sub>3</sub>CX<sub>2</sub>C Fe–S-based motif used to chelate an organic molecule, it is plausible that SAM radical-based chemical transformations were some of the first functions associated with early protein-based biocatalysts.

### 3. GLYCYL RADICAL ENZYME ACTIVATING ENZYMES

The glycy radical enzymes (GREs) are a family of enzymes that house a stable, catalytically essential glycy radical in their active state.<sup>56</sup> Examples include PFL, anaerobic ribonucleotide reductase, benzylsuccinate synthase, 4-hydroxyphenylacetate decarboxylase, and glycerol dehydratase, among others. These oxygen-sensitive enzymes play key roles in microbial anaerobic metabolism.<sup>57</sup> The glycy radicals are generated by glycy radical enzyme activating enzymes (GRE-AEs), which are radical SAM enzymes. The GRE-AEs function either as distinct enzymatic entities or as subunits of the GREs that they activate. In either case, the GRE-AEs represent the simplest chemistries catalyzed by radical SAM enzymes, because the species generated upon H-atom abstraction by the deoxyadenosyl radical is the product of the reaction.

#### 3.1. Pyruvate Formate-Lyase Activating Enzyme

Pyruvate formate-lyase activating enzyme (PFL-AE) catalyzes the activation of pyruvate formate lyase (PFL), a central enzyme in anaerobic glucose metabolism in microbes. The activation of PFL by PFL-AE involves the stereospecific (pro-S) H-atom abstraction from PFL G734 (*E. coli* numbering) by a SAM-derived 5'-deoxyadenosyl radical generated by PFL-AE (Figure 14). PFL-AE was among the earliest enzymes identified to utilize SAM and iron to catalyze a radical reaction.

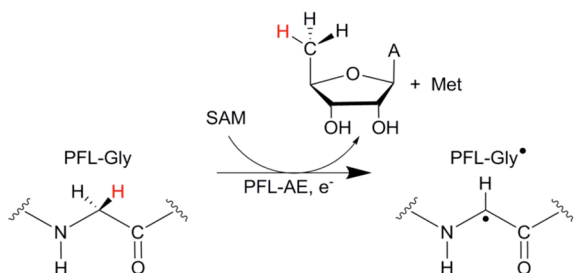


**Figure 14.** PFL-AE reaction scheme catalyzing the activation of PFL by stereospecific (pro-S) hydrogen atom abstraction from PFL G734 (in *E. coli*).

**3.1.1. Early Studies on Pyruvate Formate-Lyase and Its Activation.** The enzyme-catalyzed reversible cleavage of pyruvate to formate and acetyl-CoA was first described by the Werkman and Lipmann laboratories in the 1940s and 1950s;<sup>58</sup> in 1968 Chase and Rabinowitz proposed the name pyruvate formate-lyase for the enzyme catalyzing this reaction.<sup>59</sup> Characterization of this enzyme was hampered by its oxygen sensitivity, and by the loss of other required but unknown factors during cell fractionation. Joachim Knappe and co-workers first reported in 1965 that SAM was a cofactor,<sup>60</sup> and over the succeeding 35 years the Knappe laboratory led the way in unraveling the key mysteries of this extremely challenging and intriguing enzyme. They showed in 1969 that in addition to the pyruvate formate-lyase (PFL, which they also referred to as Enzyme I), a second enzyme (referred to as Enzyme II) was required for the reaction and was activated by Fe(II) and dithiols.<sup>3</sup> Enzyme II was ultimately shown to be responsible for catalyzing the activation of pyruvate formate-lyase itself, in a

reaction linked to the reductive cleavage of SAM. Knappe's predicted Enzyme II is now known as the radical SAM enzyme pyruvate formate-lyase activating enzyme (PFL-AE). In a seminal paper published in 1984, Knappe and co-workers reported that activation of PFL by the Fe(II)- and SAM-dependent PFL-AE resulted in the introduction of an unprecedented organic free radical localized on a PFL residue.<sup>2</sup> Four years later the same group reported the primary structures of PFL and PFL-AE, and noted "a cluster of three cysteines...which may be significant for the putative Fe-binding and redox-functional properties of this enzyme."<sup>61</sup> This cysteine "cluster" was, of course, the canonical radical SAM superfamily CX<sub>3</sub>CX<sub>2</sub>C motif.

The amino acid radical present in activated PFL was eventually shown to reside on glycine 734,<sup>4</sup> and to be generated by stereospecific abstraction of the α-C pro-S H-atom of G734.<sup>62</sup> The nature of the PFL-AE however remained somewhat more mysterious. PFL-AE was reported to contain an unidentified covalent chromophore ( $\lambda_{\text{max}} = 388 \text{ nm}$ ) and strictly require Fe(II) for activity.<sup>63</sup> Subsequent work in the Kozarich laboratory using recombinant PFL-AE homologously overexpressed in *Escherichia coli* and purified from inclusion bodies by denaturation demonstrated that no covalent chromophore was present in this case, and yet the enzyme was still active under reducing conditions in the presence of Fe(II) and SAM.<sup>64</sup> Kozarich and co-workers also reported that PFL-AE binds one Fe(II) per protein upon reconstitution, and that the protein could alternatively be reconstituted with similar ratios of Co(II) or Cu(II). Further, Cu(II), Zn(II), and Cd(II) were found to inhibit enzyme activity.<sup>64</sup>

**3.1.2. The Iron–Sulfur Cluster of PFL-AE and Its Role in Catalysis.** Despite this mounting evidence for a mononuclear iron site in PFL-AE, it was demonstrated in 1997 that PFL-AE was, in fact, an iron–sulfur cluster containing enzyme.<sup>5</sup> Careful anaerobic purification of PFL-AE from overexpressing *E. coli* cells without denaturation yielded protein with a reddish-brown color and a UV–vis spectrum characteristic of iron–sulfur clusters (Table 2).<sup>5</sup> Quantitative analysis of the isolated enzyme revealed the presence of 1.5 irons and 1.7 acid-labile sulfides per protein monomer.<sup>5</sup> Resonance Raman spectroscopy revealed the presence of both [4Fe–4S]<sup>2+</sup> and [2Fe–2S]<sup>2+</sup> clusters in the enzyme as-isolated, with only [4Fe–4S]<sup>2+</sup> clusters present upon dithionite reduction.<sup>5</sup> EPR spectroscopy revealed that the cluster could be reduced to the [4Fe–4S]<sup>+</sup> state in the presence of SAM (Table 2).<sup>5</sup> While the iron and sulfide to protein stoichiometry and cluster lability led at the time to a proposal that PFL-AE contained subunit-bridging [4Fe–4S] clusters, further investigations concluded that PFL-AE is monomeric and binds a [4Fe–4S] cluster. It was also noted in this paper that PFL-AE, the activase subunit of the anaerobic ribonucleotide reductase, and biotin synthase all contained the same CX<sub>3</sub>CX<sub>2</sub>C motif likely responsible for cluster coordination; together with the common requirement for SAM, this suggested "a commonality of mechanism that may represent a new paradigm for radical generation in biological systems."<sup>5</sup>

Modification of growth and purification conditions for PFL-AE ultimately led to isolation of enzyme containing primarily [3Fe–4S]<sup>+</sup> clusters,<sup>65</sup> which could be converted to [4Fe–4S] clusters upon reduction.<sup>66</sup> Further optimization of expression and purification conditions led to purified protein containing primarily [4Fe–4S]<sup>2+</sup> clusters, with stoichiometry close to one [4Fe–4S]<sup>2+</sup> cluster per protein monomer.<sup>67</sup> Enzyme activity

Table 1. Kinetic Parameters Associated with Radical SAM Enzymes

enzyme	substrate/Analogue	rate constant (min <sup>-1</sup> )	K <sub>M</sub>	no. of turnover events <sup>a</sup>	role of SAM <sup>b</sup>
BioB <sup>68</sup>	dethiobiotin	0.12 ± 0.03	10 ± 5 μM (SAM)	3	S
LipA <sup>69</sup>	octanoyl derivative of the H-protein	0.175 ± 0.01		0.378	S
ThiC <sup>70</sup>	5-aminoimidazole ribonucleotide (AIR)	0.14 ± 0.03	17 ± 3 μM (SAM)	5.2	S
NocL <sup>71</sup>	tryptophan	0.0416		~1.75	S
PFL-AE <sup>64,65</sup>	PFL	0.12	1.2 ± 0.4 μM (PFL) 2.8 ± 0.3 μM (SAM)	150	S
LAM <sup>8,72</sup>	lysine	~2000	4.3 ± 0.5 mM (lysine) 2.8 × 10 <sup>-8</sup> M (SAM)	>1000	C
EAM <sup>73</sup>	glutamate	366 ± 12	2.3 ± 0.2 mM		C
SPL <sup>74</sup>	DNA spore photoproduct	0.021 ± 0.004 (dinucleoside) 0.30 ± 0.01 (dinucleotide)		~10	C
Hpd-AE <sup>75</sup>	4-hydroxyphenyl acetate decarboxylase (Hpd)	0.25 ± 0.007	0.44 ± 0.04 mM (SAM)		S
BtrN <sup>76</sup>	2-deoxy-scyllo-inosamine (DOIA)	1.2 ± 0.1	0.022 ± 0.004 mM (DOIA) 0.46 ± 0.10 mM (SAM)		S
ThiH and ThiGH complex <sup>77</sup>	tyrosine	0.192 ± 0.048 ( <i>p</i> -cresol) (ThiH) 0.318 ± 0.036 ( <i>p</i> -cresol) (ThiGH)		~3 2.3	S
HydG <sup>78</sup>	tyrosine	0.108 ± 0.012 ( <i>p</i> -cresol) 0.036 ± 0.001 (CN <sup>-</sup> )	0.3 ± 0.03 mM (tyrosine) 2.6 ± 1.1 μM (SAM)	3	S
AtsB	serine on target sulfatase	0.32 ± 0.01 (Ser peptide)			S
anSMEkp <sup>79</sup>	(18-mer Ser or Cys peptide)	1.14 ± 0.12 (Cys peptide)			S
anSMEcp <sup>80</sup>	cysteine on target sulfatase (17- or 18-mer Ser or Cys peptides)	17-mer (Cys peptide) - (FGly) 0.0185  Kp18mer (Cys peptide) - (FGly) 2.3 ± 0.1  Kp18mer (Ser peptide) - (FGly) 0.85 ± 0.001		~3.5	S
BlsE <sup>81</sup>	cytosylglucuronic acid (CGA)	1.62 ± 0.30	1.93 ± 2.4 μM (CGA)		S
MoaA <sup>82</sup>	GTP	0.045 ± 0.003 (GTP)	1.4 ± 0.2 μM (GTP) 4.1 ± 1.3 μM (SAM)	0.5	S
MiaB <sup>83</sup>	i <sup>6</sup> A <sup>37</sup> containing 17 base tRNA oligonucleotide	0.018		1.2	S
RimO <sup>83</sup>	ribosomal S12-aspartyl 89 (13-mer)	0.019 13-mer (Asp peptide)		1.7	S
GenK <sup>84</sup>	gentamicin X <sub>2</sub>	0.018		22	S
HemN <sup>85</sup>	coproporphyrinogen III			5–8	S
AlbA <sup>86</sup>	precursor peptide SboA	0.075			S
DesII <sup>87</sup>	TDP-4-amino-4,6-dideoxy-D-glucose	1.0 ± 0.1	50 ± 1.2 μM		E
QueE <sup>88</sup>	6-carboxy-5,6,7,8-tetrahydropterin	5.4 ± 1.2	20 ± 7 μM (CPH <sub>4</sub> ) 45 ± 1 μM (SAM)		C
TsrM <sup>89</sup>	tryptophan	0.26		~50	N

<sup>a</sup>Reported as total moles product per mole enzyme. <sup>b</sup>Role of SAM during catalysis. S = substrate, C = cofactor, E = either, N = neither.

was correlated with cluster content, showing that the cluster was catalytically essential.<sup>5,65</sup> EPR spectroscopy was used to demonstrate clearly for the first time that (1) the [4Fe–4S]<sup>+</sup> state is the catalytically active state of the cluster, and (2) the [4Fe–4S]<sup>+</sup> cluster is oxidized to the [4Fe–4S]<sup>2+</sup> cluster concomitant with substrate turnover.<sup>21</sup> These experiments were carried out by reducing PFL-AE with photoreduced 5-deazariboflavin; the reduction requires exposure to an intense halogen lamp, and removal of excess reductant is as simple as putting the sample in the dark.<sup>21</sup> The PFL-AE samples were reduced for a range of times to produce enzyme with varying [4Fe–4S]<sup>+</sup> content (as confirmed by quantitative EPR spectroscopy).<sup>21</sup> Each sample was then placed in the dark, which effectively removes the reductant, and SAM and PFL were added. These samples then were analyzed using

quantitative EPR spectroscopy, as the enzyme product in this case is the paramagnetic PFL glycyl radical. Because the glycyl radical has distinct EPR spectral properties relative to the [4Fe–4S]<sup>+</sup> cluster, it was possible to identify and quantify each paramagnetic species individually. What the data set revealed was a 1:1 correlation between the amount of [4Fe–4S]<sup>+</sup> in the reduced PFL-AE sample and the amount of glycyl radical generated upon addition of PFL (Figure 6).<sup>21</sup> Further, the results showed that the [4Fe–4S]<sup>+</sup> cluster was converted to an EPR silent state upon reaction with PFL; this EPR silent state was ultimately shown to be the [4Fe–4S]<sup>2+</sup> state.<sup>21,67</sup>

These results revealed a key feature of radical SAM chemistry: radical SAM reactions utilize a reduced [4Fe–4S]<sup>+</sup> for cluster to transfer an electron to SAM, reductively cleaving it to generate methionine and a dAdo<sup>•</sup>, with the dAdo<sup>•</sup>

**Table 2. Spectroscopic Properties of the Radical SAM [4Fe–4S] FeS Cluster**

enzyme	organism	$\lambda_{\max}$ (nm) <sup>a</sup>	sample type	EPR ( <i>g</i> -values) <sup>b</sup>	[4Fe–4S] cluster Mössbauer parameters (mm/s) <sup>c</sup>	ref
Radical SAM Enzymes Without Auxiliary Fe–S Clusters						
LAM	<i>Clostridium subterminale</i> SB4	420 <sup>f,h</sup>	as-isolated <sup>f,h</sup>	2.03, 2.00, 1.99		8, 22, 90
			oxidized <sup>f,h</sup>	2.03, 2.01		
			reduced <sup>f,h</sup>	— <sup>j</sup>		
			reduced + SAM <sup>f,h</sup>	2.00, 1.90, 1.85		
RNR-AE <sup>p</sup>	<i>Escherichia coli</i>	420 <sup>e</sup>	as-isolated <sup>e</sup>	2.03, 2.00	[4Fe–4S] <sup>2+</sup> : $\delta = 0.43$ ; $\Delta E_Q = 1.0$ (82%) <sup>e</sup>	7a, 91
			reduced <sup>e</sup>	2.03, 1.93; 2.02, 1.92	[4Fe–4S] <sup>2+</sup> : $\delta = 0.46$ ; $\Delta E_{Q1} = 1.04$ (30%) <sup>e</sup>	
			reduced + SAM <sup>e</sup>	2.00, 1.91	[4Fe–4S] <sup>+</sup> : $(\delta_1 = 0.53$ ; $\Delta E_{Q1} = 0.92$ , $\delta_2 = 0.59$ ; $\Delta E_{Q2} = 1.61$ ) (50%) <sup>e</sup>	
					[4Fe–4S] <sup>2+</sup> : $\delta = 0.47$ ; $\Delta E_Q = 1.00$ (49%) [4Fe–4S] <sup>+</sup> : $(\delta_1 = 0.62$ ; $\Delta E_{Q1} = 1.70$ , $\delta_2 = 0.53$ ; $\Delta E_{Q2} = 0.73$ ) (40%) <sup>e</sup>	
<i>Lactococcus lactis</i>		as-isolated <sup>e</sup>	2.03, 2.01, 2.00			92
			reduced <sup>e,o</sup>	2.02, 1.93; 2.04, 1.94 <sup>o</sup>		
			reduced + SAM <sup>e</sup>	2.00, 1.92, 1.86; 2.00, 1.92, 1.86 <sup>o</sup>		
PFL-AE	<i>Escherichia coli</i>	420 <sup>f</sup>	reduced <sup>f,o</sup>	2.02, 1.94, 1.88 <sup>o</sup>		5, 16a, 17
			reduced + SAM <sup>f,o</sup>	2.01, 1.89, 1.88; 2.01, 1.88, 1.87 <sup>o</sup>		
			as-isolated <sup>f</sup>		[4Fe–4S] <sup>2+</sup> : $(\delta_1 = 0.45$ ; $\Delta E_{Q1} = 1.15$ , $\delta_2 = 0.45$ ; $\Delta E_{Q2} = 1.10$ ) (8%) <sup>f</sup>	
			reduced <sup>f,o</sup>		[4Fe–4S] <sup>2+</sup> : $(\delta_1 = 0.45$ ; $\Delta E_{Q1} = 1.15$ , $\delta_2 = 0.45$ ; $\Delta E_{Q2} = 1.10$ ) (66%) <sup>f</sup>	
		420 <sup>e</sup>	as-isolated + SAM <sup>f,q</sup>		[4Fe–4S] <sup>+</sup> : $(\delta_1 = 0.50$ ; $\Delta E_{Q1} = 1.32$ , $\delta_2 = 0.58$ ; $\Delta E_{Q2} = 1.89$ ) (12%) <sup>f</sup>	66, 93
			as-isolated + dAdoH <sup>f</sup>		[4Fe–4S] <sup>2+</sup> : $(\delta = 0.72$ ; $\Delta E_Q = 1.15$ ) (32%) <sup>f,q</sup>	
			whole cells		[4Fe–4S] <sup>2+</sup> : $(\delta = 0.44$ ; $\Delta E_Q = 1.20$ ) (19%) ( $\delta_1 = 0.39$ ; $\Delta E_{Q1} = 0.52$ ), ( $\delta_2 = 1.00$ ; $\Delta E_{Q2} = 2.07$ ) (77%)	
					[4Fe–4S] <sup>2+</sup> : $(\delta_1 = 0.43$ ; $\Delta E_{Q1} = 1.20$ ), ( $\delta_2 = 0.45$ ; $\Delta E_{Q2} = 0.71$ ), ( $\delta_3 = 0.97$ ; $\Delta E_{Q3} = 2.08$ ) (75%)	
		420 <sup>e,m</sup>	as-isolated <sup>e</sup>	2.01		94
			reduced <sup>e</sup>	2.03, 1.93		
			reduced + SAM <sup>e,m</sup>	2.01, 1.92, 1.89		
			reduced + SAH <sup>e,m</sup>	2.04, 1.93, 1.90		
SPL	<i>Bacillus subtilis</i>	400, 472 <sup>d</sup>	as-isolated <sup>d</sup>			95
			as-isolated <sup>e</sup>	2.03	[4Fe–4S] <sup>2+</sup> : $\delta = 0.44$ ; $\Delta E_Q = 1.06$ (40%) <sup>e</sup>	
			reduced <sup>e</sup>	2.03, 1.93		
			reduced + SAM <sup>e</sup>	2.02, 1.93		
		420 <sup>f</sup>	as-isolated <sup>f</sup>	2.02		97
			reduced <sup>f</sup>	2.03, 1.93, 1.89; 2.04, 1.94, 1.89		
			reduced + SAM <sup>f</sup>	2.03, 1.93, 1.92		
	<i>Clostridium acetobutylicum</i>	420 <sup>e</sup>	as-isolated <sup>e</sup>		[4Fe–4S] <sup>2+</sup> : $\delta = 0.43$ ; $\Delta E_Q = 1.09$ (42%) <sup>e</sup>	98
			as-isolated <sup>f</sup>		[4Fe–4S] <sup>2+</sup> : $\delta = 0.45$ ; $\Delta E_Q = 1.22$ (27%) <sup>f</sup>	
			reduced <sup>e</sup>	2.04, 1.94		
			413 <sup>f</sup>	1.99		
Geobacillus stearothermophilus		420 <sup>e</sup>	as-isolated <sup>f</sup>	2.03, 1.93, 1.92		74b
			reduced <sup>f</sup>	2.03, 1.92, 1.82		
			reduced + SAM <sup>f</sup>	2.04, 1.93, 1.89		
HemN	<i>Escherichia coli</i>	410 <sup>f</sup>	reduced + SAM <sup>e</sup>	2.04, 1.93, 1.89		99
			as-isolated <sup>f</sup>		[4Fe–4S] <sup>2+</sup> : $\delta_1 = 0.43$ , $\Delta E_{Q1} = 1.17$ (67%); $\delta_2 = 0.57$ ; $\Delta E_{Q2} = 1.23$ (22%) <sup>f</sup>	
			as-isolated + SAM <sup>f</sup>		[4Fe–4S] <sup>2+</sup> : $\delta_1 = 0.43$ , $\Delta E_{Q1} = 1.10$ (67%); $\delta_2 = 0.68$ ; $\Delta E_{Q2} = 1.04$ (22%) <sup>f</sup>	
			reduced <sup>f</sup>	2.06, 1.94, 1.89		
			reduced + SAM <sup>f</sup>	— <sup>j</sup>		
ThiGH	<i>Escherichia coli</i>	390 <sup>g</sup> , 410 <sup>g</sup>	as-isolated <sup>g</sup>	2.01		101
			reduced <sup>g</sup>	2.03, 1.92		
			reduced + SAM <sup>g</sup>	2.00, 1.87		
DesII	<i>Streptomyces venezuelae</i>	420 <sup>e</sup>	as-isolated <sup>d</sup>	2.01		87, 102

Table 2. continued

enzyme	organism	$\lambda_{\max}$ (nm) <sup>a</sup>	sample type	EPR ( <i>g</i> -values) <sup>b</sup>	[4Fe–4S] cluster Mössbauer parameters (mm/s) <sup>c</sup>	ref
Radical SAM Enzymes Without Auxiliary Fe–S Clusters						
			reduced <sup>e</sup>	2.01, 1.96, 1.87		
Elp3	<i>Methanocaldococcus jannaschii</i>	420 <sup>e</sup>	as-isolated <sup>e</sup>	2.00, 1.96		103
			reduced <sup>e</sup>	2.03, 1.93		
			reduced + SAM <sup>e</sup>	2.02, 1.93		
AviX12	<i>Streptomyces viridochromogenes</i>	450 <sup>d</sup>	oxidized <sup>d</sup>	2.03, 2.02, 2.00		104
			reduced <sup>d</sup>	— <sup>j</sup>		
ThiC	<i>Arabidopsis thaliana</i>	410 <sup>d,f,l</sup>	as-isolated <sup>d,l</sup>			105
	<i>Salmonella enterica</i>	410 <sup>f</sup>	as-isolated <sup>f</sup>			106
			reduced <sup>f</sup>	1.92		
	<i>Caulobacter crescentus</i>	415 <sup>g</sup>	as-isolated <sup>f</sup>		[4Fe–4S] <sup>2+</sup> : $\delta = 0.46$ ; $\Delta E_Q = 1.11$ (53%) <sup>f</sup>	41
			as-isolated <sup>g</sup>	2.00	[4Fe–4S] <sup>2+</sup> : $\delta = 0.45$ ; $\Delta E_Q = 1.12$ (43%) <sup>g</sup>	
			reduced <sup>g</sup>	2.02, 1.93		
Bss-AE <sup>p</sup>	<i>Thauera aromatica</i> T1	420, <sup>e</sup> 390 <sup>g</sup>	as-isolated <sup>e,f,g</sup>	2.02	[4Fe–4S] <sup>2+</sup> : $\delta = 0.43$ ; $\Delta E_Q = 1.09$ (92%) <sup>f,z</sup>	107
			reduced <sup>e,g</sup>	2.04, 1.94; <sup>e</sup> 2.06, 1.94 <sup>g</sup>		
Dph2	<i>Pyrococcus horikoshii</i>	400 <sup>f</sup>	as-isolated <sup>f</sup>		[4Fe–4S] <sup>2+</sup> : $\delta = 0.43$ ; $\Delta E_Q = 1.13$ (73%) <sup>f</sup>	32, 108
			reduced <sup>f</sup>	2.03, 1.92, 1.86		
HcgA	<i>Methanococcus maripaludis</i> S2	410 <sup>g</sup>	as-isolated <sup>g</sup>			109
			reduced <sup>g</sup>	2.04, 1.93		
			reduced + SAM <sup>g</sup>	2.03, 1.92		
NirJ	<i>Paracoccus pantotrophus</i>		as-isolated <sup>f</sup>	— <sup>j</sup>		110
			reduced <sup>f</sup>	2.02, 1.93		
			reduced + SAM <sup>f</sup>	2.00, 1.89		
RlmN	<i>Escherichia coli</i>	410 <sup>g</sup>	as-isolated <sup>f,g,aa</sup>	N.R. <sup>i</sup>	[4Fe–4S] <sup>2+</sup> : $\delta = 0.44$ ; $\Delta E_Q = 1.14$ (93%); <sup>f</sup> (95%) <sup>g</sup>	111
Cfr	<i>Staphylococcus aureus</i>	400, <sup>g</sup> 410 <sup>g</sup>	as-isolated <sup>f,g,aa</sup>	N.R. <sup>i</sup>	[4Fe–4S] <sup>2+</sup> : $\delta = 0.44$ ; $\Delta E_Q = 1.10$ (86%); <sup>f</sup> (98%) <sup>g</sup>	111, 112
			reduced <sup>g</sup>	2.04, 1.93, 1.89		
			reduced + SAM <sup>g</sup>	— <sup>j</sup>		
			reduced + SAH <sup>g</sup>	2.00, 1.93, 1.82		
Viperin	<i>Homo sapiens</i>	415, <sup>e,g</sup> 410 <sup>d</sup>	as-isolated <sup>g</sup>	2.01		113
			reduced <sup>g</sup>	2.02, 1.92, 1.91		
			reduced + SAM <sup>g</sup>	2.03, 1.95, 1.88		
GD-AE	<i>Clostridium butyricum</i>		reduced <sup>g</sup>	N.R. <sup>i</sup>		31
NocL	<i>Nocardia</i> sp. ATCC 202099	393 <sup>g</sup>	as-isolated <sup>g</sup>	— <sup>j</sup>		71
			reduced <sup>g</sup>	2.02, 1.91		
			reduced + SAM <sup>g</sup>	2.01, 1.89, 1.80 <sup>m</sup>		
			reduced + Trp <sup>g</sup>	2.02, 1.89, 1.85		
NosL	<i>Streptomyces actuosus</i>	400 <sup>g</sup>	as-isolated <sup>g</sup>			114
			reduced <sup>g</sup>	2.02, 1.91		
PhnJ	<i>Escherichia coli</i>	403, <sup>e</sup> 410 <sup>g</sup>	reduced <sup>g</sup>	2.01, 1.92, 1.87		115
PhpK	<i>Kitasatospora phosalicinaea</i>	420 <sup>g</sup>	as-isolated <sup>g</sup>	2.00		116
			reduced <sup>g</sup>	1.93		
CofH	<i>Nostoc punctiforme</i>	405 <sup>f</sup>	as-isolated <sup>f</sup>			117
CofG	<i>Methanocaldococcus jannaschii</i>	420 <sup>f</sup>	as-isolated <sup>f</sup>			117
QueE	<i>Bacillus subtilis</i>	410 <sup>g</sup>	as-isolated <sup>g,aa</sup>	2.00	[4Fe–4S] <sup>2+</sup> : $\delta = 0.44$ ; $\Delta E_Q = 1.13$ (80%) <sup>g</sup>	88
			reduced <sup>g</sup>	— <sup>j</sup>		
			reduced + SAM <sup>g</sup>	2.00, 1.91, 1.86		
TsrM	<i>Streptomyces laurentii</i>	420 <sup>e</sup>	as-isolated <sup>e</sup>			89
YtkT	<i>Streptomyces</i> sp. TP-A0356	410 <sup>g</sup>	as-isolated <sup>g</sup>			118
GenK	<i>Micromonospora echinospora</i>	420 <sup>e</sup>	as-isolated <sup>e</sup>			84
BlsE	<i>Streptomyces griseochromogenes</i>	420 <sup>g</sup>	as-isolated <sup>g</sup>	2.01		81
			reduced <sup>g</sup>	2.02, 1.93		
			reduced + SAM <sup>g</sup>	2.00, 1.96, 1.87		
MqnE	<i>Thermus thermophilus</i>	415 <sup>f</sup>	as-isolated <sup>f</sup>			119

Table 2. continued

enzyme	organism	$\lambda_{\max}$ (nm) <sup>a</sup>	sample type	EPR ( <i>g</i> -values) <sup>b</sup>	[4Fe–4S] cluster Mössbauer parameters (mm/s) <sup>c</sup>	ref
Radical SAM Enzymes Coordinating Auxiliary Fe–S Clusters						
BioB	<i>Escherichia coli</i>	410 <sup>d,k</sup>	as-isolated <sup>d,k</sup>			120
		420 <sup>e,k</sup>	as-isolated <sup>e,k</sup>		[4Fe–4S] <sup>2+</sup> : ( $\delta_1 = 0.44$ ; $\Delta E_{Q1} = 1.13$ (72%), $\delta_2 = 0.85$ ; $\Delta E_{Q2} = 0.51$ (8%)) <sup>e,k,t</sup>	121
			reduced <sup>e,k</sup>	2.04, 1.93 <sup>e,k,t</sup>	[4Fe–4S] <sup>+</sup> : $\delta = 0.85$ ; $\Delta E_Q = 0.51$ (80%) <sup>e,k,t</sup>	
			as-isolated <sup>e,k</sup>		[4Fe–4S] <sup>2+</sup> : $\delta_1 = 0.45$ ; $\Delta E_{Q1} = 1.16$ <sup>e,k,x</sup>	122
			as-isolated + SAM <sup>e,k</sup>		[4Fe–4S] <sup>2+</sup> : ( $\delta_1 = 0.45$ ; $\Delta E_{Q1} = 1.16$ ; $\delta_2 = 0.40$ ; $\Delta E_{Q2} = 0.86$ ; $\delta_3 = 0.64$ ; $\Delta E_{Q3} = 1.26$ ) <sup>e,k,x</sup>	
			reduced <sup>d,k,u</sup>	~2.00, 1.94, 1.94		
			reduced + SAM <sup>e,k,u</sup>	~2.00, 1.93, 1.85		
LipA	<i>Escherichia coli</i>	420 <sup>e,k</sup>	as-isolated <sup>e,k</sup>	— <sup>j</sup>	$\delta = 0.44$ ; $\Delta E_Q = 1.20$ (50%) <sup>e,k</sup>	121b, 123
		420 <sup>e,k</sup>	reduced <sup>e,k</sup>	2.04, 1.93		
		413 <sup>f,k</sup>	reduced <sup>f,k</sup>	2.06, 1.95, 1.92		124
		400 <sup>f,g,k,n</sup>	as-isolated <sup>f,g,k</sup>		[4Fe–4S] <sup>2+</sup> : ( $\delta_1 = 0.45$ , $\Delta E_{Q1} = 0.98$ ; $\delta_2 = 0.46$ , $\Delta E_{Q2} = 1.30$ ) (95%) <sup>f,k</sup> (64%) <sup>g,k</sup>	125
			as-isolated <sup>f,g,n</sup>		[4Fe–4S] <sup>2+</sup> : ( $\delta_1 = 0.46$ , $\Delta E_{Q1} = 0.92$ ; $\delta_2 = 0.45$ , $\Delta E_{Q2} = 1.22$ ) (95%) <sup>f,n</sup> (64%) <sup>g,n</sup>	
			reduced <sup>f,g,k</sup>	2.03, 1.93		
			reduced <sup>f,n</sup>	2.03, 1.93		
MiaB	<i>Escherichia coli</i>	(416, 460, 560) <sup>d,e,k</sup>	as-isolated <sup>d,e,k</sup>	2.01		126
			reduced <sup>d,e,k</sup>	2.06, 1.93		
	<i>Thermotoga maritima</i>	420 <sup>e,k</sup>	as-isolated <sup>e,k</sup>	2.01	[4Fe–4S] <sup>2+</sup> : ( $\delta_1 = 0.46$ , $\Delta E_{Q1} = 1.27$ ; $\delta_2 = 0.44$ , $\Delta E_{Q2} = 1.03$ ) (71%) <sup>f,k</sup> [4Fe–4S] <sup>+</sup> : ( $\delta_1 = 0.50$ , $\Delta E_{Q1} = 1.32$ ; $\delta_2 = 0.58$ , $\Delta E_{Q2} = 1.89$ ) (29%) <sup>e,k</sup>	24b, 127
			reduced <sup>e,k</sup>	2.05, 1.93		
MoaA	<i>Homo sapiens</i>	415 <sup>d,k</sup>	as-isolated <sup>g,k</sup>	2.00	[4Fe–4S] <sup>2+</sup> : $\delta = 0.48$ , $\Delta E = 1.26$ ; (40%) <sup>g,k,n</sup>	128
		410 <sup>f,g,k</sup>				
			reduced <sup>g,k</sup>	2.03, 1.92, 1.89		
HydE	<i>Thermotoga maritima</i>	400 <sup>e,k</sup>	as-isolated <sup>e,k</sup>			129
			reduced <sup>e,k</sup>	2.04, 1.93		
HydG	<i>Thermotoga maritima</i>	400 <sup>e,k</sup>	reduced <sup>e,k</sup>	N.R. <sup>i</sup>		129
	<i>Clostridium acetobutylicum</i>	400, <sup>e,k</sup> 395 <sup>g,k</sup>	as-isolated <sup>g,k</sup>			78b, 130
			reduced <sup>g,n,o</sup>	2.03, 1.91, 1.89		
			reduced + SAM <sup>g,n,o</sup>	2.03, 1.92, 1.91; 1.99, 1.88, 1.84		
	<i>Shewanella oneidensis</i>	N.R. <sup>i</sup>	reduced <sup>g,m,n</sup>	2.05, 1.94, 1.91		131
			reduced + SAM <sup>g,n</sup>	2.01, 1.88, 1.84		
NifB	<i>Azotobacter vinelandii</i>	400 <sup>g,k</sup>	as-isolated <sup>g,k</sup>			132
NifEN-B	<i>Azotobacter vinelandii</i>	N.R. <sup>f,i,k</sup>	oxidized <sup>f,k</sup>			133
			reduced <sup>f,k</sup>	2.02, 1.95, 1.94		
			reduced + SAM <sup>f</sup>	1.94 <sup>j,v</sup>		
Hpd-AE <sup>P</sup>	<i>Clostridium scatologenes</i>	420 <sup>g</sup>	as-isolated <sup>g,r</sup>	2.02	[4Fe–4S] <sup>2+</sup> : $\delta = 0.44$ ; $\Delta E_Q = 1.22$ (82%) <sup>g,z</sup>	75, 134
			reduced <sup>g,r</sup>	2.04, 1.94		
			reduced + SAM <sup>g,r</sup>	2.04, 1.94		
		390 <sup>f</sup>	as-isolated <sup>f,s</sup>	— <sup>j</sup>		
			reduced <sup>f,s</sup>	2.04, 1.94		
			reduced + SAM <sup>f,s</sup>	2.04, 1.94		
	<i>Clostridium difficile</i>	385 <sup>f</sup>	as-isolated <sup>s</sup>	— <sup>j</sup>		
			reduced <sup>s</sup>	2.04, 1.94		
			reduced + SAM <sup>s</sup>	2.04, 1.94		
anSME	<i>Clostridium perfringens</i>	420, <sup>e,k</sup> 400 <sup>g,k</sup>	as-isolated <sup>e,f,g,k</sup>		[4Fe–4S] <sup>2+</sup> : $\delta = 0.44$ ; $\Delta E_{qQ} = 1.14$ (95%) <sup>f,k</sup> (75%) <sup>g,k</sup>	80b, 135
			reduced <sup>e,k</sup>	2.05, 1.94		
			reduced + SAM <sup>e,k</sup>	1.99, 1.90		
	<i>Bacteroides thetaiotaomicron</i>	400 <sup>e,k</sup>	reduced <sup>e,k</sup>	2.05, 1.92		135b, 136
			reduced + SAM <sup>e,k</sup>	1.98, 1.90, 1.84		
BtrN	<i>Bacillus circulans</i>	420 <sup>f,g,k</sup>	as-isolated <sup>f,g,k</sup>		[4Fe–4S] <sup>2+</sup> : $\delta = 0.44$ ; $\Delta E_{qQ} = 1.13$ (87%) <sup>f,k</sup> (98%) <sup>g,k</sup>	76, 137

Table 2. continued

enzyme	organism	$\lambda_{\max}$ (nm) <sup>a</sup>	sample type	EPR ( <i>g</i> -values) <sup>b</sup>	[4Fe–4S] cluster Mössbauer parameters (mm/s) <sup>c</sup>	ref
Radical SAM Enzymes Coordinating Auxiliary Fe–S Clusters						
			reduced <sup>d,k</sup>	2.04, 1.92		
			reduced + SAM <sup>d,k</sup>	1.99, 1.83		
			reduced + SAM + substrate <sup>d,k,w</sup>	2.05, 1.96, 1.87		
AtsB	<i>Klebsiella pneumoniae</i>	395 <sup>f,g,k,aa</sup>	as-isolated <sup>g</sup>	N.R. <sup>i</sup>	[4Fe–4S] <sup>2+</sup> : $\delta = 0.44$ , $\Delta E_Q = 1.17$ (94%) <sup>f,g</sup>	79, 80b
RimO	<i>Escherichia coli</i>	410 <sup>f,g,k</sup>	as-isolated <sup>f,k</sup>	2.01	[4Fe–4S] <sup>2+</sup> : $\delta = 0.43$ , $\Delta E_Q = 1.07$ (90%) <sup>f,k</sup>	138
			as-isolated + SAM <sup>f,k</sup>		[4Fe–4S] <sup>2+</sup> : $(\delta_1 = 0.43, \Delta E_{Q1} = 1.07$ (58%); $\delta_2 = 0.70, \Delta E_{Q2} = 1.24$ (16%); $\delta_3 = 0.37, \Delta E_{Q3} = 0.81$ (16%)) <sup>f,k</sup>	
			as-isolated <sup>g,k</sup>		[4Fe–4S] <sup>2+</sup> : $\delta = 0.43$ , $\Delta E_Q = 1.12$ (62%) <sup>g,k</sup>	
			as-isolated + SAM <sup>g,k</sup>		[4Fe–4S] <sup>2+</sup> : $(\delta_1 = 0.43, \Delta E_{Q1} = 1.12$ (44%); $\delta_2 = 0.70, \Delta E_{Q2} = 1.24$ (9%); $\delta_3 = 0.37, \Delta E_{Q3} = 0.81$ (9%)) <sup>g,k</sup>	
			reduced <sup>f,k</sup>	2.06, 1.98, 1.94		
			reduced <sup>g,k</sup>	2.04, 1.93		
			reduced + SAM <sup>g,k</sup>	2.04, 1.93		
<i>Thermotoga maritima</i>		420 <sup>e,f,g,k</sup>	as-isolated <sup>e,f,g,k</sup>		[4Fe–4S] <sup>2+</sup> : $\delta_1 = 0.45, \Delta E_{Q1} = 1.15$ (56%); $(\delta_2 = 0.48, \Delta E_{Q2} = 1.24; \delta_3 = 0.60, \Delta E_{Q3} = 2.07; \delta_4 = 0.30, \Delta E_{Q4} = 0.90)$ (32%) <sup>e,k</sup>	83, 139
			reduced <sup>e,k</sup>	2.03, 1.93, 1.90; 2.04, 1.94, 1.88		
			reduced <sup>e,k,aa</sup>	2.03, 1.93, 1.90; 2.05, 1.94, 1.88	[4Fe–4S] <sup>2+</sup> : $(\delta_1 = 0.55, \Delta E_{Q1} = 1.90; \delta_2 = 0.50, \Delta E_{Q2} = 1.30)$ <sup>e,k</sup>	
PqqE	<i>Klebsiella pneumoniae</i>	420 <sup>e,k</sup>	as-isolated <sup>e,k</sup>	2.05, 1.94		140
		420 <sup>g,k</sup>	as-isolated <sup>g,k</sup>	2.01		
			reduced <sup>g,k</sup>	2.06, 1.96, 1.91		
			reduced + SAM <sup>g,k</sup>	2.00, 1.94, 1.90 <sup>m</sup>		
YqeV <sup>y</sup>	<i>Bacillus subtilis</i>	420 <sup>e,k</sup>	reduced <sup>e,k</sup>	N.R. <sup>i</sup>		141
TYW1	<i>Pyrococcus abyssi</i>	410 <sup>e,k</sup>	as-isolated <sup>e,k</sup>		[4Fe–4S] <sup>2+</sup> : $\delta = 0.44; \Delta E_Q = 1.13$ (78%) <sup>e,k</sup>	142
			as-isolated + SAM <sup>e,k</sup>			
			reduced <sup>e,k,o</sup>	2.02, 1.90, 1.86		
			reduced + SAM <sup>e,k,o</sup>	1.98, 1.86, 1.83		
AlbA	<i>Bacillus subtilis</i>	410 <sup>e,k</sup>	as-isolated <sup>e,k</sup>	— <sup>j</sup>		86
		430 <sup>e,n</sup>	reduced <sup>e,k</sup>	2.03, 1.92		
			as-isolated <sup>e,n</sup>	2.01		
			reduced <sup>e,n</sup>	2.03, 1.92		
FbiC	<i>Thermobifida fusca</i>	420 <sup>e</sup>	as-isolated <sup>e</sup>			117
SkfB	<i>Bacillus subtilis</i>	410 <sup>e,k</sup>	as-isolated <sup>e,k</sup>	2.01		143
			reduced <sup>e,k</sup>	2.04, 1.93		
		410 <sup>e,n</sup>	as-isolated <sup>e,n</sup>	2.01		
			reduced <sup>e,n</sup>	2.03, 1.93		

<sup>a</sup>Represents nonreduced  $\lambda_{\max}$  with as-reconstituted enzyme. Exceptions are marked as indicated. <sup>b</sup>Represents spectral *g*-values for the radical SAM [4Fe–4S] cluster; however, overlapping [4Fe–4S] cluster signals may be reflected in the cited *g*-values. Spectral values where radical SAM [4Fe–4S] signal discrimination has been performed is indicated. Unless otherwise indicated, samples that underwent reduction were reduced with dithionite. <sup>c</sup>Represents selected (simulated) Mössbauer parameters consistent with the radical SAM [4Fe–4S] cluster. Unless otherwise indicated, spectral values reported at 4.2 K. <sup>d</sup>Aerobic purification, no Fe–S reconstitution. <sup>e</sup>Aerobic purification, anaerobic Fe–S reconstitution. <sup>f</sup>Anaerobic purification, no Fe–S reconstitution. <sup>g</sup>Anaerobic purification and Fe–S reconstitution. <sup>h</sup>Enzyme not Fe–S reconstituted, but undergoes activation with Fe. <sup>i</sup>N.R. = data available, but was not reported. <sup>j</sup>Diamagnetic. <sup>k</sup>Intact enzyme. <sup>l</sup>Truncated enzyme. <sup>m</sup>Additional spectral features observed; please see reference. <sup>n</sup>Site-directed mutagenesis performed on non-radical SAM Fe–S cluster. <sup>o</sup>S-Deazariboflavin reduction data available. <sup>p</sup>Radical SAM Fe–S cluster part of a larger oligomeric structure with subunits that coordinate Fe–S clusters. <sup>q</sup>Represents a mixed <sup>56</sup>Fe/<sup>57</sup>Fe [4Fe–4S] cluster. <sup>r</sup>Enzyme purified with a hexahistidine tag. <sup>s</sup>Enzyme purified with a streptavidin tag. <sup>t</sup>Spectrum from Ollagnier 2000 Biochemistry. <sup>121b</sup> Cited references have slightly different but comparable Mössbauer parameters. <sup>u</sup>Samples underwent cryoreduction. <sup>v</sup>SAM serves as a substrate, causing Fe–S cluster to become diamagnetic. <sup>w</sup>Assignment was made before discovery of an auxiliary cluster on the enzyme. <sup>x</sup>% Fe not reported. <sup>y</sup>Reference uses YqeV and MtaB interchangeably. <sup>z</sup>Experiment performed at 80 K. <sup>aa</sup>EPR or UV-vis spectral data available on <sup>57</sup>Fe-enriched (reconstituted) samples.

abstracting a H-atom from substrate. These and other kinetics studies demonstrated that PFL-AE could undergo multiple turnover events, with the 150 PFL activations per PFL-AE reported in Table 1 not the upper limit, but rather a number limited by the PFL:PFL-AE ratio in the steady-state kinetics assays. As can be seen from the data summarized in Table 1, PFL-AE is one of the few radical SAM enzymes demonstrated

to be truly catalytic. Many of the enzymes studied to date undergo very few turnover events in vitro, reflecting both the difficulties in preparing and assaying active radical SAM enzymes and the challenging issues related to product stability/quantitation.

### 3.1.3. Defining the Unique SAM–Cluster Interaction in Radical SAM Enzymes.

The CX<sub>3</sub>CX<sub>2</sub>C motif in PFL-AE,

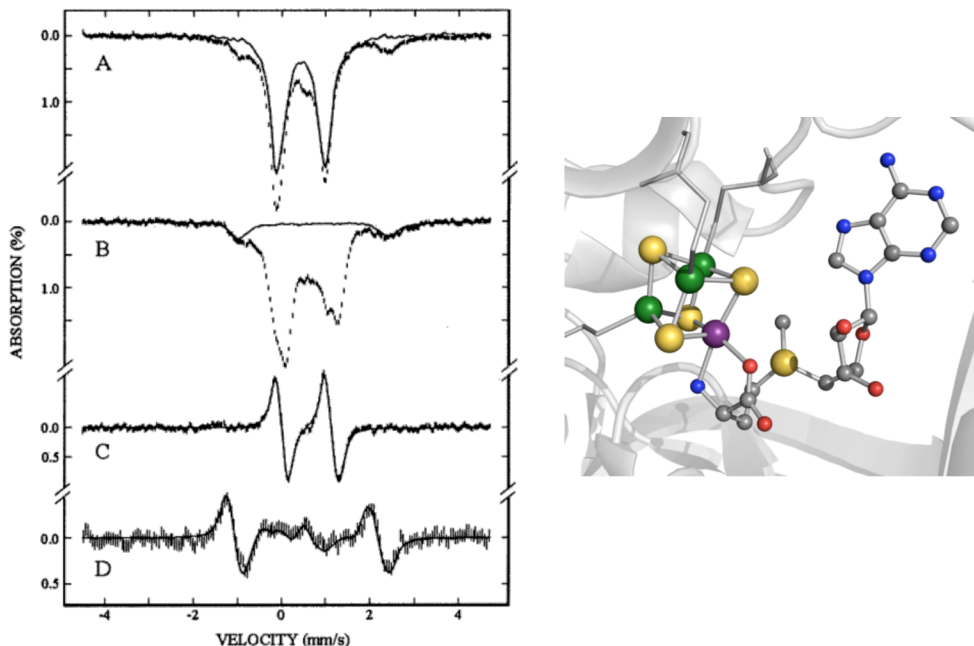


**Figure 15.** Left: Mössbauer spectra of  $^{56}\text{Fe}$  PFL-AE reconstituted with  $^{57}\text{Fe}$  for incorporation into the unique iron site in the absence (A) and presence (B) of SAM. The solid line in (A) is the experimental spectrum of  $[\text{4Fe}-\text{4S}]^{2+}$  clusters in PFL-AE normalized to 70% of the total Fe absorption of (A). The solid line in (B) is the spectrum of the control sample containing only the reconstitution ingredients and SAM but without PFL-AE and is normalized to 15% of the total Fe absorption of (B). A difference spectrum of (B) minus (A) is shown in (C). Spectrum (D) is a difference spectrum of the samples (A) and (B) recorded in a parallel field of 8 T. Reprinted with permission from ref 93a. Copyright 2002 American chemical Society. Right: Illustration of the PFL-AE  $[\text{4Fe}-\text{4S}]$  cluster with  $^{57}\text{Fe}$  (purple sphere) in the unique site bound by SAM, with the other sites occupied by natural abundance iron ( $^{56}\text{Fe}$ , green spheres) (PDB ID 3CB8).

together with the evidence that the catalytically relevant cluster was a  $[\text{4Fe}-\text{4S}]$  cluster, suggested the possibility of a site-differentiated  $[\text{4Fe}-\text{4S}]$  cluster in which three irons are coordinated by cysteinyl residues and the fourth iron has a noncysteine ligand. The first direct evidence for a site-differentiated cluster in the radical SAM enzymes was provided by an EPR spectroscopic study of LAM.<sup>90</sup> In this study, Frey and co-workers showed that oxidation of the  $[\text{4Fe}-\text{4S}]$  state of LAM with air or ferricyanide generated an EPR signal characteristic of  $[\text{3Fe}-\text{4S}]$  clusters, and similar to that previously reported for aconitase.<sup>90,144</sup> The observation that this  $[\text{3Fe}-\text{4S}]$  state could be converted back to the  $[\text{4Fe}-\text{4S}]$  state upon addition of iron and reductant (also similar to aconitase) strongly suggested that LAM, like aconitase, contains a site-differentiated  $[\text{4Fe}-\text{4S}]$  cluster in which one iron is rendered labile due to its lack of protein ligation. Similarly, anaerobically purified PFL-AE containing  $[\text{4Fe}-\text{4S}]^{2+}$  clusters were found to readily convert to the  $[\text{3Fe}-\text{4S}]^+$  state by air oxidation.<sup>93a</sup> Removal of the released iron by gel filtration followed by addition of 1 equiv of  $^{57}\text{Fe}$  produced enzyme whose Mössbauer spectroscopic parameters were typical of  $[\text{4Fe}-\text{4S}]^{2+}$  clusters. Upon addition of SAM to this protein, a significant change in the Mössbauer isomer shift, from 0.45 to 0.7, occurred (Figure 15) (Table 2).<sup>93a</sup> This shift is indicative of a change in coordination of the  $^{57}\text{Fe}$  to a harder, more ionic environment, and provided the first evidence that SAM binds to the  $[\text{4Fe}-\text{4S}]$  cluster of PFL-AE. In a complementary set of experiments, PFL-AE was overexpressed in  $^{57}\text{Fe}$  enriched medium, generating protein containing  $[\text{4Fe}-\text{4S}]$  clusters isotopically enriched in  $^{57}\text{Fe}$ .<sup>93a</sup> This protein was oxidized in air to generate the  $[\text{3Fe}-\text{4S}]^+$  cluster, and then 1 equiv of natural abundance Fe(II) was added to rebuild the  $[\text{4Fe}-\text{4S}]$  cluster. Again, the protein exhibited Mössbauer spectral

parameters consistent with the presence of  $[\text{4Fe}-\text{4S}]^{2+}$  clusters (Table 2).<sup>93a</sup> In this case, however, addition of SAM did not perturb these parameters. Together, the interpretation of these two results was that when Fe was added to rebuild a  $[\text{4Fe}-\text{4S}]$  cluster from a  $[\text{3Fe}-\text{4S}]$  cluster, the supplementary Fe entered primarily or exclusively the unique iron site that was not coordinated by the  $\text{CX}_3\text{CX}_2\text{C}$  motif; further, only this unique site was perturbed by the addition of SAM.<sup>93a</sup> Thus, these results provided the first evidence that SAM interacts directly with the  $[\text{4Fe}-\text{4S}]$  cluster of PFL-AE by coordinating the unique iron of the cluster.<sup>93a</sup>

The finer details of the SAM–cluster interaction were illuminated by electron–nuclear double resonance (ENDOR) spectroscopic studies of PFL-AE in complex with specifically isotopically labeled SAMs. By examining the coupling between the electron spin on the  $[\text{4Fe}-\text{4S}]^+$  and the nuclear spins on [ $\text{methyl-}^{13}\text{C}$ ]-SAM and [ $\text{methyl-D}_3$ ]-SAM, it was demonstrated that the sulfonium sulfur of SAM was in orbital overlap with the  $[\text{4Fe}-\text{4S}]$  cluster in the PFL-AE/SAM complex.<sup>17</sup> These results provided the first indication that the reduction of SAM by the  $[\text{4Fe}-\text{4S}]$  cluster occurred by an inner-sphere mechanism through direct orbital overlap.<sup>17</sup> Subsequent ENDOR studies of the PFL-AE/SAM complex using SAM isotopically labeled with  $^{13}\text{C}$  at the carboxyl carbon, with  $^{17}\text{O}$  at the carboxyl oxygen, and with  $^{15}\text{N}$  at the amino nitrogen of SAM, unequivocally demonstrated for the first time that SAM chelates the unique iron of the  $[\text{4Fe}-\text{4S}]$  cluster via the amino and carboxyl moieties of the methionine portion of SAM (Figure 16).<sup>16a,67</sup> Remarkably, the same SAM chelate structure has now been observed in every radical SAM crystal structure in which SAM is present; it seems clear that the coordination of SAM to the unique iron of the  $[\text{4Fe}-\text{4S}]$  cluster is a unifying

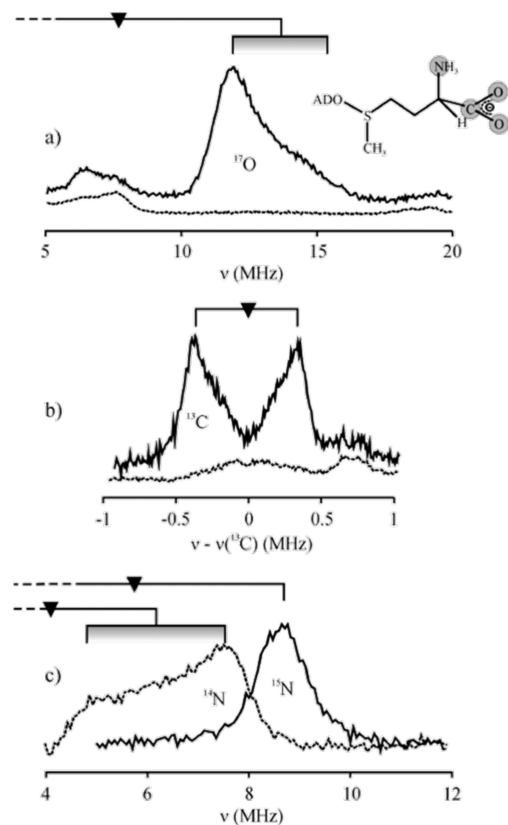


**Figure 16.** 35-GHz pulsed ENDOR spectra of PFL-AE with  $^{17}\text{O}$  (A) and  $^{13}\text{C}$  (B) carboxylato-labeled and  $^{15}\text{N}$ -amino-labeled (C) SAM as compared to data from an unlabeled sample, at  $g_{\perp}$ . Reprinted with permission from ref 67. Copyright 2005 American Chemical Society.

feature of radical SAM catalysis, playing a critical role in mediating the subsequent catalytic chemistry.

Insight into the behavior of the iron–sulfur cluster of PFL-AE in vivo was obtained by Mössbauer spectroscopic studies of whole *E. coli* cells overexpressing PFL-AE.<sup>93b</sup> The results demonstrate that in aerobic culture, the PFL-AE contains a mixture of [4Fe–4S] and [2Fe–2S] clusters; however, upon equilibrating the culture under anaerobic conditions, all of the iron–sulfur clusters converted to the [4Fe–4S] state, indicating that under anaerobic conditions the [2Fe–2S]<sup>2+</sup> clusters undergo reductive coupling to form [4Fe–4S]<sup>2+</sup> clusters, or alternatively that the [2Fe–2S] clusters are scavenged under anaerobic conditions building the more reduced [4Fe–4S]<sup>2+</sup> clusters.<sup>93b</sup> Only the diamagnetic [4Fe–4S]<sup>2+</sup> clusters were observed in the anaerobic cultures, indicating that even under anaerobic conditions in vivo, the amounts of the catalytically active [4Fe–4S]<sup>+</sup> state are too small to observe. This may indicate that the catalytically active [4Fe–4S]<sup>+</sup> oxidation state is achieved only immediately prior to catalysis, after the PFL-AE is complexed with its substrate PFL and poised for H-atom abstraction. The most intriguing observation from these studies, however, was that the [4Fe–4S]<sup>2+</sup> cluster contained a pair of valence-localized irons. While the vast majority of biological [4Fe–4S]<sup>2+</sup> clusters, including the [4Fe–4S]<sup>2+</sup> in purified PFL-AE, contain two pairs of valence-delocalized irons ( $\text{Fe}^{2.5+}$ – $\text{Fe}^{2.5+}$  pairs), the [4Fe–4S]<sup>2+</sup> cluster in PFL-AE in whole cells contains one valence delocalized ( $\text{Fe}^{2.5+}$ – $\text{Fe}^{2.5+}$ ), and one valence localized ( $\text{Fe}^{3+}$ – $\text{Fe}^{2+}$ ) pair (Figure 17).<sup>93b</sup> The  $\text{Fe}^{2+}$  of this localized pair is assigned to the distinct peak at +1.9 mm/s

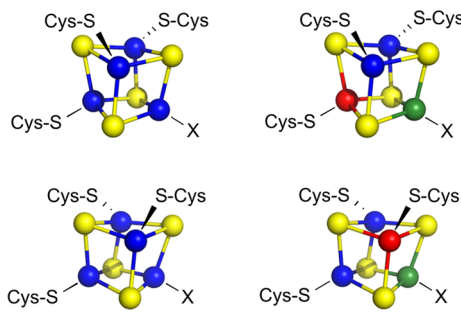


**Figure 17.** Representative valence delocalization of biological  $[4\text{Fe}-4\text{S}]^{2+}$  clusters containing two  $\text{Fe}^{2.5+}$ – $\text{Fe}^{2.5+}$  pairs (left, top and bottom). Representative valence localization of  $[4\text{Fe}-4\text{S}]^{2+}$  clusters in PFL-AE isolated from whole cells containing one  $\text{Fe}^{2.5+}$ – $\text{Fe}^{2.5+}$  pair and one  $\text{Fe}^{3+}$ – $\text{Fe}^{2+}$  pair (right, top and bottom) (PDB ID 3CB8).

in the Mössbauer spectrum, which is the high-energy half of the quadrupole doublet assigned to a high-spin  $\text{Fe}^{2+}$  ( $\delta = 0.97 \text{ mm/s}$  and  $\Delta E_Q = 2.08 \text{ mm/s}$ ) (Table 2). A valence-localized  $[4\text{Fe}-4\text{S}]^{2+}$  cluster has only been described for one other protein, ferredoxin:thioredoxin reductase, which has a very unusual redox-active disulfide in close proximity to the cluster that appears to influence the valence localization.<sup>145</sup> In PFL-AE, it remains unclear what causes the valence localization *in vivo*. Amazingly, 100% of the PFL-AE  $[4\text{Fe}-4\text{S}]^{2+}$  clusters are valence localized *in vivo*, while 100% are valence delocalized in the purified enzyme. It is clear that SAM does not induce valence localization of the  $[4\text{Fe}-4\text{S}]$  cluster of PFL-AE,<sup>93</sup> but the observed valence localization *in vivo* is almost certainly a result of something coordinating to the unique iron. To explore the possibilities, a range of small molecules were added to purified PFL-AE in the  $[4\text{Fe}-4\text{S}]^{2+}$  state, and the valence localization/delocalization was examined by Mössbauer spectroscopy.<sup>93b</sup> Several of these small molecules, including AMP and adenosine, were found to induce valence localization. Whether one or more of these small molecules are responsible for the valence localization observed *in vivo* has not yet been determined.

**3.1.4. X-ray Crystal Structure of PFL-AE.** PFL-AE was the first glycyl radical enzyme activating enzyme to be structurally characterized, and remains one of the smallest radical SAM enzyme for which a structure has been solved.<sup>29</sup> The enzyme is composed of a  $(\beta\alpha)_6$  partial TIM barrel, with essentially no additional secondary structural elements, unlike other structurally characterized radical SAM enzymes (Figure 18).<sup>29</sup> The  $[4\text{Fe}-4\text{S}]$  cluster resides at the top of the barrel, coordinated by the cysteines of the radical SAM CX<sub>3</sub>CX<sub>2</sub>C motif. A conserved patch of amino acids near the  $[4\text{Fe}-4\text{S}]$  cluster was proposed to be the site of interaction with the *in vivo* electron donor flavodoxin,<sup>29</sup> and recent studies have shown that flavodoxin binds PFL-AE with low micromolar affinity.<sup>146</sup> Structures were solved of the enzyme crystallized in the presence of SAM (2.25 Å), and in the presence of SAM plus a 7-mer peptide (RVSG<sub>734</sub>YAV) analogue of the Gly734 region of PFL (2.8 Å), although ordered SAM binding is observed only in the latter structure, suggesting that substrate binding helps to order SAM in the active site. SAM binds to the unique iron of the  $[4\text{Fe}-4\text{S}]$  cluster as had been previously demonstrated via ENDOR spectroscopy, and it packs close to the peptide substrate such that the C5' of SAM is only 4.1 Å from the  $\alpha$ -C of Gly734 where the H-atom is abstracted during PFL activation. Contacts between the PFL-AE side chains and

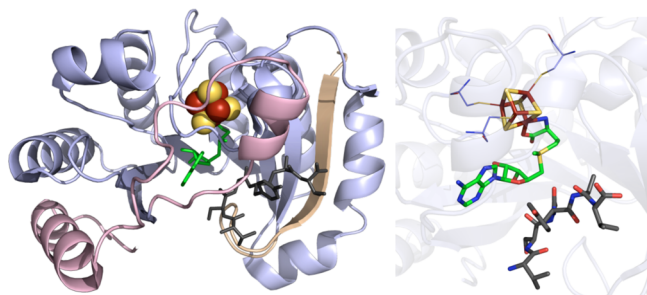


**Figure 18.** PFL-AE crystal structure (PDB ID 3CB8). Left: N-terminal domain colored in wheat, radical SAM domain in light blue, C-terminal domain in light pink, [4Fe–4S] cluster in yellow and rust spheres, SAM in green sticks, 7-mer peptide in dark gray sticks. Right: Active site of PFL-AE where [4Fe–4S] cluster (yellow and rust), SAM (green carbons), and 7-mer peptide (gray carbons) are depicted in sticks with oxygens colored red and nitrogens colored blue. Cysteines (light blue carbons) involved in ligating cluster are depicted in lines.

the peptide backbone appear to orient the Gly734 in the active site and control the peptide conformation. The stereospecificity of H-atom abstraction from PFL by PFL-AE is consistent with the resulting orientation of Gly734 relative to the CS' of SAM. A loop containing a conserved GRE-AE motif (DGXGXR) moves toward the active site in the peptide-bound structure, with this motif making several contacts with the bound peptide. A docking model using the “radical domain” of PFL (residues 712–759) revealed that this portion of PFL could fit in the splayed active site barrel of PFL-AE, with the Gly734  $\alpha$ -C positioned 4.6 Å from the S'C of SAM, poised for H-atom abstraction (Figure 19).<sup>29</sup>

### 3.1.5. PFL-AE Mechanism and the Interaction with PFL.

The [4Fe–4S] cluster of PFL-AE binds SAM in the

oxidized [4Fe–4S]<sup>2+</sup> or the reduced and catalytically active [4Fe–4S]<sup>+</sup> state.<sup>16a,17,67,93a</sup> Similar to all other radical SAM enzymes, the reduced cluster can transfer an electron via an inner-sphere process to the bound SAM, promoting homolytic S–C5' bond cleavage generating methionine and a dAdo<sup>•</sup> intermediate. The methionine presumably is initially bound to the unique iron of the cluster, although spectroscopic studies have not yet provided evidence for this methionine-bound state in PFL-AE. The dAdo<sup>•</sup> intermediate abstracts the pro-S H-atom from Gly734 to generate dAdoH and the active glycyl radical form of PFL.<sup>62</sup> Subsequent turnovers of PFL-AE require methionine and dAdoH replacement with SAM, substrate PFL binding, and the PFL-AE cluster reduction to the 1+ state.

The PFL crystal structure published in 1999 revealed that the Gly734 resides in a buried location within the structure, ~8 Å from the surface of the protein (Figure 20).<sup>147</sup> Gly734, together with two conserved cysteine residues (Cys418 and Cys419), define the active site of PFL, where the C–C bond of pyruvate is cleaved in a radical-mediated process to produce formate and the acetyl group transferred to CoA.<sup>147</sup> Evidence supports a mechanism in which the Gly734 radical abstracts a H-atom from Cys419 to generate a thiyl radical, and it is this thiyl radical that interacts directly with substrate pyruvate to mediate the chemical reaction. Thus, the close proximity of Gly734, Cys419, and Cys418 in an active site buried in the protein, where radical mechanisms are able to occur in a relatively protected fashion, is not surprising. The protected location of the Gly734 radical likely gives rise to its remarkable stability, with a half-life measured at >24 h.<sup>148</sup> However, the buried location of Gly734, together with the biochemical evidence for direct H-atom abstraction from this residue by a dAdo<sup>•</sup> generated in the PFL-AE active site,<sup>62</sup> and the structural studies of PFL-AE providing evidence that Gly734 bound in close proximity to the cluster-bound SAM in the active site of PFL-AE,<sup>29</sup> pointed to significant conformational changes for PFL during the activation process. Biochemical and biophysical studies utilizing enzyme activity assays, fluorescence, CD, and EPR spectroscopy have provided evidence that, while the PFL crystal structure revealed a protein in a “closed” state, with Gly734 buried in the active site, the presence of PFL-AE promoted conversion to an alternate “open” conformation in which Gly734 is more solvent-exposed.<sup>149</sup> It is presumably in this open conformation that the radical domain of PFL binds to the active site of PFL-AE, allowing formation of the radical at Gly734 (Figure 20). Consistent with these proposed large conformational changes in PFL during activation by PFL-AE, recent surface plasmon resonance studies indicate that the PFL/PFL-AE binding is slow, with the rate limited by large conformational changes.<sup>150</sup> Upon generation of the Gly734, the radical domain presumably reinserts Gly734 into the core of the PFL structure, thereby conferring the remarkable stability of Gly734. Interestingly, combining binding affinity data with information on the cellular abundance of PFL, PFL-AE, and SAM leads to the conclusion that these three species exist primarily in a ternary complex *in vivo*.<sup>150</sup>

### 3.2. The Anaerobic Ribonucleotide Reductase Activating Enzyme

The anaerobic ribonucleotide reductase activating enzyme, like PFL-AE, activates its target protein by the abstraction of a specific H-atom to generate the catalytically essential glycyl radical.

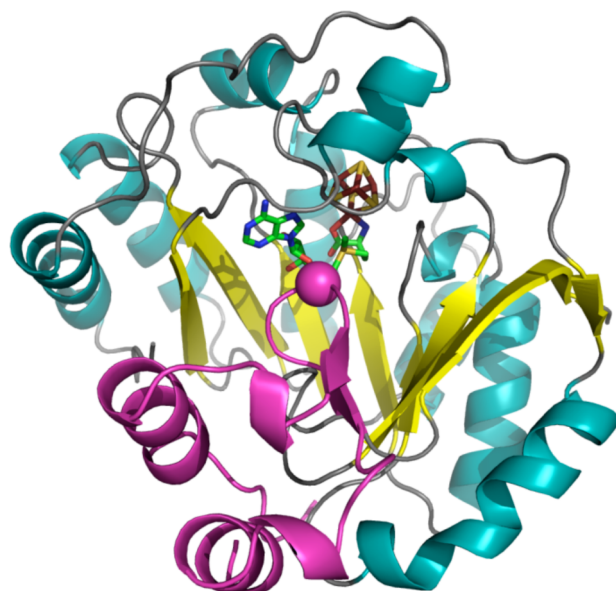


**Figure 19.** Docking model of PFL-AE (PDB ID 3CB8). Best dock as produced by ZDOCK, with C $\alpha$  of G734 in spacefill and radical domain of PFL (residues 712–759) in magenta. PFL-AE helices in cyan, strands in yellow, and loops in gray. The [4Fe–4S] cluster (yellow and rust) and SAM (green carbons) are depicted in sticks with oxygens colored red and nitrogens colored blue. Reprinted with permission from ref 29. Copyright 2008 National Academy of Sciences.

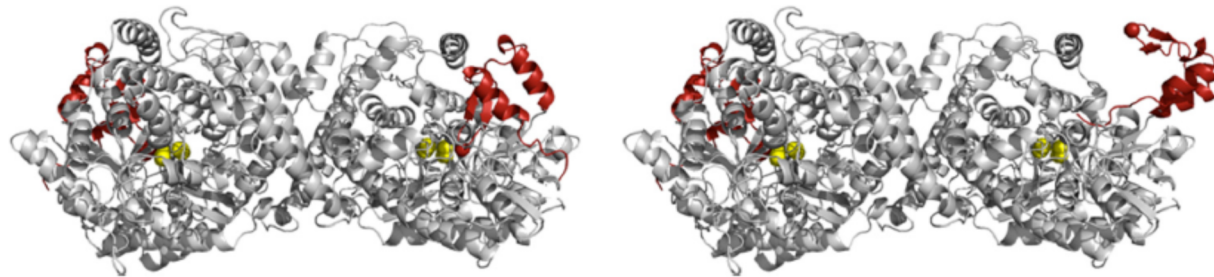


**Figure 20.** Schematic representation of PFL: left, crystal structure of closed conformation (PDB ID 2PFL); and right, model for the open conformation. Radical domain shown in red where Gly734 is a red sphere and active site residues Cys418 and Cys419 are yellow spheres. Reprinted with permission from ref 149. Copyright 2010 American Society for Biochemistry and Molecular Biology.

**3.2.1. Identification of an Anaerobic Ribonucleotide Reductase Containing a Glycyl Radical.** While the “aerobic” ribonucleotide reductase (Type 1, found widely in mammals and aerobic bacteria) had been known since the 1970s to contain a tyrosyl radical cofactor implicated in catalysis,<sup>18b,151</sup> the existence of an alternative ribonucleotide reductase present in anaerobic *E. coli* was first reported in 1988 by Barlow.<sup>152</sup> In 1989, Reichard and co-workers showed that this enzyme reduced CTP to dCTP, thereby differentiating its activity from the aerobic *E. coli* enzyme that reduced nucleotide diphosphates.<sup>153</sup> This anaerobic RNR (aRNR) requires strictly anaerobic conditions for optimal activity.<sup>153</sup> Hydroxyurea, which is known to potently scavenge the tyrosyl radical present in the aerobic RNR, only weakly inhibits the anaerobic RNR.<sup>153</sup> A year later, work in the Reichard laboratory demonstrated that the anaerobic RNR was dependent on SAM for activity.<sup>154</sup> The authors concluded that the anaerobic RNR used SAM and “a loosely bound metal” to generate the radical required for reduction at the 2' position of CTP.<sup>154</sup>

The sequence of the *nrdD* gene, encoding the anaerobic ribonucleotide reductase, was published in 1993, and Reichard and co-workers noted the presence of a pentapeptide on the aRNR, RVCY, that showed a strong resemblance to the pentapeptide of PFL, RVSGY, that had recently been shown to harbor a catalytically essential glycyl radical.<sup>7b</sup> Reichard and co-workers postulated that Gly681 of this peptide harbored a glycyl radical required for ribonucleotide reduction by aRNR,<sup>7b</sup> a hypothesis subsequently confirmed by specific isotopic labeling and site-directed mutagenesis of the aRNR coupled with analysis by EPR spectroscopy.<sup>155</sup> Reichard and co-workers also showed in 1993 that the aRNR bound an iron–sulfur cluster with EPR properties characteristic of a [3Fe–4S]<sup>+</sup> cluster, with the enzyme activity correlating with iron content.<sup>7a</sup> The cluster signal went away upon reductive activation of the enzyme, and a new EPR signal appeared that they assigned to an organic radical on Gly681. Although the iron–sulfur cluster was attributed at the time to the aRNR, we now know that the cluster is associated specifically with the aRNR activating enzyme as is discussed in the next section.

**3.2.2. A [4Fe–4S] Cluster in the Activating Enzyme for the aRNR.** In 1995 an open reading frame downstream of the *nrdD* gene was identified; this ORF encoded the 17.5 kDa iron-dependent protein (NrdG) eventually identified as the activating protein for the anaerobic RNR.<sup>156</sup> It was subsequently shown that this small activase protein (designated  $\beta$ ) formed a tight complex with the anaerobic RNR protein (designated  $\alpha$ ), with  $\alpha_2\beta_2$  stoichiometry.<sup>157</sup> As was also incorrectly originally proposed for PFL-AE, the [4Fe–4S] cluster was thought to bridge the  $\beta_2$  dimer.<sup>91a,157a</sup> This

hypothesis was supported by the observation of [2Fe–2S]<sup>2+</sup> clusters bound to the  $\alpha_2\beta_2$  enzyme, which, upon reductive activation, converted to a mixture of [4Fe–4S]<sup>+</sup> and [4Fe–4S]<sup>2+</sup> clusters (Table 2).<sup>158</sup> It was shown shortly thereafter, however, that each  $\beta$  peptide bound four irons and four sulfides, and that the aRNR activating enzyme was a [4Fe–4S]<sup>2+</sup> and not a [2Fe–2S]<sup>2+</sup> enzyme, with the observation of the latter clusters being due to air degradation of the former.<sup>91b</sup> Site-directed mutagenesis studies demonstrated that the three cysteines in the CX<sub>3</sub>CX<sub>2</sub>C motif, and no other cysteine residues, were required for cluster coordination and catalytic activity.<sup>159</sup>

Like PFL-AE, the aRNR activase was found to undergo reductive cluster conversion from [3Fe–4S] to [4Fe–4S] without addition of exogenous iron and sulfide.<sup>92b</sup> Subsequent studies showed that the presence of SAM perturbed the EPR spectrum of the [4Fe–4S]<sup>+</sup> cluster,<sup>160</sup> and that in the presence of DTT, the [4Fe–4S]<sup>+</sup> cluster was converted to an EPR silent state concomitant with formation of the glycyl radical (Table 2).<sup>91c</sup> These results were important in establishing a redox catalytic role for the [4Fe–4S] cluster in the activation of the anaerobic RNR exploiting SAM as a cofactor. This paper provided further insight into the relationship between the aRNR and its activase, demonstrating the activase alone could bind SAM and catalyze its reductive cleavage, but the activity was enhanced in the presence of the  $\alpha_2$  RNR.<sup>91c</sup> A similar study on the enzyme from *Lactobacillus lactis* reached the same conclusion: that NrdD is the ribonucleotide reductase that is activated by its activase NrdG.<sup>157b</sup> While  $\beta_2$  forms a tight complex with  $\alpha_2$ , and was thus viewed for some time as a subunit of the aRNR holoenzyme,  $\beta_2$  was ultimately demonstrated to activate multiple  $\alpha_2$ , and thus, like PFL-AE,  $\beta_2$  is a true activating enzyme.<sup>91b</sup> The physiological reducing system for the aRNR-AE, flavodoxin and flavodoxin reductase in the presence of NADPH, was shown to be incapable of reducing the iron–sulfur cluster of the aRNR-AE to the catalytically active state, consistent with the redox potential of the aRNR-AE [4Fe–4S]<sup>2+/+</sup> couple being more negative than the relevant couples of the flavodoxin system.<sup>160</sup> In the presence of SAM and the aRNR ( $\alpha_2$ ), however, the flavodoxin/flavodoxin reductase system was capable of generating the glycyl radical on  $\alpha_2$ , suggesting that electron transfer from the flavodoxin system to the aRNR-AE is coupled to, and driven by, the reductive cleavage of SAM and the subsequent generation of the glycyl radical on aRNR.<sup>160</sup> The strict requirement for the presence of all of the players in this high-cost, high-stakes chemistry is testament to the complexity of these enzyme systems.



**Figure 21.** The X-ray crystal structures of the activating enzyme substrates from left to right: GD, PFL, and aRNR (PDB IDs: 1R8W, 2PFL, and 1HK8, respectively). All structures possess a core 10-stranded  $\beta$ -barrel motif assembled in a manner antiparallel to two parallel five-stranded  $\beta$ -sheets. The  $\beta$ -barrel core is surrounded by  $\alpha$ -helices forming the  $\beta/\alpha$ -barrel. Radical domains, highlighted in magenta, for GD, PFL, and aRNR are composed of the amino acids 731–782, 702–754, and 540–586 (where aRNR possesses a mostly disordered C-terminal domain), respectively.

### 3.3. The $B_{12}$ -Independent Glycerol Dehydratase Activating Enzyme

A  $B_{12}$ -independent glycerol dehydratase (GD) has been discovered that has significant sequence homology to PFL and is activated by a protein (GD-AE) with homology to PFL-AE.<sup>161</sup> The X-ray crystal structure of GD<sup>162</sup> reveals a tertiary fold similar to that of PFL<sup>147a</sup> and the aRNR,<sup>163</sup> and the C-terminal domain of GD aligns well (rmsd  $\sim 0.7$  Å) with the radical domain of PFL that is the site of interaction with PFL-AE (Figure 21).<sup>162</sup> The purified inactive GD can be activated under anaerobic conditions in the presence of SAM by GD-AE that had been subjected to iron–sulfur cluster reconstitution conditions, providing further evidence for similarity to the PFL/PFL-AE system.<sup>162</sup> The reduced form of GD-AE exhibits EPR spectral features consistent with the presence of one or more  $[4\text{Fe}-4\text{S}]^+$  clusters that are perturbed upon addition of SAM.<sup>31</sup> When GD is added to the GD-AE/SAM complex, a glycyl radical is formed as detected by EPR spectroscopy.<sup>31</sup> Therefore, in many significant ways, the GD/GD-AE and PFL/PFL-AE systems are analogous. However, while PFL-AE has been shown to cleave the S–C(5') bond of SAM generating dAdoH and methionine (via a dAdo $^\bullet$  intermediate), GD-AE has been found to cleave the S–C( $\gamma$ ) bond of SAM to generate methylthioadenosine (MTA) and 2-aminobutyrate as products.<sup>31</sup> Presumably, a 2-aminobutyryl radical intermediate is utilized in the GD-AE-catalyzed activation of GD, although this has yet to be directly demonstrated. This was an important observation as it demonstrated the potential for radical SAM enzymes to cleave alternate S–C bonds during radical catalysis.

### 3.4. Other Glycyl Radical Enzyme Activating Enzymes

Benzylsuccinate synthase (BSS) is a central enzyme in anaerobic toluene catabolism, catalyzing the conversion of toluene + fumarate  $\rightarrow$  benzylsuccinate. BSS is a glycyl radical enzyme with an  $\alpha_2\beta_2\gamma_2$  oligomeric structure, with the large  $\alpha$  subunits exhibiting similarity to PFL and harboring the glycyl radical.<sup>164</sup> The BSS also contains Fe–S clusters putatively residing on the  $\beta$  and  $\gamma$  subunits that are of unknown function (Table 2).<sup>107</sup> The BSS is activated by a specific activating enzyme that has not yet been characterized but is presumably similar to PFL-AE.

4-Hydroxyphenylacetate decarboxylase (HPD), which catalyzes the formation of *p*-cresol, is another glycyl radical enzyme

that, like BSS, contains additional subunits.<sup>165</sup> A mechanism for this enzyme has recently been proposed on the basis of QC/MM calculations, which invokes a Cys503 radical as an oxidant, abstracting an electron from substrate, while Glu637 abstracts a proton.<sup>166</sup> Like BSS, HPD contains auxiliary iron–sulfur clusters in addition to a glycyl radical; the clusters bind to small subunits in  $\beta_4\gamma_4$  octamers and may be involved in quenching the radicals of activated enzymes when substrate is absent.<sup>134,167</sup> The HPD activating enzyme (HPD-AE) is monomeric and contains approximately eight iron atoms and eight acid-labile sulfides per monomer, with an extinction coefficient consistent with the presence of two clusters per protein.<sup>134</sup> EPR spectra of the dithionite-reduced HPD-AE indicate the presence of  $[4\text{Fe}-4\text{S}]^+$  clusters (Table 2). The amino acid sequence of HPD-AE contains, in addition to the radical SAM CX<sub>3</sub>CX<sub>2</sub>C motif, eight additional cysteines present in the two motifs CX<sub>5</sub>CX<sub>2</sub>CX<sub>3</sub>C and CX<sub>2</sub>CX<sub>4</sub>CX<sub>3</sub>C, suggesting that this protein could bind up to three  $[4\text{Fe}-4\text{S}]$  clusters.<sup>134</sup> It is interesting to note that all GRE-AEs with the exception of PFL-AE and aRNR-AE contain similar auxiliary cluster motifs.<sup>134</sup> Although it had been proposed on the basis of the results with GD-AE that the GRE-AEs containing auxiliary Fe–S clusters might catalyze cleavage of alternate S–C bonds of SAM,<sup>31</sup> it has been recently reported that HPD-AE cleaves the S–C(5') bond of SAM.<sup>75</sup> The “classical” SAM cleavage exhibited by HPD-AE thus calls into question the proposed correlation between additional clusters and alternate mechanisms of SAM cleavage.

A glycyl radical enzyme was recently found to catalyze the C–N bond cleavage involved in the conversion of choline to trimethylamine.<sup>168</sup> There are currently no published studies on the activating system for this glycyl radical enzyme.

## 4. ENZYMES CATALYZING SULFUR INSERTION

Among the earliest recognized radical SAM enzymes were two that catalyzed sulfur insertion into C–H bonds; these were biotin synthase, catalyzing thiazole ring formation in the final step of biotin biosynthesis, and lipoyl synthase, which catalyzes the insertion of two sulfur atoms into C–H bonds of an octanoyl moiety to generate the lipoyl cofactor.

#### 4.1. Biotin Synthase

##### 4.1.1. Initial Identification of Fe–S Cluster and SAM Dependence.

The product of the *bioB* gene, now commonly referred to as biotin synthase (BioB), was first characterized in a cell-free extract by Ifuku and co-workers in 1992 (for the *E. coli* enzyme)<sup>169</sup> and Ohshiro et al. in 1994 (for the enzyme from *Bacillus subtilis*).<sup>170</sup> It also demonstrated that the *bioB* gene product was capable of converting dethiobiotin to biotin in a reaction that was dependent on Fe<sup>2+</sup> and SAM, in addition to a few other components including an unidentified protein partner (Figure 22). In 1994, Flint and co-workers reported

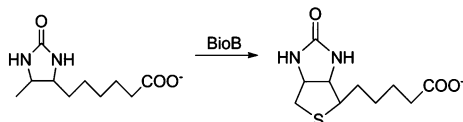


**Figure 22.** The conversion of dethiobiotin to biotin catalyzed by biotin synthase (BioB).

the first purification of *E. coli* BioB.<sup>12a</sup> The enzyme behaved as a dimer, and iron and sulfide analysis together with EPR spectroscopic evidence supported the presence of one redox-active [2Fe–2S] cluster per monomer. The iron–sulfur cluster was EPR silent in the isolated state, and became EPR active ( $g = 2.00, 1.95, 1.90$ ) upon reduction with dithionite, although the EPR spin quantitation accounted for only 10–15% of the expected iron–sulfur clusters.<sup>12a</sup> Regardless, the data indicated that a [2Fe–2S]<sup>2+</sup> cluster in the isolated protein could be reduced to a [2Fe–2S]<sup>+</sup> cluster by dithionite. Flint and co-workers also demonstrated *in vitro* that the purified *bioB* gene product was active in converting dethiobiotin to biotin in the presence of NADPH, SAM, Fe<sup>3+</sup> or Fe<sup>2+</sup>, and additional cofactors that were subsequently identified as flavodoxin, flavodoxin reductase, fructose 1,2-bisphosphate, cysteine, and DTT, although it was observed at most only 3 biotin produced per protein dimer, and a turnover number of 1 per hour.<sup>171</sup> This low number of turnovers and slow rate of catalysis is something that continues to beleaguer BioB research to the current day (Table 1), as will be addressed again later in this section.

Importantly, Flint and co-workers pointed out the similarity of biotin synthase to isopenicillin N synthase (IPNS), which also inserts sulfur into an unactivated C–H bond and also depends on loosely bound iron, but then noted that while IPNS required O<sub>2</sub> for its reaction, biotin synthase did not.<sup>171</sup> They also pointed out the dual presence of the CX<sub>3</sub>CX<sub>2</sub>C motif in both BioB and lipoate synthase, which also catalyzes insertion of sulfur into unactivated C–H bonds. They also noted the apparent similarities in reaction between biotin synthase, lysine 2,3-aminomutase, and the anaerobic ribonucleotide reductase, including the involvement of an Fe–S cluster and SAM, and the mechanism involving abstraction of a H-atom from an unactivated carbon. Because LAM and the aRNR-AE appeared to utilize radical chemistry, Flint and co-workers suggested that biotin synthase would also operate via radical chemistry.<sup>171</sup> These authors also alluded to the “remote possibility” that the unstable iron–sulfur cluster in biotin synthase might serve as the sulfur donor in biotin biosynthesis;<sup>12a</sup> this role for the [2Fe–2S] cluster in biotin synthase is now widely accepted, as will be discussed further below. Thus, in this very first report of the characterization of purified biotin synthase, a number of key ideas were put forth that placed biotin synthase hypothetically

with the other early iron–sulfur cluster and SAM dependent enzymes. Shortly thereafter, Andree Marquet and co-workers demonstrated that highly purified BioB was active in the absence of any other protein if photoreduced deazaflavin was present.<sup>172</sup> Further, they showed that during the BioB reaction, SAM was cleaved to produce dAdoH and methionine, in a ratio of approximately three per biotin produced. They surmised that two SAM cleavage events were required to cleave two C–H bonds in dethiobiotin, while the third equivalent was attributed to an abortive process.<sup>172</sup>

##### 4.1.2. The Iron–Sulfur Clusters of Biotin Synthase.

A thorough spectroscopic characterization of biotin synthase by Michael Johnson and co-workers provided the first detailed picture of the Fe–S clusters in this enzyme.<sup>120</sup> They used UV-vis, VTMCD, EPR, and resonance Raman spectroscopies of biotin synthase in its as-isolated state and after reduction with dithionite. The as-isolated enzyme appeared to contain [2Fe–2S]<sup>2+</sup> clusters at a stoichiometry of one [2Fe–2S] cluster per subunit. Resonance Raman spectroscopy indicated the presence of at least one noncysteine ligand to this cluster. Prolonged reduction with dithionite resulted in the formation of [4Fe–4S] clusters, which were either entirely in the diamagnetic 2+ oxidation state or partially in the paramagnetic 1+ state depending on the details of the reduction (Table 2).<sup>120</sup> Resonance Raman spectroscopy pointed to complete cysteinyl ligation for this [4Fe–4S] cluster, and EPR spectroscopy showed that the 1+ state existed as a mixture of spin states, with both S = 1/2 ( $g = 2.044, 1.944, 1.914$ ) and S = 3/2 ( $g = 5.6$ ) states observed (Table 2).<sup>120</sup> The authors proposed that the [4Fe–4S]<sup>2+/+</sup> cluster was formed by reductive coupling of two [2Fe–2S] clusters at the subunit interface, and that the [4Fe–4S] cluster played a role in the reductive cleavage of SAM to initiate radical chemistry. It was also proposed that oxidative conversion of the [4Fe–4S] cluster to [2Fe–2S] clusters might play a physiological role in regulating enzyme activity in response to oxidative stress.<sup>120</sup>

Subsequent studies by Fontecave and co-workers<sup>121b</sup> and Jarrett and co-workers,<sup>173</sup> however, demonstrated that biotin synthase could be reconstituted to contain one [4Fe–4S] cluster per subunit, or two per dimer. Oxidative degradation resulted in conversion of the [4Fe–4S] clusters to [2Fe–2S] clusters, and rereduction regenerated the [4Fe–4S] clusters. Jarrett and co-workers further demonstrated that reductive conversion of [2Fe–2S] to [4Fe–4S] clusters involved rapid dissociation of iron followed by rate-limiting reassociation to produce the [4Fe–4S] clusters; this observation is also inconsistent with the previously proposed reductive coupling of [2Fe–2S] clusters to form [4Fe–4S] clusters.<sup>173</sup> It also showed that biotin synthase containing two [4Fe–4S] clusters per dimer could undergo rapid and reversible oxidation and reduction, supporting that the [4Fe–4S] cluster was the catalytically essential state of the enzyme. Further, it was shown that mutagenesis of the three cysteines that comprise the radical SAM motif yields inactive enzyme,<sup>174</sup> which was incompetent for reductive cleavage of SAM.<sup>121c</sup> Two additional cysteines were also found to be required for activity.<sup>175</sup> Taken together, these results argued against the previously proposed subunit-bridging [4Fe–4S] clusters.

In an important series of papers, Jarrett and co-workers and Johnson and co-workers provided the first clear evidence that both [2Fe–2S] and [4Fe–4S] clusters were playing a critical role in biotin synthase activity. Ugulava et al. used electrochemistry coupled with UV-vis spectroscopy to show that

reduction of the  $[2\text{Fe}-2\text{S}]$  clusters to generate  $[4\text{Fe}-4\text{S}]$  clusters occurred at widely separated potentials of  $-140$  and  $-430$  mV, while reduction of the  $[4\text{Fe}-4\text{S}]^{2+}$  to the  $[4\text{Fe}-4\text{S}]^+$  state occurred at lower potentials between  $-440$  and  $-505$  mV (Figure 23).<sup>24a</sup> A subsequent Mössbauer study provided

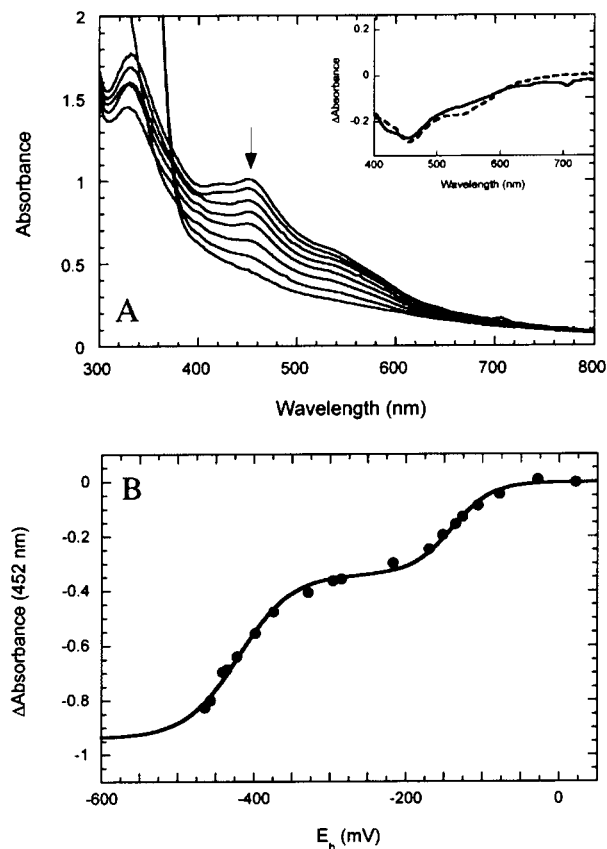


**Figure 23.** Reduction of BioB containing  $[2\text{Fe}-2\text{S}]^{2+}$  clusters. (A) UV-visible spectra of BioB were recorded as the cell potential was lowered by titration with dithionite. (Inset) Difference spectra associated with the first wave of reduction (solid curve) and the second wave of reduction (dashed curve) having maxima at 460 nm. (B) The absorbance change at 452 nm was followed as a function of the measured cell potential. Reprinted with permission from ref 24a. Copyright 2001 American Chemical Society.

evidence that the  $[2\text{Fe}-2\text{S}]$  and  $[4\text{Fe}-4\text{S}]$  clusters in biotin synthase occupy distinct sites in the enzyme.<sup>176</sup> Detailed UV-visible, resonance Raman, and Mössbauer spectroscopic studies by Cosper et al. showed that the  $-140$  mV potential was likely due to residual  $[2\text{Fe}-2\text{S}]$  cluster residing in the radical SAM cluster site, with the lower potential  $-430$  mV cluster assigned to the catalytic  $[2\text{Fe}-2\text{S}]$  cluster.<sup>177</sup> Given the differing potentials of the radical SAM and  $[2\text{Fe}-2\text{S}]$  clusters, Ugulava et al. were able to isolate BioB containing one  $[2\text{Fe}-2\text{S}]$  and one  $[4\text{Fe}-4\text{S}]$  cluster per monomer after incubation under assay conditions,<sup>24a</sup> and to show that this mixed cluster state of biotin synthase gave rise to optimal enzyme activity.<sup>178</sup> Spectroscopic evidence indicated that the  $[2\text{Fe}-2\text{S}]$  cluster was degraded and the  $[4\text{Fe}-4\text{S}]$  cluster retained during turnover, affording the first results supporting the proposal that the  $[2\text{Fe}-2\text{S}]$  cluster of biotin synthase was the source of sulfur in the synthesis of biotin, as is discussed in the following section.<sup>24a,178</sup>

Ollagnier-de Coudens et al. used EPR and Mössbauer spectroscopic studies coupled to analysis of SAM cleavage products to demonstrate that the  $[4\text{Fe}-4\text{S}]^+$  cluster of biotin synthase provides an electron to SAM, promoting its reductive cleavage to dAdoH and Met while leaving the cluster in the diamagnetic  $[4\text{Fe}-4\text{S}]^{2+}$  state (Table 2).<sup>121c</sup> They also demonstrated that only three of the eight cysteines in biotin synthase (residues 53, 57, and 60, in a  $\text{CX}_3\text{CX}_2\text{C}$  motif) were required for the SAM cleavage activity, indicating that these three cysteines coordinate the  $[4\text{Fe}-4\text{S}]$  cluster. Johnson and co-workers subsequently used resonance Raman, Mössbauer, and EPR spectroscopies to demonstrate that SAM binds to a unique iron site of the  $[4\text{Fe}-4\text{S}]$  cluster of biotin synthase, supporting an inner-sphere electron transfer mechanism for reduction of SAM by the  $[4\text{Fe}-4\text{S}]^+$  cluster.<sup>122</sup>

Johnson, Huynh, and co-workers provided further support for distinct roles for two different iron–sulfur clusters in biotin synthase.<sup>179</sup> Like Jarrett and co-workers, they showed that as-isolated biotin synthase containing  $[2\text{Fe}-2\text{S}]$  clusters could be reconstituted with iron and sulfide to a form that contained one  $[2\text{Fe}-2\text{S}]$  and one  $[4\text{Fe}-4\text{S}]$  cluster per monomer. They also used EPR and Mössbauer spectroscopies to demonstrate that while the  $[4\text{Fe}-4\text{S}]$  cluster was stable and was bound by SAM during catalysis, most of the  $[2\text{Fe}-2\text{S}]$  cluster was degraded during turnover, thus further supporting the Jarrett proposal that the  $[2\text{Fe}-2\text{S}]$  cluster served as the source of sulfur in biotin biosynthesis (Figure 24).<sup>178,179</sup> Johnson and co-workers

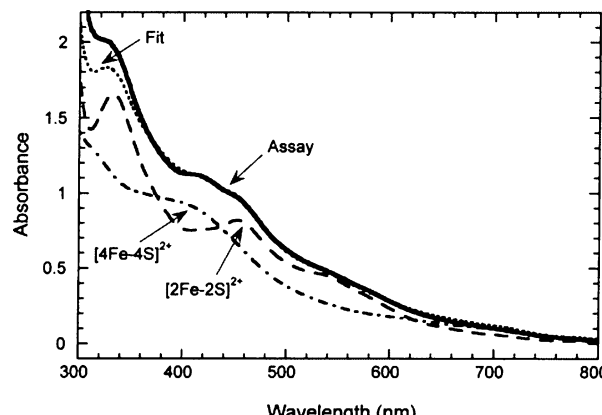


**Figure 24.** UV-visible spectrum of BioB under assay conditions reveals features characteristic of both  $[4\text{Fe}-4\text{S}]^{2+}$  and  $[2\text{Fe}-2\text{S}]^{2+}$  clusters. Reprinted with permission from ref 24a. Copyright 2001 American Chemical Society.

found, however, that the rate of decay of the  $[2\text{Fe}-2\text{S}]$  cluster was significantly faster than the initial rate of formation of biotin. They interpreted these results as indicating that if the  $[2\text{Fe}-2\text{S}]$  cluster is the sulfur donor in biotin biosynthesis, then S insertion must not be rate-limiting. Alternatively, they suggested that  $[2\text{Fe}-2\text{S}]$  cluster degradation could lead to formation of an intermediate protein-bound polysulfide or persulfide that served as the sulfur donor.<sup>179</sup>

**4.1.3. X-ray Crystal Structure of Biotin Synthase.** Biotin synthase, along with HemN, were the first radical SAM enzymes to be crystallographically characterized. The structure, solved to 3.4 Å resolution, revealed the presence of both a radical SAM  $[4\text{Fe}-4\text{S}]$  cluster coordinated by the  $\text{CX}_3\text{CX}_2\text{C}$  motif with SAM coordinated to the unique iron and a  $[2\text{Fe}-2\text{S}]$  cluster (Figure 25).<sup>40</sup> The  $[2\text{Fe}-2\text{S}]$  cluster was found to

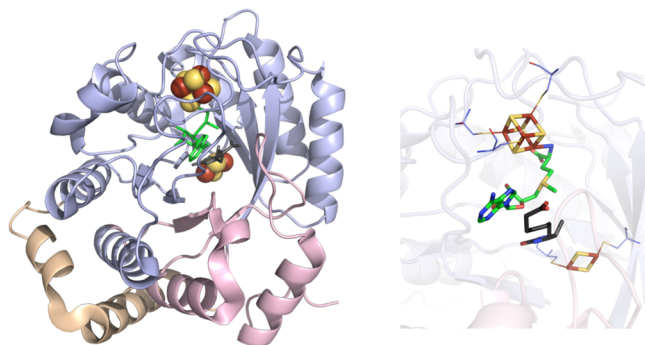


**Figure 25.** BioB crystal structure (PDB ID 1R30). Left: N-terminal domain colored in wheat, radical SAM domain in light blue, C-terminal domain in light pink, [4Fe–4S] and [2Fe–2S] clusters in yellow and rust spheres, SAM in green sticks, dethiobiotin in dark gray sticks. Right: Active site of BioB where [4Fe–4S] and [2Fe–2S] clusters (yellow and rust), SAM (green carbons), and dethiobiotin (gray carbons) are depicted in sticks with oxygens colored red and nitrogens colored blue. Cysteines (light blue carbons) involved in ligating clusters are depicted in lines.

be coordinated by four conserved residues (Cys97, Cys128, Cys188, and Arg260); the arginine ligand was unprecedented at the time in biology and was quite unexpected, although it was consistent with the early spectroscopic work indicating incomplete cysteinal ligation of the [2Fe–2S] cluster.<sup>120</sup> Interestingly, although it is completely conserved and a highly unusual ligand for an iron–sulfur cluster, the Arg260 is not essential for BioB activity in vitro or in vivo, as demonstrated by Broach and Jarrett.<sup>180</sup> Dethiobiotin was observed to be bound between SAM and the [2Fe–2S] cluster, with the C9 atom ~3.9 Å, and C6–4.1 Å, from the 5'-C of SAM, and thus in an appropriate position for H-atom abstraction upon reductive cleavage of SAM to generate the dAdo<sup>•</sup> intermediate.<sup>40</sup> The closest bridging sulfide of the [2Fe–2S] cluster was found to be only 4.6 Å from C9, supporting a mechanism whereby a carbon radical generated at C9 could react with this bridging sulfide to form one of the new C–S bonds in biotin. The two iron–sulfur clusters and the enzyme active site were all found within a TIM barrel fold, and the authors pointed out the intriguing similarity between the biotin synthase structure and those of AdoCbl radical enzymes (section 2.7).<sup>40</sup>

**4.1.4. Source of the Sulfur in Biotin Biosynthesis.** The origin of the sulfur inserted into dethiobiotin in the last step of biotin biosynthesis has been a longstanding question. Dennis Flint first brought up the “remote possibility” that the [2Fe–2S] cluster of biotin synthase was the source of this sulfur atom.<sup>12a</sup> In a subsequent paper utilizing cell-free extracts, Shaw and co-workers demonstrated label transfer into biotin from <sup>35</sup>S-cysteine, but not from <sup>35</sup>S-labeled methionine, indicating that cysteine and not methionine or SAM served as the sulfur

source in biotin biosynthesis.<sup>11</sup> Marquet and co-workers provided further insight into the source of sulfur by removing iron and sulfide from purified biotin synthase, and then reconstituting with Fe<sup>2+</sup> and <sup>34</sup>S<sup>2-</sup>.<sup>181</sup> The reconstituted enzyme was catalytically active, and the resulting biotin product was approximately 65% <sup>34</sup>S-labeled.

The coupled spectroscopic and biochemical studies of Jarrett and co-workers provided the first clear evidence that both [4Fe–4S] and [2Fe–2S] clusters were present in active forms of biotin synthase, and that while the [2Fe–2S] cluster was degraded during turnover, the [4Fe–4S] was stable (Figures 23 and 24) (section 4.1.2).<sup>24a,176,178</sup> This latter observation was subsequently confirmed by Johnson and co-workers<sup>179</sup> and by Marquet and co-workers.<sup>182</sup> The presence of two different clusters in the active enzyme, as well as the observation of [2Fe–2S] cluster degradation during turnover, led to the proposal that the [2Fe–2S] cluster was the source of sulfur in biotin biosynthesis. This proposal is consistent with the earlier evidence that cysteine is the source of sulfur, considering that the iron sulfur cluster assembly pathways utilize cysteine desulfurase enzymes to liberate sulfur from cysteine. The X-ray crystal structure of biotin synthase provided support for this hypothesis, showing dethiobiotin bound between the [4Fe–4S] and the [2Fe–2S] clusters and with C9 of dethiobiotin only 4.6 Å away from the closest bridging sulfide of the [2Fe–2S] cluster (Figure 25) (section 4.1.3).<sup>40</sup> With this structure, one could visualize the abstraction of an H-atom from C9 of dethiobiotin, followed by some modest structural changes that would allow the radical at C9 to capture a bridging sulfide of the [2Fe–2S] cluster. A mechanism for such a C–S bond-forming step is shown in Figure 26.

Another hypothesis advanced around the same time was that biotin synthase was a PLP-dependent enzyme that exhibited cysteine desulfurase activity, and that it was this activity that provided the sulfur from cysteine for biotin biosynthesis.<sup>183</sup> Subsequent studies from other laboratories, however, found no evidence for PLP-dependent cysteine desulfurase activity with biotin synthase.<sup>177</sup> Marquet and co-workers showed in 2006 that biotin synthase reconstituted with iron and selenide synthesized selenobiотin, lending further credence to the [2Fe–2S] cluster acting as the sulfur source.<sup>184</sup> It is generally now accepted that biotin synthase is not a PLP-dependent cysteine desulfurase, and it is conceivable that the erroneous reports of this activity may have resulted from contamination of the biotin synthase preparations with a cysteine desulfurase such as IscS, utilized in iron–sulfur cluster assembly.

**4.1.5. Biotin Synthase Mechanism.** A consensus mechanism for biotin synthase is provided in Figure 26 and is supported by numerous experimental findings. Using specifically deuterated dethiobiotin substrates, Marquet and co-workers were able to demonstrate deuterium transfer from both C6 and C9 of dethiobiotin into product dAdoD, providing

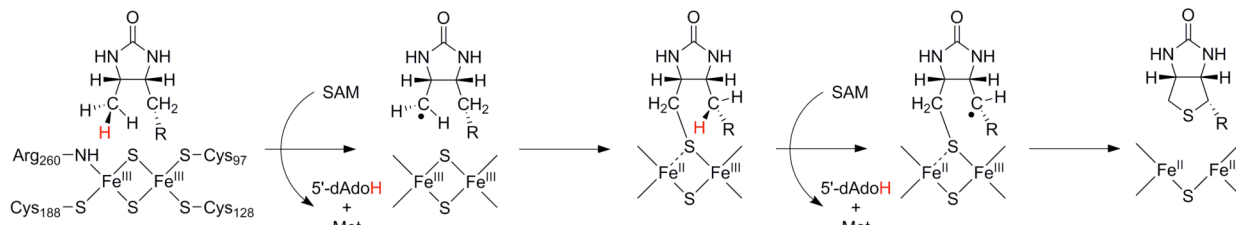


**Figure 26.** The mechanism of biotin formation from dethiobiotin as catalyzed by BioB.

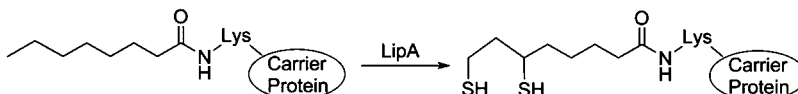


**Figure 27.** LipA reaction scheme catalyzing the conversion of octanoyl-acyl carrier protein to lipoyl-acyl carrier protein.

evidence that a SAM-derived deoxyadenosyl radical intermediate abstracts an H-atom from each of these positions during biotin biosynthesis;<sup>12c</sup> this result suggested the need for two moles of SAM for each mole of biotin synthesized, an implication that was subsequently confirmed experimentally.<sup>185</sup> Biotin synthase, like other radical SAM enzymes, is presumed to utilize a reduced  $[4\text{Fe}-4\text{S}]^{+}$  cluster to reductively cleave SAM, generating the 5'-deoxyadenosyl radical intermediate that abstracts an H-atom from dethiobiotin. The H-atom abstraction events from dethiobiotin, and the subsequent insertion of sulfur, have been shown to occur in a stepwise fashion.<sup>185</sup> Initial H-atom abstraction and sulfur insertion occurs at C9,<sup>12c</sup> producing a C9-dethiobiotinyl radical that reacts with a bridging sulfide of the  $[2\text{Fe}-2\text{S}]^{2+}$  cluster to produce a stable 9-mercaptodethiobiotin (MDTB) intermediate.<sup>185</sup> Such a reaction of a carbon radical with a bridging sulfide of a cluster to generate an intermediate in the thiol oxidation state necessitates concomitant reduction of the  $[2\text{Fe}-2\text{S}]^{2+}$  cluster to the 1+ state, as shown in Figure 26; thus it follows that, after this first sulfur insertion step, the  $[2\text{Fe}-2\text{S}]$  cluster should be EPR active. In support of this proposed  $[2\text{Fe}-2\text{S}]$  cluster reduction during the first half of the biotin synthase reaction, an EPR signal has been observed to form and decay during turnover in a manner that quantitatively correlates with the formation and decay of MDTB.<sup>179,186</sup> Remarkably, HYSCORE spectroscopic studies have demonstrated that the MDTB intermediate is a ligand to the  $[2\text{Fe}-2\text{S}]^{+}$  cluster of biotin synthase in this EPR-active intermediate state, providing strong support for the mechanism shown in Figure 26.<sup>187</sup> To complete the synthesis of biotin, the dAdoH and methionine products must be released and a second molecule of SAM bound, and the radical SAM  $[4\text{Fe}-4\text{S}]^{2+}$  cluster must be rereduced to the  $[4\text{Fe}-4\text{S}]^{+}$  state. A second reductive cleavage of SAM to generate a dAdo<sup>•</sup> occurs, and a H-atom is abstracted from C6 to generate a C6-MDTB radical that reacts with the same sulfide to close the thiphane ring and generate biotin.

The roles of individual amino acids in the active site of biotin synthase have been probed in a number of studies. Mutation of a set of conserved residues (YNHNLD) individually to alanine produced inactive variants in all cases except for the H152A, which showed low activity.<sup>188</sup> These residues are all in the vicinity of the active site; however, all variants appeared to assemble proper iron–sulfur clusters; it was proposed that this conserved sequence was important for interactions with SAM and dethiobiotin. The roles of these residues were further clarified when a more extensive series of variants in which Asn153 and Asp155 were changed to other residues, including some capable of retaining hydrogen-bonding interactions.<sup>46</sup> Most of the variants exhibited some catalytic activity, although altered products of SAM cleavage were observed, leading to the conclusion that these residues are important for retaining and controlling intermediates in the active site.<sup>46</sup>

#### 4.2. Lipoyl Synthase

**4.2.1. Octanoic Acid as a Precursor for Lipoic Acid.** An abstract published in 1964 reported that octanoic acid served as the precursor for lipoic acid.<sup>189</sup> Ronald Parry provided the first

published experimental verification of this transformation by showing that  $[1-^{14}\text{C}]\text{-octanoic acid}$  was specifically incorporated into lipoic acid *in vivo*.<sup>190</sup> Further, by use of specifically tritiated octanoic acids, Parry was able to show that the introduction of sulfur at C6 and C8 of octanoic acid occurred without loss of tritium from C5 or C7; these results were taken to indicate that the mechanism of sulfur insertion was unlikely to involve unsaturation at C5 or C7.<sup>190</sup> Parry also noted the similarity of these results to those he had previously reported for biotin biosynthesis,<sup>191</sup> and suggested that the biosyntheses of these two important cofactors might proceed via comparable mechanisms. Parry further elucidated the stereochemistry of sulfur insertion at C6 of octanoic acid.<sup>192</sup> White examined lipoic acid production in *E. coli* growing on [methyl- $^2\text{H}_3$ ]-acetate and demonstrated that the synthesis of lipoic acid from octanoic acid occurred with loss of only a single deuterium at C8.<sup>193</sup> They were able to infer from their results, together with the knowledge of the stereochemistry of fatty acid biosynthesis and the known conformation of lipoic acid at C6, that sulfur insertion at this position occurs with inversion of configuration. Further studies by White showed that hydroxylated octanoic acids were not likely intermediates in lipoic acid biosynthesis, thereby suggesting that sulfur is inserted directly at the saturated C6 and C8 carbons of octanoic acid.<sup>194</sup> Further, they showed that 8-thiooctanoic acid served as a precursor for lipoic acid, indicating that this species was likely an intermediate in lipoic acid biosynthesis.

**4.2.2. Similarity to Biotin Synthase.** The *lip* locus of *E. coli* was cloned and characterized by Cronan and co-workers in 1991 and by Ashley and co-workers in 1992.<sup>195</sup> The latter group reported that the *lip* locus encoded a protein of approximately 36 kDa that had sequence similarity to BioB.<sup>195b</sup> The *lipA* gene was subsequently implicated in the sulfur insertion step(s) of lipoate biosynthesis,<sup>196</sup> and most specifically in the insertion of the first sulfur into octanoic acid (Figure 27).<sup>196b</sup> The product of the *lipB* gene was subsequently shown to be responsible for ligation of lipoyl groups to proteins, and to be redundant with the product of the *lipA* gene.<sup>197</sup>

**4.2.3. In Vitro Activity Requires an Iron–Sulfur Cluster, SAM, and Preattachment of the Octanoyl Substrate.** Sequencing of the *lipA* gene showed that it would encode a protein with a CX<sub>3</sub>CX<sub>2</sub>C motif, the same motif that at the time was known to be present in biotin synthase, PFL-AE, and ARR-AE.<sup>196b</sup> Like these proteins, LipA was shown to be an Fe–S protein.<sup>123,124</sup> Initial work by Fontecave and co-workers identified a  $[2\text{Fe}-2\text{S}]$  cluster in the protein after purification, refolding, and reconstitution with iron and sulfide. As had been observed with biotin synthase, the  $[2\text{Fe}-2\text{S}]$  clusters converted to  $[4\text{Fe}-4\text{S}]$  clusters upon reduction (Table 2) (sections 4.1.1, 4.1.2),<sup>123</sup> and air exposure of the  $[4\text{Fe}-4\text{S}]$  state converted these to  $[2\text{Fe}-2\text{S}]$  clusters.<sup>121b</sup> A major breakthrough in lipoate synthase research came the following year, when Marletta and co-workers isolated and characterized *E. coli* LipA that had been expressed in a soluble form.<sup>124b</sup> Their purified LipA contained approximately four irons and four sulfides per protein, and exhibited electronic absorption and

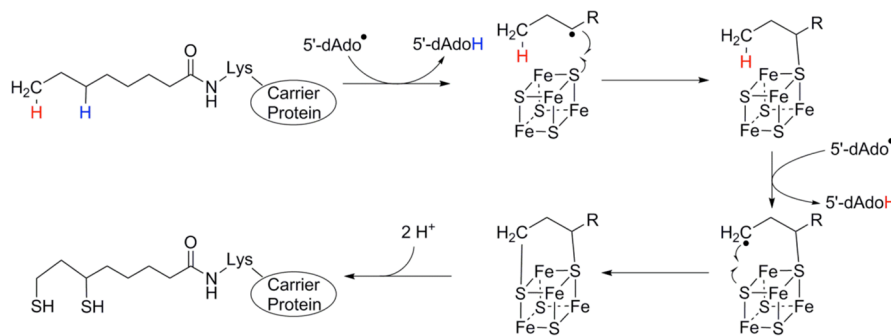


**Figure 28.** The mechanism of lipoyl-acyl carrier protein from octanoyl-acyl carrier protein as catalyzed by LipA.

EPR spectral properties consistent with the presence of  $[3\text{Fe}-4\text{S}]^+$  and  $[4\text{Fe}-4\text{S}]$  clusters in the as-isolated state, and a mixture of  $[4\text{Fe}-4\text{S}]^+$  and  $[4\text{Fe}-4\text{S}]^{2+}$  in the reduced state (Table 2). More importantly, Marletta and co-workers were able to demonstrate for the first time the *in vitro* enzymatic activity of LipA.<sup>124b</sup> The assays were carried out under anaerobic reducing conditions in the presence of SAM, octanoyl-ACP, LipB (lipoyl-ACP-protein-N-lipoyltransferase), and apo-PDC (pyruvate dehydrogenase complex); the requirement for SAM together with the presence of iron–sulfur clusters in LipA placed this enzyme in the growing radical SAM enzyme class. Further, their LipA assays clearly demonstrated that, contrary to previous thinking, octanoic acid was not a substrate for LipA. Rather, LipA utilized octanoyl-acyl carrier protein (octanoyl-ACP) as a substrate for sulfur insertion to form the lipoyl-ACP, which then lipoylated the pyruvate dehydrogenase complex.<sup>124b</sup> Thus, LipA was found to not be a lipoate synthase, but rather a lipoyl synthase, requiring preattachment of the octanoyl group to a carrier protein before sulfur insertion could be catalyzed (Figure 27). Cronan and co-workers subsequently demonstrated that lipoyl synthase would also use the octanoylated E<sub>2</sub> subunit of PDC as a substrate,<sup>198</sup> while Booker and co-workers showed that the octanoylated H-protein of the glycine cleavage system could also serve as a LipA substrate.<sup>69</sup>

#### 4.2.4. A Mechanism for LipA Involving Two $[4\text{Fe}-4\text{S}]$ Clusters

**Clusters.** It is now established that the *E. coli* lipoyl synthase binds two distinct  $[4\text{Fe}-4\text{S}]$  clusters<sup>125</sup> and requires 2 equiv of SAM to synthesize 1 equiv of lipoyl cofactor.<sup>69</sup> The higher iron content of this protein as compared to earlier reports was due in part to the coexpression of the *isc* biosynthetic operon responsible for the synthesis of iron–sulfur clusters, as described by Roach and co-workers<sup>124c</sup> and Booker and co-workers.<sup>125</sup> Using site-directed mutagenesis combined with iron and sulfur analysis and spectroscopy, this latter group demonstrated that one of the  $[4\text{Fe}-4\text{S}]$  clusters bound the CX<sub>3</sub>CX<sub>2</sub>C radical SAM motif, while the second bound a CX<sub>4</sub>CX<sub>5</sub>C motif conserved only among lipoyl synthases; these clusters were spectroscopically distinguishable by EPR of the reduced state of the protein.<sup>125</sup> Removing either cluster by site-directed mutagenesis eliminated production of both dAdoH and lipoyl cofactor. Booker and co-workers also provided evidence for direct H-atom abstraction from the octanoyl group by the dAdo<sup>•</sup>, by showing that deuterium is transferred from [octanoyl-d<sub>15</sub>]H-protein to the dAdo<sup>•</sup> to generate the monodeuterated dAdoD product.<sup>69</sup> Further, they demonstrated that two dAdoH are produced per lipoyl cofactor synthesized. Roach and co-workers subsequently demonstrated that the sulfur insertions catalyzed by LipA occur in a stepwise manner,

with thiolation at the C6 position occurring first.<sup>199</sup> This observation, together with the previously reported isotope effect for sulfur insertion at C8,<sup>190</sup> leads to a mechanism such as that shown in Figure 28, with the second sulfur insertion step being rate determining.

## 5. RADICAL SAM MUTASES

The radical SAM mutases catalyze rearrangement reactions classically viewed as B<sub>12</sub>-type rearrangement reactions (section 2.7). Indeed, it was the recognition that lysine 2,3-aminomutase catalyzed a reaction directly analogous to a B<sub>12</sub>-dependent reaction, and yet utilized SAM, that initially suggested a similarity between B<sub>12</sub> and SAM radical reactions.<sup>10</sup> Lysine 2,3-aminomutase remains one of the best understood radical SAM enzymes, with extensive spectroscopic, biochemical, and structural information in the literature. It is also the best understood radical SAM enzyme that uses SAM catalytically, and thus most closely mimics the role for B<sub>12</sub> in the adenosylcobalamin-dependent radical reactions (section 2.7).

### 5.1. Lysine 2,3-Aminomutase

Lysine 2,3-aminomutase (LAM) catalyzes the interconversion of L- $\alpha$ -lysine to L- $\beta$ -lysine (Figure 29), a reaction directly analogous to B<sub>12</sub>-dependent aminomutases.

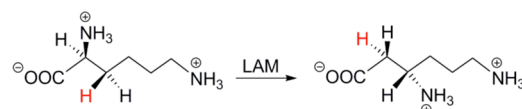


**Figure 29.** LAM reaction scheme catalyzing the conversion of L- $\alpha$ -lysine to L- $\beta$ -lysine.

#### 5.1.1. Early Characterization of a B<sub>12</sub>-Independent Aminomutase.

Barker and co-workers published the first purification and characterization of lysine 2,3-aminomutase (LAM) in 1970.<sup>8</sup> In this seminal paper, they demonstrated that LAM was a pyridoxal phosphate (PLP) enzyme activated by SAM and ferrous ion. They noted that the enzyme was quite air-sensitive, but could be activated by anaerobic incubation in the presence of sulfhydryls. Quite surprisingly, given the dependence of all other aminomutases known at the time on coenzyme B<sub>12</sub>, LAM activity was not dependent on B<sub>12</sub>.<sup>8</sup> Further, the observation that neither hydrogen nor nitrogen from lysine exchange with the medium during the reaction indicated that the reaction occurred via intramolecular transfer. Aberhart et al. showed that this migration, like those of B<sub>12</sub>-dependent aminomutases, occurred with inversion of configuration at both carbons involved.<sup>200</sup> Specifically, they demonstrated that the 3-pro-R hydrogen of  $\alpha$ -lysine was

transferred to the 2-pro-R position of  $\beta$ -lysine, while the 3-pro-S hydrogen of  $\alpha$ -lysine was retained at C3 and the C2 hydrogen of  $\alpha$ -lysine was retained at the 2-pro-S position in  $\beta$ -lysine.<sup>201</sup> They also demonstrated that amino group transfer took place intramolecularly, but that hydrogen transfer appeared to be primarily intermolecular.<sup>201</sup>

**5.1.2. SAM as a dAdo $^{\bullet}$  Precursor in LAM.** Moss and Frey provided the first evidence that the 5'-deoxyadenosyl moiety of SAM was involved in the hydrogen transfer.<sup>10</sup> They utilized S-[2,8,5'- $^3$ H]-adenosylmethionine, and found that tritium was incorporated into both L- $\alpha$ -lysine and L- $\beta$ -lysine. By quantifying the tritium content in both isomers, they were able to determine an equilibrium constant ( $5.3 \pm 0.3$  in the forward direction at pH 7.7 and 30 °C). Because they saw no tritium incorporation into lysine when using S-[2,8- $^3$ H]-adenosylmethionine or S-[methyl- $^3$ H]-adenosylmethionine, they concluded that the tritium incorporation occurs from the 5'-position of SAM. They proposed that the dAdoH moiety of SAM played a role analogous to that of the dAdoH moiety of adenosylcobalamin in B<sub>12</sub>-dependent rearrangements. Although there were contradictory reports subsequently published,<sup>202</sup> these initial results from the Frey lab have been substantiated by numerous additional studies.

Further support for this role for SAM in the LAM-catalyzed reaction was provided by utilizing S-[5'- $^3$ H]-adenosylmethionine in the presence of excess LAM, which resulted in all of the tritium ending up in lysine or  $\beta$ -lysine.<sup>203</sup> The tritium transfer from the 5'-position of SAM into the reactant/product of LAM, together with further label transfer experiments utilizing [3,3- $^2$ H<sub>2</sub>]-lysine<sup>203</sup> or [3- $^3$ H]-lysine,<sup>204</sup> provided evidence that SAM served as a precursor of a dAdo $^{\bullet}$  during LAM catalysis, and that this radical intermediate mediated hydrogen transfer from C3 to C2 of lysine. Using SAM labeled with  $^{14}$ C at either the carboxyl carbon of the methionine moiety or the 8-position of the adenine ring, Moss and Frey demonstrated the conversion of SAM to methionine and dAdoH during LAM catalysis.<sup>205</sup> They postulated at the time that the dAdoH moiety of SAM was transferred to another species associated with the enzyme, perhaps another cofactor, to generate the adenosyl species responsible for H-atom abstraction.

**5.1.3. The Role of PLP in LAM.** Han and Frey provided the first chemical model for the role of PLP in 1,2-amino migrations such as that catalyzed by LAM.<sup>206</sup> They provided the first demonstration of a 1,2-imino rearrangement via a radical mechanism, and their results provided support for the hypothesis that PLP could facilitate such migrations via formation of an amino acid-PLP aldimine radical. The PLP binds to a lysine of LAM (Lys346 in the enzyme from *B. subtilis*) present in a PGGGGK motif that is conserved among LAMs from *Bacillus* and *Clostridium* species, and serves as a site of covalent attachment of the lysine substrate.<sup>207</sup>

**5.1.4. The Iron–Sulfur Cluster in LAM and Its Interaction with SAM.** It was reported in 1991 that purified LAM contained iron and sulfide in a 1:1 ratio, providing the first indication that this enzyme contained an iron–sulfur cluster.<sup>9</sup> The purified enzyme was also found to contain cobalt, zinc, and copper, with the cobalt appearing to be important for activity; the apparent involvement of cobalt was intriguing given the mechanistic similarity to B<sub>12</sub> enzymes, but subsequent studies showed that cobalt was not in fact required for activity.<sup>22</sup> EPR spectroscopy indicated that the iron–sulfur clusters in the anaerobically purified enzyme were [4Fe–4S] $^{+}$  clusters (Table 2), which upon oxidation converted to [3Fe–

4S] $^{+}$  clusters.<sup>90</sup> Reduction to the [4Fe–4S] $^{+}$  state was found to be dependent on the presence of SAM or SAH and a strong reducing agent. The [4Fe–4S] $^{+}$ /SAM state was found to exhibit full activity in the absence of any additional reducing agent.<sup>22</sup> The SAM analogue azaSAM also binds to LAM and allows reduction to the [4Fe–4S] $^{+}$  state, exhibiting EPR spectral features similar to those observed with SAH; interestingly, the protonation state of the azaSAM did not affect the ability to reduce the [4Fe–4S] $^{2+}$  cluster.<sup>208</sup> Selenium K-edge X-ray absorption spectroscopy of LAM in various states of turnover with S-adenosyl-L-selenomethionine (SeSAM) revealed that SeSAM is cleaved by LAM to generate SeMet, and that this SeMet is positioned near one of the irons of the [4Fe–4S] cluster at a distance of approximately 2.7 Å;<sup>209</sup> these results implicated a unique iron site in the [4Fe–4S] cluster, as well as the direct involvement of the cluster in catalysis.

Significant insight into the SAM–[4Fe–4S] cluster interaction was provided by electron–nuclear double resonance (ENDOR) spectroscopic studies of LAM in complex with isotopically labeled SAM (Figure 11).<sup>16b</sup> These experiments were similar to those carried out with PFL-AE as described earlier in this Review, and examined ENDOR spectra of LAM in the [4Fe–4S] $^{+}$  state in complex with labeled SAM (individually labeled either at the carboxylate with  $^{17}$ O, at the amino nitrogen with  $^{15}$ N, or at the methyl with either  $^{13}$ C or  $^{2}$ H). The LAM was reduced with dithionite under ambient conditions to probe the geometry of the [4Fe–4S] $^{+}$  state, or frozen in the [4Fe–4S] $^{2+}$  state in the presence of SAM and then cryoreduced, to probe the geometry of the 2+ state. The results reveal the direct coordination of the [4Fe–4S] $^{2+/+}$  clusters by SAM via the amino and carboxylate groups, and the close proximity of the methyl of SAM to the [4Fe–4S] cluster. The results also suggested some differences in binding geometry of SAM in LAM versus PFL-AE that could be important mechanistically.

**5.1.5. The Structure of LAM.** Lysine 2,3-aminomutase was originally characterized as a hexamer with one active site per subunit.<sup>210</sup> The heterologous expression of LAM from *Clostridium subterminale* SB4 in *E. coli*<sup>211</sup> ultimately led to an X-ray crystal structure of LAM (2.1 Å resolution, Figure 30)<sup>39</sup> in which the protein crystallized as a tetramer composed of two domain-swapped dimers linked by zinc coordination. Each subunit consisted of an  $(\beta\alpha)_6$  partial TIM barrel, with the [4Fe–4S] cluster, SAM, and PLP occupying the barrel. SAM was found coordinated to the unique iron of the [4Fe–4S] cluster via the amino and carboxylate moieties, as had previously been elucidated by using ENDOR spectroscopy.<sup>16b</sup> Further, the selenium of SeSAM appeared poised to coordinate the unique iron as well upon S–C(5') bond cleavage, corroborating previous selenium XAS experiments showing a close Fe–Se distance upon reductive cleavage of SAM.<sup>209</sup> PLP and L- $\alpha$ -lysine were held in position by a series of H-bond and ionic contacts; the position of lysine was such that it was poised for abstraction of the 3-pro-R hydrogen of lysine by the dAdo $^{\bullet}$  intermediate.

**5.1.6. The Mechanism of LAM.** A consensus mechanism for LAM is provided in Figure 31. Lysine binds in the active site as an aldimine adduct of PLP. SAM was shown using ENDOR to bind to both the [4Fe–4S] $^{2+}$  and the [4Fe–4S] $^{+}$  oxidation states via coordination of the amino and carboxylate groups of SAM to the unique iron of the cluster. One-electron reduction of the 2+ cluster puts it in the catalytically active state, whereby it can transfer an electron to SAM to initiate the reductive

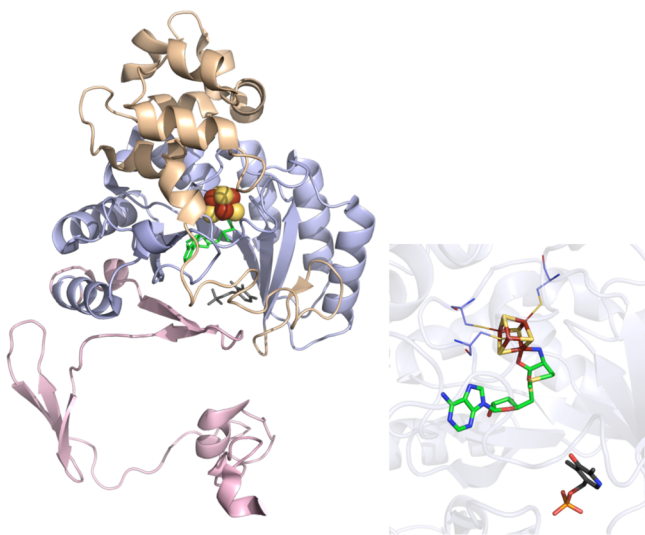


**Figure 30.** LAM crystal structure (PDB ID 2ASH). Left: N-terminal domain colored in wheat, radical SAM domain in light blue, C-terminal domain in light pink, [4Fe-4S] cluster in yellow and rust spheres, SAM in green sticks, PLP in dark gray sticks. Right: Active site of LAM where [4Fe-4S] cluster (yellow and rust), SAM (green carbons), and PLP (gray carbons) are depicted in sticks with oxygens colored red, nitrogens colored blue, and phosphorus in orange. The cysteine residues (light blue carbons) involved in ligating cluster are depicted in lines.

cleavage to methionine and dAdo<sup>•</sup>. The dAdo<sup>•</sup> then abstracts the 3-pro-R H-atom of bound lysine substrate to yield a substrate radical intermediate with the unpaired electron at C3, the  $\beta$ -carbon. Use of the alternative substrate 4-thia-L-lysine allowed observation of the C3-radical of 4-thialysine, an analogue of the substrate C3 radical shown in the mechanism (species 2 in Figure 11).<sup>72,212</sup> Further support for the involvement of a C3 radical in the mechanism was provided by another alternative substrate, *trans*-4,5-dehydrolysine, which resulted in formation of the observable allylic 4,5-dehydrolysyl

radical by abstraction of an H-atom from C3.<sup>213</sup> Cyclization of the substrate radical shown in Figure 31 to the azacyclopropylcarbinyl radical followed by ring-opening generates the product radical intermediate. This product radical intermediate was detected in LAM during turnover<sup>214</sup> and was shown, using isotopically labeled lysine substrate, to be a lysine-based  $\pi$ -radical centered at C2 of  $\beta$ -lysine, with coupling to the  $\alpha$ -C proton, the nitrogen on the  $\beta$ -C, and the  $\beta$ -C proton giving rise to hyperfine structure.<sup>215</sup> The hyperfine couplings allowed these authors to determine dihedral angles and ultimately the structure of the radical intermediate. Electron spin–echo envelope modulation (ESEEM) experiments were used to examine the coupling of this radical intermediate to a deuteron introduced at the 4'-position of PLP; the results supported the presence of an aldimine linkage between PLP and the  $\beta$ -nitrogen of  $\beta$ -lysine (species 3 in Figure 11).<sup>216</sup> This radical intermediate was also shown to be kinetically competent.<sup>217</sup>

Studies on the mechanism of LAM have provided the most direct evidence to date for the involvement of a 5'-deoxyadenosyl radical intermediate in the radical SAM enzymes. Magnusson et al. synthesized the SAM analogue S-3',4'-anhydroadenosyl-L-methionine (anSAM) and demonstrated that upon reaction with LAM under assay conditions, a new steady-state radical species was observed.<sup>20a</sup> By using deuterated lysine and/or anSAM deuterated at the 5' position or at all five carbons of the ribose moiety, they were able to demonstrate that this was an allylically stabilized radical with the spin distributed equally between the C5' and C3' carbons of the ribosyl moiety.<sup>20</sup> They further showed that this radical was kinetically competent, supporting the involvement of the dAdo<sup>•</sup> in the mechanism of LAM, and, by extension, in the radical SAM enzymes in general.<sup>20b</sup>

**5.1.7. LAM and LAM-like Enzymes from Other Organisms.** The studies described in the preceding sections were carried out primarily on the LAM from *C. subterminale* SB4. The enzyme has also been isolated from *B. subtilis*, and a number of the structural and mechanistic features seen in the *Clostridial* enzyme are also observed in the enzyme from *B. subtilis*, including the presence of a [4Fe-4S] cluster, the

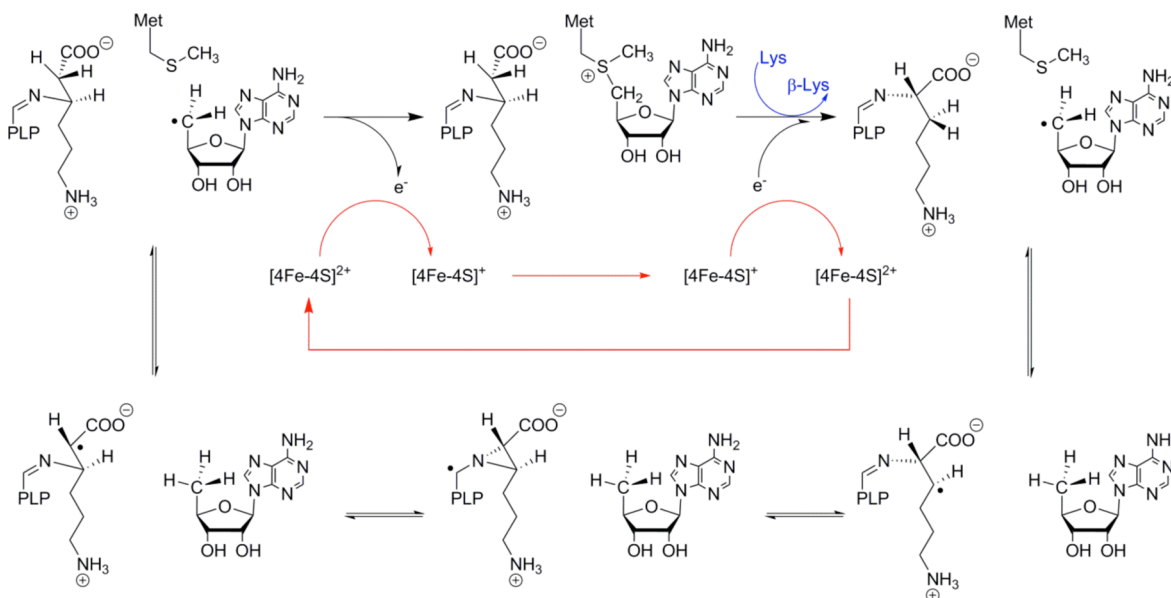


**Figure 31.** The conversion of L- $\alpha$ -lysine to L- $\beta$ -lysine as catalyzed by lysine 2,3-aminomutase.

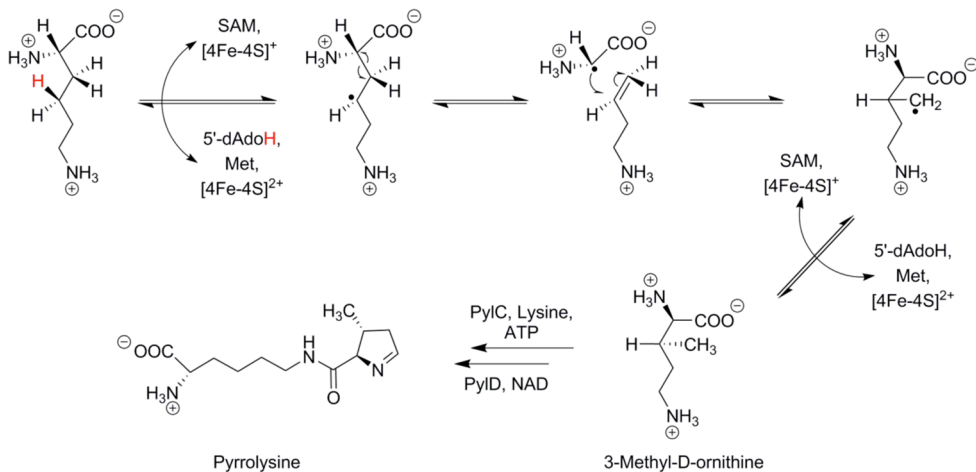


**Figure 32.** The synthesis of 3-methyl-D-ornithine from L- $\alpha$ -lysine as catalyzed by PylB in the first step of pyrrolysine biosynthesis.

requirement of a strong reducing agent and SAM for enzyme activity, and the ability to observe substrate radicals during steady-state turnover.<sup>218</sup> Interestingly, the LAM from *B. subtilis* is stable in air, unlike the enzyme from *C. subterminale* SB4 (and unlike most other radical SAM enzymes) that require handling under strictly anaerobic conditions. The *E. coli* gene P39280 shares 30% sequence identity with those for LAM from *C. subterminale* SB4 and from *B. subtilis*; however, the conserved lysine that serves as the site of attachment for PLP is not present. This gene is located adjacent to *efp*, encoding for elongation factor P, and downstream from *groES* and *groEL*; its function at present is not known.<sup>218</sup> It should be noted that although several homologues of LAM have been identified,<sup>219</sup> their putative function may be to catalyze a mutase reaction other than that of lysine. For example, the identified glutamate-2,3-aminomutase from *Clostridium difficile* is similar to LAM, but lacks Lys-binding residues Asp 293 and Asp 330.<sup>73</sup>

## 5.2. Pyrrolysine Biosynthesis: Carbon Backbone Rearrangement Catalyzed by the Lysine Mutase PylB

Pyrrolysine is the 22nd amino acid encoded by the genetic code and in Archaea is known to only occur in the *Methanoscincus* family.<sup>220</sup> Members of this family can utilize trimethylamine, dimethylamine, or monomethylamine as precursors to methane by the actions of MttB, MtbB, or MtmB.<sup>221</sup> These methyltransferase proteins methylate the Co(I) states of the corrinoid cofactors bound to either MttC, MtbC, or MtmC, forming Co(III)-CH<sub>3</sub> moieties. The Co(III)-CH<sub>3</sub> bound proteins then act as substrates for MtBA where the thiol group of coenzyme M is subsequently methylated, which then serves to directly generate methane, or to enter subsequent pathways resulting in release of either CO<sub>2</sub> or cellular carbon.<sup>222</sup> Mass spectral analysis and X-ray crystallography were used to confirm that the in frame UAG amber codon present in *mttb*, *mtbb*, and *mtmb* sequences was encoded as pyrrolysine.<sup>220b,223</sup> In the crystal structure of methylornithine synthase, pyrrolysine was found to bind ammonia at the carbon of the imine bond, leading to the hypothesis that the role of this amino acid was to bind and activate methylammonium species toward nucleophilic attack by the Co(I) corrinoid groups of MttC, MtbC, or MtmC.<sup>220b,222c</sup>

Pyrrolysine is synthesized from two molecules of lysine via reactions catalyzed by the *pylBCD* gene products (Figure 32).<sup>222c</sup> PylB contains the CX<sub>3</sub>CX<sub>2</sub>C motif, identifying it as a member of the radical SAM superfamily of enzymes, while PylC

shows sequence similarity with amino acid ligases and carbamoyl phosphate synthetase, and PylD is proposed to be a dehydrogenase given its similarity to leucine and 3-hydroxybutyrate dehydrogenases.<sup>222c</sup> Insight into pyrrolysine biosynthesis was provided by two independent studies that showed *E. coli* could not synthesize pyrrolysine in the absence of *pylB*, but could make desmethylpyrrolysine (a pyrrolysine analog that lacks the ring methyl group) when supplemented with exogenous D-ornithine.<sup>222c,224</sup> Desmethylpyrrolysine biosynthesis required only *pylC* and *pylD*, and indirectly suggested that PylB's activity was directed toward the synthesis of (2R,3R)-3-methyl-D-ornithine from lysine as a first step in pyrrolysine synthesis. Cells transformed with *pylC* produced D-ornithyl-N<sup>ε</sup>-L-lysine when doped with D-ornithine, indicating that PylC forms an amide bond between D-ornithine (or (2R,3R)-3-methyl-D-ornithine) and the ε-amine of a second lysine molecule to yield a dipeptide product in a reaction that hydrolyzes ATP.<sup>222c,224,225</sup> The final biosynthetic step is catalyzed by PylD, which oxidizes the terminal amine of D-ornithyl-N<sup>ε</sup>-L-lysine (or (2R,3R)-3-methyl-D-ornithyl-N<sup>ε</sup>-L-lysine) in a reaction that produces ammonia and a semi-aldehyde derivative; a spontaneous condensation-heterocyclization step then yields either desmethylpyrrolysine or pyrrolysine.<sup>222c,224,225</sup>

The reaction catalyzed by PylB places this enzyme in the mutase subclass of radical SAM enzymes, and is the first example of a radical SAM enzyme catalyzing a mutase reaction involving carbon backbone rearrangement reactions similar to those carried out by coenzyme B<sub>12</sub> enzymes.<sup>48,227</sup> The X-ray crystal structure of PylB from *Methanoscincus barkeri* at 1.5 Å resolution shows the monomeric protein is comprised of single domain that houses the site-differentiated [4Fe-4S] cluster and SAM (Figure 33).<sup>43</sup> Sequence analysis reveals that PylB is most similar to HydE and BioB (sections 12.2.5 and 4.1), and superimposition shows that PylB overlays with the available structures (PylB PDB ID 3T7V, HydE PDB ID 3CIW, BioB PDB ID 1R30) with minimal differences in root-mean-square deviation values ( $\leq 1.8$  Å). Remarkably, the PylB structure revealed the presence of both SAM and methylornithine despite the fact that neither SAM nor lysine were exogenously added to the protein, suggesting that the (2R,3R)-3-methyl-D-ornithine product was synthesized *in vivo* and along with SAM remained tightly bound within the active site during the purification process; a complex network of hydrogen bonds and

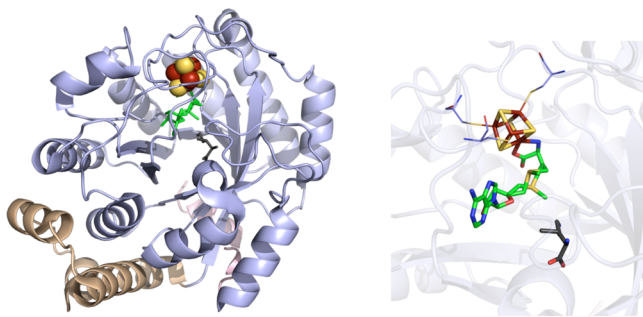


**Figure 33.** PylB crystal structure (PDB ID 3T7V). Left: N-terminal domain colored in wheat, radical SAM domain in light blue, C-terminal domain in light pink, [4Fe–4S] cluster in yellow and rust spheres, SAM in green sticks, methylornithine in dark gray sticks. Right: Active site of PylB where [4Fe–4S] cluster (yellow and rust), SAM (green carbons), and methylornithine (gray carbons) are depicted in sticks with oxygens colored red and nitrogens colored blue. Cysteines (light blue carbons) involved in ligating cluster are depicted in lines.

hydrophobic interactions within the active site appears to bind and stabilize both SAM and methylornithine, respectively.<sup>43</sup> The existence of methylornithine bound in close proximity to the SAM bound [4Fe–4S] cluster allowed for the modeling of lysine in the active site and a proposition for its conversion to product to be put forth. The proposed reaction mechanism invokes H-atom abstraction from the C4 position of lysine by the 5'-deoxyadenosyl radical that is generated upon SAM cleavage. Resulting  $\text{C}\alpha\text{-C}\beta$  bond homolysis of the lysine radical species would generate a glycyl radical and 4-aminobutene; recombination of the glycyl radical with the 2 position of 4-aminobutene (formerly the 4 position of lysine) would yield a (3R)-3-methyl-d-ornithine radical intermediate that could then abstract an H-atom from an unknown source to form (3R)-3-methyl-d-ornithine.<sup>43,228</sup> Theoretical QM/MM analysis has suggested that either the  $\text{C}\alpha\text{-C}\beta$  homolytic cleavage event or the recombination of the glycyl radical with aminobutene could be rate limiting due to the considerable energy barriers associated with these steps.<sup>229</sup> While it is unknown what molecule may serve as the source of the H-atom that is abstracted by the proposed (3R)-3-methyl-d-ornithine radical intermediate, it is certainly plausible that it could be dAdoH, and the apparent tight binding of SAM within the active site cavity certainly may suggest that PylB uses SAM as a cofactor and not a cosubstrate (sections 2.3, 2.5). While direct experimental evidence for the copurification and/or tight binding of SAM is lacking, making it difficult to assign the role of SAM as cofactor, it has been postulated that the apparent high affinity of methylornithine to the active site may act to govern pyrrolysine biosynthesis through the controlled release of product, an event possibly triggered by PylC binding to PylB.<sup>228</sup> Future work should help resolve these issues, as well as the details of the fragmentation–recombination reaction, especially the mechanism whereby the presumed glycyl radical is directed toward the 2 position of 4-aminobutene; computational work has indicated that this may be directed by the aminobutene fragment undergoing an intramolecular rotation that alters the dihedral angle of the carbon backbone.<sup>229</sup>

## 6. ENZYMES CATALYZING COMPLEX REARRANGEMENTS AND CYCLIZATIONS

### 6.1. MoaA

All molybdenum-containing metalloenzymes except for the Mo-nitrogenase utilize the molybdopterin cofactor (Moco) at their active sites to catalyze a diverse series of redox reactions in the global carbon, sulfur, and nitrogen cycles. The coordination complex of Moco is composed of a molybdenum ion coordinated to a low molecular weight tricyclic pterin scaffold ligand via dithiolene coordination (Figure 34).<sup>230</sup>

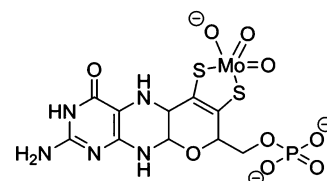


**Figure 34.** The molybdopterin cofactor (Moco) is composed of a molybdenum ion coordinated by a low molecular weight tricyclic pterin ligand via dithiolene coordination.

**6.1.1. Molybdopterin Cofactor Biosynthesis.** The Moco cofactor biosynthetic pathway is a five-step process involving radical SAM-based biochemistry as an essential step. A model of Moco biosynthesis in *E. coli* was proposed in 1992<sup>230b</sup> to involve eight Moco-specific genes (*moaABCDE*, *mobAB*, *moeB*), based on early investigations of phenotype suppression and of *chl* mutants defective in molybdate uptake and processing.<sup>230b,231</sup> In this model, MoaA–MoaC was responsible for molybdopterin precursor Z biosynthesis, while the MoaD and MoaE were responsible for converting the precursor into molybdopterin. Precursor Z (now termed 1,1'-dihydroxy-2',4'-cyclic pyranopterin monophosphate (cPMP))<sup>232</sup> was found to originate from a guanosine derivative,<sup>233</sup> where GTP was identified as a likely source, given its identity as a common starting material in the biosynthesis of pterins and pteridines as part of GTP cyclohydrolase I-type chemistry (Figure 35).<sup>233a</sup>

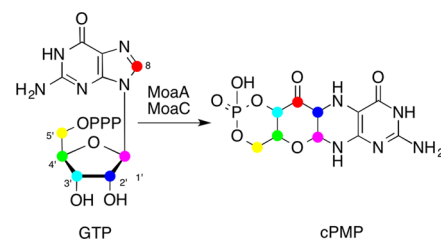


**Figure 35.** The observed rearrangement of carbon atoms in the MoaA/MoaC reaction.

Interestingly, early comparison of the amino acid-encoded gene sequence of *moaA*<sup>234</sup> from *E. coli* was found to be similar to the NifB protein from *K. pneumoniae*,<sup>235</sup> the FixZ protein from *Rhizobium leguminosarum* (homologue to NifB),<sup>236</sup> as well as to PQQ synthesis protein III from *A. calcoaceticus*.<sup>237</sup> In retrospect, all of these proteins contain the radical SAM CX<sub>3</sub>CX<sub>2</sub>C motif, linking MoaA to radical-initiated catalysis.

**6.1.2. Identification of Two [4Fe–4S] Clusters in MoaA.** Early spectroscopic and biochemical characterization of the Fe–S clusters of MoaA has served as a foundational example in understanding the role of multiple Fe–S clusters in radical SAM enzymology. The discovery that MoaA binds Fe–

S clusters at two tricysteine motifs ( $\text{CX}_3\text{CX}_2\text{C}$  and  $\text{CX}_2\text{CX}_{13}\text{C}$ )<sup>238</sup> led Hänelmann and co-workers to perform the first thorough functional characterization of the MoaA and MoaC proteins.<sup>239</sup> Human MOCS1A and MOCS1B, which derive from bicistronic cDNA, serve as homologues to bacterial genes *moaA* and *moaC* (*cnx2* and *cnx3* in plants), respectively.<sup>239</sup> Complementary UV-vis, MCD, and Mössbauer spectroscopy showed that human MoaA (MOCS1A) contained oxygen-sensitive Fe–S clusters at the N-terminal and C-terminal regions that were predominantly [4Fe–4S] cluster in character (Table 2).<sup>128</sup> Comparison of Mössbauer spectra between wild-type and the C80/84/87S triple mutant provided different signal contributions that could be assigned as a discrete, site-differentiated Fe–S cluster at the C-terminus.<sup>128</sup>

**6.1.3. The X-ray Crystal Structure of MoaA.** The MoaA enzyme was the first radical SAM enzyme with two discrete [4Fe–4S] clusters to be characterized crystallographically (Figure 36).<sup>240</sup> Its structure has provided a substantive model

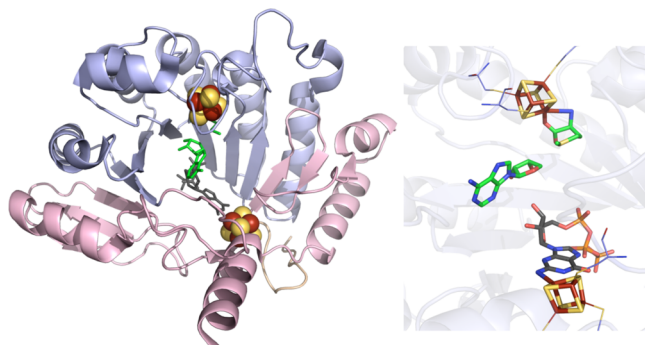


**Figure 36.** MoaA crystal structure (PDB ID 2FB3). Left: N-terminal domain colored in wheat, radical SAM domain in light blue, C-terminal domain in light pink, [4Fe–4S] clusters in yellow and rust spheres, dAdoH and Met in green sticks, GTP in dark gray sticks. Right: Active site of MoaA where [4Fe–4S] cluster (yellow and rust), dAdoH and Met (green carbons), and GTP (gray carbons) are depicted in sticks with oxygens colored red, nitrogens colored blue, and phosphates in orange. Cysteines (light blue carbons) involved in ligating clusters are depicted in lines.

for structural comparisons for radical SAM enzymes involving multiple [4Fe–4S] clusters. MoaA has a partial  $(\beta\alpha)_6$  TIM barrel, with the N- and C-terminal [4Fe–4S] clusters found on opposite ends of the hydrophilic channel of the TIM barrel at a distance of approximately 17 Å.<sup>240,241</sup> The N-terminal cluster is coordinated as part of a 31-residue loop extending from  $\beta$ -strand 1 to  $\alpha$ -helix 1 of the TIM barrel, and is similar to HemN and BioB (sections 11.1.2 and 4.1.3).<sup>240</sup> The C-terminal cluster is coordinated between two loops that lead to the C-terminus of the enzyme. Because precursor Z synthesis requires the activity of the MoaC enzyme in addition to MoaA, it may be that the incompleteness of the MoaA TIM barrel accommodates a complex with MoaC.<sup>240</sup>

In the substrate-bound structures of MoaA, SAM was found coordinated to the N-terminal cluster as an N/O chelate to the N-terminal site-differentiated Fe, while the sulfonium sulfur was 3.3 Å from the site-differentiated Fe and 3.6 Å from the nearest sulfide (Figure 36).<sup>240</sup> SAM was found extended across the top of the barrel, but the binding of SAM in the active site resulted in no significant protein and cluster conformational changes relative to its absence. In addition to the Fe–S cluster binding motifs, five conserved arginine residues and two lysine residues

line the inside of the TIM barrel, likely to stabilize the negative charge of the triphosphate group of 5'-GTP.<sup>240</sup> Structures with GTP bound have shown that the ribose and base are relatively flexible, with the triphosphate part tightly anchored within the hydrophilic channel (Figure 36).<sup>242</sup> A basis for specific nucleotide hydrogen bonding by GTP over ATP can be rationalized, complementing equilibrium dialysis experiments that showed 40%, 60%, and 100% residual binding by 5'-ATP, 5'-ITP, and 5'-XTP, respectively.<sup>242</sup> Equilibrium dialysis experiments have shown that GTP binding is not dependent on SAM binding, and that the position 6 oxo group and the amino group at position 2 are important for guanine recognition by MoaA.<sup>242</sup> While crystallographic studies indicate that no active site closure is apparent upon substrate binding, the multiple electrostatic interactions between triphosphate and protein arginine and lysine residues tightly confine the generation of radical intermediates from the dAdo $^\bullet$ . Structure elucidation of the triple arginine mutant R17/266/268A has shown distinct conformational changes in 5'-GTP binding, resulting in a more open active site.<sup>242</sup>

**6.1.4. A Role for the C-Terminal Cluster in MoaA.** The precise role that the C-terminal site-differentiated Fe–S cluster serves has been proposed to be that of a Lewis acid, in a manner similar to that of the [4Fe–4S] cluster of aconitase.<sup>240,243</sup> Crystal structures of MoaA with GTP bound (with the radical SAM tricysteine motif substituted as trialanine) have shown that the guanine base N1 nitrogen and exocyclic amine closely interact with the C-terminal cluster at distances of 2.8 and 2.4 Å, respectively; however, these distances are too long to be considered bonds.<sup>242</sup> Elucidation of the interaction of GTP with the C-terminal cluster of MoaA resulted from elegant ENDOR studies of the C24/28/31S MoaA complexed with [ $^{14}\text{N}$  or  $^{15}\text{N}$ ]-5'-GTP and [ $^{14}\text{N}$ ]-5'

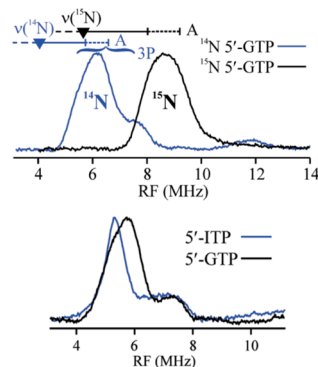


**Figure 37.** Top panel:  $^{15}\text{N}$  ENDOR evidence of 5'-GTP interaction with C-terminal [4Fe–4S], using  $^{14}\text{N}$  and  $^{15}\text{N}$  5'-GTP substrate and C24S/C28S/C31S MoaA. Bottom panel: Comparison of  $^{14}\text{N}$  ENDOR of substrate analogue 5'-ITP with 5'-GTP that have equivalent  $^{14}\text{N}$  hyperfine interaction with the C-terminal [4Fe–4S] cluster. Reprinted with permission from ref 38. Copyright 2006 American Chemical Society.

(Figure 37).<sup>244</sup> It was clear from the ENDOR studies of [ $^{14}\text{N}$  or  $^{15}\text{N}$ ]-5'-GTP complexed with the MoaA variant that at least one nitrogen coordinated to the unique iron of the C-terminal cluster; but was it the purine ring nitrogen N1 or the amino nitrogen N2? By using natural abundance [ $^{14}\text{N}$ ]-ITP, which lacks the amino group of GTP, Hoffman and co-workers demonstrated that the coordinated nitrogen was, in fact, the

purine ring nitrogen N1 (Figure 37).<sup>244</sup> The ENDOR-determined distance of the GTP substrate to the Fe–S cluster has been shown to be consistent with guanine binding to the cluster as the enol tautomer, which may be significant in substrate activation and/or ring cyclization.<sup>244</sup>

#### 6.1.5. Mechanism of a Complex Rearrangement Initiated by H-Atom Abstraction.

MoaA and MoaC together perform the synthesis of cPMP (Figure 38), but

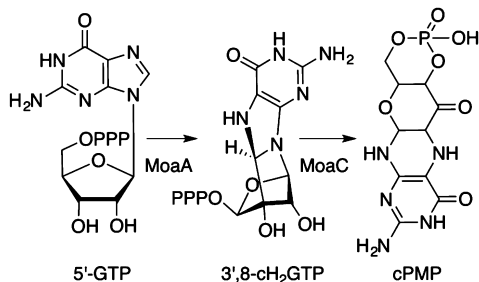


Figure 38. Proposed specific transformations that are catalyzed by enzymes MoaA and MoaC.

assignment of specific roles has been difficult, given the historic instability of detected pterin products. As noted by Hänelmann and Schindelin, the most difficult step in the precursor Z synthesis is fragmentation of the GTP C2'–C3' bond and insertion of the C8 atom,<sup>242</sup> recent studies indicate that MoaA is responsible for this remarkable reaction, which is initiated by H-atom abstraction from the C3' position.<sup>245</sup> Using a library of <sup>2</sup>H isotopologues of 5'-GTP, single deuterium label transfer to dAdoH was found to occur with 3'-<sup>2</sup>H-GTP, and detection of an oxygen-sensitive pterin product was detected by LC–MS<sup>245</sup> but was difficult to confirm using other characterization methods. However, the unique MoaA product, (8S)-3',8-cyclo-7,8-dihydroguanosine 5'-triphosphate (3',8-cH<sub>2</sub>GTP), was identified, isolated, and characterized by chemical derivatization, MS, and NMR spectroscopy by separate laboratories (Figure 38).<sup>82,246</sup> This product was shown to serve as the substrate for MoaC, producing cyclic pyranopterin monophosphate.<sup>82</sup>

The accumulated crystallographic, spectroscopic, and biochemical data result in a proposed mechanism for MoaA catalysis, shown in Figure 39. H-atom abstraction at the C3'-

carbon results in generation of a radical on the ribose ring that in turn cyclizes with the C8 guanine base carbon atom.<sup>82,245</sup> This results in generation of an aminyl radical that becomes oxidized to make the 3',8-cH<sub>2</sub>GTP product that is proposed to undergo general acid/base catalysis with MoaC to make cPMP.<sup>82</sup> Considering that the abstraction site on GTP is 5.3 Å from the C5' carbon atom of SAM, that the guanine ring nitrogen atom interacts with the C-terminal cluster as an enol tautomer (in the absence of SAM), and that the ribose and base are rotationally flexible in the crystal structure, the differential anchoring of the ribose and base with the C-terminal cluster prior to substrate H-atom abstraction is likely significant in cyclization reaction performed by MoaA. Further work investigating the interaction between the guanine N1 nitrogen and the Fe–S cluster with substrate and SAM, as well as with the product 3',8-cH<sub>2</sub>GTP, will provide additional details to this remarkable transformation.

#### 6.2. ThiC

ThiC is one of two radical SAM enzymes required in the pathway for thiamin biosynthesis. While ThiC catalyzes a complex rearrangement, ThiH, described in section 10.1, catalyzes cleavage of the C<sub>α</sub>–C<sub>β</sub> bond of tyrosine (Figure 40).

**6.2.1. Radical SAM Chemistry in the Synthesis of Thiamine Pyrophosphate.** Thiamine pyrophosphate (Vitamin B1) was discovered in 1932, its structure was elucidated in 1936, and it was the first such compound to be recognized as an essential metabolic cofactor.<sup>247</sup> It is an essential vitamin used by enzymes in central metabolism such as pyruvate dehydrogenase and α-ketoglutarate dehydrogenase to stabilize acyl carbanions.<sup>248</sup> It consists of 4-amino-5-hydroxymethyl-2-methylpyrimidine (HMP) and 4-methyl-5-(β-hydroxyethyl)thiazole phosphate carboxylate (THZ-P) moieties, which are independently synthesized and then ultimately combined by the actions of ThiE and ThiL to form TPP (Figure 40).<sup>249</sup> In all bacteria characterized to date, the syntheses of the HMP-PP and THZ-P carboxylate moieties both require the activity of radical SAM enzymes.<sup>250</sup> ThiC, the radical SAM enzyme involved in the synthesis of HMP-PP, catalyzes a complex rearrangement and is described in this section, while ThiH, which catalyzes a C–C bond cleavage required for synthesis of THZ-P, is described in section 10.1.

**6.2.2. Conversion of 4-Aminoimidazole Ribonucleotide (AIR) to HMP-P by ThiC.** In vivo thiamine biosynthesis is integrated with purine biosynthesis, where common metabolites serve as precursors in respective pathways.<sup>251</sup> Involvement of purine precursor 4-aminoimidazole ribonucleotide (AIR) has been known for several decades,<sup>252</sup> and description of its metabolic context is well documented.<sup>253</sup> Cumulative in vivo isotopic labeling studies that have spanned several decades have shown that all carbon and nitrogen atoms of HMP originate from AIR (Figure 41),<sup>251,254</sup> with only a single gene thiC required for AIR to HMP conversion in *E. coli* and *B. subtilis*.<sup>255</sup> Anaerobic handling of a cell-free extract containing overexpressed ThiC was shown to convert AIR to HMP, requiring SAM.<sup>256</sup> Because ThiC possesses a nontraditional CX<sub>2</sub>CX<sub>4</sub>C motif, its association as a radical SAM enzyme was not made initially. However, discovery of a plant-encoded ThiC protein that appeared to contain bound [Fe–S] clusters implicated ThiC as a Fe–S containing protein that could cleave SAM anoxically.<sup>105a</sup> In turn, collective data from the Downs and Begley laboratories demonstrated that anaerobically purified ThiC, in the presence of reductant, SAM, AIR, ATP, and

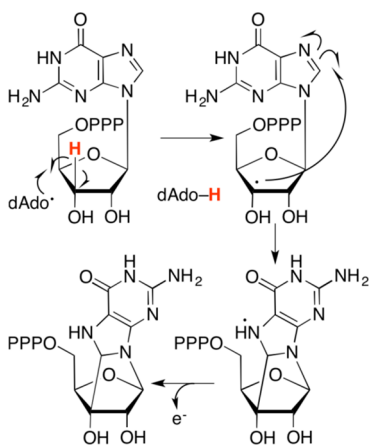
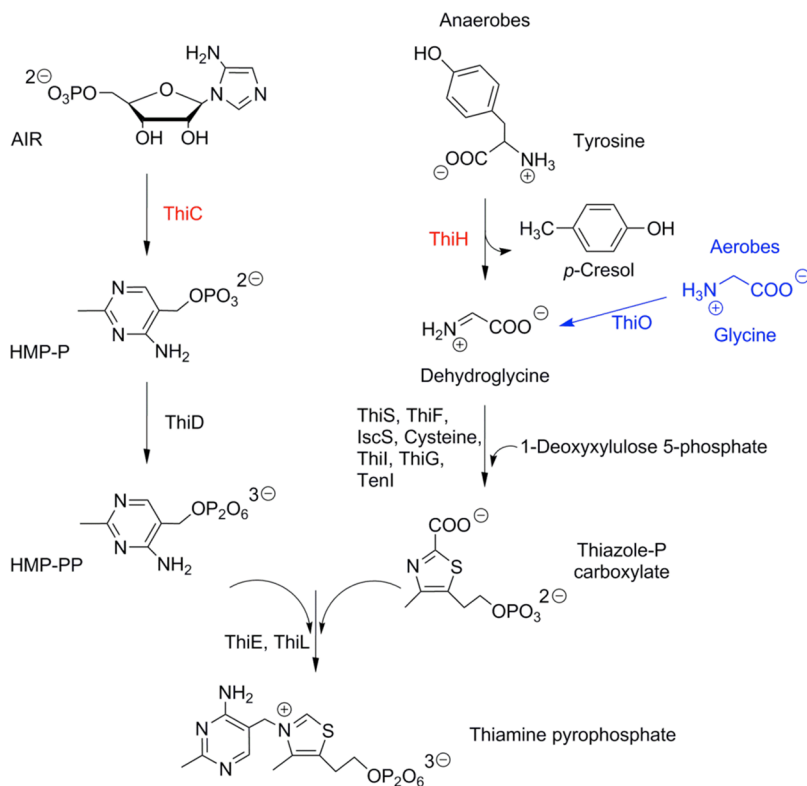
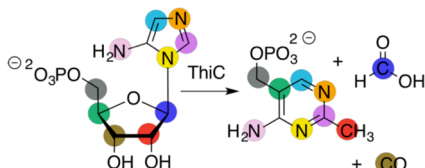


Figure 39. Proposed mechanism of formation of 3',8-cH<sub>2</sub>GTP by radical SAM enzyme MoaA.



**Figure 40.** The biosynthesis of thiamine pyrophosphate. 4-Amino-5-hydroxymethyl-2-methylpyrimidine pyrophosphate (HMP-PP) (left) is ultimately coupled with 4-methyl-5-( $\beta$ -hydroxyethyl)thiazole phosphate carboxylate (thiazole-P carboxylate) (right) to form thiamine pyrophosphate. The radical SAM enzymes ThiC and ThiH are highlighted in red. The generation of dehydroglycine differs between aerobes and anaerobes, which is highlighted as well.



**Figure 41.** Carbon and nitrogen isotopic label studies in the ThiC conversion of AIR to HMP-P. All carbon and nitrogen atoms originate from AIR, and the two carbon atoms (from the C-1' and C-3' positions) not incorporated into HMP-P produce formic acid and carbon monoxide, respectively.

$MgCl_2$ , stimulated dAdoH and HMP production.<sup>41,106</sup> Characterization of the anaerobically prepared enzyme (by UV-vis, EPR, and Mössbauer spectroscopy) revealed the presence of one [4Fe–4S] cluster (Table 2).<sup>41</sup> Recently, a significant improvement of in vitro catalytic activity of ThiC has been reported, which involves multiple turnovers of AIR (Table 1).<sup>70</sup> Similar to radical SAM enzymes that have been kinetically characterized (Table 1), ThiC is inhibited by SAM-derived metabolites S-adenosylhomocysteine, dAdoH, methionine, homocysteine, as well as S-methyl-5'-thioadenosine and adenosine.<sup>70</sup>

**6.2.3. Mechanistic Insight into the Complex Rearrangement Catalyzed by ThiC.** ThiC catalyzes a remarkable complex rearrangement involving the opening of the imidazole C4–C5 bond, and inserting the C4' and C5' carbons to make a pyrimidine ring (Figure 41). Interestingly, recent deuterium labeling studies with AIR have identified the site of H-atom abstraction by ThiC.<sup>257</sup> Characterization of the dAdoH product (by LC–MS and NMR) has shown that substrate labeled at

both the C4' and the C5' positions resulted in a mixture of mono- and bis-labeled dAdoH products with a 1:1 stoichiometry. However, individual labels at C4' or C5' positions of AIR result in a single deuterium transfer to dAdoH.<sup>257</sup> Such a pattern implicates H-atom abstraction at both positions, because multiple deuterium labels in dAdoH product can only occur if product or substrate radical recombines with dAdoH.<sup>257</sup> Corroborative data that support this hypothesis include recent trapping of a carbon-based radical generated by ThiC.<sup>258</sup> While the radical was tentatively assigned as protein-associated, in principle it could represent a substrate radical intermediate of the reaction following abstraction at either the C4' or the C5' positions.

While substrate radical initiation has been defined, its propagation is clearly less understood. The observation of multiple deuterium labels in dAdoH product requires abstraction at the C4' and C5' positions.<sup>257</sup> While abstraction at the C4' position would confer a direct transfer of carbon atoms to the imidazole ring, it would leave final abstraction difficult in the net fragmentation of the ribose ring at the C-5' position. The AIR C1' and C3' carbon atoms are ultimately expelled as formic acid and carbon monoxide, respectively (Figure 41), requiring likely radical propagation to the substrate C1' and C3' positions.<sup>257</sup> To this end, isolation of product intermediates and characterization of product radicals likely will provide critical insight to the nature of radical rearrangement.

**6.2.4. The Structure of ThiC.** Structural characterization has uncovered potentially significant insights to the chemical reaction catalyzed by ThiC and further expanded our understanding of the radical SAM superfamily (Figure 42).<sup>41</sup> The enzyme has been structurally characterized from bacterial

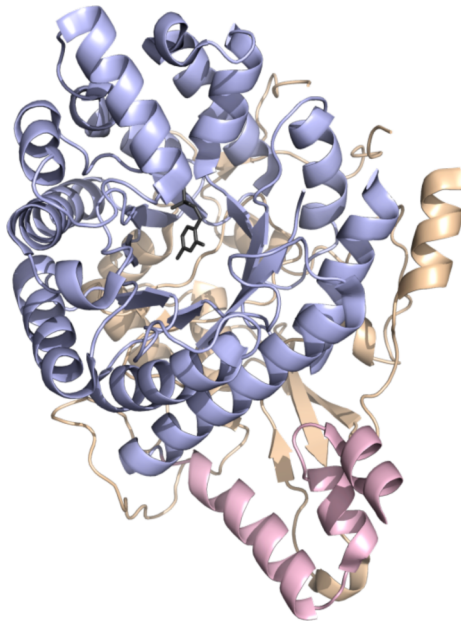


**Figure 42.** ThiC crystal structure (PDB ID 3EPO). N-terminal domain colored in wheat, radical SAM domain in light blue, C-terminal domain in light pink, HMP-P in dark gray sticks.

(*Caulobacter crescentus*) and eukaryotic (*Arabidopsis thaliana*) organisms.<sup>41,105b</sup> Like other characterized radical SAM enzymes, ThiC has an aromatic residue within the tricysteine motif; this aromatic residue likely interacts with the adenine moiety of SAM, while the characteristic glycine-rich “GGE” and “G<sub>x</sub>LxGxE” motifs implicate similar protein–SAM interactions.<sup>41</sup> Like BioB and HydE (sections 4.1.3 and 12.2.5.2), ThiC contains a complete  $(\beta\alpha)_8$  TIM barrel. While BioB, HydE, and other radical SAM enzymes house the tricysteine motif in a single loop as part of the N-terminal region of the TIM barrel that also houses the substrate binding site, the ThiC structure is unique, as has been described in detail elsewhere.<sup>259</sup> In ThiC, the tricysteine motif that binds the radical SAM cluster is in a domain distinct from the TIM barrel, which contains the substrate binding site.<sup>41</sup> ThiC is in fact structurally similar to adenosylcobalamin-dependent enzymes including glutamate mutase, methylmalonyl-CoA mutase, lysine 5,6-aminomutase, and ornithine 4,5-aminomutase, by housing the radical precursor cofactor adenosylcobalamin in a separate domain from the TIM barrel domain that encloses the substrate binding site.<sup>259</sup> In the ThiC structure, a segment of conserved sequence residues in the TIM barrel constitutes a broad surface that likely define the interface across which the Fe–S cluster domain and the TIM barrel interact, an attribute that is more similar to characterized AdoCbl-dependent structures than to characterized radical SAM structures.

**6.2.5. Pathways Utilizing Multiple Radical SAM Enzymes.** ThiC is part of a biosynthetic machinery that applies multiple and discrete sets of radical SAM enzymes to facilitate complex rearrangements in their products. As more members of the radical SAM enzyme superfamily are characterized, the number of multiple radical SAM enzymes involved in discrete steps of biosynthetic reactions is expected to increase. In the case of thiamine biosynthesis, an additional radical SAM enzyme ThiH is employed to ultimately synthesize the thiazole-P carboxylate moiety of thiamine phosphate (section 10.1). While no crystal structure has been obtained

to date for ThiH, its amino acid sequence is expected to form the canonical SAM tertiary fold (section 2.6). That a biosynthesis employs multiple radical SAM enzymes with different protein architectures poses some intriguing evolutionary questions with respect to relationships between the radical SAM enzymes, as they relate to radical AdoCbl enzymes. The similarity of the radical SAM enzyme ThiC to radical AdoCbl enzymes appears to be a potential link between two distinct enzyme classes, where a structural basis has been defined (section 2.7). While other examples of biosynthetic pathways that employ multiple, yet discrete, sets of radical SAM enzymes are documented (HydE and HydG in [FeFe]-hydrogenase biosynthesis (sections 12.2.4 and 12.2.5) as well as CofH/CofG in the F<sub>420</sub> biosynthesis (section 6.4)), discovery and characterization (coupled with structural characterization) of new members of the superfamily will better delineate the evolutionary link they have within the radical SAM superfamily, and by extension, to radical AdoCbl enzymes.

### 6.3. Synthesis of Pyrrolopyrimidines: QueE and ToyC

Pyrrolopyrimidines, or 7-deazapurine-containing molecules, are a structurally diverse family of nucleotide analogues that are ubiquitous in nature.<sup>260</sup> Those identified from *Streptomyces* (such as toyocamycin discovered in 1956)<sup>261</sup> have demonstrated antibiotic and antineoplastic activities, while other pyrrolopyrimidines, such as queosine, have been found as modified bases in tRNA.<sup>262</sup> Biosynthetically, pyrrolopyrimidine compounds are synthesized in three steps via a common set of biotransformations starting from the precursor GTP, supported by early radiotracer studies with tubercidin and more recently with characterization of the biosynthetic gene structure of toyocamycin.<sup>263</sup> Using the biosynthesis of queosine as a model, GTP is first converted to 7,8-dihydronopterin triphosphate by GTP cyclohydrolase I. Next, it is converted to 6-carboxy-5,6,7,8-tetrahydopterin by its associated synthase QueD or ToyB. Finally, it undergoes a rearrangement with another enzyme (QueE or ToyC) to make 7-carboxy-7-deazaguanine (CDG).<sup>263a</sup>

QueE (ToyC) was identified as a radical SAM enzyme, because it contained the CX<sub>3</sub>CX<sub>2</sub>C motif, and was consistent with earlier genetic and experimental evidence suggesting the involvement of an Fe-containing protein with an encoded amino acid sequence similar to the *nrdG* gene (section 3.2).<sup>263g,264</sup> QueD was shown to produce 6-carboxy-5,6,7,8-tetrahydopterin, and activity of QueC was found to produce 7-cyano-7-deazaguanine (preQ<sub>0</sub>).<sup>260c,263c</sup> This provided evidence that QueE performs the reaction shown in Figure 43, effectively a radical ring contraction reaction with loss of NH<sub>4</sub><sup>+</sup>.<sup>260c</sup> Recent characterization of QueE has confirmed that it serves as a radical SAM enzyme, where it coordinates a [4Fe–4S] cluster and it catalyzes the reductive cleavage of SAM.<sup>88</sup> An EPR

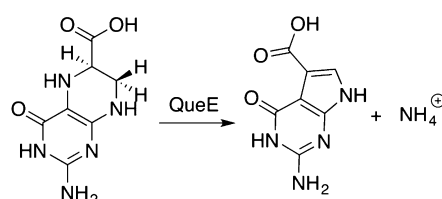


**Figure 43.** Reaction of the heterocyclic rearrangement catalyzed by radical SAM enzyme QueE.

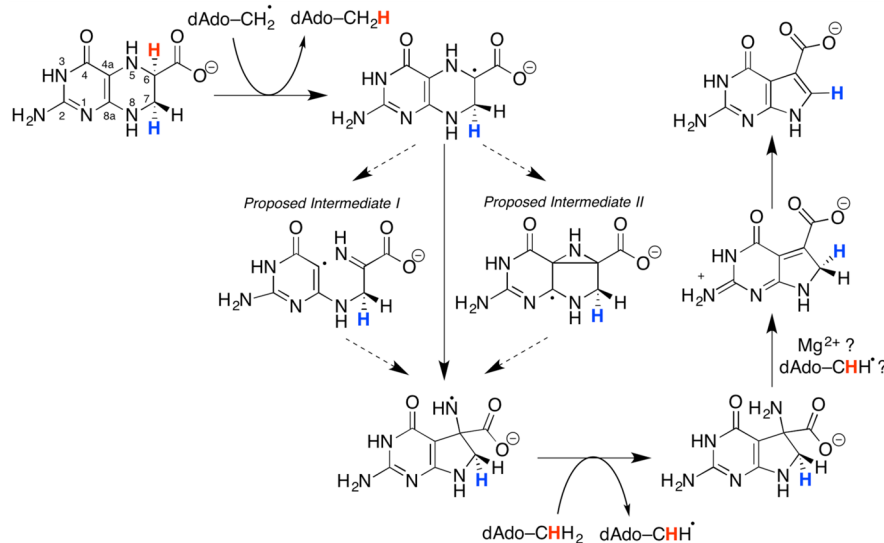


**Figure 44.** Proposed mechanism in the QueE heterocyclic rearrangement.

spectrum of QueE was obtainable only in the presence of reductant and SAM; this characteristic is similar to LAM where coordination of SAM to the site-differentiated cluster increases the reduction potential of the cluster (Table 2 and sections 2.4, 2.5, 5.1.4).<sup>88</sup> For QueE, SAM was shown to function catalytically; <sup>2</sup>H atom transfer experiments using [6-<sup>2</sup>H]-6-carboxy-5,6,7,8-tetrahydropterin substrate have confirmed this, with multiple <sup>2</sup>H labels observed in dAdoH, consistent with a SAM cofactor undergoing several turnovers.<sup>88</sup> In contrast, no label transfer to dAdoH was observed with substrate labeled at the 7R or 7S locations, and consistent with previous radiotracer studies, the 7S deuterium label was retained in the product.<sup>88,263f</sup>

A working chemical mechanism is depicted in Figure 44.<sup>88</sup> Insertion of a substrate radical at the C6 position of 6-carboxy-5,6,7,8-tetrahydropterin is expected to result in either homolytic C–N bond cleavage resulting in a ring-opening mechanism (forming an imine and a radical at the C4a position), or an azacyclopropylcarbinyl radical (as has been proposed for LAM, section 5.1.6). In either step, a nitrogen-centered radical is proposed to occur, and H-atom abstraction from dAdoH would regenerate the dAdo<sup>·</sup> and subsequently SAM.<sup>88</sup> The following steps (aromatization of the five-membered ring and loss of ammonia) are currently unresolved questions in the chemical mechanism; however, it is noted that Mg<sup>2+</sup> plays an important, yet unidentified role in the reaction. The addition of Mg<sup>2+</sup> results in 11-fold more product formed relative to its absence.<sup>88</sup> The recently published structure of QueE reveals a specific binding of Mg<sup>2+</sup> near the substrate, as well as a modified ( $\beta_6/\alpha_3$ ) TIM barrel structure.<sup>477</sup>

#### 6.4. Biosynthesis of the F<sub>420</sub> Cofactor: FbiC/CofH and CofG

The hydride transfer F<sub>420</sub> cofactor is a deazaflavin derivative used as an essential cofactor by enzymes involved in a variety of processes, including energy metabolism, antibiotic biosynthesis, and DNA repair.<sup>265</sup> As a naturally occurring compound, it was first discovered in mycobacteria<sup>266</sup> and later purified from methanogenic bacteria.<sup>267</sup> Its structure was discovered<sup>268</sup> to contain a 8-hydroxy-7-desmethyl-5-deazariboflavin chromophore (factor F<sub>0</sub>) responsible for a 420 nm absorbance when oxidized.<sup>267</sup>

The biosynthesis of the 5-deazaflavin ring has been a subject of considerable interest spanning several decades that is outside the scope of this Review. Discovery of putative involvement of radical SAM chemistry in the biosynthesis of F<sub>0</sub> has been more recent, following complete genome sequencing for an expanding library of organisms.<sup>269</sup> Gene knockouts in the F<sub>420</sub>-producing bacterium *Mycobacterium bovis* BCG identified that knockouts of *fbiC* abolished F<sub>0</sub> and F<sub>420</sub> production.<sup>270</sup> Genome sequencing of *Methanocaldococcus jannaschii* revealed paralogues to the *fbiC* gene (*cogG* (MJ0446) and *cogH* (MJ1431))<sup>269</sup> homologous to the N-terminal and C-terminal regions of protein encoded by *fbiC*, with each containing a CX<sub>3</sub>CX<sub>2</sub>C motif.<sup>271</sup> For the enzymes from *M. jannaschii*, both CogG and CogH together were required for F<sub>0</sub> production, although the bifunctional polypeptide FbiC from *Mycobacterium smegmatis* was shown to produce more F<sub>0</sub> overall.<sup>271,272</sup> Additionally, partially purified *M. smegmatis* FbiC in cell-free extracts was shown to produce F<sub>0</sub> when incubated with 5-amino-6-ribitylamino-2,4(1H,3H)-pyrimidinedione, SAM, reductant, and 4-hydroxyphenylpyruvate.<sup>271</sup>

Recent biochemical and functional studies of purified and reconstituted FbiC as well as CogG and CogH have provided considerable insights into the role of radical SAM chemistry in the synthesis of the F<sub>0</sub> cofactor.<sup>117</sup> The purified FbiC containing approximately 1 Fe/protein could be reconstituted to contain 9.5 ± 1.2 Fe/protein, consistent with the presence of two [4Fe–4S] clusters.<sup>117</sup> The purified enzyme catalyzes the uncoupled reductive cleavage of SAM in the absence of substrate, as has been observed for other radical SAM enzymes (section 2.3). Previous studies using enzyme *in vivo* or in cell-free extracts had been unable to differentiate between 4-hydroxyphenylpyruvate and tyrosine as substrates due to the activity of tyrosine transaminase, so both molecules were tested with the purified enzyme.<sup>117,271</sup> While small amounts of F<sub>0</sub> were observed with 4-hydroxyphenylpyruvate, these same small amounts of product were observed without any added substrate, presumably due to the presence of substrate bound to the purified enzyme. When tyrosine was examined as a potential substrate, the F<sub>0</sub> levels increased 77-fold over the background level, indicating that tyrosine is the true substrate.<sup>117</sup> When the assay was repeated with [<sup>U-13</sup>C]-

tyrosine, the  $F_0$  product exhibited a 7 Da mass shift, reflecting the incorporation of the *p*-cresolate ring of tyrosine into  $F_0$ . Together, the cumulative data indicate that FbiC alone, or the combination of CofH and CofG (see below), catalyzes the reaction (Figure 45).<sup>117</sup> While use of dithionite as a reductant

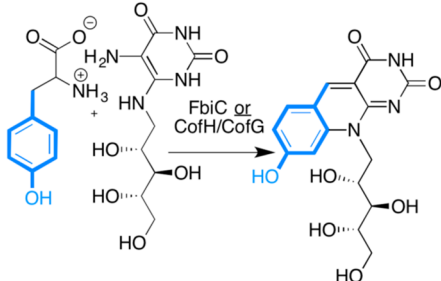


**Figure 45.**  $F_0$  synthase reaction catalyzed by bifunctional enzyme FbiC. The monofunctional units of FbiC can be isolated separately and, *in vitro*, catalyze the same reaction, with tyrosine and 5-amino-6-ribitylamino-2,4(1*H*,3*H*)-pyrimidinedione to make the 8-hydroxy-7-desmethyl-5-deazariboflavin chromophore  $F_0$ .

resulted in the production of nearly four dAdoH molecules per  $F_0$ , use of the physiological reductant flavodoxin/flavodoxin reductase resulted in just over two dAdoH molecules per  $F_0$ , suggesting that two SAM molecules are required and cleaved during  $F_0$  synthesis, presumably one at each of the radical SAM clusters in the enzyme.<sup>117</sup>

Additional insight into the roles of each of the radical SAM [4Fe–4S] clusters has been provided by studies of the purified CofG and CofH proteins. Both enzymes were successfully overexpressed and purified with an iron content of just under two Fe per protein, but with UV-vis absorption features consistent with the presence of [4Fe–4S] clusters (Table 2); CofH required coexpression of the *E. coli* *suf* operon to obtain significant soluble protein.<sup>117</sup> Both enzymes reductively cleaved SAM when incubated with dithionite as a reductant. Incubation of CofG, CofH, SAM, dithionite, tyrosine, and 5-amino-6-ribitylamino-2,4(1*H*,3*H*)-pyrimidinedione resulted in production of  $F_0$ . Interestingly, production of  $F_0$  was found to not require 5-amino-6-ribitylamino-2,4(1*H*,3*H*)-pyrimidinedione, and subsequently 5-amino-6-ribitylamino-2,4(1*H*,3*H*)-pyrimidinedione was found to copurify with CofH but not CofG, supporting the hypothesis that CofH acts first, in the early steps of  $F_0$  biosynthesis.<sup>117</sup> Further experiments in which CofH and CofG were incubated separately with SAM and substrates under reducing conditions, and then the small molecule products (if any) of these separate reactions were incubated with the other enzyme, demonstrated clearly that CofH functions first in  $F_0$  biosynthesis, and produces a stable product that is then used by CofG to synthesize  $F_0$  (Figure 46).

Because CofH acts first in  $F_0$  biosynthesis, it presumably uses tyrosine as a substrate; like ThiH and HydG, which also utilize tyrosine, CofH is proposed to catalyze  $C_\alpha$ – $C_\beta$  bond cleavage (sections 10.1, 12.2); CofG is expected to have a unique reaction mechanism that likely involves H-atom abstraction of the *p*-cresol product or initiation by a product radical produced from CofH.<sup>117</sup> CofH likely facilitates a  $C_\alpha$ – $C_\beta$  bond cleavage at a single, site-differentiated Fe–S cluster, similar to ThiH. Considering that the FbiC radical SAM domains are discrete, the site-differentiated clusters are expected to be distant from one another, catalyzing separate reactions where the domains are linked together resulting in a more efficient biotransforma-

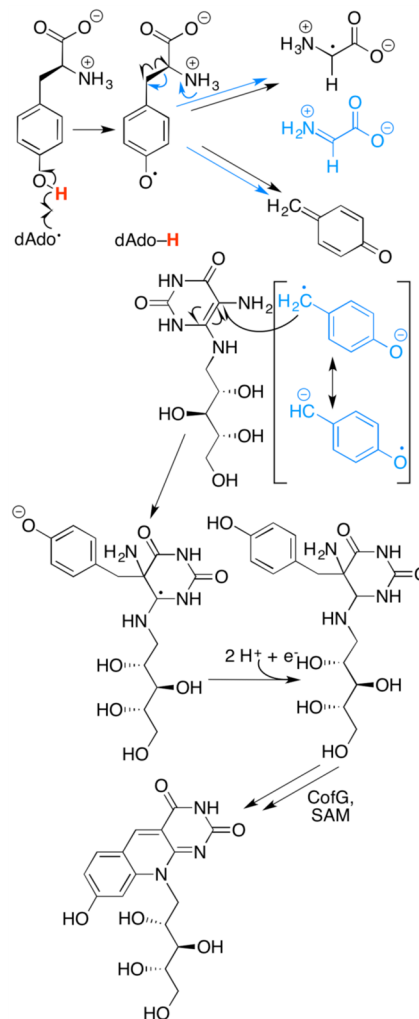


**Figure 46.** Proposed mechanism of radical initiation and probable involvement of CofH. Tyrosine homolytic  $C_\alpha$ – $C_\beta$  bond cleavage products are depicted in black, while heterolytic bond cleavage products are depicted in aqua.

tion (by analogy similar to NifEN-B in FeMoco biosynthesis, section 12.1). Characterization of a bifunctional radical SAM enzyme with discrete CX<sub>3</sub>CX<sub>2</sub>C motifs in a single enzyme is unique with respect to the enzyme superfamily, and that likely can serve as a template for understanding other complex biotransformations that employ multiple radical SAM enzymes involved in discrete steps of biosynthesis (e.g., HydE and HydG in [FeFe]-hydrogenase H-cluster maturation, section 12.2).

## 6.5. Synthesis of Menaquinone: MqnC and MqnE

Menaquinone (Vitamin K<sub>2</sub>) serves as an electron shuttle between membrane-bound proteins in the respiratory chain.<sup>273</sup> In *E. coli*, its biosynthesis starts from chorismate, and is understood to involve eight enzymes encoded by the *men* operon.<sup>274</sup> Analysis of whole genome sequences from *Helicobacter pylori*, *Campylobacter jejuni*, and *Streptomyces coelicolor*, however, has indicated that these organisms do not have orthologues to the *men* genes found in *E. coli* despite their ability to synthesize menaquinone.<sup>275</sup> For these other organisms, an alternative fthalosine pathway synthesizes menaquinone from chorismate. Following a proposed outline of the alternative pathway put forth by Hiratsuka et al., the conversion of dehypoxanthine fthalosine to cyclic dehypox-

yanthine fthalosine was associated with a gene *SCO4550* that encodes MqnC, a protein that contains the canonical radical SAM CX<sub>3</sub>CX<sub>2</sub>C motif.<sup>276</sup> Successful reconstitution of the radical SAM enzyme MqnC has revealed that it is involved in the cyclase reaction (Figure 47).<sup>277</sup> Deuterium labeling of the

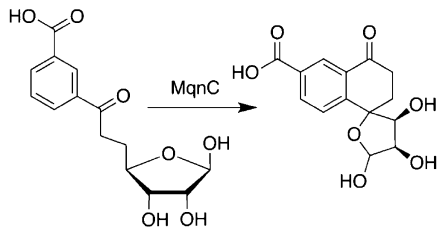


Figure 47. Transformation catalyzed by radical SAM enzyme MqnC.

dehypoxanthine fthalosine substrate has determined that the C4 hydrogen is abstracted by the dAdo<sup>•</sup>.<sup>277</sup> The resulting C4 radical is proposed to cyclize with the aromatic ring at the position *para* to the attached carboxylate, and subsequent deprotonation is proposed to result in the cyclic structure (Figure 48). That SAM appears to serve as a cosubstrate in the

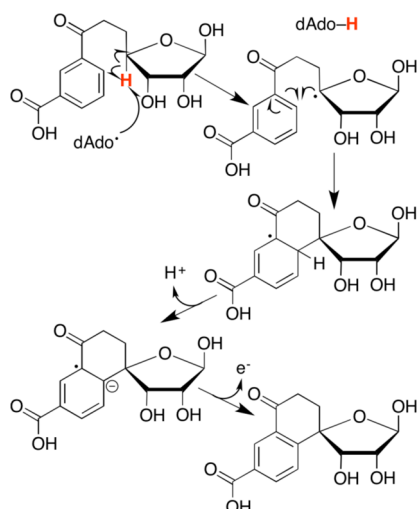


Figure 48. Ring cyclization mechanism catalyzed by radical SAM enzyme MqnC.

reaction at a single, site-differentiated [4Fe–4S] cluster is similar to other identified radical SAM enzymes that facilitate C–C bond formation.<sup>277</sup>

In addition to MqnC, further radical SAM enzyme involvement in the biosynthetic precursor to dehypoxanthine fthalosine has been recently discovered.<sup>119</sup> The fthalosine-dependent menaquinone biosynthetic pathway was identified on the basis of the observation of fthalosine as an intermediate through MS and NMR techniques,<sup>276</sup> following a series of bioinformatic, gene deletion, labeling, and biochemical characterization studies.<sup>278</sup> The first step in this pathway was initially proposed to involve chorismate, pyruvate, an adenosine precursor, and the gene *SCO4506* that encodes the enzyme MqnA.<sup>276</sup> The MqnA orthologue *TTHA0803* (*T. thermophilus*) was shown to catalyze the formation of 3-[1-carboxyvinyl]-oxy]benzoic acid, and required an additional enzyme to catalyze formation of fthalosine.<sup>276</sup> Subsequent bioinformatic analysis of menaquinone biosynthetic genes encoding putative ketoacid decarboxylases or radical SAM enzymes identified a possible

candidate *SCO4494* (now annotated as *mqnE*) that contained a sequence encoding a CX<sub>3</sub>CX<sub>2</sub>C motif.<sup>119</sup> Overexpression of the *T. thermophilus* orthologue of the *mqnE* gene (*TTHA0804*) produced an oxygen-sensitive Fe–S containing enzyme that exhibited an absorbance maximum at 415 nm (Table 2).<sup>119</sup> Interestingly, incubation of MqnE with 3-[1-carboxyvinyl]-oxy]benzoic acid, SAM, and reductant resulted in production of aminofthalosine, bicarbonate, and presumably methionine (Figure 49). Conversion of aminofthalosine to dehypoxanthine fthalosine was attained when assay mixtures were incubated with purified MqnB enzyme.<sup>119</sup>

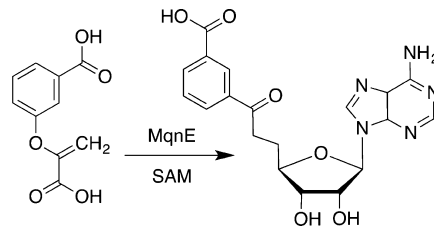


Figure 49. Transformation catalyzed by radical SAM enzyme MqnE.

The reaction catalyzed by MqnE is unique in the radical SAM superfamily in that the dAdo<sup>•</sup> is added to a substrate vinylic enol ether double bond (Figure 50).<sup>119</sup> While the radical

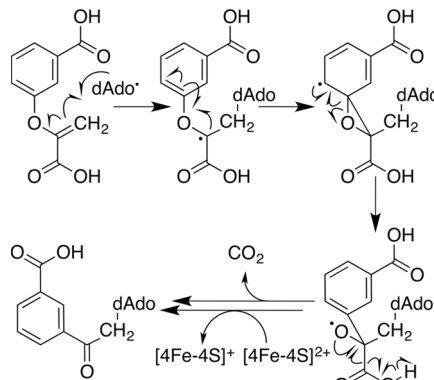
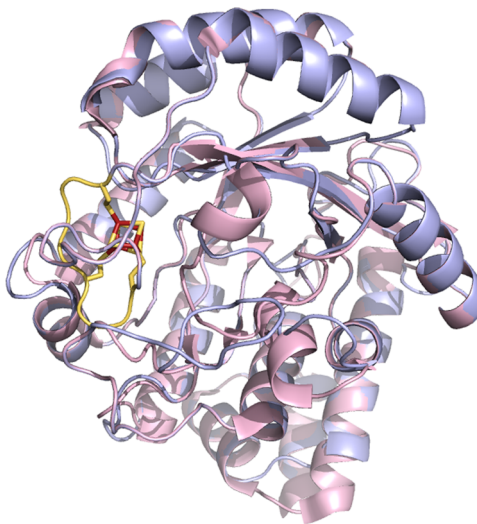


Figure 50. Mechanism of dAdo<sup>•</sup> addition to a vinylic ether double bond, catalyzed by radical SAM enzyme MqnE.

is generated and serves as a cosubstrate, the product 5'-dAdoH is not produced in the reaction. Addition of dAdo<sup>•</sup> to the substrate has been proposed to result in the formation of a captodatively stabilized substrate radical similar to Gly734 in PFL (section 3.1.5). Radical rearrangement generating an alkoxy radical would result in decarboxylation, while electron transfer to the oxidized [4Fe–4S]<sup>2+</sup> would terminate the product radical, forming the product keto group (Figure 50).<sup>119</sup>

The proposed mechanism and observed products in the MqnE reaction are suggestive of a novel biochemical transformation different from all other radical SAM enzymes characterized to date that cleave the SAM S–C(S') bond.<sup>119</sup> While most of the enzymes in the superfamily perform H-atom abstraction, MqnE utilizes dAdo<sup>•</sup> to carry out C–C bond formation at the C-5' position. Such chemical distinctions between H-atom abstraction and radical addition might be expected to correlate with active site structural differences; however, amino acid sequence comparison shows that MqnE is predicted to have a complete (βα)<sub>8</sub> TIM barrel with analogous SAM binding motifs as observed in other superfamily members

(Figure 51) (section 2.6).<sup>34,279</sup> These similarities suggest that the mechanism of dAdo<sup>•</sup> generation and substrate radical



**Figure 51.** Structure homology model of the amino acid sequence of MqnE (*T. thermophilus*) (blue), aligned to the HydE crystal structure (PDB ID 3CIX) (pink) (section 12.2.5.2). Radical SAM motif is colored in yellow, cysteines involved in ligating the [4Fe–4S] are shown as yellow sticks, while the [4Fe–4S] cluster is depicted as yellow and rust sticks. For clarity, the [2Fe–2S] cluster of HydE has been omitted. MqnE structural model was generated using the protein structure prediction server Phyre2,<sup>279</sup> where the HydE template model yielded the top hit.

propagation in MqnE is comparable to radical SAM enzymes that perform H-atom abstraction reactions. Alternatively, differences in the fate of the generated dAdo<sup>•</sup> species could be rationalized by variances in substrate proximity to the SAM-bound Fe–S cluster. While the basis for the unusual chemistry catalyzed by MqnE remains unclear, future structural and spectroscopic characterization in the presence of substrate and SAM will likely provide new insights into the subtle active site characteristics that control dAdo<sup>•</sup> reactivity.

#### 6.6. Synthesis of Modified Side Chain Rings of Thiopeptides: NosL or NocL

Thiopeptides represent a class of polythiazolyl antibiotics that have clinical interest against drug-resistant bacterial pathogens.<sup>280</sup> They are comprised of a macrocyclic core, consisting of a nitrogen-containing six membered ring with variable side chains and rings. Thiopeptide formation is facilitated through conserved post-translational modifications on a ribosomally produced precursor peptide, including cyclodehydrations, dehydrations, and intramolecular cyclizations to synthesize the nitrogen heterocycle product.

Thiopeptides such as nosiheptide and thiostrepton have side chain rings (indolic acid and quinalic acid, respectively) that are synthesized independently of the precursor peptide. The nosiheptide side chain ring 3-methyl-2-indolic acid (MIA) is synthesized by genes *nosL* and *nosN*, which were identified as putative SAM-dependent enzymes.<sup>281</sup> Homologous *nocL* and *nocN* genes were discovered as important in the nocathiacin I biosynthesis.<sup>282</sup> The NosN protein was found to have a high amino acid sequence similarity to Tlm-Orf11 in tallysomycin biosynthesis (section 7.3),<sup>283</sup> while NosL was similar to radical SAM enzyme ThiH.<sup>281</sup> Mutant strain SL4006 (lacking the NosN protein) produced a side ring-opened NOS analogue

containing a 3-methylindolyl group linked to the thiopeptide by a single thioester linkage.<sup>281</sup> Collectively, the ordering of these radical SAM-dependent enzymes suggested NosL acts first to make MIA from tryptophan, and NosN later performs a methyltransferase reaction (Figure 52).

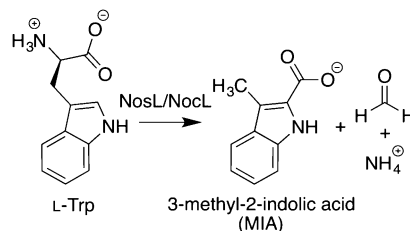


**Figure 52.** Radical fragmentation–recombination reaction catalyzed by radical SAM enzymes NosL and NocL.

Biochemical characterization of the NosL and NocL (NosL homologue in nocathiacin I biosynthesis) together has provided an understanding of this novel radical SAM biotransformation.<sup>71,114</sup> NosL and NocL were purified and reconstituted anaerobically from recombinant strains SL4101 and SL4151 respectively, where the enzyme was found to bind a single [4Fe–4S] cluster that upon incubation with tryptophan, SAM, and dithionite resulted in formation of MIA.<sup>71,114</sup> The EPR signal of reduced NosL and NocL was found to be axial ( $g = 2.02$  and  $1.91$ ). Interestingly, reduction of NocL in the presence of tryptophan resulted in the formation of a new signal ( $g = 2.02, 1.89, 1.85$ ) (Table 2). Feeding of the NosL SL4101 strain with either [ $1-^{13}\text{C}$ ] or [ $3-^{13}\text{C}$ ]-labeled tryptophan resulted in label incorporation in the 2-carboxylate and 3-methyl group of MIA, respectively.<sup>114</sup> Incubation with the purified NosL with [ $^2\text{H}_8$ ]-tryptophan resulted in production of [ $^2\text{H}_6$ ]-MIA without observable deuterium transfer to dAdoH; formaldehyde was detected as a byproduct, as well as 3-methylindole and glyoxylate.<sup>114</sup> HPLC–MS analysis of turnover samples revealed the production of glycine, suggestive of a glycyl radical intermediate.<sup>114</sup> Further evidence for a free glycyl radical is supported by EPR spectra performed at 77 K, where low-level formation of carbon-based free radical was detected in the NocL protein.<sup>71</sup>

A preliminary mechanism for the NosL/NocL biotransformation can be found in Figure 53. H-atom abstraction at the ring indole nitrogen atom generates a tryptophanyl substrate radical, which undergoes  $\text{C}_\alpha-\text{C}_\beta$  bond cleavage to form a glycyl radical and a 3-methyleneindole-based radical. Because glyoxylate and low levels of glycine were identified as reaction products, an oxidized glycine intermediate (either a glycyl radical or a dehydroglycine) is produced from the initial substrate radical and can be quenched to make the glycine-based product.<sup>114</sup> From here, it is proposed that the product radicals terminate at the indole C2 position, resulting in formation of a new C–C bond between the Trp C1 carboxylate and the methylindole. Oxidation and subsequent fragmentation of the original Trp C-2 carbon atom results in formation of product and formaldehyde.<sup>114</sup> Interestingly, the mechanism is similar to the ThiH/HydG proteins, in that substrate initiation occurs at a solvent exchangeable position, that  $\text{C}_\alpha-\text{C}_\beta$  bond cleavage occurs, culminating in oxidation of the glycine backbone, and that glyoxylate is detected as a product under certain conditions (sections 10.1 and 12.2.4).<sup>71,78,114,284</sup> Mechanistic insight to the final step of the reaction (loss of

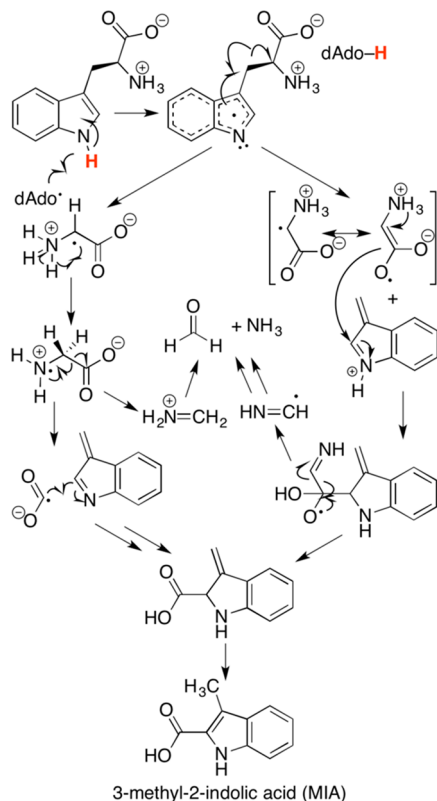


**Figure 53.** Proposed fragmentation–recombination mechanism in the conversion of L-Trp to MIA catalyzed by NosL and NocL.

the C2 carboxylate) will require further investigation, but the observed radical fragmentation–recombination has merit to be a general mechanism within the subclass of radical SAM enzymes that perform amino acid  $C_{\alpha}$ – $C_{\beta}$  bond cleavage events.

## 7. ENZYMES CATALYZING METHYLATION AND METHYLIOTHIOLATION REACTIONS

As was discussed in section 2.5, homolytic cleavage of the S–C(methyl) bond of SAM has not been well established in the radical SAM superfamily; however, numerous enzymes use radical SAM chemistry to transfer methyl groups, or methylthio groups, to substrates, as detailed in this section. Radical SAM methyltransferases (RSMTs) can be divided into three classes on the basis of their domain structure, and these classes most likely also delineate mechanistic differences (Figure 54).<sup>285</sup> The class A RSMTs have a single radical SAM domain and utilize a conserved cysteine as a key component of the methylation reaction, with one SAM transferring a methyl group by an  $S_N2$  reaction to the cysteinyl residue, and the second SAM serving as a precursor of a dAdo<sup>•</sup> that abstracts an H-atom from the methyl cysteine prior to methyl group transfer to substrate. The class B RSMTs contain both a radical SAM domain and a cobalamin-binding domain; for these enzymes it is thought that one SAM serves to methylate the cobalamin cofactor, while the second serves as a precursor of a dAdo<sup>•</sup> that abstracts an H-atom from the substrate prior to methyl group transfer to substrate. The class C RSMTs contain a radical SAM domain, as well as a C-terminal domain similar to that found in HemN. These RSMTs do not have conserved cysteines beyond the radical SAM motif, and do not bind cobalamin, and therefore presumably utilize a mechanism distinct from the class A and B RSMTs.

### 7.1. Class A Radical SAM Methyltransferases Methylenate the 23S rRNA at A2503

**7.1.1. A Novel rRNA Methylation.** The staphylococcal Cfr (chloramphenicol-florfenicol resistance) protein was first identified in 2000 and later noted in 2004 for the similarity of its N-terminal cysteine-rich region to Fe–S cluster binding radical SAM proteins.<sup>286</sup> Cfr is a methyltransferase that modifies the adenine 2503 position in 23S RNA of the bacterial large ribosomal subunit via methylation of C8 (Figure 55).<sup>287</sup> Methylation of aromatic sp<sup>2</sup>-hybridized carbons is

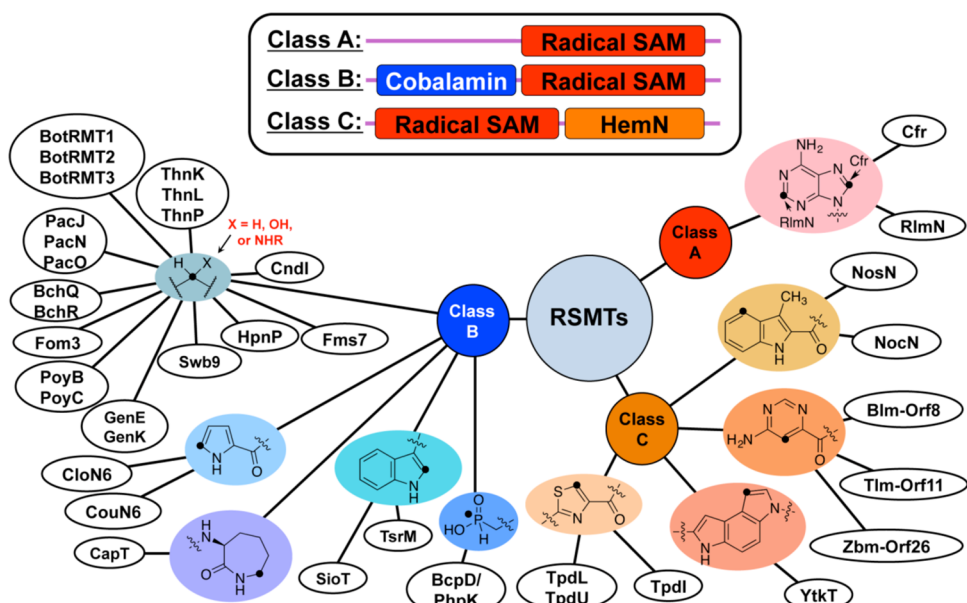


**Figure 54.** Representative radical SAM methyltransferase enzymes (RSMTs). Enzymes are organized by their class, which are differentiated by the top panel. Members of each class are differentiated by the type of methyl transfer catalyzed.

unusual among methyltransferases, which typically methylate at the nucleophilic O or N atoms of the nucleotide moiety.

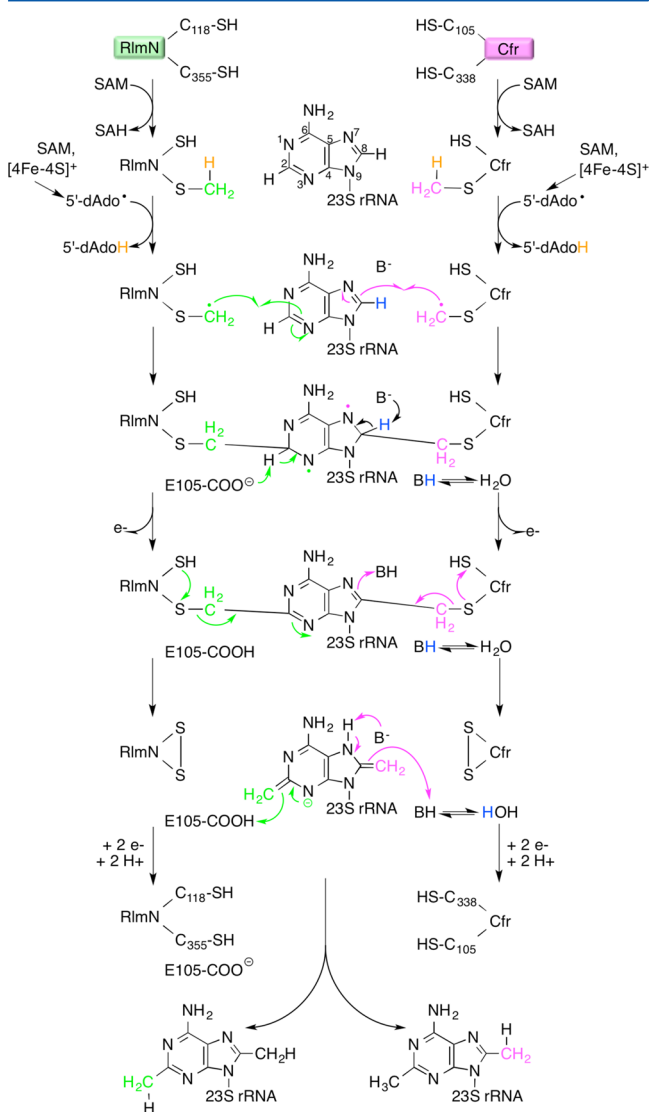


**Figure 55.** The modification of adenosine 2503 in 23S RNA of the bacterial large ribosomal subunit via methylation of the C2 or C8 position as catalyzed by RlmN or Cfr (two representative members of the class A RSMTs), respectively. The proposed mechanism for methylation of C2 by RlmN is depicted along the left side as shown using green arrows. The proposed mechanism for methylation of C8 by Cfr is depicted along the right side as shown using magenta arrows.

Because of earlier work showing high sequence homology, especially within the C-terminal region, of RlmN from *E. coli* with Cfr from *Staphylococcus aureus*,<sup>54a,286,288</sup> Toh and co-workers set out to determine if RlmN was indeed the *E. coli* counterpart of the staphylococcal methyltransferase.<sup>289</sup> Their results show that RlmN functions to methylate the C2 position on A2503 in 23S RNA (denoted m<sup>2</sup>A, Figure 55). However, unlike Cfr, which confers resistance against a variety of antibiotics that target A2503 for modification thereby inhibiting peptidyl transferase activity of the ribosome,<sup>290</sup> RlmN is innate and possibly important for ribosomal activity in bacteria.<sup>289</sup>

**7.1.2. Mechanistic Studies.** Published work on the first in vitro characterization of MTases demonstrated that RlmN and Cfr posttranslationally methylate A2503 at the C2 and C8

positions, respectively; although Cfr can act upon C2 as well, it is not the preferred site of methylation.<sup>111a</sup> Both of the enzymes bind only one [4Fe-4S] cluster and require two SAM molecules.<sup>111c</sup> Akin to MiaB, which also requires two SAMs (section 7.4.1), it was believed that one SAM gets reductively cleaved to form the dAdo<sup>•</sup> and the other donates the necessary methyl group.<sup>111a,127</sup>

Activity assays on these enzymes detected Met, dAdoH, and SAH as byproducts of the reaction to form the methylated A2503 product.<sup>111a</sup> Use of S-adenosyl-L-[methyl-<sup>3</sup>H]-methionine resulted in incorporation of the tritium into A2503, suggesting that the methyl group came from SAM. It was believed that the first SAM molecule was cleaved to generate a dAdo<sup>•</sup>, which carried out an H-atom abstraction at C2 of the adenosine substrate generating a substrate radical that was methylated by the second SAM molecule. This proposed mechanism, however, required homolytic cleavage of C–H aromatic carbon bond and generation of energetically unfavorable σ-radical.<sup>111a</sup>

In 2011,<sup>291</sup> Yan et al. modified their earlier proposal based on results using [2-<sup>2</sup>H]-adenosine. On the basis of previous findings, one would expect formation of [S'-<sup>2</sup>H]-dAdoH due to abstraction of the deuterium from substrate; however, no [S'-<sup>2</sup>H]-dAdoH was observed via MS, indicating that H-atom abstraction does not occur directly from C2 of substrate.<sup>291</sup> When [methyl-<sup>2</sup>H<sub>3</sub>]-SAM was used in activity assays with either RlmN or Cfr, however, singly deuterated dAdoH and doubly deuterated A2503 were observed as products. It was therefore postulated that the one SAM molecule donates the methyl group while one H-atom is abstracted from that methyl during catalysis. It was proposed that the dAdo<sup>•</sup> generated by radical SAM chemistry abstracted a hydrogen from the second SAM molecule to form SAM methyl radical that then combines with the substrate; a resulting hydride shift in the adenosine ring would then lead to expulsion of SAH and generation of final product.

Grove et al. provided data supporting an alternate mechanism in which RlmN and Cfr do not use SAM for direct transfer of the methyl group to substrate but rather for methylation of a conserved cysteine residue (Figure 55).<sup>111b</sup> Under single turnover conditions including methyl-d<sub>3</sub>-SAM, a 7-mer rRNA (2500–2506), and either RlmN or Cfr, there was no MS evidence for the transfer of d<sub>3</sub>-methyl from SAM to the 7-mer substrate; the substrate was indeed methylated but no deuterium was incorporated. Upon further investigation after growing up and isolating RlmN and Cfr from an *E. coli* methionine auxotroph in the presence of d<sub>3</sub>-methionine, single turnover assay conditions produced a doubly deuterated adenosine product, suggesting that d<sub>3</sub>-methyl is initially incorporated into the proteins during growth and then transferred to the C2 of the adenosine. Additionally, incorporation of a deuterium into dAdoH was observed; therefore, the dAdo<sup>•</sup> must abstract an H-atom from the methylated amino acid of protein generating a protein-based radical.<sup>111b</sup> Tryptic digestions and MS identified the labeled amino acid in RlmN as Cys355 (Cys338 in Cfr).<sup>111c</sup> These results are consistent with previous mutagenesis studies, which revealed that Cys to Ala changes in the CX<sub>3</sub>CX<sub>2</sub>C motif completely eliminate catalytic activity in RlmN,<sup>111a,287</sup> while mutation of two other conserved cysteines in Cfr makes the protein unable to methylate C8 on A2503.<sup>292</sup> Moreover, Grove et al. demonstrated the apoRlmN is catalytically inactive, however, upon reconstitution of the cluster and in the presence

of SAM, there is rapid release of SAH along with the methylated adenosine.<sup>111c</sup> RlmN and Cfr thus appear to possess a dual-purpose for the [4Fe–4S] cluster: the common need to generate a dAdo<sup>•</sup> but also the unique need to methylate substrate.<sup>111c</sup>

The current mechanism involves an initial S<sub>N</sub>2 reaction transferring the methyl group from one SAM molecule to Cys355 on RlmN and releasing SAH (Figure 55).<sup>111b</sup> Next, reductive cleavage of the second SAM molecule generates a dAdo<sup>•</sup> that abstracts an H-atom from methylated Cys355 forming a carbon radical and dAdoH. The methylcysteinyl radical attacks the sp<sup>2</sup>-hybridized C2 of A2503, resulting in carbon–carbon bond formation and a resonance-delocalized radical on the neighboring base of the nucleotide. Direct evidence for such a covalent intermediate has been provided by Fujimori and co-workers, who generated variants in which Cys118 of RlmN was changed to either alanine or serine; they found that these variants were unable to “resolve” the proposed covalent intermediate to form methylated product.<sup>293</sup> Further, they demonstrated using tandem mass spectrometry that the Cys118 variants of RlmN contained a covalently bound, methylene-linked adenosyl modification at Cys355.<sup>293</sup> The remainder of the mechanism involves loss of an electron to an Fe–S cluster and removal of a proton from C2 to give rise to an alkylated product linked to Cys355 of the protein. Intramolecular attack by Cys118 thiolate on Cys355 results in disulfide bond formation and an enamine intermediate, and final methylated product formation occurs through tautomerization and acquiring a proton from solvent. A similar mechanism is postulated for Cfr; however, differences are most likely present in the Cfr active site due to its preferential methylation of C8 over C2 of the substrate.<sup>111b</sup>

Most recently, data were presented to help elucidate the ability for Cfr to carry out two separate reactions with SAM in its active site.<sup>112b</sup> Wild-type (WT) Cfr was found to catalyze the uncoupled reductive cleavage of SAM, while C388A Cfr, which lacks the cysteine that accepts the methyl group from SAM, did not.<sup>112b</sup> These results suggested that Cys388, and/or methylated Cys388, is essential for the reductive SAM cleavage that is not coupled to substrate turnover. This difference in reactivity was not due to differences in SAM binding, because both WT and mutant Cfr were shown to bind SAM with similar affinity; EPR spectroscopy, however, established that oxidation of the reduced [4Fe–4S]<sup>1+</sup> cluster upon addition of SAM occurred only in the WT enzyme (Table 2).<sup>112b</sup> Together, these results suggest that methylated Cys388 properly positions SAM for reductive cleavage.

**7.1.3. Insights from the Structure of RlmN.** While in vitro studies have provided substantive insight into methylation transfer, a structural understanding of dAdo<sup>•</sup> interaction with substrate has helped to elucidate the observed differences between RlmN and Cfr described in section 7.1.2. The RlmN structure (representing the first structurally characterized radical SAM methyltransferase) (Figure 56) contains a  $\beta\alpha_6$  partial TIM barrel similar to PFL-AE, as well as an N-terminal accessory domain that is similar to the nucleic acid recognition helix-hairpin-helix fold found in the MraW methyltransferase family.<sup>294</sup> Similar to other structurally characterized radical SAM enzymes, the SAM sulfonium sulfur atom is oriented 3.2 Å from the unique Fe of [4Fe–4S] cluster.<sup>34,295</sup> Interestingly, the structure contains a methylated Cys355 (part of the  $\beta\gamma$  extension) at a distance of 6 Å from the bound SAM methionine methyl group, which would require a second

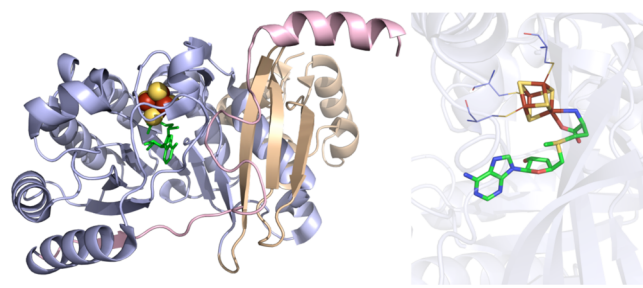


**Figure 56.** RlmN crystal structure (PDB ID 3RFA). Left: N-terminal domain colored in wheat, radical SAM domain in light blue, C-terminal domain in light pink, [4Fe–4S] cluster in yellow and rust spheres, and SAM in green sticks. Right: Active site of RlmN where [4Fe–4S] cluster (yellow and rust) and SAM (green carbons) are depicted in sticks with oxygens colored red and nitrogens colored blue. Cysteines (light blue carbons) involved in ligating cluster are depicted in lines.

equivalent of SAM capable of specific coordination to the site-differentiated Fe site. This observation is consistent with the multiple equivalents of SAM used, as well as with the mechanism proposed by Grove et al. (noted in section 7.1.2).

RlmN and Cfr catalyze similar methyltransfer events that differ in the specific site of transfer, yet both share a comparable affinity for SAM in the presence and absence of substrate.<sup>112b</sup> Such an observation has suggested that methylation of Cfr Cys338 influences structural changes in the active site mimicking substrate binding in the active site of other radical SAM enzymes.<sup>112b</sup> Interestingly, the RlmN structure possesses distinct structural elements lacking in Cfr that confer its specificity in reaction. Structural sequence mapping of Cfr on the RlmN structure showed strict sequence conservation within the active site cleft, which can be interpreted to represent a common radical initiation event.<sup>295</sup> Structural elements lacking in the Cfr sequence include the loss of conformationally flexible regions present in RlmN, such as the extended  $\alpha 1/\beta 2$  loop. Such observations are consistent with the in vitro experiments described in section 7.1.2, where differences in SAM cleavage were observed between the C355A RlmN and C338A Cfr enzymes. It appears here that slight differences in SAM and/or substrate binding in the active site lead to the enhanced functionality observed with Cfr to act on both positions C2 and C8 of A2508 as compared to the singly active RlmN at site C2.<sup>112b</sup>

## 7.2. Class B RSMTs: Cobalamin–Radical SAM Partnership

An emerging subclass among the MTases merges the unique features of radical SAM- and cobalamin-binding domains and has been recently reviewed and classified as Class B radical SAM methyltransferases (RSMTs).<sup>285</sup> Class B RSMTs potentially utilize two molecules of SAM, as seen with Class A RSMTs, in conjunction with cobalamin-mediated methyl transfer to carry out catalytic activity as illustrated in Figure 57. Included in this section is discussion of a few of the recently characterized class B RSMTs, including PhpK, TsrM, GenK, and HpnP.

PhpK, isolated from *Kitasatospora phosalacinea*, is a P-methyltransferase that carries out methyl transfer from methylcobalamin to 2-acetylaminoc-4-hydroxymethylphosphinylbutanoate (*N*-acetyldeethylphosphinothricin, NAcDMPT) to form the only known carbon–phosphorus–carbon linkage to occur in nature, 2-acetylaminoc-4-hydroxymethylphosphinylbutanoate (*N*-acetylphosphinothricin, NAcPT).<sup>116</sup> Assay condi-

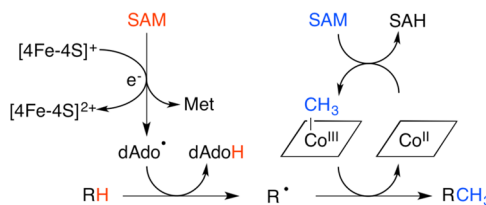


Figure 57. Proposed reaction scheme for class B RSMTs.

tions of reconstituted PhpK including SAM, dithionite, NAcDMPT,  $\text{CH}_3\text{Cbl}(\text{III})$ , and 5'-methylthioadenosine/S-adenosylhomocysteine nucleosidase (MTAN) (to prevent product inhibition), in conjunction with NMR spectroscopy enabled observation of the conversion of NAcDMPT to NAcPT. Two-dimensional  $^1\text{H}$ - $^{31}\text{P}$  gradient heteronuclear single-quantum correlation (gHSQC) spectroscopy to observe H-P cross-peaks in response to passive couplings from  $^{13}\text{C}$  (from  $^{13}\text{CH}_3\text{Cbl}(\text{III})$ ) to  $^1\text{H}$  and  $^{31}\text{P}$  nuclei demonstrated that  $^{13}\text{CH}_3\text{Cbl}(\text{III})$ , in the presence of PhpK, serves as the sole methyl donor to NAcDMPT.<sup>116</sup> It is speculated that a dAdo $^\bullet$ , resulting from SAM cleavage, abstracts an H-atom from substrate generating a phosphinate radical, which then interacts with  $\text{CH}_3\text{Cbl}(\text{III})$  resulting in transfer of the methyl group and release of Cbl(II) (Figure 58). Although it is unclear whether Cbl acts as a cosubstrate or cofactor, perhaps in accordance with similar  $\text{CH}_3\text{Cbl}$  chemistry such as Cbl-dependent methionine synthase, SAM is required to replenish the methyl group bound to Cbl enabling further turnover.<sup>296</sup>

The first known tryptophan methyltransferase, TsrM isolated from *Streptomyces laurentii*, was found to be responsible for the initial step of the complex transformation of tryptophan to thiostrepton A.<sup>89,280a,297</sup> Thiostrepton A is an antibiotic isolated more than 50 years ago<sup>298</sup> and is known for its activity against various pathogens, malaria, and possibly even cancer.<sup>299</sup> Initial in vitro activity assays of reconstituted TsrM including tryptophan, SAM, and dithionite demonstrated neither generation of any methylated products nor any nonproductive cleavage of dAdoH. However, due to the observed presence of a potential cobalamin-binding domain, addition of  $\text{CH}_3\text{Cbl}(\text{III})$  to the assay mixture generated SAH, indicating SAM is a potential methyl donor, as well as an unidentified compound that exhibited UV-vis and emission spectra characteristic of tryptophan.<sup>89</sup> Analysis via LC-MS determined this product to be methyltryptophan, and subsequent labeling experiments along with NMR spectroscopy revealed that the methyl was transferred to the C2 position of the indole ring. One exceptional finding was that in the absence of dithionite as the reductant, TsrM continued to generate SAH, thereby indicating that radical SAM chemistry was not a required precursor to methyl group transfer. Instead, it was concluded

that SAM functions solely as methyl donor to Cbl, forming methylcobalamin and expelling SAH. The final step in methyltryptophan formation necessitates generation and transfer of a methyl radical species from methylcobalamin to the C2 position of tryptophan, activated through possible ligation to a radical SAM [4Fe-4S] cluster (Figure 59).<sup>89</sup> The accumulated

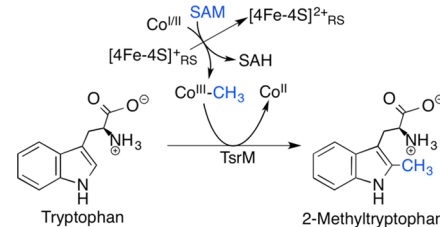
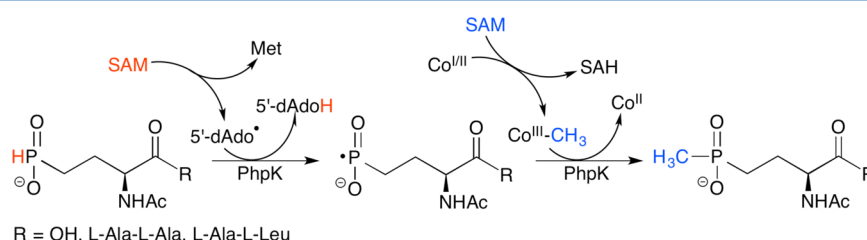


Figure 59. TsrM reaction scheme catalyzing the conversion of tryptophan to 2-methyltryptophan.

data on TsrM thus suggest that, while it is a member of the radical SAM superfamily and catalyzes methyl transfer, it does not, in fact, catalyze SAM-based radical chemistry.

Initial characterization of GenK, an enzyme involved in gentamicin biosynthesis, as a Cbl-dependent radical SAM MTase from gene knockout studies was further substantiated through in vitro activity assays with purified and reconstituted GenK from *Micromonospora echinospora*.<sup>84,300</sup> GenK, SAM, and Cbl/MeCbl all functioned to convert GenX<sub>2</sub> to the antibiotic Geneticin or G418, a precursor to gentamicin; in addition, the reaction produced dAdoH and SAH in a 1:1 ratio (Figure 60). Isotope labeling studies with  $^{13}\text{CD}_3$ -methyl-SAM detected  $^{13}\text{CD}_3$  bound to both G418 and Cbl indicating SAM is the preliminary methyl donor to Cbl, followed by secondary transfer of the methyl group to GenX<sub>2</sub>.<sup>84</sup> A possible mechanism includes homolytic cleavage of a SAM molecule giving rise to the dAdo $^\bullet$  followed by H-atom abstraction from GenX<sub>2</sub> forming the substrate radical and dAdoH. Quenching of the GenX<sub>2</sub> radical via transfer of a methyl radical from methylcobalalmin gives rise to Cbl(II) and G418. Conceivably, Co(II) is further reduced to Cbl(I), thereby enabling remethylation to occur from an incoming SAM molecule.<sup>84</sup>

Another protein recently added to the growing list of radical SAM enzymes, HpnP, is believed to act as a methyltransferase as it appears to be involved in the methylation of the C2 in hopanoids (Figure 61). Hopanoids, so named after a natural resin used in varnish for paintings that was derived from the genus *Hopea*, are functionalized pentacyclic hydrocarbon compounds produced in many cyanobacteria, as well as in  $\alpha$ -proteobacteria and acidobacteria and function in plasma membrane rigidity much like the function of sterols in eukaryotes.<sup>301</sup> Classification of *hpnP* from the *Rhodopseudomo-*

Figure 58. PhpK reaction scheme catalyzing the conversion of *N*-acetyldemethylphosphinothricin, NAcDMPT, to *N*-acetylphosphinothricin, NAcPT.

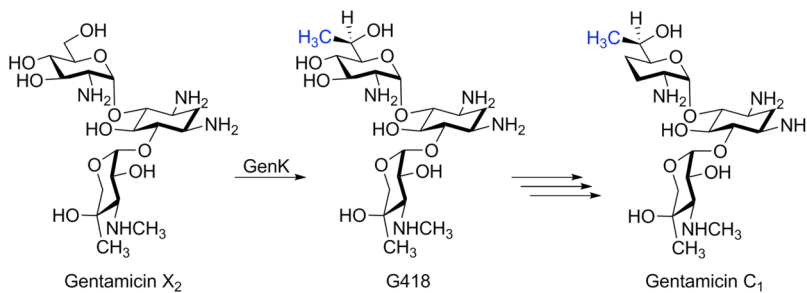


**Figure 60.** GenK reaction scheme catalyzing the conversion of Gentamicin  $X_2$  to G418.

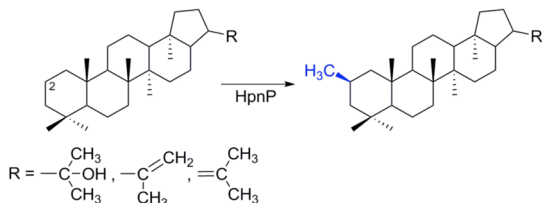


**Figure 61.** HpnP reaction scheme catalyzing the methylation of the C2 position in bacterial hopanoids. A few representative hopanoids are shown here.

*nas palustris* TIE-1 genome as a putative radical SAM enzyme was due to the presence of the CX<sub>3</sub>CX<sub>2</sub>C motif among the ORF 4269.<sup>302</sup> Because of earlier work showing that *R. palustris* cells fed with labeled methionine generate 2-methylhopanoids with the methyl group labeled at the C2 position,<sup>303</sup> it was speculated that the *hpnP* gene product may be responsible for such a methylation reaction. Analysis of an ORF 4269 gene deletion strain demonstrated an inability for methylation to occur in any one of the six known C2 methylated triterpenoids; however, insertion of the *hpnP* gene back into the ORF restored production of the methylated products.<sup>302</sup>

### 7.3. Class C Radical SAM Methyltransferases: Similar to HemN

The third class of radical SAM-dependent methyltransferases is a subcategory that has amino acid sequence similarities to radical SAM enzyme HemN.<sup>285</sup> As described in section 11.1.2, the HemN crystal structure comprises an incomplete ( $\beta\alpha$ )<sub>6</sub> TIM barrel motif in addition to a unique C-terminal domain that is putatively involved in substrate binding. The N-terminal “trip-wire” domain assigned to be important in substrate recognition in HemN is absent, however, in the Class C methyltransferase family.<sup>241</sup> As noted in section 11.1.2, a defining feature of the HemN reaction is the likely involvement of two SAM molecules at the active site.<sup>85,241</sup> While the class C enzymes are methyltransferases, they are thought to utilize a different mechanism than the class A or B enzymes, given that they contain neither a conserved cysteine nor a cobalamin-binding domain that could be used in methyl transfer.<sup>285</sup> Interestingly, this subfamily has several notable bioinformatic markers that differentiate it from the rest of the enzyme superfamily. It has been suggested that many of the identified, HemN-like oxygen-independent coproporphyrinogen III oxidases may actually be Class C radical SAM methyltransferase enzymes.<sup>285</sup>

Mechanistic information on the involvement of the HemN-like domain remains limited due to lack of enzyme characterization. Thiazole heterocycle methylation enzymes (TpdI, TpdL, and TpdU)<sup>304</sup> as well as pyrimidine ring methylation enzymes (Blm-Orf8, Tlm-Orf11, and Zbm-Orf26)<sup>283,305</sup>

involved in bleomycin antibiotic biosyntheses are identified as class C members.<sup>285</sup> As this enzyme subfamily is involved in the biosynthesis of several important thiopeptides and antibiotics, advances are likely to be significant in differentiating the role that the cobalamin serves in Class B methyltransferases to the role served by the HemN-like domain. However, as has been seen with other members of the radical SAM superfamily, the tasks of enzyme isolation and substrate identification often remain as the most significant hurdles in mechanistic characterization.

**7.3.1. NocN: Methyltransferase in Nosiheptide and Nocathiacin Biosynthesis.** As described in the section of NosL/NocL (section 6.6), thiopeptides represent a class of polythiazolyl antibiotics that have clinical interest against drug-resistant bacterial pathogens.<sup>280</sup> The nosiheptide and nocathiacin side chain ring 3-methyl-2-indolic acid (MIA) is synthesized by genes *nosL* and *nosN* (*nocL* and *nocN*, respectively), where each was identified as putative radical SAM-dependent enzymes.<sup>281,282</sup> The encoded NosL and NocL enzymes catalyze the conversion of tryptophan to make MIA, via H-atom abstraction at the tryptophan indole nitrogen atom (Figure 52).<sup>71,114</sup> The *nosN* and *nocN* genes were identified as SAM-dependent methyltransferase enzymes putatively involved in the synthesis of the C4-hydroxymethyl group, because feeding studies showed that the substituent originated from the methyl group of SAM.<sup>281,282,306</sup> To confirm this hypothesis, a mutant strain SL4006 (lacking the NosN protein) produced a side ring-opened NOS analogue containing a 3-methylindolyl group linked to the thiopeptide by a single thioester linkage, lacking a 4-methyl substituent.<sup>281</sup> Thus, the NosN/NocN activity has been proposed to follow the fragmentation/recombination event performed by NocL/NosL.

The accumulated data above, along with characterization of NosL, provide a working mechanism of activity for NosN. Provided that MIA serves as the substrate of NosN, the generated dAdo<sup>•</sup> may be anticipated to abstract a methyl H-atom from a second equivalent of SAM bound to the enzyme in a fashion similar to that proposed for RlmN<sup>291</sup> as would be potentially consistent with a HemN-like structure (section 7.1.2).<sup>241</sup> Such a mechanism would generate a methyl carbon-centered radical that would undergo addition to C4 of MIA. Because the substrate MIA represents a reduced species, methyl radical addition would result in an oxidized intermediate similar to those proposed in NosL/NocL MIA synthesis (section 6.6).<sup>71,114</sup> Hydride shift to the sulfonium sulfur atom, followed by one-electron reduction, would result in the generation of SAH and the 3,4-dimethylindolic acid product.

NosN is a class C methyltransferase that by analogy to HemN likely employs multiple equivalents of SAM as part of the catalytic mechanism (section 11.1.3). However, to date an

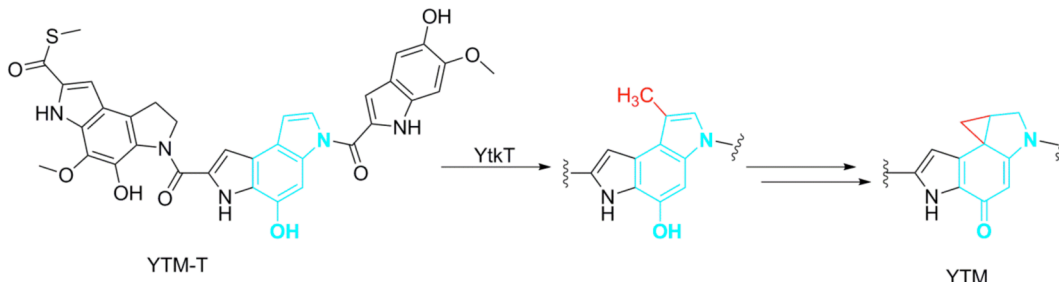


**Figure 62.** YtkT reaction scheme catalyzing the methylation of a yatakemycin (YTM) intermediate prior to cyclopropane ring formation.

in vitro investigation of the enzyme remains lacking; thus confirmation that MIA serves as the substrate has not been shown yet. Nonetheless, it is noteworthy that mutant strain SL4006 can produce a side ring-opened NOS analogue with a 3-methylindolyl group, meaning that the NosN enzyme might be expected to act on the MIA moiety on the thiopptide framework, rather than MIA.<sup>281</sup> In addition to the above, structural insight into the exact role that the HemN-like C-terminal region serves (as a defining characteristic of the subclass) remains limited, aside from putative involvement in substrate.<sup>285</sup> Because the HemN crystal structure was solved in the absence of substrate, limited structural information relating to substrate binding has been obtained. However, as more class C methyltransferases are characterized, structural studies in the presence of substrate should be informative in defining the enzyme subclass.

**7.3.2. Methylation during the Synthesis of the Natural Product Yatakemycin: YtkT.** Yatakemycin (YTM) is a naturally occurring antitumor agent in the family of CC1065 and the duocarmycins antibiotics and also exhibits certain antifungal properties. Exploring the Yatakemycin gene cluster led to identification of the *ytkT* gene; inactivation of *ytkT* via gene replacement curbed generation of the final product, YTM.<sup>118</sup> HPLC and LC–MS analysis showed buildup of YTM-T (Figure 62), demonstrating YtkT is necessary for YTM biosynthesis via C-methyltransferase activity. YtkT is highly homologous to HemN, and reconstitution of the purified YtkT along with reduction with dithionite displayed typical UV–vis absorption features common among many other radical SAM enzymes. Activity assays involving YTM-T, YtkT, SAM (as the methyl donor) under anaerobic reducing conditions yielded YTM (Figure 62).<sup>118</sup> When compared to cyclopropane fatty acid synthase, the mechanism for the YtkT-catalyzed reaction has been proposed to proceed via the S<sub>N</sub>2 transfer of the methyl group of SAM to the double bond of a cyclopropane ring followed by proton transfer and ring closing.<sup>118</sup>

#### 7.4. Radical SAM Methylthiotransferases

Posttranslational modifications, evident in all organisms, can range from simple functional group additions to complex multienzyme modifications. Of the five naturally occurring methylthio modifications, one takes place on the strictly conserved aspartic acid residue (Asp89) of ribosomal protein S12, while the other four alter the adenosine base (A-37) residing adjacent to the 3'-end of the anticodon in tRNA that reads codons beginning with U (except the tRNA<sup>IV</sup> Ser) (Figure 63).<sup>307</sup> Both modifications, either to the tRNA or to the ribosomal S12, could lead to alteration of functions potentially important for carrying out efficient and accurate ribosomal translation,<sup>308</sup> whereas prevention of such mod-

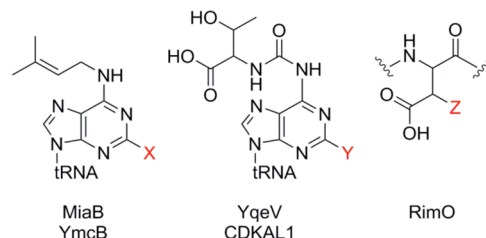


**Figure 63.** Methylthiolations of nucleic acid and protein residues. Left: Methylthiolations as catalyzed by MiaB (*E. coli* and *T. maritima*) and YmcB (*B. subtilis*) where the tRNA adenosine base is modified from i<sup>6</sup>A (when X = H) to ms<sup>2</sup>i<sup>6</sup>A (when X = SCH<sub>3</sub>). Middle: Methylthiolations as catalyzed by YqeV (*B. subtilis*) and CDKAL1 (mammalian tRNA<sup>Lys</sup> UUU) where the tRNA adenosine base is modified from t<sup>6</sup>A (when Y = H) to ms<sup>2</sup>t<sup>6</sup>A (when Y = SCH<sub>3</sub>). Right: Methylthiolation as catalyzed by RimO (*E. coli* ribosomal S12) where Asp89 (when Z = H) is modified to  $\beta$ -methylthio Asp89 (when Z = SCH<sub>3</sub>).

ifications in organisms such as bacteria could lead to antibiotic resistance.<sup>309</sup>

#### 7.4.1. Modification of tRNA<sup>Phe</sup> A-37 by MiaB.

Modification of the adenosine site, A-37, to 2-methylthio-N-6-isopentenyl adenosine (ms<sup>2</sup>i<sup>6</sup>A-37) of tRNA<sup>Phe</sup> is known to be initialized by MiaA in *E. coli*, which catalyzes the transfer of a dimethylallyl group to the N-6 nitrogen of adenine to generate i<sup>6</sup>A-37.<sup>310</sup> The next step(s) of the modification consists of sulfur insertion and methylation at position 2 of the adenine moiety resulting in conversion of i<sup>6</sup>A-37 to ms<sup>2</sup>i<sup>6</sup>A-37 and requires the input of SAM, iron, and cysteine.<sup>311</sup> Transcriptional studies of the *mia* operon identified the protein product MiaB as possessing the common CX<sub>3</sub>CX<sub>2</sub>C Fe–S cluster binding motif but lacking conserved SAM binding motifs; this led to the conclusion that MiaB likely catalyzes the thiolation of i<sup>6</sup>A-37 but not the methylation step, and therefore necessitated a third enzyme to carry out the final methylation event.<sup>312</sup>

Pierrel and co-workers successfully isolated and characterized MiaB as the first known Fe–S cluster-containing tRNA modifying enzyme. Reconstitution incorporated a single [4Fe–4S] cluster into MiaB (Table 2), and replacement of Cys with Ala of the CX<sub>3</sub>CX<sub>2</sub>C motif abolished formation of the ms<sup>2</sup>i<sup>6</sup>A-37 product.<sup>24b,126</sup> Further work by Pierrel and co-workers aimed to answer two important questions: does MiaB function as a radical SAM enzyme, and is MiaB sufficient for modification of i<sup>6</sup>A to ms<sup>2</sup>i<sup>6</sup>A or is a third protein required? They demonstrated the bifunctional nature of MiaB, showing it carried out both the thiolation and the methylation of i<sup>6</sup>A-37 using two molecules of SAM, one for reductive cleavage to generate a dAdo<sup>•</sup> and the other as a methyl donor. Assays with [<sup>3</sup>H]-methyl-SAM, reducing agent, MiaB, and the i<sup>6</sup>A

oligoribonucleotide led to incorporation of the labeled methyl group into ms<sup>2</sup>i<sup>6</sup>A, as well as formation of dAdoH.<sup>127a</sup> The next question to be answered was the source of the sulfur for donation to i<sup>6</sup>A. While it was determined that neither dithionite nor SAM were the source of the sulfur, selenium reconstituted MiaB produced Se-modified substrate, suggesting that sulfur added during the process of reconstitution was the ultimate sulfur source. This observation led to the hypothesis that a dAdo<sup>•</sup> abstracts an H-atom directly from position 2 of the adenine ring, thereby preparing it for sulfur insertion to generate a s<sup>2</sup>i<sup>6</sup>A intermediate. Cleavage of the second SAM molecule allows for methylation of s<sup>2</sup>i<sup>6</sup>A to give the final product, ms<sup>2</sup>i<sup>6</sup>A, and SAH.<sup>127a</sup>

Removal of the radical SAM cluster by mutation of the CX<sub>3</sub>CX<sub>2</sub>C cysteines revealed the presence of second [4Fe–4S] cluster coordinated by three N-terminal cysteines; this cluster had UV-vis absorption, resonance Raman, and Mössbauer spectral features similar to those of the radical SAM bound [4Fe–4S] cluster (Table 2), yet with differing redox and EPR signatures.<sup>127b</sup> X-band EPR of WT versus mutant MiaB displays an additional feature at *g* = 5, suggesting weak interactions between two paramagnetic clusters that are separated by approximately 12–20 Å.<sup>127b</sup> As both clusters are required for one turnover event of ms<sup>2</sup>i<sup>6</sup>A formation, it was suggested that the N-terminal cluster, as seen with BioB and suggested with LipA (sections 4.1.4, 4.2.4), possibly functions as the S-donor for the conversion of i<sup>6</sup>A to s<sup>2</sup>i<sup>6</sup>A.<sup>127b</sup>

**7.4.2. Methylthiolation of Ribosomal Protein S12.** Like MiaB, a highly homologous gene from *E. coli*, *yliG*, whose protein product was later termed RimO (for ribosomal modification), is capable of carrying out methylthio posttranslational modifications. Unlike MiaB that modifies tRNA, however, RimO acts on an amino acid, specifically Asp89 of the ribosomal protein S12 from *E. coli*.<sup>313</sup> Incubation of the modified S12 with Raney nickel catalyst demonstrated the added group to be a thioether (–SCH<sub>3</sub>) not a methylthiol (–CH<sub>2</sub>SH) and further verified the final product to be β-methylthio-aspartic acid, termed ms-Asp or ms-D89.<sup>313</sup> Additional similarities of RimO to MiaB include: (1) the need for two molecules of SAM to carry out catalytic activity (one for generation of the dAdo<sup>•</sup> and one for methyl donation) (Table 1), (2) the presence of two [4Fe–4S] clusters, where one cluster acts to reductively cleave one molecule of SAM and the second possibly functions as the sulfur donor as implicated for MiaB, BioB, and LipA, and (3) the dual role of carrying out both thiolation and methylation of the target substrate.<sup>138,139,313a,314</sup>

Sequence alignments of MiaB and its homologues, as well as the *Thermotoga maritima* RimO crystal structure, reveal three structural domains in these enzymes: an N-term UPF0004 domain, a radical SAM domain, and a C-terminal TRAM domain.<sup>139,313a,315</sup> In MiaB, the N-terminal domain contains three conserved cysteines found to bind one [4Fe–4S] cluster. The central radical SAM domain binds a second [4Fe–4S] cluster (Table 2).<sup>127b</sup> As observed with the methyltransferase RumA, where the RNA substrate is bound by the TRAM domain, it is reasonable to infer that the TRAM domain for MTTases is also likely responsible for substrate binding and recognition.<sup>315,316</sup> Differences in the MiaB and RimO TRAM domains could help elucidate specificity to tRNA or to ribosomal protein S12, respectively. For MiaB, the mainly positively charged TRAM domain is poised to attract negatively charged tRNA substrates, whereas in RimO, the negatively

charged TRAM domain makes it possible for interaction with the positively charged S12 protein.<sup>317</sup>

The recently solved reconstituted *TmRimO* crystal structure (Figure 64) provides the first evidence for a potential source of

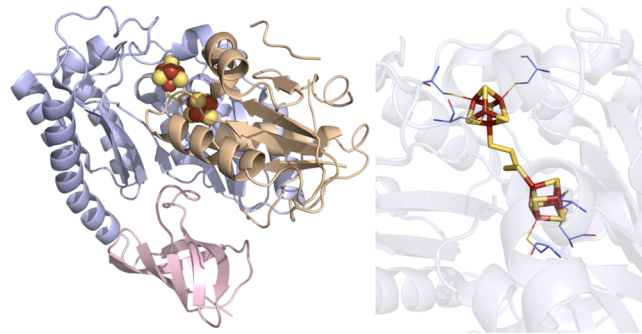


**Figure 64.** RimO crystal structure (PDB ID 4JC0). Left: N-terminal UPF0004 domain colored in light orange, radical SAM domain in light blue, C-terminal TRAM domain in light pink, [4Fe–4S] clusters in yellow and rust spheres, and SAM in green sticks. Right: Active site of RimO where the [4Fe–4S] clusters (yellow and rust) and pentasulfide moiety (yellow) are depicted in sticks. Cysteines (light blue carbons) involved in ligating clusters are depicted in lines.

the sulfur needed for the thiolation step of catalysis.<sup>318</sup> While reconstitution of the protein afforded two [4Fe–4S] clusters, it also led to exogenously bound sulfide. In this structure, the TRAM domain binds at the surface of the TIM barrel that contains the radical SAM domain but lies at the opposite end of the barrel from the radical SAM cluster. The UPF0004 domain binds at the opposite edge of the TRAM domain in the barrel and in very close proximity to the radical SAM cluster. The second cluster lies at the innermost point of the C-terminal region near the interface of the UPF0004 domain and the radical SAM domain, placing it at only 8 Å away from and bound to the radical SAM cluster through a pentasulfide moiety. This structure demonstrates an iron-accessible site of the second cluster capable of ligating a sulfur moiety without creating steric hindrance for the binding of SAM to the radical SAM cluster in a typical geometric fashion observed with other radical SAMs.<sup>40,240</sup> It was also observed that docking of the S12 substrate effectively closes off the active site.<sup>318</sup>

Additional studies investigating the function of the second cluster along with the relevance of exogenously bound sulfur in the RimO crystal structure utilized HYSCORE and EPR of MiaB lacking the radical SAM cluster binding motif. The ligands CH<sub>3</sub>S<sup>–</sup>, CH<sub>3</sub>Se<sup>–</sup>, or CH<sub>3</sub><sup>77</sup>Se<sup>–</sup> were found to coordinate the unique iron of the second cluster of MiaB, and to be utilized as cosubstrates capable of multiple turnovers for thiomethyl transfer to tRNA in activity assays. These results were repeated for RimO, showing that S (or Se in these studies) bound to the unique iron of the second cluster is the target of SAM methylation.<sup>318</sup>

Recently, Landgraf and co-workers have provided experimental evidence for RimO and MiaB mechanisms wherein the SAM-methyl is first donated to a persulfide-bound moiety of the auxiliary [4Fe–4S] cluster.<sup>83</sup> Feeding of unlabeled SAM to either RimO or MiaB, in the absence of product and reductant, generated ~1 equiv of SAH; moreover, early doping of unlabeled SAM to either RimO or MiaB followed by the addition of *d*<sub>3</sub>-SAM, product, and reductant into the assay mixture resulted in an initial surge of unlabeled product prior to

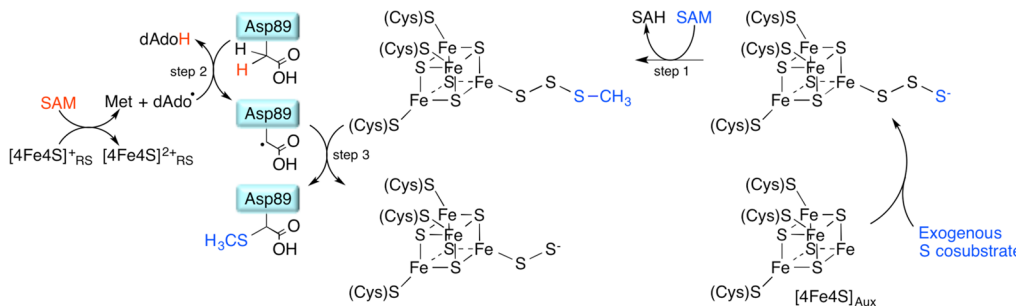


Figure 65. Proposed RimO mechanism catalyzing the methylthiolation of Asp89 of the ribosomal S12 protein.

a slower formation of labeled product.<sup>83</sup> These results indicate that the initial step of  $S_{\text{N}2}$  methyl transfer from SAM to the sulfane sulfur site at the auxiliary [4Fe–4S] cluster is rate-limiting in comparison to the ensuing more rapid radical-dependent methylthio transfer from cluster to substrate.<sup>83</sup> Interestingly, the presence of a persulfide moiety also enables for multiple turnovers per enzyme because when one sulfur is enlisted for methylthio transfer to substrate, another sulfur is then present and ready for methylation and subsequent relocation. A similar “ping pong” mechanism is proposed for the MTases, Cfr and RlmN, where product methylation proceeds first through donation of a methyl group from SAM onto an intermediate labile acceptor prior to radical-initiated methyl transfer to substrate (section 7.1.2).

These results lead to a model distinct from other sulfur insertion enzymes, in which MiaB and RimO do not cannibalize the second Fe–S cluster for sulfur donation but instead bind a sulfur ligand to the second cluster, allowing for the binding of SAM to the first cluster and, therefore, repeated turnover via activation and donation of a sulfur cosubstrate without degradation of secondary Fe–S cluster (Figure 65).<sup>318</sup> It remains to be determined how transfer of cluster-bound  $-\text{SCH}_3$  ligand takes place as well as what differences exist between RimO and MiaB to account for substrate attack at an  $\text{sp}^3$ -hybridized carbon or an aromatic carbon, respectively.

**7.4.3. Classification of MTTases.** The growing family of MTTases has been subdivided into five clades using bioinformatics analysis:<sup>141,315</sup> (1) the MiaB family and its homologues, found exclusively in bacteria and eukaryotic organelles; (2) the RimO family, found only in bacteria; (3) the MtaB family, found in eubacteria (named for methylthio-threonylcarbamoyl-adenosine transferase B), includes YqeV from *B. subtilis*; (4) the e-MtaB family, found in archaea and eukarya (named for eukaryotic methylthio-threonylcarbamoyl-adenosine B), includes CDKAL1; and (5) MTL1, found only in  $\epsilon$ -proteobacteria (named for methylthiotransferase-like family-1).

As MiaB has been shown to carry out the  $\text{i}^6\text{A}$  to  $\text{ms}^2\text{i}^6\text{A}$  modification, it is hypothesized that additional members of these clades exist that carry out the same or similar methylthio modifications. One example of yet to be identified MTTases within the MiaB clade are enzymes catalyzing an alternate modification at A-37 of tRNA; it is known that *E. coli* YrdC (and the related yeast Sua5) act in the initial base modification from A-37 to  $\text{t}^6\text{A}$ -37 in which a threonylcarbamoyl group is added onto the nitrogen- $\text{N}^6$  of the adenosine ring.<sup>319</sup> The second step of conversion must therefore involve sulfur insertion and methylation of  $\text{t}^6\text{A}$  into 2-methylthio- $\text{N}^6$ -threonylcarbamoyladenosine ( $\text{ms}^2\text{t}^6\text{A}$ ), although the enzymes involved in methylthio transfer remain to be elucidated. Moving

on to enzymes within the MtaB clade, protein products of both *ymcB*, an orthologue of *miaB*, and *yqeV*, both from *B. subtilis*, effect transfer of a methylthiolate moiety to modified  $\text{i}^6\text{A}$  and  $\text{t}^6\text{A}$  adenosine bases of tRNA to generate  $\text{ms}^2\text{i}^6\text{A}$  and  $\text{ms}^2\text{t}^6\text{A}$ , respectively. Using chimeric proteins for YmcB/YqeV followed by LC–MS analysis, they identified five conserved cysteine residues within the radical SAM domain, separate from those in the Fe–S cluster binding motif, which might be involved in substrate specificity for either the  $\text{i}^6$  or the  $\text{t}^6$  modified bases.<sup>320</sup>

Around the same time of the published work by Anton et al. on members of the MtaB family, results from Arragain and co-workers characterized a member of the e-MtaB family, human CDKAL1, showing it capable of converting  $\text{t}^6\text{A}$ -37 into  $\text{ms}^2\text{t}^6\text{A}$ -37 in tRNA.<sup>141</sup> Mutational analysis of triple Cys to Ala mutant of the radical SAM motif revealed that it lacked the desired adenine modification, indicating that the Fe–S cluster was necessary for methylthiotransferase activity. Upon reconstitution, CDKAL1 appears to bind two [4Fe–4S] clusters with UV–vis and EPR features characteristic of other radical SAM enzymes.<sup>141</sup> Using CDKAL1 pancreatic  $\beta$ -cell knockout mice, Wei et al. demonstrated that CDKAL1 carries out its MTTase activity on tRNA<sup>Lys</sup> (UUU) with no base modification present in the knockout mice.<sup>321</sup> Structural studies of the  $\text{ms}^2\text{t}^6\text{A}$  modified base in bacterial tRNA<sup>Phe</sup> show the methylthiol group functions to stabilize codon–anticodon interactions through cross-strand stacking with the base of the first nucleotide of the mRNA codon; such interactions improve translational fidelity by preventing frame shifting and misreading during translation.<sup>322</sup> While it was determined that CDKAL1 is required for precise translation of AAA and AAG codons, mistranslation of one of the two lysine codons present in the human insulin gene could be responsible for improper synthesis and/or folding of proinsulin (i.e., immature insulin), therefore leading to onset of type 2 diabetes as seen in mice.<sup>321</sup> Development of treatments aiming to improve the quality of proinsulin may be of benefit to humans carrying CDKAL1 that is not fully functional.<sup>323</sup>

## 8. DEHYDROGENATION REACTIONS BY RADICAL SAM ENZYMES

Radical SAM chemistry serves as a powerful anaerobic means to catalyze oxidation of different substrates. Radical SAM dehydrogenases are a growing class of enzymes that utilize reductive SAM cleavage to initiate two electron oxidations of organic substrates. Two types of radical SAM-dependent dehydrogenation reactions have been studied to date, and despite the different cellular processes in which the enzymes themselves are involved, the dehydrogenation reactions of the substrates are likely mechanistically similar. The following section details the biochemical characterization of members from these two classes of dehydrogenases, wherein the first type

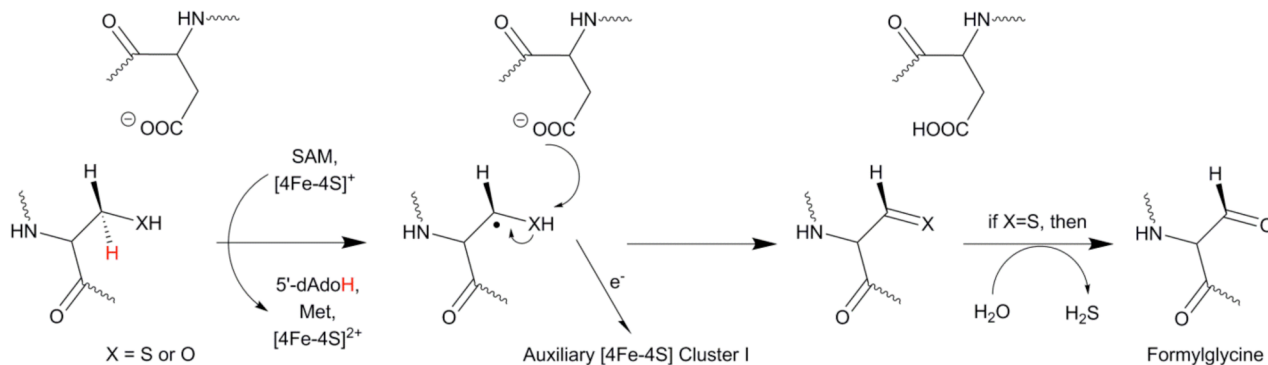


**Figure 66.** Mechanism of formylglycine generation for cysteine (anSMEcp) and serine type (AtsB/anSMEkp) sulfatase maturing enzymes. The order of H-atom abstraction and proton abstraction events has not yet been established.

invokes the oxidation of a protein bound cysteine or serine residue to an aldehyde, while the second involves the oxidation of a secondary alcohol to a ketone.

### 8.1. Formylglycine Generation during Sulfatase Maturation: The anSMEs

Arylsulfatases utilize a protein-derived formylglycine (FGly) as a cofactor in the cleavage of sulfate monoesters from a variety of substrates like sulfated polysaccharides, sulfolipids, and steroid sulfates.<sup>324</sup> Two classes of sulfatase enzymes exist, and while both utilize FGly generating enzymes (FGEs) to form FGly, the first class carries out the oxidation reaction of a cysteine residue on the target sulfatase with O<sub>2</sub>, whereas the second class catalyzes the anaerobic oxidation reactions of either cysteine or serine residues using radical SAM chemistry, and these enzymes are referred to as anaerobic sulfatase maturing enzymes (anSMEs).<sup>325</sup>

**8.1.1. AnSMEs as Radical SAM Enzymes.** AtsA is an arylsulfatase in *K. pneumonia* that is activated by the anSME AtsB, which catalyzes formylglycine generation from a conserved serine residue.<sup>326</sup> AtsB was identified as an iron–sulfur protein with three conserved cysteine motifs,<sup>326b</sup> and was predicted to belong to the radical SAM superfamily.<sup>1</sup> AtsB from *Klebsiella pneumonia* (anSMEkp) was subsequently shown to require SAM for its activity and to be inhibited by metal chelators.<sup>327</sup> An anSME from *C. perfringens*, anSMEcp, was the subject of a study that provided the first demonstration of in vitro maturation, with a conserved cysteine residue on the sulfatase as the substrate.<sup>135a</sup> This study also showed that this anSME catalyzed the reductive cleavage of SAM generating dAdoH.<sup>135a</sup>

**8.1.2. The Fe–S Clusters and Enzymatic Activities of AnSMEs.** The first detailed characterization of the iron–sulfur clusters of an anSME was published in 2008.<sup>79</sup> In this study, Grove et al. demonstrated that by coexpressing AtsB (from *K. pneumonia*) with the iron–sulfur cluster assembly machinery encoded by the *isc* operon, they could produce a soluble AtsB that bound 8.7 ± 0.4 Fe and 12.2 ± 2.6 sulfides in the isolated state, with most of the iron present in [4Fe–4S]<sup>2+</sup> clusters as determined by Mössbauer spectroscopy (Table 2).<sup>79</sup> Reconstitution with iron and sulfide yielded protein with 12.3 ± 0.2 Fe and 9.9 ± 0.4 sulfides per protein, with essentially all of the iron located in [4Fe–4S] clusters. This provided confirmation of the earlier inferences based on the presence of three cysteine motifs that AtsB bound three [4Fe–4S] clusters. When the cysteine residues of the radical SAM motif were changed to alanines by site-directed mutagenesis, the protein was found to bind approximately eight irons and sulfides,

consistent with the presence of two remaining [4Fe–4S] clusters. Kinetic studies demonstrated multiple turnovers of a peptide substrate (Table 1), with production of a 1:1 ratio of formylglycine to dAdoH, thereby indicating that SAM is consumed as a substrate in the reaction. They also demonstrated that AtsB, previously considered to be a “Ser-type” sulfatase maturation enzyme that oxidizes a serine residue on the substrate sulfatase, could also oxidize a cysteine residue in the substrate peptide, and with 4-fold greater activity.

Around the same time, another study published by Benjdia et al. arrived at the same conclusion: the anSMEs were dual substrate enzymes that could act on either cysteine or serine residues in their substrate proteins.<sup>135b</sup> Benjdia et al. purified and characterized both a Cys-type anSME (from *C. perfringens*, referred to as anSMEcp), which matures Cys-type sulfatases in vivo, and a Ser-type anSME from *Bacteroides thetaiotaomicron*, which catalyzes the maturation of only Ser-type sulfatases in vivo. The purified reconstituted enzymes from both organisms were characterized using UV–vis spectroscopy, and anSMEcp was further studied using EPR and resonance Raman spectroscopies. The results provide evidence for primarily [4Fe–4S]<sup>2+/+</sup> cluster content bound to the radical SAM motif in these enzymes (Table 2). No conclusive evidence was obtained at the time for cluster binding to the other two cysteine motifs in these proteins,<sup>135b</sup> although a subsequent study confirmed the presence of two additional [4Fe–4S] clusters.<sup>136</sup> Interestingly, Benjdia and co-workers found that peptide substrates corresponding to their target sulfatase in vivo could contain either cysteine or serine at the target residue position, and still function as substrates for formylglycine generation.

**8.1.3. Mechanistic Studies of AnSMEs.** Initially it was presumed that the mechanism of the anSMEs would involve coordination of the substrate cysteine or serine residue to one of the auxiliary iron–sulfur clusters, followed by an H-atom abstraction on the substrate’s β-C to generate a substrate radical.<sup>79</sup> Electrons transfer from the bound substrate radical to the [4Fe–4S]<sup>2+</sup> to which it is bound, accompanied by radical combination to generate a C=O double bond, or a C=S double bond that hydrolyzes to C=O, yielding formylglycine (Figure 66).<sup>79</sup> Importantly, MS analysis of assay mixtures consisting of a deuterated 17-mer peptide that comprised the sulfatase consensus motif and the [β,β<sup>2</sup>H] cysteine residue at the target position showed production of a new peptide with a mass loss of 19 Da, consistent with oxidation of the cysteinyl residue to FGly.<sup>80a</sup> Moreover, an apparent KIE of 5.6 suggested that Cβ–H/D bond cleavage serves as a rate-determining step

in the reaction. HPLC coupled to MS and NMR analysis also demonstrated that substrate derived deuterium was incorporated into 20–30% of the dAdoH produced, confirming that the 5'-deoxyadenosyl radical abstracted the  $\beta$ -C H-atom during the oxidation of cysteine to FGly.<sup>80a</sup> Importantly, assays performed with threonyl and *allo*-threonyl containing peptides located at the target position respectively show ketone product formation with varying efficiency, suggesting that the 5'-deoxyadenosyl radical stereospecifically abstracts the pro-S H-atom from the cysteine substrate.<sup>80b</sup>

The role of the auxiliary clusters during catalysis has been somewhat a matter of debate. Evidence in support of their role in binding substrate is lacking, and in fact recent site-directed mutagenesis experiments have shown that individual substitutions of the conserved cysteine residues in AtsB typically result in expression of insoluble proteins, implicating these cysteines in coordination of accessory Fe–S clusters that play a role in stabilizing the protein architecture.<sup>80b</sup> Berteau and co-workers demonstrated that the two auxiliary [4Fe–4S] clusters were both necessary to obtain efficient cleavage of SAM, suggesting that the accessory clusters may be involved in shuttling electrons to and/or from the radical SAM active site during catalysis.<sup>136</sup> By monitoring flavodoxin semiquinone levels during anSMEcp turnover, Grove and co-workers have now shown that the electron generated from substrate oxidation is ultimately transferred back to oxidized flavodoxin, and the authors indicate that this probably occurs via the movement of the electron through the auxiliary [4Fe–4S] clusters.<sup>80b</sup> This observation opens the possibility for the enzyme to recycle electrons over multiple catalytic events, assuming the external electron acceptor species (like flavodoxin) can in turn then reduce the radical SAM [4Fe–4S]<sup>2+</sup> cluster. Along these lines, recent X-ray crystallographic results of the anSMEcp protein (which are detailed below) have unequivocally demonstrated that the accessory clusters are not involved in substrate coordination and appear to confirm the role of these clusters in acting as conduits for inter- and intramolecular electron flow.

**8.1.4. Structure of anSME and Clarification of the Role of the Auxiliary Clusters.** Structures of anSMEcp with SAM bound with and without peptide substrate show the ( $\beta\alpha$ )<sub>6</sub> partial TIM barrel with an N-terminal radical SAM [4Fe–4S] cluster coordinated by SAM in the same configuration commonly observed (Figure 67).<sup>328</sup> Importantly, each structure shows two C-terminal [4Fe–4S] clusters fully ligated by protein derived cysteine residues. The distance from the SAM cluster to the auxiliary cluster is 16.9 Å while the distance to the auxiliary II cluster is 26.7 Å away; the two auxiliary clusters are bound at a distance of 12.9 Å from one another. The structures with two separate peptide substrates bound reveal that the C $\beta$  target cysteine residue is positioned at a distance of 4.1 Å from the 5'-carbon of SAM, thus nicely orienting the pro-S H-atom for abstraction. Importantly, the target cysteine residues of the peptides do not ligate either auxiliary cluster, and, when bound, the cysteine to be modified is located 8.9 Å from the radical SAM cluster, 8.6 Å from cluster I, and 20.8 Å from cluster II. Given the available biochemical data summarized above and the distances observed in the peptide bound structures, the authors suggest that auxiliary cluster I is the immediate electron acceptor accompanying oxidation of the cysteinyl radical to FGly, with auxiliary cluster II serving as a redox center for the subsequent oxidation of cluster I (Figure 66). The general base responsible for deprotonation of the cysteine side chain during

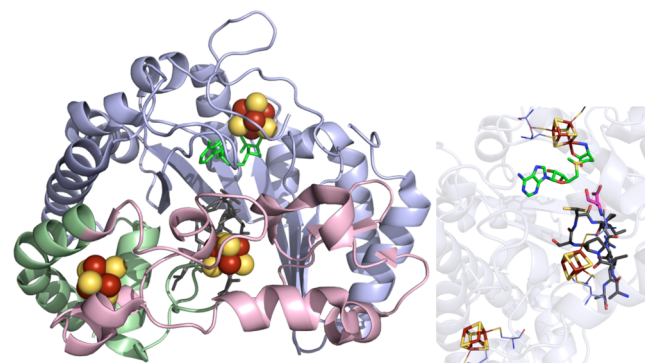


**Figure 67.** anSME crystal structure (PDB ID 4K39). Left: N-terminal/radical SAM domain colored in light blue, SPASM domain in light pink, remaining two  $\alpha$ -helices in light green, [4Fe–4S] clusters in yellow and rust spheres, SAM in green, and peptide in gray sticks. Right: Active site of anSME where the [4Fe–4S] clusters (yellow and rust), SAM (green carbons), and peptide (gray carbons) depicted in sticks with oxygens colored red and nitrogens colored blue. D277 (magenta carbons, depicted in sticks) has been identified as the catalytic base (see Figure 66). Cysteines (light blue carbons) involved in ligating clusters are depicted in lines.

catalysis was assigned to Asp277, and activity assays performed with an D277N mutant retained  $\leq 1\%$  of the ability to generate FGly.<sup>328</sup>

The anSME active site is buried in a cleft created by the radical SAM and the C-terminal SPASM domains requiring the target peptide to adopt a tight turn upon binding. Similar to the PFL-AE Gly-peptide structure, the substrate analogue bound anSME structure shows that this system also relies on activase derived backbone hydrogen-bonding interactions to bind and stabilize the peptide substrate, which potentially may act as a generic binding mode for radical SAM enzymes that act on other proteins as their substrates (section 3.1 and Figure 18). The anSME structure is the first for an enzyme harboring the SPASM domain, which is representative of a subfamily of radical SAM comprising  $\sim 1400$  members each containing a 7-cysteine motif (CX<sub>9–15</sub>GX<sub>4</sub>C-gap-CX<sub>2</sub>CX<sub>5</sub>CX<sub>3</sub>C-gap-C), which coordinates additional Fe–S clusters in these enzymes.<sup>328</sup> The first part of the SPASM domain containing two cysteines has been previously visualized in the MoaA structure (MoaA lacks a full SPASM domain as its sequence terminates shortly after the two cysteine residues, thus providing a site for substrate binding to the auxiliary cluster) (section 6.1).<sup>240,242</sup> Goldman and co-workers note that these two cysteines flank a beta hairpin region (referred to as a twitch subdomain) that extends the  $\beta$  sheet of the radical SAM core domain and in both enzymes is associated with Fe–S cluster coordination; the auxiliary cluster I in anSME superimposes over the position of the accessory cluster in MoaA.<sup>328</sup> Intriguingly, additional parallels to non-SPASM harboring radical SAM enzymes certainly appear to exist as the twitch subdomain shares high sequence homology with the BtrN dehydrogenase enzyme (see below).<sup>328</sup> BtrN binds a single accessory [4Fe–4S] cluster, and the link between anSME and MoaA suggests that the SPASM/twitch subfamily may be a structural motif utilized more generally by approximately 16% of uncharacterized radical SAM enzymes that coordinate auxiliary Fe–S clusters.<sup>328</sup>

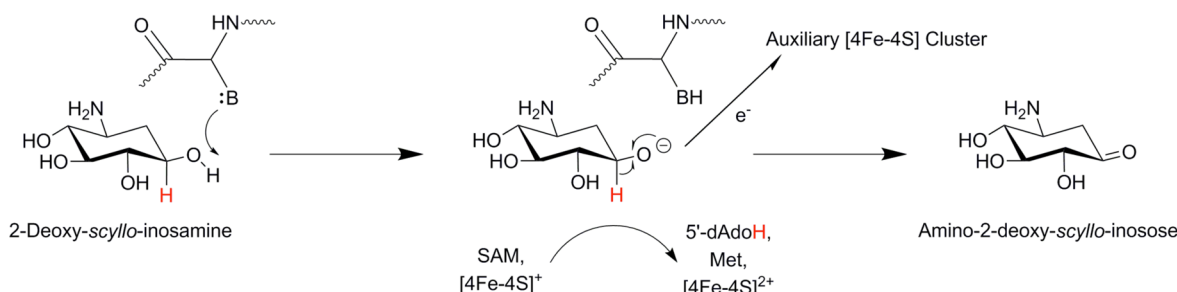


**Figure 68.** The dehydrogenation reaction catalyzed by BtrN during butirosin biosynthesis. The order of H-atom abstraction and proton abstraction events has not yet been definitively established, and along these lines it has only recently been suggested that formation of the  $\alpha$ -hydroxylalkyl radical by H-atom abstraction may activate the C3-hydroxyl functional group by decreasing its  $pK_a$ . Goldman et al. have identified the putative base involved in catalysis as being Arg152.<sup>328</sup>

## 8.2. Dehydrogenation in Antibiotic Synthesis: BtrN and the Synthesis of Butirosin

The gene cluster encoding for the biosynthesis of butirosin, a 2-deoxystreptamine containing aminoglycoside antibiotic, includes an open reading frame encoding the protein, BtrN, containing the canonical radical SAM cysteine motif ( $\text{CX}_3\text{CX}_2\text{C}$ ). Eguchi and co-workers demonstrated that BtrN catalyzes the oxidation of the secondary alcohol 2-deoxy-scylloinosamine (DOIA) to the ketone 3-amino-2,3-dideoxy-scylloinosose (amino-DOI) under anaerobic conditions in a SAM-dependent reaction, with one SAM cleaved producing one dAdoH and one methionine per DOIA oxidized (Figure 68).<sup>76a</sup> Assays carried out with [ $3^2\text{H}$ ]-DOIA result in the production of a mixture of unlabeled, monodeuterated, and dideuterated dAdoH, demonstrating that the dehydrogenation reaction is initiated by abstraction of an H-atom from the C3 position of DOIA.<sup>76a</sup> The observation of multiply deuterated dAdoH further indicates that the H-atom abstraction step is reversible and can occur multiple times prior to reaction with substrate.<sup>76a</sup> EPR spectroscopic studies carried out at 50 K under steady-state turnover conditions using either unlabeled DOIA or [ $2,2^2\text{H}_2$ ]-DOIA have provided evidence for a radical intermediate at C3 of DOIA.<sup>76b</sup> When EPR measurements were carried out at 10 K during steady-state turnover, multiple [4Fe–4S] species were observed, and by comparison to samples of enzyme with and without SAM, two of these species were assigned as the unbound ( $g = 1.92, 2.04$ ) and bound ( $g = 1.83, 1.99$ ) forms of the [4Fe–4S]<sup>+</sup> state of the enzyme (Table 2).<sup>76b</sup> The third EPR-active species ( $g = 1.87, 1.96, 2.05$ ) was assigned as the BtrN/SAM/DOIA ternary complex by comparison to the EPR spectra of enzyme–substrate and enzyme–product complexes (Table 2).<sup>76b</sup>

Through mutagenesis studies, BtrN was subsequently shown to contain not one, but two [4Fe–4S] clusters after reconstitution.<sup>137</sup> Upon generation of a BtrN variant in which the three cysteines of the radical SAM motif were changed to alanine residues, the enzyme only bound a single [4Fe–4S] cluster based on quantitative elemental analyses and Mössbauer characterization (Table 2).<sup>137</sup> Outside of the radical SAM cysteine motif in BtrN, there are five additional cysteine residues. Generation of variants in which each of these cysteinyl residues are changed to alanines revealed that while variant C69A behaved like wild-type protein, the C235A variant produced less soluble protein with bound Fe–S clusters but displayed turnover activity ≤10% of wild type; the remaining mutations at positions Cys169, Cys187, and Cys232 yielded insoluble proteins.<sup>137</sup> These results suggest that these residues

serve as ligands to the second [4Fe–4S] cluster, which was initially thought to be site differentiated and coordinate substrate at its unique iron site.<sup>137</sup> Coordination of the C3 hydroxyl of DOIA would facilitate deprotonation of this group, as well as H-atom abstraction by the dAdO<sup>•</sup>. Electron transfer from the resulting substrate radical to the coordinated [4Fe–4S]<sup>2+</sup> cluster could occur via an inner-sphere mechanism yielding the oxidized product. This electron added to the auxiliary [4Fe–4S] cluster could then be transferred back to the radical SAM cluster, regenerating the enzyme for catalysis. Interestingly, Grove et al. observed an axial EPR signal ( $g = 1.83, 1.99$ ) during enzyme turnover similar to that reported by Yokoyama; while Yokoyama assigned this to the BtrN–SAM complex, Grove et al. ultimately assigned this signal to the reduced auxiliary cluster as the signal is unlike that of any radical SAM protein (Table 2).<sup>76b,137</sup> This auxiliary cluster could not be reduced by chemical means, likely due to its exceptionally low redox potential or inaccessibility to reducing agents, results that future work will hopefully clarify.<sup>137</sup>

Several aspects of the mechanism and role of the auxiliary cluster in BtrN have been clarified by the recent determination of the X-ray structure of this enzyme in substrate free and bound states (Figure 69).<sup>328</sup> First, the structures reveal that the auxiliary cluster is fully protein ligated both in the presence and in the absence of DOIA, clearly ruling out that the possibility that the cluster coordinates substrate and is involved in its deprotonation; the DOIA substrate is instead bound in a hydrophilic pocket located between the radical SAM and

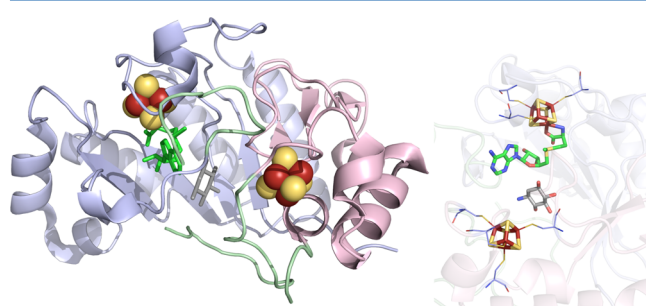


**Figure 69.** BtrN crystal structure (PDB ID 4M7T). Left: Radical SAM domain colored in light blue, C-terminal domain in light pink, linker regions in light green, [4Fe–4S] clusters in yellow and rust spheres, SAM in green, and DOIA in gray sticks. Right: Active site of BtrN where the [4Fe–4S] clusters (yellow and rust), SAM (green carbons), and DOIA (gray carbons) depicted in sticks with oxygens colored red and nitrogens colored blue. Cysteines (light blue carbons) involved in ligating clusters are depicted in lines.

auxiliary FeS clusters. Moreover, the BtrN structure reveals that the enzyme is designed to avoid a DesII-like elimination reaction (section 10.3), given the existence of hydrogen-bonding interactions with the functional group of substrate and the observation that DOIA binds in an equatorial chair conformation. These observations coupled with those made by Grove et al.<sup>80b</sup> suggest that the auxiliary cluster in BtrN functions as an electron acceptor during the dehydrogenation reaction, possibly driving the oxidation of the intermediate radical species. While the order of H-atom abstraction and proton abstraction events are not yet resolved (Figure 68), it has only recently been suggested that formation of the  $\alpha$ -hydroxyalkyl radical by H-atom abstraction may activate the C3-hydroxyl functional group by decreasing its  $pK_a$ .<sup>328</sup> Furthermore, Goldman et al. have identified the putative base involved in catalysis as being Arg152, although experimental confirmation of this is still needed.<sup>328</sup>

## 9. FORMATION OF NEW C–C, C–N, AND C–S BONDS

### 9.1. The Synthesis of Pyrroloquinoline Quinone: PqqE

Pyrroloquinoline quinone (PQQ) is a prokaryotic cofactor derived from the post-translational modification of and then excision from a peptide. The biosynthesis of PQQ requires the *pqq* operon, which encodes six gene products designated PqqA–F.<sup>237,329</sup> PqqA is a 23-residue peptide that is thought to be the substrate for PQQ biosynthesis.<sup>329b</sup> A key step in the biosynthesis of PQQ involves the fusion of glutamate and tyrosine, which are strictly conserved in PqqA, to form the intermediate AHQQ (3a-(2-amino-2-carboxyethyl)-4,5-dioxo-4,5,6,7,8,9-hexahydroquinoline-7,9-dicarboxylic acid) (Figure 70);<sup>330</sup> in vivo experiments indicate both PqqA and PqqE are required for this initial biosynthetic step,<sup>329b</sup> although the details remain elusive. AHQQ is subsequently converted to

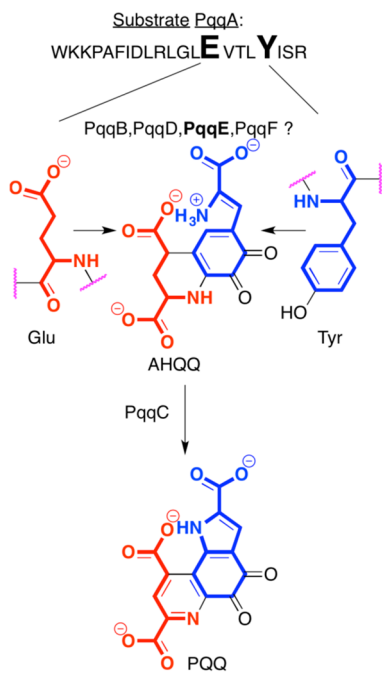


**Figure 70.** Involvement of radical SAM enzyme PqqE in pyrroloquinoline quinone (PQQ) biosynthesis. PqqE is proposed to be involved in the condensation of peptide residues Glu and Tyr, but its specific substrate is unknown.

PQQ in an 8-electron oxidation and cyclization catalyzed by PqqC.<sup>331</sup> The functions of PqqD, PqqB, and PqqF have not been experimentally determined, although the latter two are thought to function as proteases based on sequence alignments.

PqqE contains the canonical radical SAM cysteine motif CX<sub>3</sub>CX<sub>2</sub>C in its N-terminal region as well as a second C-terminal cysteine motif.<sup>332</sup> When PqqE from *Klebsiella pneumonia* was heterologously overexpressed in *E. coli* and purified under strictly anaerobic conditions, it was found to be a dark red-brown protein with 10.4 ± 0.9 Fe and 7.0 ± 1.0 inorganic sulfide per protein.<sup>140a</sup> The UV-vis spectrum showed features at 390, 420, and 550 nm, and EPR spectroscopy revealed a small isotropic signal at g = 2.01 attributed to a [3Fe–4S]<sup>+</sup> cluster accounting for 0.01 spin/protein (Table 2). Reduction of this purified protein with dithionite results in bleaching of the visible absorption features and appearance of a rhombic EPR signal with g = 2.06, 1.96, and 1.91 attributed to a [4Fe–4S]<sup>+</sup> cluster (0.17 spin/protein) (Table 2).<sup>140a</sup> Addition of SAM results in modest changes in the EPR spectral features. PqqE has also been shown to cleave SAM in the presence of the reducing agent dithionite with multiple turnovers observed in the presence of excess reductant. This reductive cleavage of SAM appears to be an uncoupled reaction, because no substrate was provided and there was no evidence for PqqE itself serving as the substrate. Interestingly, when the PqqE-catalyzed reductive cleavage of SAM is carried out in D<sub>2</sub>O, deuterium is found to be incorporated into the product dAdoH, indicating that the dAdo<sup>•</sup> intermediate abstracts a H-atom from an exchangeable site, or is reduced and then abstracts a proton from an exchangeable site. When assays of PqqE were carried out in the presence of the putative substrate PqqA, however, no modification of the PqqA peptide was observed. It was postulated that perhaps one of the other gene products of the *pqq* operon was required, in addition to PqqE, to catalyze the initial reaction in PQQ biosynthesis.<sup>140a</sup> A possible link between PqqE and PqqD was suggested by BLAST searching that revealed a number of putative radical SAM proteins with a fused PqqD domain, including AlbA (section 9.3.1).<sup>140b</sup> Hydrogen/deuterium exchange experiments provided evidence for interaction between PqqE and PqqD, as the presence of PqqE provided partial protection of PqqD to H/D exchange.<sup>140b</sup> Further, the addition of PqqD to reduced PqqE significantly altered the EPR spectral features associated with the [4Fe–4S]<sup>+</sup> cluster of the latter. Additional evidence for interaction of the two proteins was provided by far-UV CD data. PqqE and PqqD therefore appear to interact; however, even with both proteins present, no modifications in PqqA were observed under conditions where SAM is reductively cleaved.<sup>140b</sup> It may be that PqqA requires initial modification, for example, hydroxylation of the conserved tyrosine, prior to the radical SAM reaction catalyzed by PqqE.<sup>140b</sup>

### 9.2. Modification of tRNA at G37 To Generate Wybutosine: TYW1

Another radical SAM involved in the post-translational modification of nucleosides is one that acts in the complex tricyclic base modification of a guanosine at position 37 in tRNA. Generation of the modified residue to wybutosine (yW) is potentially important in stabilizing codon–anticodon interactions through base-stacking, as well as in reinforcing the reading frame. To determine the genes responsible for yW biosynthesis in *Saccharomyces cerevisiae*, ribonucleome analysis was employed and resulted in the identification of four new

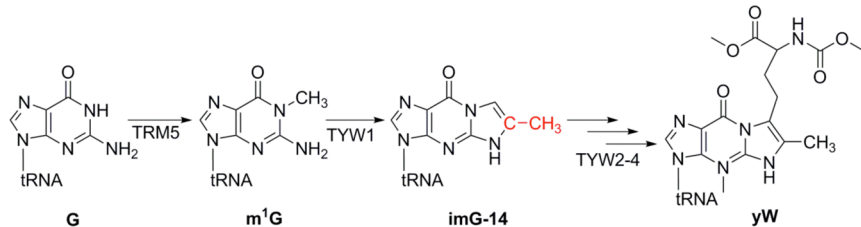


**Figure 71.** The biosynthesis of yW. G at position 37 is transformed to imG-14 through the actions of TRM5 and TYW1, which is subsequently converted to yW through the actions of TYW2, TYW3, and TYW4.

genes, *tyw1–4*, as those involved in the multistep modification pathway.<sup>333</sup> Sequence alignments of various TYW1 homologues established the presence of the Fe–S cluster-binding CX<sub>3</sub>CX<sub>2</sub>C motif as well as the SAM-coordinating GGE motif; mutation of any one of the cysteines or the glutamate completely abolished yW synthesis.<sup>333</sup> It was shown that a  $\Delta tyw1$  strain accumulated *N*-methylguanosine (m<sup>1</sup>G), which is the product of the first step of the modification of guanosine known to be catalyzed by TRM5; this therefore indicated that TYW1 was responsible for the second step of the reaction, condensation of m<sup>1</sup>G with an unknown 2-carbon fragment to form 4-demethylwyosine (imG-14) (Figure 71).<sup>334</sup>

The second substrate required for conversion of m<sup>1</sup>G to imG-14 was identified by Young and Bandarian, who assayed TYW1 under anaerobic reducing conditions in the presence of SAM, tRNA<sup>Phe</sup>, and TRM5 (to convert G to m<sup>1</sup>G), along with each one of four potential carbon donors: acetyl-CoA, acetyl phosphate, phosphoenolpyruvate, and pyruvate.<sup>335</sup> Only pyruvate led to successful conversion from m<sup>1</sup>G to imG-14. Further, assays carried out with [1-<sup>13</sup>C]-, [2-<sup>13</sup>C]-, and [3-<sup>13</sup>C]-pyruvate revealed that both C2 and C3 of pyruvate are incorporated into the tricyclic ring of yW.

In addition to the radical SAM cluster bound to the CX<sub>3</sub>CX<sub>2</sub>C motif, TYW1 binds a second [4Fe–4S] cluster, and thus falls into a subgroup of radical SAM enzymes (including BioB, LipA, MoaA, and MiaB) that bind a second iron–sulfur cluster (sections 4.1, 4.2, 6.1, and 7.4.1).<sup>142</sup> The second cluster in TYW1, however, is bound to a CX<sub>12</sub>CX<sub>12</sub>C motif in the N-terminal region of the protein in a domain that is not homologous to the region binding the second cluster in these other proteins.<sup>142</sup> UV-visible, EPR, and Mössbauer spectroscopic studies have been carried out on the reconstituted enzyme from *Pyrococcus abyssi*, showing that in the as-reconstituted state it binds primarily [4Fe–4S]<sup>2+</sup> clusters (Table 2), with a total of two [4Fe–4S] clusters per protein.<sup>142</sup> While addition of SAM did not perturb the spectroscopic features, addition of pyruvate was found to introduce a shoulder in the Mössbauer spectrum at high velocity, indicative of an iron becoming more ferrous in nature presumably due to pyruvate coordination to a unique site.<sup>142</sup> Reduction of the protein produces a complex EPR spectrum that is interpreted as resulting from the superposition of two [4Fe–4S]<sup>+</sup> S = 1/2 signals (Table 2). Addition of SAM significantly perturbs one cluster signal while leaving the other essentially unchanged, consistent with coordination of SAM to one cluster. HYSCORE data for this reduced enzyme–SAM complex provide evidence for nitrogen coordination to the cluster. Interestingly, addition of pyruvate to the reduced enzyme–SAM complex leaves the SAM-cluster signal unchanged but causes the second cluster signal to disappear; the loss of the second cluster EPR signal was shown, using Mössbauer

spectroscopy, to be a result of cluster oxidation to the [4Fe–4S]<sup>142</sup> state.

The crystal structure of TYW1 in its apo-state (Figure 72) was solved several years before the spectroscopic character-

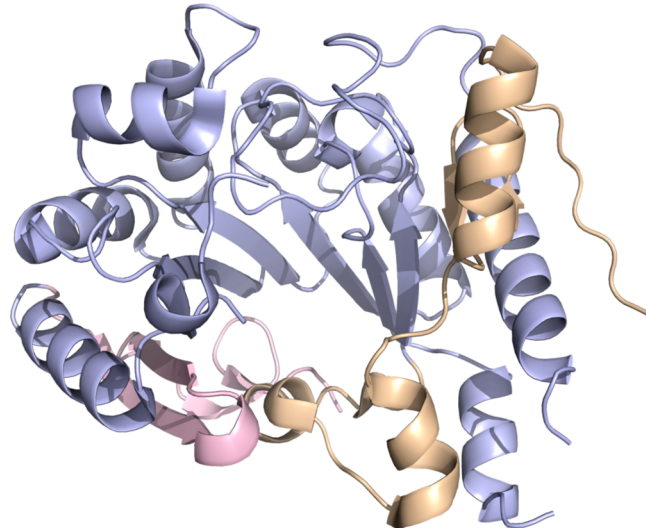


**Figure 72.** phTYW1 crystal structure (PDB ID 2YX0). N-terminal domain colored in wheat, radical SAM domain in light blue, and C-term domain in light pink.

ization of the clusters just described. As with other radical SAM enzymes, it adopts a partial ( $\beta\alpha$ )<sub>6</sub> TIM barrel; although no clusters could be resolved in the solved structure, the presence of two sets of three cysteine residues suggested the possibility of two iron–sulfur cluster binding sites. The radical SAM cluster site is within the partial TIM barrel and to one side of a positively charged cleft.<sup>336</sup> The second cluster binding site is located opposite the cleft from the radical SAM cluster binding site and near the putative tRNA substrate binding site. A conserved Lys41 known to be required for in vivo activity was found to lie next to the second Fe–S cluster binding site.<sup>336</sup>

Two different mechanistic proposals for TYW1 catalysis have been put forth recently, and these are summarized nicely in a recent review.<sup>337</sup> One of these mechanistic proposals, illustrated in Figure 73, involves covalent catalysis whereby pyruvate forms a Schiff base with Lys41. Radical SAM-based H-atom abstraction from m<sup>1</sup>G generates a substrate radical that then reacts with pyruvate. The second cluster is proposed to play a redox role, donating or accepting an electron to/from pyruvate to form formate or CO<sub>2</sub>, respectively. Subsequent transimination and deprotonation generates imG-14.

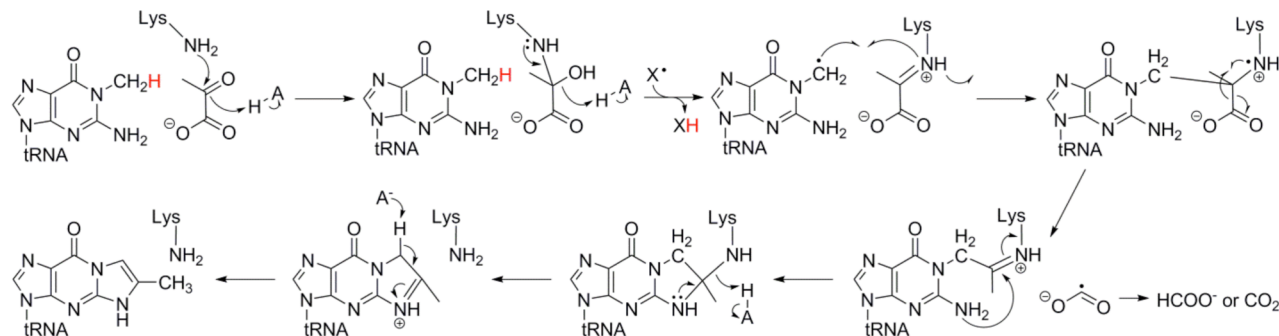


Figure 73. Proposed mechanism for the conversion of *N*-methylguanosine ( $m^1G$ ) to 4-demethylwyosine (img-14) catalyzed by TYW1.

### 9.3. Catalysis of Thioether Cross-Link Formation in Antimicrobial Peptides

A growing number of ribosomally synthesized antimicrobials containing post-translational modifications involving a Cys-to- $\alpha$ -C thioether linkage are being discovered, collectively known as sactipeptides.<sup>338</sup> In several known cases, biosynthesis of these sactipeptides requires a radical SAM enzyme, as described in the following sections.

**9.3.1. AlbA and the Synthesis of Subtilisin A.** Subtilisin A is a ribosomally synthesized natural product produced by *B. subtilis* with demonstrated antimicrobial and spermicidal activity.<sup>339</sup> It is a head-to-tail cyclized 35-residue peptide with three thioether bonds linking three cysteine residues to the  $\alpha$ -carbons of two phenylalanines and one threonine (Figure 74).<sup>340</sup> These sulfur to  $\alpha$ -carbon linkages

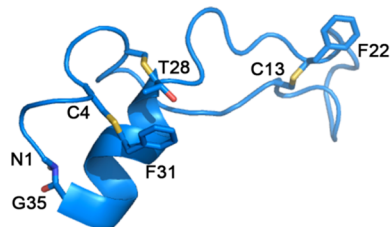


Figure 74. Solution NMR structure of Subtilisin A (PDB ID 1PXQ).

have so far been found in four other bacterial natural products.<sup>338</sup> Biosynthesis of subtilisin A requires the *sbo-alb* operon, with *sboA* and *sboX* encoding precursor peptides and *albA-G* encoding proteins required for processing and export of, as well as immunity to, subtilisin A.<sup>341</sup> AlbA and AlbF have been implicated in the cyclization and cross-linking of the peptide precursor.<sup>341b</sup> AlbA contains the canonical CX<sub>3</sub>CX<sub>2</sub>C motif of the radical SAM enzymes, and recent biochemical and spectroscopic characterization confirms that is a member of this diverse superfamily.<sup>86</sup> Purified AlbA reconstituted with iron and sulfide contains 7.6 ± 0.3 Fe and 7.7 ± 0.4 sulfide per protein, and exhibits UV-vis spectroscopic features characteristic of an iron–sulfur protein. The EPR spectrum of the as-reconstituted enzyme is nearly featureless; however, upon reduction with dithionite an EPR signal ( $g = 2.03, 1.92$ ) appears that is characteristic of a [4Fe–4S]<sup>+</sup> cluster (Table 2).<sup>86</sup> Mutation of the cysteines of the CX<sub>3</sub>CX<sub>2</sub>C motif to alanines resulted in protein that contained less iron (~5 per protein) but still had characteristic UV-vis and EPR spectroscopic features of [4Fe–4S] clusters, supporting the hypothesis that AlbA binds a second [4Fe–4S] cluster in addition to the radical SAM cluster. AlbA was also found to catalyze the reductive cleavage of SAM

to produce dAdoH and methionine; however, this activity was abolished in the triple Cys to Ala variant of the radical SAM cysteine motif. AlbA was shown to catalyze the maturation of subtilisin A from the precursor peptide in vitro, and the second iron–sulfur cluster was found to be required for formation of all three thioether linkages.<sup>86</sup> A proposed mechanism for AlbA is shown in Figure 75.

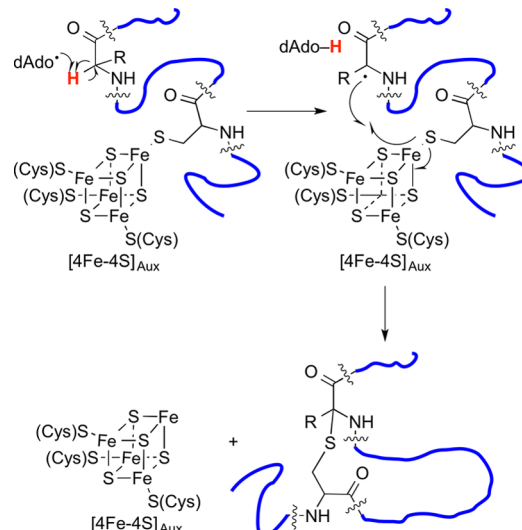
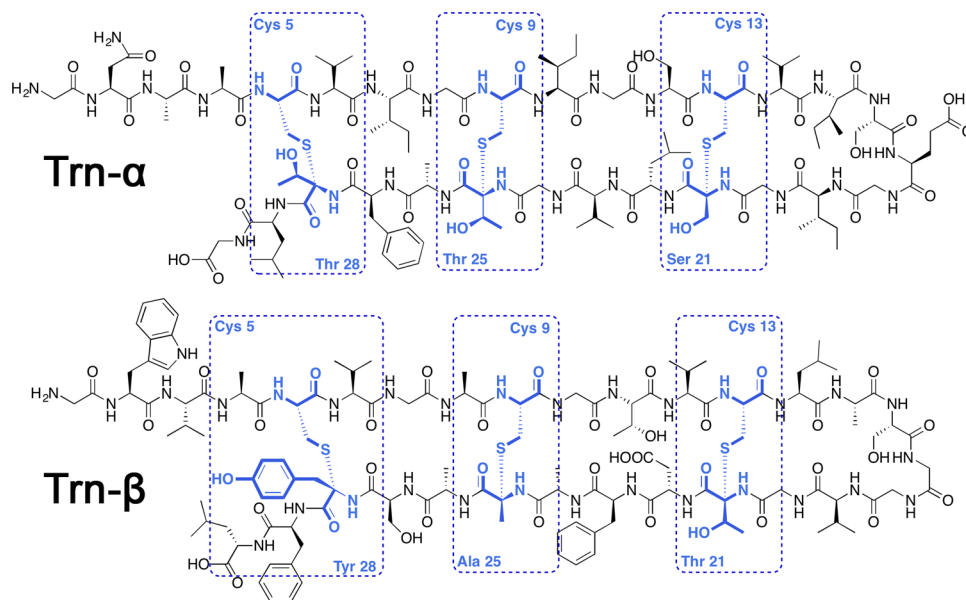


Figure 75. Proposed hydrogen atom abstraction mechanism in thioether bond formation observed for radical SAM enzymes AlbA and SkfB.

**9.3.2. Biosynthesis of Thuricin CD.** Thuricin CD is a two-component bacteriocin active against *C. difficile* recently isolated from human fecal matter.<sup>342</sup> Thuricin CD, like subtilisin A, contains three thioether cross-links between cysteine residues and the  $\alpha$ -carbons of the modified amino acids, which are two threonines and a serine in Trn $\alpha$  and one tyrosine, one alanine, and one threonine in Trn $\beta$  (Figure 76).<sup>342,343</sup> Sequencing of the *thuricin CD* operon revealed that two gene products, TrnC and TrnD, belong to the radical SAM protein superfamily.<sup>342</sup> Genome mining based on the TrnC and TrnD radical SAM proteins has revealed 15 additional thuricin CD-like gene clusters in a variety of environments.<sup>344</sup>

**9.3.3. Biosynthesis of Thurincin H.** Thurincin H is a bacteriocin produced by *Bacillus thuringiensis* SF361 that is derived from a 31 amino acid peptide. Thurincin H has recently been shown to contain four cysteine-to- $\alpha$ -carbon thioether cross-links, with each cross-link appearing to have the D configuration at the  $\alpha$ -carbon.<sup>345</sup> The operon for thurincin H



**Figure 76.** Thuricin CD, like subtilisin A, contains three thioether cross-links between cysteine residues and the  $\alpha$ -carbons of the modified amino acids, which are two threonines and a serine in Trn $\alpha$  and one tyrosine, one alanine, and one threonine in Trn $\beta$ .

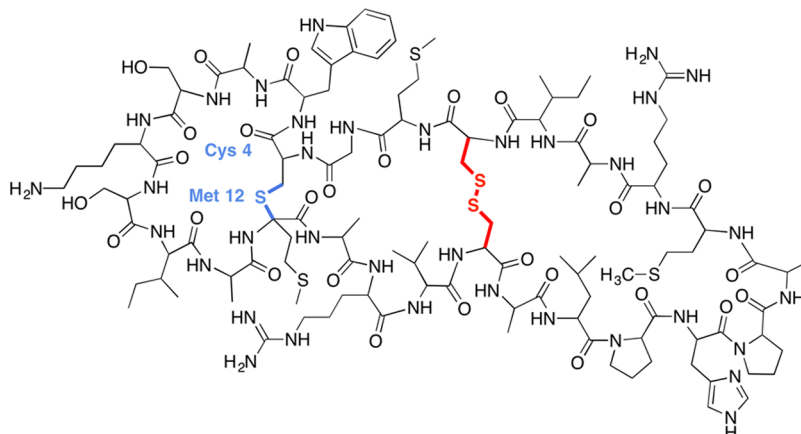


**Figure 77.** Structure of sporulation killing factor (SKF). The thioether bond is highlighted in blue, while the cysteine disulfide bond is highlighted in red.

production includes 10 open-reading frames, three of which are tandem repeats of the gene encoding the precursor peptide.<sup>346</sup> One of the seven remaining open-reading frames, designated ThnB, has sequence characteristics of the radical SAM superfamily.<sup>346</sup> Although ThnB has not yet been biochemically characterized, the similarity between its putative reaction and those catalyzed by TrnC, TrnD, SkfB, and AlbA suggests that its properties will be similar to these enzymes.<sup>345</sup>

**9.3.4. SkfB and the Maturation of Sporulation Killing Factor.** Sporulation killing factor (SKF, Figure 77),<sup>347</sup> like subtilisin A and thuricin CD, is a head-to-tail cyclic peptide.<sup>348</sup> SKF contains a single thioether cross-link between a cysteine residue and the  $\alpha$ -carbon of a methionine residue.<sup>348</sup> The *skf* operon includes four genes required for generation of SKF; these include *skfA*, encoding the 55 residue precursor peptide, and *skfB*, with sequence features of a radical SAM enzyme.<sup>347</sup> Two additional genes in the operon are required for export and immunity, while a seventh gene is of unknown function.<sup>347</sup> Purified SkfB can be reconstituted with iron and sulfide to yield a protein containing  $8.29 \pm 0.07$  Fe and  $8.36 \pm 0.14$  S per protein, and UV-vis and EPR spectroscopic data are consistent

with the presence of at least one [4Fe–4S] cluster (Table 2).<sup>143</sup> When the cysteines in the CX<sub>3</sub>CX<sub>2</sub>C radical SAM motif are changed to alanines by site-directed mutagenesis, the reconstituted enzyme contains  $4.5 \pm 0.2$  Fe per protein and has UV-vis and EPR spectral features that are consistent with the presence of a [4Fe–4S] cluster.<sup>143</sup> Thus, the wild-type SkfB appears to have two [4Fe–4S] clusters. The reconstituted enzyme is capable of catalyzing the reductive cleavage of SAM under reducing conditions.<sup>143</sup> Further, HPLC–MS analysis was used to demonstrate that SkfB catalyzes the formation of a single thioether bond in the precursor peptide SkfA.<sup>143</sup> A C4S substitution in SkfA abolished cross-link formation, indicating that SkfB was not capable of ether bond formation. Further, switching the position of the cysteine and the methionine involved in the cross-link also abolished thioether bond formation, demonstrating specificity of SkfB for the directionality of the thioether linkage. Interestingly, the methionine involved in the thioether linkage could be changed to a number of hydrophobic or aromatic amino acids while retaining full ability to form the thioether linkage, while replacing the methionine with hydrophilic amino acids reduced or eliminated

thioether bond formation; these results suggest the presence of a hydrophobic pocket at the acceptor site of thioether bond formation that is critical for catalysis.<sup>143</sup> An SkfB variant in which the cysteines of the second cluster were changed to alanines was able to bind a [4Fe–4S] cluster (Table 2) and to reductively cleave SAM; however, the ability to catalyze thioether bond formation was abolished, demonstrating the importance of the second [4Fe–4S] cluster in the enzymatic mechanism.<sup>143</sup> A mechanism for SkfB that is similar to that for AlbA has been proposed (Figure 7S).

## 10. USING RADICAL SAM CHEMISTRY TO CLEAVE C–X (X = C, N, P) BONDS

### 10.1. Cleavage of the $\alpha$ – $\beta$ Bond of Amino Acids: ThiH

Thiamine pyrophosphate (TPP) biosynthesis follows distinct pathways in anaerobic and aerobic organisms, given the presence of ThiH in anaerobes and ThiO in aerobes. However, these two pathways converge in the synthesis of the common intermediate dehydroglycine (DHG), which in anaerobes is formed via tyrosine cleavage and in aerobes is formed through the oxidation of glycine (Figure 40 and section 6.2).<sup>284b,249</sup> Following its production, dehydroglycine is ultimately incorporated into 4-methyl-5-( $\beta$ -hydroxyethyl)-thiazole phosphate carboxylate on the pathway to formation of thiamine pyrophosphate in a multistep process involving ThiG, ThiF, ThiI, IscS, and 1-deoxyxylulose-5-phosphate.<sup>255a</sup>

Early genetic studies revealed a connection between thiamine synthesis and Fe–S cluster metabolism in *Salmonella enterica* and suggested a role for ThiH in this process.<sup>350</sup> It was soon discovered that ThiH likely belonged to the radical SAM superfamily, and subsequent mutational analysis of *Salmonella enterica thiH* demonstrated the conserved site-differentiated [4Fe–4S] cluster and SAM binding motifs were required for the in vivo function of the enzyme.<sup>1,351</sup> Initial characterization of ThiH showed that it purified with nearly 1:1 stoichiometry with ThiG.<sup>101a</sup> Spectroscopic analysis of ThiGH samples demonstrated the purified sample's [3Fe–4S]<sup>+</sup> EPR signal could be converted to an axial [4Fe–4S]<sup>+</sup> signal upon treatment with dithionite (Table 2). Importantly, thiazole synthase activity in *E. coli* lysate mixtures was stimulated upon addition of purified ThiGH, SAM, and a reducing agent and depended upon addition of tyrosine, leading to the proposal that the deoxyadenosyl radical was responsible for initiating tyrosyl radical formation.<sup>352</sup> Reconstitution of purified ThiGH resulted in a significant increase in [4Fe–4S]<sup>2+/+</sup> content (Table 2). Subsequent addition of SAM to reduced samples resulted in a concomitant perturbation of the reduced cluster's axial signal, providing direct evidence that ThiH coordinated a site-differentiated cluster capable of interacting with SAM.<sup>284b</sup> Conversely, spectral analysis of reduced samples exposed to both SAM and tyrosine showed a significant decrease in the amount of [4Fe–4S]<sup>+</sup> signal present, suggesting that tyrosine triggered the reduced [4Fe–4S]<sup>+</sup> cluster to cleave SAM, generating the diamagnetic [4Fe–4S]<sup>2+</sup> state.

Turnover experiments performed with L-[U-<sup>14</sup>C]-tyrosine and S-adenosyl-L-[methyl-<sup>14</sup>C]-methionine showed the concurrent consumption of these molecules, and ~1 equiv of 4-methyl-5-( $\beta$ -hydroxyethyl) thiazole phosphate was formed per mole of ThiGH.<sup>284b</sup> By radiographically monitoring product separation by thin layer chromatography, Kriek and co-workers found initiating with L-[U-<sup>14</sup>C]-tyrosine produced the formation of two radiolabeled products. These molecules with

distinct polarities in conjunction with GC–MS and <sup>13</sup>C NMR techniques were identified as *p*-cresol and glyoxylate.<sup>284b</sup> Kinetics experiments further demonstrated the reaction stoichiometry proceeded with formation of 1.3 equiv of dAdoH to 1 equiv each of *p*-cresol and glyoxylate. Efforts to improve turnover number led to the finding that ThiGH is susceptible to product inhibition by dAdoH with methionine; the cooperative inhibition is overcome through the addition of 5'-methylthioadenosine/S-adenosylhomocysteine nucleosidase (MTAN), which hydrolyzes dAdoH.<sup>27b,77</sup> Subsequent kinetic analysis of both ThiGH and monomeric ThiH under saturating tyrosine, SAM, and reductant conditions offered improvements in activity and allowed for the determination of rate constants for ThiH's tyrosine lyase activity.<sup>77</sup> Kinetics for both ThiGH and ThiH were observed to be biphasic in nature, with a burst preceding a slower steady-state phase of  $53 \pm 6 \times 10^{-4}$  and  $1.6 \pm 0.2 \times 10^{-4} \text{ s}^{-1}$ , respectively, for ThiGH formation of *p*-cresol, suggesting product release was rate limiting (Table 1). During the burst phase, efficient coupling of dAdoH production to tyrosine cleavage occurs, but during the steady-state phase the uncoupled cleavage of SAM increases dramatically as the tyrosine kinetics become more strongly influenced by the accumulation of products. Moreover, addition of exogenous glyoxylate and ammonia to assay mixtures inhibits tyrosine turnover, possibly as a consequence of glyoxylate (or dehydroglycine) binding in the active site.<sup>77</sup>

Glyoxylate formation occurs following the hydrolysis of dehydroglycine, the latter of which is the common intermediate linking thiamine biosynthesis in aerobes and anaerobes (Figure 40). Dehydroglycine formation has been proposed to occur through two mechanisms, both initiated by an H-atom abstraction from the hydroxyl group on the phenol moiety of tyrosine by the 5'-deoxyadenosyl radical. Assays performed with several tyrosine analogues have shown a strict dependence on the phenol group for SAM cleavage.<sup>77</sup> The resulting tyrosyl radical then undergoes C <sub>$\alpha$</sub> –C <sub>$\beta$</sub>  bond cleavage through a heterolytic process forming dehydroglycine directly or a homolytic process forming a glycyl radical, which may oxidize to dehydroglycine (Figure 78). The reactivity of dehydroglycine poses an intriguing issue, as the intermediate is readily hydrolyzed to glyoxylate upon exposure to aqueous environments yet must be transferred from ThiH to ThiG during biosynthesis. The copurification and characterization of the ThiGH complex undoubtedly speaks to the intimate relationship these protein partners have in vivo. Challand et al. observed the addition of glyoxylate to assays limits C <sub>$\alpha$</sub> –C <sub>$\beta$</sub>  tyrosine bond cleavage, suggesting dehydroglycine might modulate uncoupled cleavage of SAM as a mechanism ensuring dehydroglycine production and incorporation into the thiazole carboxylate is a coordinated event between ThiH and ThiG.<sup>77</sup>

It should be noted that several other radical SAM enzymes, most notably HydG (section 12.2.4) and NosL/NocL (section 6.6), also catalyze the cleavage of the C <sub>$\alpha$</sub> –C <sub>$\beta$</sub>  bonds of the amino acids tyrosine or tryptophan, apparently by initial abstraction of a solvent-exchangeable H-atom from the aromatic ring.

### 10.2. Repair of Thymine Dimers in DNA: Spore Photoproduct Lyase

Spore photoproduct lyase (SPL) is a DNA repair enzyme first identified in *B. subtilis* that catalyzes the monomerization of the UV-induced thymine dimer spore photoproduct (SP, 5-thyminyl-5,6-dihydrothymine) to two thymines (Figure

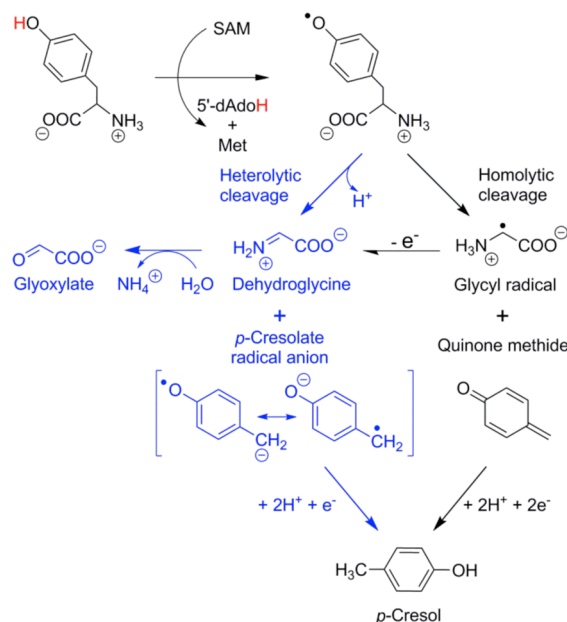


**Figure 78.** The mechanism of  $\text{C}\alpha\text{-C}\beta$  tyrosine bond cleavage as catalyzed by ThiH. Bond breakage may either occur through a heterolytic process forming dehydroglycine directly or through a homolytic process forming a glycyl radical.

79).<sup>353</sup> Unlike the better known DNA photolyase system,<sup>354</sup> however, SPL is catalytically active in the absence of light.<sup>353c</sup> Sequencing of the gene encoding SPL revealed some sequence homology between SPL and DNA photolyase in their C-terminal regions, suggesting an evolutionary relationship and perhaps mechanistic similarities.<sup>355</sup> It was demonstrated, however, that SPL specifically bound to and repaired SP, and was incapable of binding or repairing cyclobutane pyrimidine dimers such as those repaired by DNA photolyase.<sup>356</sup>

**10.2.1. Identification of SPL as a Radical SAM Enzyme.** Limited sequence similarity of the genes encoding spore photoproduct lyase to both aNR-AE and PFL-AE was first recognized in 1997, suggesting that SPL might also be an iron–sulfur protein.<sup>357</sup> Indeed, the first characterization of aerobically purified SPL showed each enzyme contained about 1 iron and approximately 1.5 sulfides.<sup>95</sup> The UV–visible spectrum of this purified protein also revealed spectral features consistent with protein-bound iron–sulfur clusters, which vanished after reduction with dithionite.<sup>95</sup> Subsequent studies using SPL anaerobically reconstituted with exogenous iron and sulfide revealed the presence of a  $[3\text{Fe}-4\text{S}]^+$  EPR signal, which converted to a  $[4\text{Fe}-4\text{S}]^+$  signal upon reduction with dithionite.<sup>96a</sup> Addition of SAM to reduced SPL resulted in a decreased intensity of the  $[4\text{Fe}-4\text{S}]^+$  signal, interpreted as

resulting from an electron transfer from the cluster to SAM.<sup>96a</sup> Further evidence for such an electron transfer was provided by SAM cleavage assays, which demonstrated that under reducing conditions, SPL produced dAdoH upon incubation with SAM.<sup>96a</sup> SPL was ultimately demonstrated to catalyze radical SAM chemistry when a  $^3\text{H}$  label at C6 of SP was traced to dAdoH after repair by SPL in the presence of SAM, demonstrating that SP repair was initiated by abstraction of an H-atom from the C6 position of SP by a dAdo $^\bullet$  (Figure 79).<sup>358</sup>

**10.2.2. The Iron–Sulfur Cluster of Spore Photoproduct Lyase and Its Interaction with SAM.** When purified under anaerobic conditions, SPL from *B. subtilis* or *Clostridium acetobutylicum* is reddish-brown in color and contains approximately three irons and three acid-labile sulfides per protein.<sup>74b,97a</sup> The protein's UV–vis spectrum is consistent with the presence of iron–sulfur clusters, and the EPR spectrum of the purified protein shows a signal at  $g = 2.02$  (Table 2), indicating a small amount of  $[3\text{Fe}-4\text{S}]^+$  clusters. Reduction of purified protein with dithionite yielded an EPR signal ( $g = 2.03, 1.93, 1.89$ ) characteristic of a  $[4\text{Fe}-4\text{S}]^+$  cluster (Table 2). Similar spectroscopic properties are observed for the enzyme aerobically purified followed by anaerobic reconstitution.<sup>96b</sup> Reconstituted protein characterized by Mössauer spectroscopy revealed inhomogeneity of the iron species, with four different quadrupole doublets modeled, including a  $[4\text{Fe}-4\text{S}]^{2+}$  cluster accounting for approximately 40% of the total iron, and a  $[2\text{Fe}-2\text{S}]^{2+}$  cluster accounting for 27% of total iron (Table 2). Similar spectroscopic properties were observed for the reconstituted enzymes from *Geobacillus stearothermophilus*<sup>99</sup> and *C. acetobutylicum*.<sup>98</sup> HYSCORE spectroscopy provided evidence for the coordination of the amino group of SAM to the iron–sulfur cluster, further confirming the intimate interaction of the  $[4\text{Fe}-4\text{S}]$  cluster and SAM required for catalysis.<sup>98</sup>

**10.2.3. Defining the Substrate for Spore Photoproduct Lyase.** Obtaining a model substrate SP for SPL biochemical and mechanistic investigations has been a longstanding challenge. Early investigations utilized DNA irradiated under a variety of conditions including low hydration levels, presence of dipicolinic acid, and/or presence of small acid-soluble proteins (SASPs).<sup>359</sup> The SASPs bind to DNA in spores and modify the conformation of DNA from B-form to more of an A-like structure, which may alter the photochemistry of SASP-bound DNA such that SP is formed at the expense of cyclobutane pyrimidine dimers.<sup>360</sup> However, despite the presence of SASPs or buffer conditions that enhance production of SP, UV irradiation of DNA is unlikely to ever produce a precise spore photoproduct without production of other photoproducts. Considerable effort has been made to synthesize a model dinucleotide spore photoproduct allowing

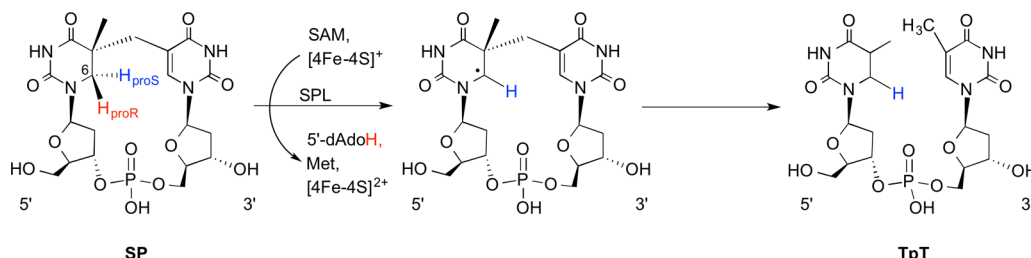


**Figure 79.** SPL reaction scheme catalyzing the conversion of SP to TpT.

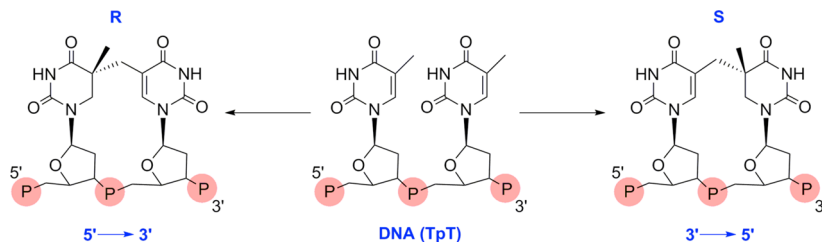


**Figure 80.** Depiction of the two possible spore photoproducts with either SR or SS configuration.

for more defined mechanistic studies. An initial report of the synthesis of two diastereomers of the dinucleotide spore photoproduct was provided by Begley and co-workers; use of 2-D ROESY allowed them to assign one of these products as the 5R-SP, with the other presumably the 5S.<sup>361</sup> It was noted in this paper that constraints of double helical DNA would favor the 5R configuration for the natural spore photoproduct.<sup>361</sup>

An SPL assay with a defined dinucleotide substrate was first reported in 2006. The defined SP substrate was generated by UV irradiation of dry DNA, followed by acid hydrolysis and HPLC purification of the SP dinucleotide, or by UV irradiation of dry films of TpT and dipicolinic acid.<sup>96b</sup> Repair reactions of the dinucleotide SP substrate demonstrated that SPL from *Bacillus subtilis*<sup>96b</sup> and *C. acetobutylicum*<sup>98</sup> were capable of catalyzing its repair to TpT. These results validated their model compound and demonstrated that SPL could catalyze repair of this minimal dinucleotide substrate in the absence of the DNA double helical structure. Further, their results supported the notion that SPL specifically binds and cleaves SP, and is incapable of catalyzing repair of cyclobutane pyrimidine dimers or 6,4-photoproducts.<sup>96b,356</sup> Another approach to generating a defined SP substrate was irradiation of an oligonucleotide containing a TT sequence in a dry film containing picolinic acid, followed by HPLC purification and enzymatic excision of the damaged oligonucleotide.<sup>99</sup> This defined SP substrate was assayed with SPL from *G. stearothermophilus*, producing thymidine.<sup>99</sup> Pieck and co-workers also showed the purified SP-lesion-containing oligo served as a substrate for SPL, and was cleanly converted to the undamaged oligo without formation of side products, indicating a tightly controlled reaction of a radical in the vicinity of DNA.<sup>99</sup>

Defining the stereochemistry of the SP substrate, specifically the stereochemistry at the C5 involved in the T-T cross-link, has been of considerable interest over the years (Figure 80). While both 5R and 5S diastereomers of SP are possible in principle, Begley argued that the natural SP would be of the 5R configuration only, due to the steric constraints imposed by the native DNA structure.<sup>361</sup> However, in 2006 two independent groups reported that SPL repairs the 5S and not the 5R configured SP.<sup>99,362</sup> Their syntheses of the 5R and 5S dinucleoside spore photoproducts, lacking the phosphodiester bridge, were based on modifications of Begley's earlier reported syntheses.<sup>361,362b,363</sup> Quantitative NOESY experiments were used to assign the stereochemistry at C5 for both the dinucleoside SPs and the derivatives containing a C3-C5 diester bridge.<sup>362</sup> Assays of the dinucleoside SPs using the SPL from *B. subtilis* and from *G. stearothermophilus* showed that the 5S-SP was repaired, while the 5R-SP was not.<sup>99,362</sup> Two subsequent studies, however, reached the opposite conclusion: SPL repairs only the 5R-configured spore photoproduct. One of these studies used SPTpT prepared by irradiation of TpT in the presence of dipicolinic acid; 2D NOESY and ROESY

experiments together with DFT calculations were used to unambiguously determine the absolute stereochemistry for this natural substrate as 5R.<sup>364</sup> The second study utilized 2D NOESY and ROESY experiments to unambiguously define the stereochemistry of synthetic 5R and 5S-SP dinucleosides lacking a phosphodiester bridge.<sup>74a</sup> Further, this latter study assayed each diastereomer with SPL and showed that SPL repairs only the 5R, and not the 5S-SP.<sup>74a</sup> A follow-up study by the same group showed that complete repair could be achieved for the 5R SPTpT containing a phosphodiester backbone.<sup>74b</sup> The discrepancy between these latter two studies regarding 5R-SP as the substrate and the earlier studies naming 5S-SP as the substrate was elucidated by Heil et al., who demonstrated that "5S", thought to be a model substrate, was in fact the 3'→5' 5S-SP, while the 5R substrate was the 5'→3' SP.<sup>365</sup> In other words, the directionality of the methylene bridge of SP, whether it originates from the methyl group of the 5'-T (giving rise to the 3'→5' SP) or from the methyl group of the 3'-T (giving rise to the 5'→3' SP), was quite relevant to the stereochemical determination as well as to the SPL repair activity. Heil et al. revealed that the earlier studies indicating that SPL repairs only the 5S-SP were carried out on 3'→5' SP (prepared synthetically), while the studies indicating SPL repairs only the 5R-SP were carried out on 5'→3' SP. Heil et al. clarified and unified these earlier studies by incorporating the 5'→3' 5R and 5S-SP, both lacking a phosphodiester backbone, into DNA oligonucleotides.<sup>365</sup> The 5'→3' 5R- and 5S-SP incorporated into oligonucleotides were then crystallized in complex with the DNA polymerase from *G. stearothermophilicus*, and the absolute stereochemistry was determined on the basis of the crystal structures. They found that the 5R lesion fit well in the DNA duplex, nearly overlaying a structure of the same enzyme with undamaged DNA. In contrast, the 5'→3' 5S-SP oligo complexed to DNA polymerase reveals a considerable distortion relative to undamaged DNA, to such an extent that it is not possible to model a phosphodiester backbone between the two ribose thymidines involved in the SP lesion. They further assayed these SP-containing oligos and found that only the 5R was repaired. They concluded that the work showing repair of the 5S-SP was carried out on the 3'→5', and not the 5'→3', forms of SP. The identity of the substrate of SPL as the 5'→3' 5R-SP was further supported by studies by Lin et al. who synthesized, structurally characterized, and assayed an SP analogue containing a formacetal linker in place of the phosphodiester bridge.<sup>366</sup>

**10.2.4. SAM: Substrate or Cofactor in the SPL-Catalyzed Reaction?** While the role of SAM as cosubstrate or cofactor has been straightforward for most radical SAM enzymes, this deceptively simple question is the subject of continuing debate for SPL. The mechanism originally proposed by Mehl and Begley<sup>367</sup> and supported experimentally by Cheek and Broderick<sup>358</sup> implicates a role for SAM as a catalytic

cofactor during SP repair, because the product thyminyl radical abstracts a hydrogen from dAdoH to regenerate dAdo<sup>•</sup> and ultimately SAM. The SPL-catalyzed SAM cleavage to produce dAdoH was however reported by Rebeil and Nicholson; they found that SP-containing DNA stimulated the cleavage of SAM, implicating SAM as a cosubstrate.<sup>96a</sup> When Cheek and Broderick carried out experiments with C6-tritiated SP-containing DNA, however, tritium was observed to be transferred into SAM and not into dAdoH, supporting SAM's role as a catalytic cofactor.<sup>358</sup> This catalytic role for SAM was further supported by Buis et al. who demonstrated that one SAM molecule can mediate the repair of hundreds of SP lesions.<sup>97a</sup> These last two results seem to be unequivocal in supporting the idea that SAM is a catalytic cofactor, because there is no way to envision hundreds of substrate turnovers using one SAM molecule in any other way. Reports of SAM conversion to Met and dAdoH during the SPL reaction, implicating SAM as a substrate, continued to accrue, however. When assaying SPL using a synthetic SP substrate, Friedel et al. reported that dAdoH was produced in excess over the repaired thymidine; the authors concluded that one SAM was cleaved per SP repaired, and that the additional dAdoH produced in excess of this amount was due to uncoupled SAM cleavage, an observation common among radical SAM enzymes in vitro that employ SAM as a cosubstrate.<sup>362a</sup> Pieck et al. also observed considerable uncoupled cleavage of SAM, which was enhanced in the presence of substrate.<sup>99</sup> Using dinucleotide SPTpT as a substrate, Chandor-Proust et al. observed approximately 1 equiv of dAdoH per SP repaired, supporting a role for SAM as a cosubstrate.<sup>368</sup> Later studies by Yang et al. showed that preduced SPL could catalyze at least 10 turnovers of SP to repaired product, supporting a catalytic role for SAM.<sup>97b</sup> These workers proposed that dAdoH observed during the reaction, which appeared in small quantities and then decreased during reaction, was actually an intermediate species,<sup>97b</sup> although that proposal was later retracted when they discovered that an enzyme contaminant in their SPL preparations was converting/hydrolyzing the dAdoH produced during catalysis.<sup>97c</sup> In 2012, Yang et al. suggested a "partially catalytic" role for SAM based on their quantitation of dAdoH and TpT produced during turnover.<sup>97c</sup> One observation we have made in analyzing these differing reports regarding the role of SAM in the SPL-catalyzed reaction is that many of the reports of SAM behaving as a cosubstrate have utilized synthetic dinucleoside or dinucleotide SP substrates, rather than SP contained within a DNA strand; our interpretation is that the dinucleoside and dinucleotide substrates are not optimal substrates, and allow more uncoupled SAM cleavage than is the case with the natural substrate. It therefore appears that SAM is a catalytic cofactor in the SPL-catalyzed reaction; however, it has a propensity to catalyze uncoupled reductive cleavage of SAM, particularly in the presence of poor substrates.

**10.2.5. Structural Characterization of SPL.** Structures of SPL from *G. thermodenitrificans* with and without the dinucleotide SP substrate have been solved.<sup>369</sup> Like most other radical SAM enzymes with solved structures, SPL contains a partial  $(\beta\alpha)_6$  TIM barrel, with a [4Fe–4S] cluster coordinated at the top of the barrel by the three cysteines of the radical SAM motif (Figure 81). SAM coordinates the cluster's unique iron via the amino and carboxyl moieties with the sulfonyl sulfur 3.6 Å from the unique iron. The SR-SP substrate lacking a phosphodiester linker binds to the active site near SAM, and is correctly oriented by a series of hydrogen-

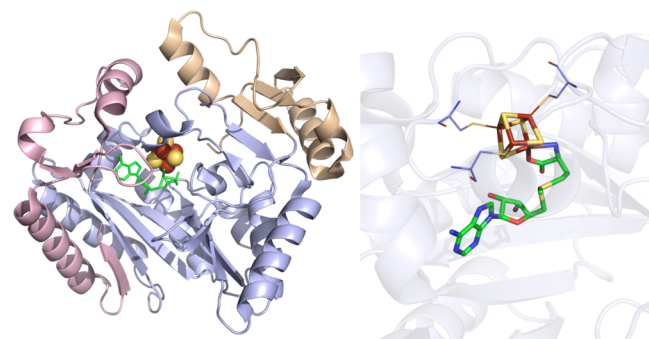


**Figure 81.** SPL crystal structure (PDB ID 4FHD). Left: N-terminal domain colored in wheat, radical SAM domain in light blue, C-terminal domain in light pink, [4Fe–4S] cluster in yellow and rust spheres, and SAM in green sticks. Right: Active site of SPL where [4Fe–4S] cluster (yellow and rust) and SAM (green carbons) are depicted in sticks with oxygens colored red and nitrogens colored blue. Cysteines (light blue carbons) involved in ligating cluster are depicted in lines.

bonding interactions. The configuration of the SR-SP in the crystal structure can accommodate a phosphodiester bridge, and soaking the crystals in pyrophosphate produced residual electron density in the vicinity of the absent bridge. Binding of the SR-SP results in structural perturbations in the active site, most significantly movement of the Tyr98 containing side chain. Further, the orientation of the SR-SP in the SPL active site points to a base-flipping mechanism during binding and repair, similarly proposed for DNA photolyase. A  $\beta$ -hairpin turn from SPL including Arg304 and Tyr305 is similar to  $\beta$ -hairpins found in other DNA repair enzymes, and likely involved in comparable substrate recognition and base flipping. The crystal structures provide support for a role for Cys141 (Cys140 in *G. thermodenitrificans*) in the hydrogen atom transfer during the SPL-catalyzed reaction. The C6 of the 5'-dihydrothymine of SP is 3.9 Å from the 5'-C of SAM, and perfectly positioned for the initial H-atom abstraction that initiates catalysis. The methylene carbon of SP, the site of the product radical after C–C bond cleavage, is further (5.3 Å) from the 5'-C of SAM than it is from the Cys140 (4.5 Å), supporting a mechanism in which a hydrogen atom is transferred from Cys140 to the product thyminyl radical to produce the repaired TpT. The presence of the conserved Tyr98 in the active site in close proximity to Cys140 also raised the intriguing question of a role for Tyr98 in a proton-coupled electron transfer pathway to quench the thiyl radical. While the crystal structures depict the structural effects on SP upon substrate binding, another group has investigated SPL's effect on the DNA structure. DNase I footprinting experiments revealed that SPL binds to an SP-containing oligonucleotide, protecting a region of approximately nine nucleotides surrounding the SP lesion.<sup>356</sup> Interestingly, within this protected region were two hypersensitive sites, suggesting that SPL binding to the lesion resulted in a distortion of the surrounding DNA.<sup>356</sup> The emerging picture in the field of SPL depicts a very dynamic interaction between enzyme and substrates. Likely, these interactions are tuned to maximize catalytic turnover while limiting deleterious enzyme–product complexes.

**10.2.6. Mechanism of Repair of SP by SPL.** A radical mechanism for repair of SP by SPL was proposed by Mehl and Begley in 1999 (Figure 82), where they proposed that an H-atom abstraction from C6 of SP could promote a radical-

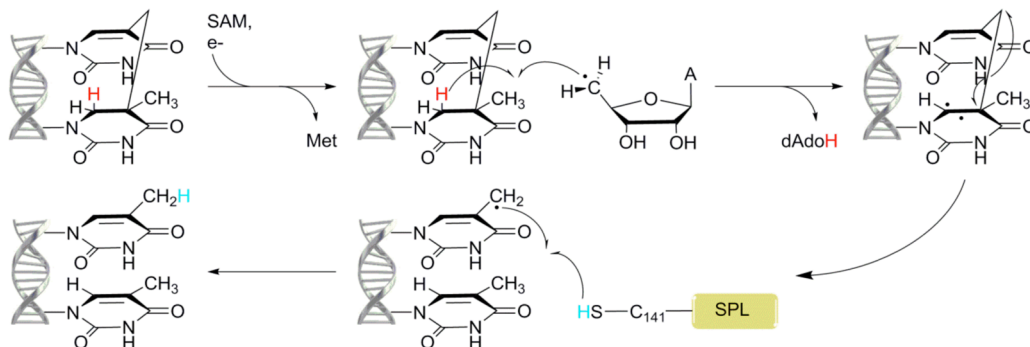


**Figure 82.** Proposed mechanism for the repair of SP as catalyzed by SPL.

mediated  $\beta$ -scission to cleave the C–C bond linking the two thymines.<sup>367</sup> This proposal was supported by a reaction in which a synthetic SP analogue with a thiophenyl group at C6 was subjected to radical generating conditions resulting in clean generation of the monomerized thymine products.<sup>367</sup> This mechanism received additional experimental support in 2002 when Cheek and Broderick demonstrated direct H-atom transfer from C6 of SP into SAM.<sup>358</sup> They utilized DNA generated in cells grown in media enriched with either [ $C_6\text{-}^3\text{H}$ ]-thymine or [methyl- $^3\text{H}$ ]-thymine. The purified DNA was then subjected to UV irradiation under optimal conditions for generation of SP. This SP-containing, tritiated DNA was used as the substrate for repair reactions with SPL in the presence of SAM under reducing conditions. The results clearly demonstrated that after turnover of C6-tritiated SP, the SAM in the reaction mixture was labeled with tritium. The results provided the first evidence for the involvement of a SAM-derived dAdo $^\bullet$  in the SPL-catalyzed reaction, and also demonstrated that Begley's initial proposal of SP repair via a C6 radical-mediated  $\beta$ -scission was most likely correct. A subsequent DFT study of the SPL-catalyzed repair reaction supported this basic mechanism, although it pointed to a possible interthymine H-atom transfer prior to regeneration of the dAdo $^\bullet$  near the end of the catalytic cycle.<sup>370</sup> More recent studies by Yang et al. using 6-pro-R or 6-pro-S-deuterated SP as a substrate demonstrated the 6-pro-R hydrogen atom is abstracted by the dAdo $^\bullet$ .<sup>97b</sup> The results reported by Cheek and Broderick also supported a catalytic role for SAM (detailed in section 10.2.4) because it was SAM and not dAdoH that contained the label after enzymatic reaction.<sup>358</sup> Buis et al. also demonstrated that SAM acted catalytically by showing that with a 1:1 ratio of SAM to SPL, hundreds of SP lesions could be repaired.<sup>97a</sup> The mechanism proposed by Mehl and Begley as well as by Cheek and Broderick would also predict that label present at the 5'-position of SAM would be incorporated into the repaired thymine in the last step in the catalytic cycle.<sup>358,367</sup> Small amounts of such label transfer have been observed.<sup>97a</sup> Subsequent studies revealed, however, that the hydrogen atom incorporated into repaired thymidine derived from solvent, not from dAdoH, thereby implicating the involvement of protein residues with exchangeable sites in the hydrogen transfer mechanism of SPL.<sup>97b</sup>

Although only three cysteines comprise the canonical SAM motif, SPL contains a fourth conserved cysteine, Cys141, shown to be essential for catalysis through a mutagenesis study.<sup>371</sup> A subsequent investigation found that a C141A variant of SPL was capable of cleaving the C–C bond of the SPTpT lesion; however, rather than producing TpT, the

product contained a sulfinate group derived from dithionite on the methyl carbon of the 3'-T of the TpT.<sup>368</sup> Their results suggested Cys141 plays a role in the final steps of the catalytic mechanism by either transferring a hydrogen atom to the allylic methyl radical of repaired TpT or stabilizing a specific state of the enzyme preventing side reactions with exogenous molecules.<sup>368</sup> The work by Yang et al. implicating a solvent-exchangeable protein site in the H-atom back-donation to the product thyminyl radical indicated Cys141 plays a role in this process.<sup>97b</sup> Further studies of the C141A variant provided additional insight, including the observation that SAM becomes a cosubstrate rather than a cofactor in the C141A variant, implicating a role for Cys141 as an H-atom donor to the product thyminyl radical.<sup>97c</sup> More recently, Carell and co-workers provided evidence that Tyr98, a conserved residue located in the active site of SPL, mediates H-atom transfer with the Cys141 residue and plays a critical role in catalysis.<sup>372</sup> Their assignment of a UV-vis feature to a tyrosyl radical has been disputed, however, and no corresponding tyrosyl radical EPR signal has yet been observed.<sup>97d</sup> Further kinetic analysis and structural characterization of variants in which Tyr98 and Tyr96 (*G. thermodenitrificans* numbering, corresponding to Tyr99 and Tyr97 in *B. subtilis*) were converted to alanine or phenylalanine provided further support for the involvement of these two tyrosine residues in the SPL-catalyzed repair of SP, with Tyr98 specifically implicated in an H-atom transfer chain during the second half of the repair reaction.<sup>97d</sup> Computational studies have provided further thermodynamic rationale for invoking intermediary amino acid radicals, as this would provide an SPL mechanism that avoids any strongly endothermic or exothermic steps.<sup>478,479</sup>

### 10.3. DesII and the Synthesis of *D*-Desosamine

Sugar deoxygenation is a common biosynthetic step in the glycodiversification of carbohydrates in biology.<sup>373</sup> Regioselective C–O bond cleavage relative to an essential 4-keto group (situated either  $\alpha$  or  $\beta$ ) yielding deoxyhexoses has been well characterized for C2, C3, and C6-type deoxygenations, although at present C4 is less well-known.<sup>374</sup> Interestingly, the biosynthesis of *D*-desosamine, which is a required component of numerous macrolide antibiotics (Figure 83), requires a C-4 deoxygenation step catalyzed by the radical SAM enzyme DesII.<sup>375</sup> Cloned and sequenced from the methymycin/neomethymycin producing strain *Streptomyces venezuelae*, DesII was identified as a "putative reductase" possessing a CX<sub>3</sub>CX<sub>2</sub>C radical SAM motif.<sup>375,376</sup> Gene knockout studies of *desI* and *desII* established that DesII performed a reaction independent of DesI, an associated PLP-dependent transaminase enzyme in C4 deoxygenation.<sup>375</sup> Product formation of

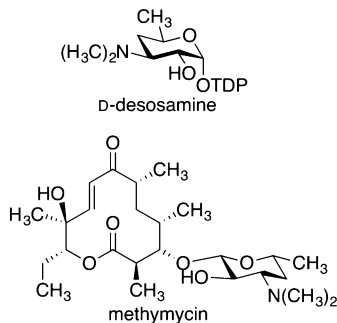


**Figure 83.** Natural products D-desosamine and methymycin. Radical SAM enzyme DesII is involved in the biosynthesis of D-desosamine.

thymidine diphosphate (TDP)-D-quinovose instead of the expected TDP-6-deoxy-4-keto-D-glucose product by DesII (in the absence of DesI) implicated a novel mechanism for C4 deoxygenation involving a possible 1,2-nitrogen shift analogous to LAM or adenosylcobalamin-dependent enzyme ethanolamine ammonia lyase.<sup>375b</sup>

DesII was found to catalyze a radical-initiated deaminase reaction.<sup>102,376</sup> When overexpressed and purified under aerobic conditions, DesII contained low iron and sulfide counts in [3Fe–4S]<sup>+</sup> clusters based on EPR spectroscopy ( $g = 2.010$ ) (Table 2).<sup>87,102</sup> Treatment of this [3Fe–4S]<sup>+</sup> form of the enzyme with dithionite converted it to an EPR-silent state, postulated in the paper to be [3Fe–4S]<sup>0</sup>.<sup>87</sup> Anaerobic reconstitution resulted in enzyme containing approximately four Fe and four sulfides per subunit and UV-vis spectrum consistent with the presence of a [4Fe–4S] cluster ( $\epsilon_{420} = 9200 \text{ M}^{-1} \text{ cm}^{-1}$ ). Reduction with dithionite in the presence of SAM produced a rhombic EPR signal ( $g = 2.01, 1.96, 1.87$ ) characteristic of a [4Fe–4S]<sup>+</sup> cluster (Table 2).<sup>87</sup> No EPR signal could be observed upon reduction in the absence of SAM, and the authors proposed that this was due to the instability of the cluster with respect to reduction in the absence of SAM.<sup>87</sup> However, when handled in the presence of SAM, reducing agent (dithionite), and in the absence of DesI, TDP-4,6-dideoxy-D-glucose was detected as the product from the TDP-4-amino-4,6-dideoxy-3-keto-D-glucose substrate (Figure 84).<sup>87,102</sup> The biological reducing system of flavodoxin and flavodoxin reductase were capable of replacing dithionite to support turnover, indicating that these or similar proteins are the electron donors *in vivo*.<sup>87</sup>

The DesII-catalyzed deamination is a redox-neutral elimination reaction requiring a single [4Fe–4S] cluster.<sup>87,377</sup> When substrate deuterated at the 3-position was used in DesII activity

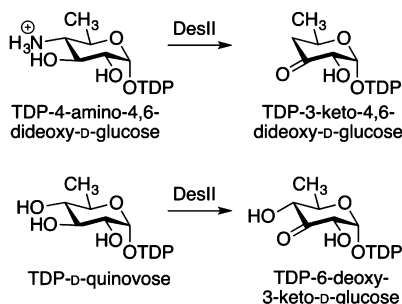


**Figure 84.** Radical SAM enzyme DesII catalyzes a redox-neutral deamination (top reaction), as well as an oxidative dehydrogenation (bottom reaction).

assays, doubly deuterated SAM and singly deuterated dAdoH were observed.<sup>87</sup> These results support a mechanism in which a dAdo<sup>•</sup> abstracts a H-atom from the C3 position of substrate to initiate the reaction (Figure 85). While incorporation of two deuterons into SAM suggests that SAM is catalytically regenerated,<sup>87</sup> the stoichiometry of product and SAM was found to be 1:1 implicating SAM as a cosubstrate.<sup>377</sup> Interestingly, redox cycling of the [4Fe–4S] cluster has been demonstrated, where the reduced [4Fe–4S] cluster can be used over several turnover events.<sup>377</sup>

While DesII has been shown to catalyze a redox-neutral deamination reaction, it can also catalyze the oxidative dehydrogenation of TDP-D-quinovose, yielding TDP-6-deoxy-3-keto-D-glucose (Figure 84).<sup>87,377</sup> In this alternate mechanism as in the deamination reaction, DesII abstracts an H-atom from the C3-position.<sup>87</sup> Additional evidence for abstraction at this position came from the observation of a substrate  $\alpha$ -hydroxylalkyl radical, when using TDP-D-quinovose as a substrate.<sup>378</sup> Assignment of this radical was supported by a decrease in EPR line width when performed in D<sub>2</sub>O that would be less consistent with a ketyl radical assignment.<sup>378</sup> Finally, solvent-dependent differences in broadening of the hydroxyl hydrogen hyperfine have brought into question the protonation state of the  $\alpha$ -hydroxylalkyl radical.<sup>378,379</sup> A thorough solvent KIE study has shown that deprotonation of the radical follows the initial H-atom abstraction event, implicating a putative role for an active site base.<sup>380</sup> However, further structural or mutagenesis studies are necessary to understand the role of specific site residues in the catalytic reaction.

DesII's remarkable versatility in catalyzing both a redox-neutral deamination reaction and an oxidative dehydrogenation reaction at a single [4Fe–4S] cluster, and initiated by abstraction at the C3 position, has some intriguing mechanistic implications. In the case of the deamination reaction, two mechanisms have been proposed (Figure 85).<sup>377,378</sup> The first mechanism bears similarity to adenosylcobalamin-dependent enzyme ethanolamine ammonia lyase, where migration of the C4 amine to the C3 position produces an ethanolamine intermediate, and loss of ammonia results in oxidation of the keto group.<sup>87,377</sup> The alternative mechanism resembles an E1cb-type elimination of ammonia, where deprotonation of the  $\alpha$ -hydroxylalkyl radical results in a stabilized enol radical formed.<sup>87,377</sup> Similarly, in the oxidative dehydrogenation reaction, deprotonation of the  $\alpha$ -hydroxylalkyl radical has been proposed to result in a single electron oxidation that may involve reduction of the [4Fe–4S]<sup>2+</sup> cluster (Figure 86).<sup>378,380</sup> This mechanism is similar to the dehydrogenation reaction catalyzed by BtrN wherein 2-deoxy-scylo-inosamine is converted to amino-2-deoxy-scylo-inosose (section 8.2, Figure 68). The idea has only recently been put forth that the oxidative dehydrogenation reactions catalyzed by enzymes like BtrN and anSME (Figures 66 and 68) occur via reduction of the [4Fe–4S]<sup>2+</sup> auxiliary clusters bound to these enzymes (section 8).<sup>328</sup> An interesting distinction to point out between these systems and that of DesII, however, relates to the ability of DesII to directly recycle the electron back to the [4Fe–4S]<sup>2+</sup> radical SAM cluster;<sup>377</sup> turnover experiments with anSME demonstrated that the electron could only be recycled back to the radical SAM cluster via an external oxidant like flavodoxin after it was transferred through auxiliary clusters I and II (section 8.1.4).<sup>80b</sup> This perhaps suggests that the structure of DesII is such that its active site pocket accommodates bound substrate in such a manner as to limit the distance between the [4Fe–

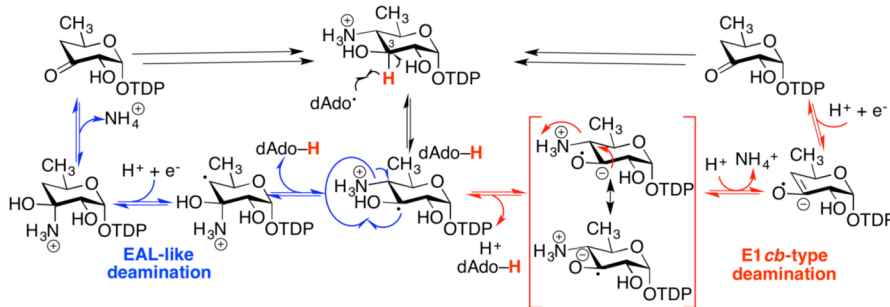


**Figure 85.** Proposed mechanism in DesII-catalyzed deamination. Depicted in blue is an ethanolamine ammonia lyase-inspired mechanism involving the formation of a carbinolamine intermediate. Depicted in red is an E1cb-type mechanism involving a stabilized enol radical. Double black full arrows represent product leaving the active site, substrate coordination, and dAdo<sup>•</sup> generation.

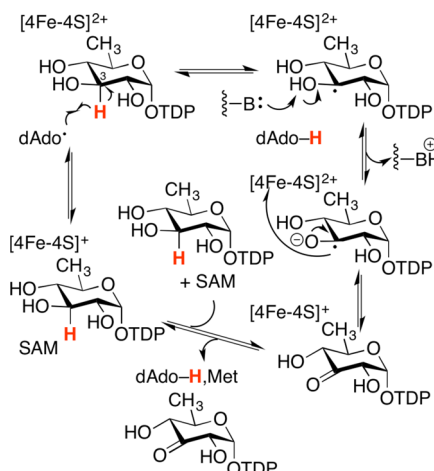


**Figure 86.** Proposed mechanism of DesII-catalyzed oxidative dehydrogenation. Note that electron transfer is proposed to occur from the product radical back to the oxidized [4Fe-4S]<sup>2+</sup> cluster, as redox cycling of the FeS cluster has been demonstrated.

4S]<sup>2+</sup> cluster and the intermediate substrate radical species produced during turnover to promote the rereduction of the Fe–S center. The recent BtrN crystal structure (Figure 69) provides evidence to support this distinction, where the substrate conformation, hydrogen-bonding interactions with the substrate functional group, and possibly proximity of the auxiliary [4Fe–4S] cluster help avoid an elimination reaction observed here for DesII (section 8.2).<sup>328</sup>

#### 10.4. PhnJ: Catalysis of C–P Bond Cleavage

The *phnJ* gene is part of the 14-gene bacterial C–P lyase gene cluster, which encodes the ability to convert alkylphosphonates to phosphate.<sup>381</sup> PhnJ contains four conserved cysteines in a CX<sub>2</sub>CX<sub>2</sub>CX<sub>5</sub>C arrangement,<sup>382</sup> and when aerobically purified binds approximately 2 Fe per protein.<sup>115a</sup> After anaerobic reconstitution with iron and sulfide, the protein exhibits UV-vis<sup>115a</sup> and EPR<sup>115b</sup> spectroscopic properties consistent with the presence of an iron–sulfur cluster that can be reduced with dithionite (Table 2). Incubation of this reconstituted enzyme with SAM, dithionite, and α-D-ribose-1-methylphosphonate-5-phosphate (PRPn) results in conversion of PRPn to α-D-ribose-1,2-cyclic-phosphate-5-phosphate (PRCP) and methane (Figure 87), in addition to dAdoH and methionine.<sup>115a</sup> Importantly, no turnover can be achieved when SAM is left out of the reaction mixture, and the collective results certainly indicate that the C–P bond cleavage catalyzed by PhnJ is a radical SAM reaction.<sup>115a</sup> All four cysteines in the CX<sub>2</sub>CX<sub>2</sub>CX<sub>5</sub>C motif

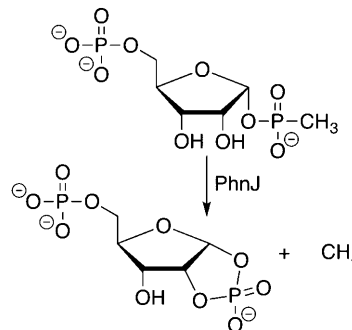


**Figure 87.** C–P bond cleavage of methylphosphonate by radical SAM enzyme PhnJ.

(cysteines 241, 244, 266, and 272 in the *E. coli* enzyme) are required for activity; however, only Cys241, Cys244, and Cys266 are needed to assemble an intact [4Fe–4S] cluster.<sup>115b</sup> Through an elegant series of experiments, Raushel and co-workers were able to show that the dAdo<sup>•</sup> produced by reductive cleavage of SAM abstracts the pro-R H from Gly32 of PhnJ to generate a glycyl radical intermediate (Figure 88).<sup>115b</sup> This glycyl radical is proposed to generate a thiyl radical at Cys272, which then attacks the phosphonate moiety of PRPn.<sup>115b</sup> Subsequent C–P bond cleavage involves H-atom abstraction from the pro-S position of Gly32 to yield methane and a covalent thiophosphate intermediate, which is released by nucleophilic attack with the 2'-hydroxyl group (Figure 88).<sup>115b</sup> This mechanism is highly reminiscent of the combined actions of PFL-AE and PFL, wherein radical SAM chemistry generates a glycyl radical on PFL, which in turn generates a thiyl radical that attacks substrate and causes C–C bond cleavage (section 3.1). Although the glycyl radical has not been directly detected in PhnJ as it has with PFL, the results reported by Raushel and co-workers indicate that PhnJ operates in a manner remarkably similar to the combined actions of pyruvate formate lyase and its activating enzyme.

#### 10.5. Elp3: Demethylation by the Elongation Complex

Elp3 is one of six subunits that comprise the elongation complex and is responsible for the histone acetyltransferase (HAT) activity of this assembly. The HAT domain of Elp3 is in the C-terminus of the protein, while a radical SAM domain has been identified in the N-terminal region.<sup>383</sup> The known biological significance of histone methylation/demethylation events in controlling transcription, coupled to the resemblance between Elp3 and HemN, suggests that Elp3 may catalyze a demethylation reaction,<sup>383</sup> although recent characterization of Elp3 from *Toxoplasma* shows that it localizes to the

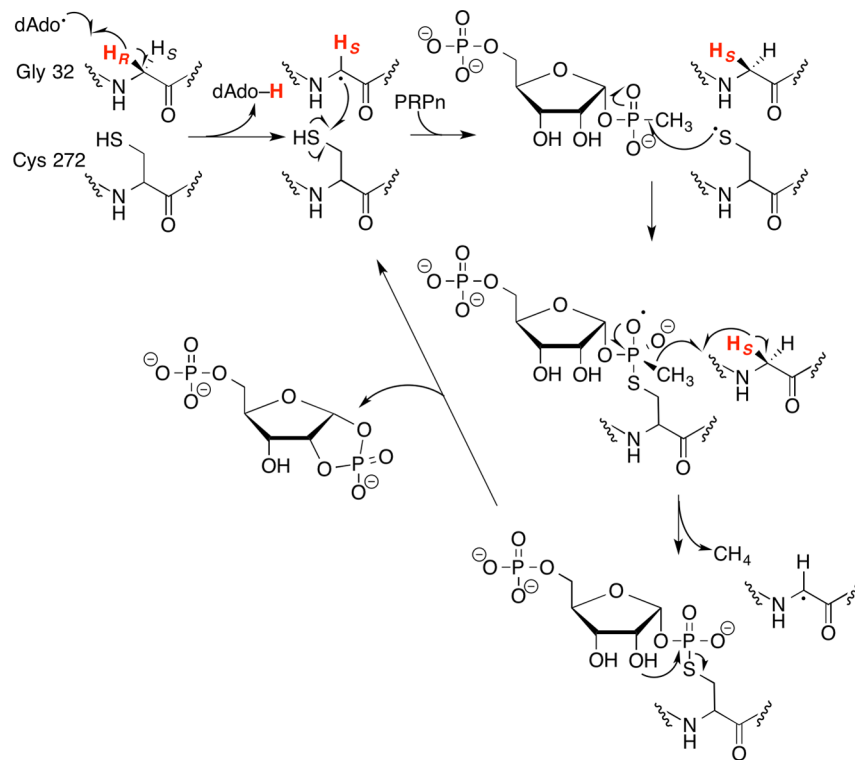


**Figure 88.** Mechanism of C–P bond cleavage catalyzed by radical SAM enzyme PhnJ.

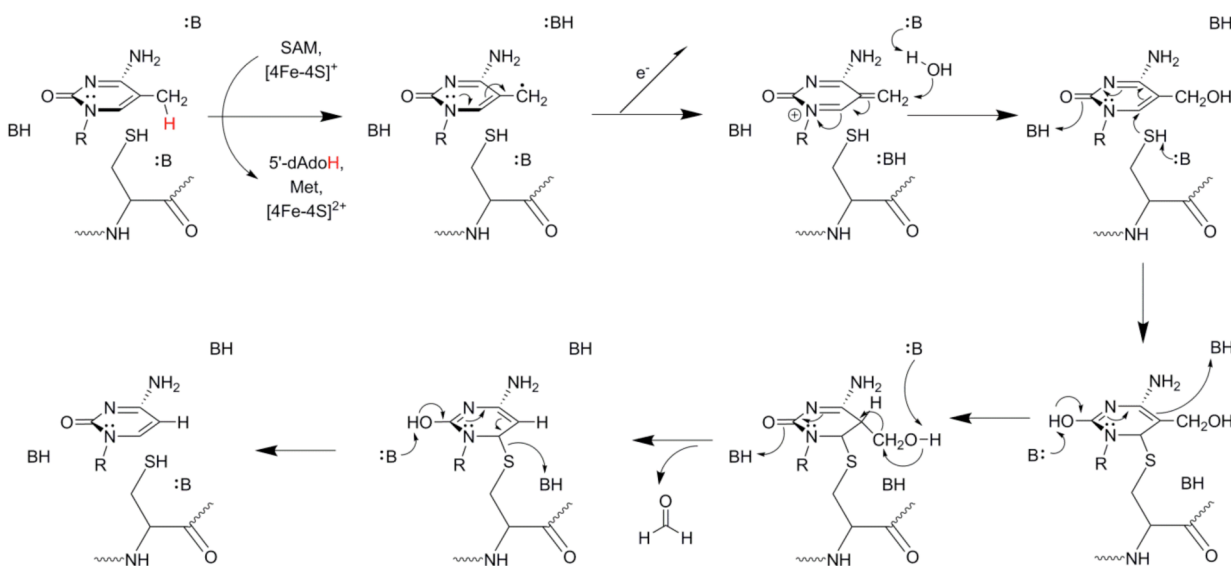


**Figure 89.** Hypothetical mechanism for the Elp3-catalyzed demethylation of DNA. An alternative pathway has been proposed, which could account for product formation in the absence of an external nucleophile; see Wu and Zhang.<sup>385b</sup>

mitochondrial surface indicating that it may have more diverse functions beyond just transcription.<sup>384</sup>

Experimental evidence in support of Elp3's role in catalyzing a demethylation reaction was ultimately provided using three independent assays in live cells.<sup>385</sup> The purified radical SAM domain of Elp3 contains small amounts of iron ( $\sim 0.3$  per protein), and a red-brown color and UV-vis features characteristic of iron–sulfur clusters.<sup>103</sup> Reconstitution with iron and sulfide increases iron content up to 1.6 per protein, with similar amounts of sulfide detected. EPR spectroscopic characterization of the reconstituted protein reveals an isotropic signal consistent with the presence of a  $[3\text{Fe}-4\text{S}]^+$  cluster ( $g = 1.96, 2.002$ ) that becomes axial upon reduction and exhibits  $g$ -values ( $g = 2.03, 1.93$ ) typical of  $[4\text{Fe}-4\text{S}]^+$  clusters. Upon addition of SAM to reduced samples, the signal attributed to the  $[4\text{Fe}-4\text{S}]^+$  cluster is slightly perturbed ( $g = 2.02, 1.93$ ) (Table 2). Biochemical experiments demonstrated the binding of SAM to the Elp3 domain, which was able to cleave SAM upon addition of reducing agents.<sup>103</sup> The cumulative evidence supports a function for Elp3 as a radical SAM demethylase, and a mechanism has been accordingly proposed (Figure 89).<sup>385b</sup>

1.96, 2.002) that becomes axial upon reduction and exhibits  $g$ -values ( $g = 2.03, 1.93$ ) typical of  $[4\text{Fe}-4\text{S}]^+$  clusters. Upon addition of SAM to reduced samples, the signal attributed to the  $[4\text{Fe}-4\text{S}]^+$  cluster is slightly perturbed ( $g = 2.02, 1.93$ ) (Table 2). Biochemical experiments demonstrated the binding of SAM to the Elp3 domain, which was able to cleave SAM upon addition of reducing agents.<sup>103</sup> The cumulative evidence supports a function for Elp3 as a radical SAM demethylase, and a mechanism has been accordingly proposed (Figure 89).<sup>385b</sup>

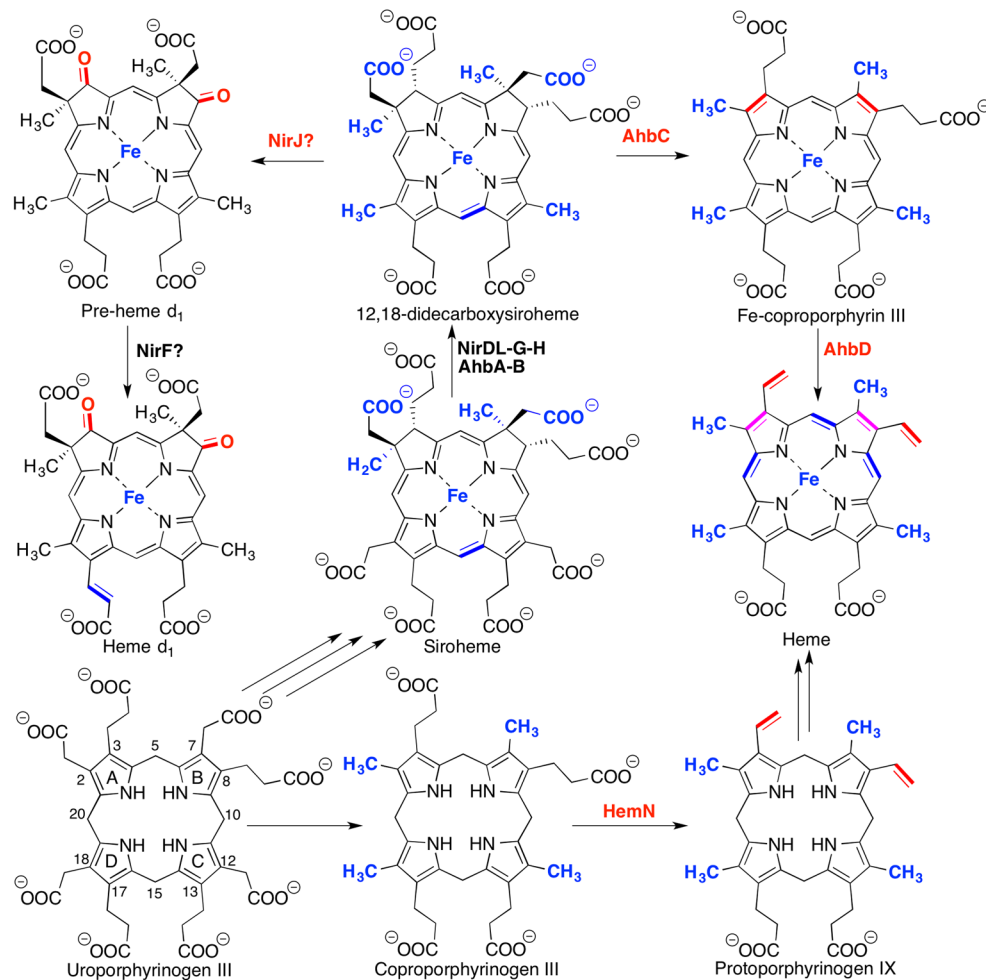


**Figure 90.** Oxygen-independent biosynthetic pathway of heme and heme  $d_1$  from uroporphyrinogen III. Biosynthetic involvement of radical SAM enzymes and the transformation catalyzed is bolded in red, while nonradical SAM enzyme transformations are bolded in blue. Pathway-dependent transformations that do not strictly require radical SAM enzyme involvement are highlighted in purple.

### 10.6. Decarboxylation during Blasticidin S Biosynthesis Catalyzed by BlsE

Blasticidin S is a peptidyl nucleoside antibiotic that functions by inhibiting peptide bond formation in the ribosome, thereby disrupting protein synthesis.<sup>386</sup> It contains a cytosyl pyranoside core structure that is found in only a few other antibiotics that include arginomycin, mildiomycin, and cytomycin. Interestingly, the biosynthetic gene clusters of at least four of these antibiotics are predicted to include a gene encoding a radical SAM enzyme. One of these radical SAM enzymes, BlsE, has now been characterized.<sup>81</sup> BlsE contains the canonical CX<sub>3</sub>CX<sub>2</sub>C radical SAM motif, and the purified 6xHis affinity tagged enzyme contains stoichiometric 1.4 iron and 1.6 sulfide per protein. Chemical reconstitution increases the quantities of iron and sulfide to 6.8 and 8.5 per protein, respectively, suggesting that an accessory iron–sulfur cluster may occupy the CX<sub>3</sub>CX<sub>2</sub>C motif that is also present in the primary sequence. The UV–vis spectrum of the enzyme shows features characteristic of bound iron–sulfur clusters, with the absorption maxima decreasing in intensity upon reduction. The isolated enzyme exhibits an EPR signal with a  $g$  value of 2.01 that is consistent with the presence of a [3Fe–4S]<sup>+</sup> cluster, while in a reduced state the axial spectral features ( $g = 2.02$  and 1.93) are typical of [4Fe–4S]<sup>+</sup> clusters (Table 2). Addition of SAM to the reduced enzyme causes a rhombic perturbation to

the reduced axial signal and yields  $g$  values of 2.00, 1.93, 1.86, which reflect SAM’s coordination to the unique iron site (Table 2). Moreover, addition of substrate to reduced samples that have been treated with SAM causes further perturbation in the EPR signal. Purified BlsE was shown to utilize cytosylglycuronic acid (CGA) as a substrate, and upon incubation with either dithionite or flavodoxin/flavodoxin reductase as electron donors decarboxylates CGA to form cytosylarabinopyranose (CAP). dAdoH was formed in excess over CAP, pointing to uncoupled SAM cleavage by this enzyme. Importantly, a requirement for the [4Fe–4S] cluster in the reductive cleavage mechanism was demonstrated as mutation of the cysteine residues in the CX<sub>3</sub>CX<sub>2</sub>C motif abolished activity.

### 11. RADICAL SAM ENZYMES IN THE SYNTHESIS OF MODIFIED TETRACYCLES

Modified tetrapyrrole derivatives such as chlorophyll, heme, cobalamins, siroheme, cytochrome heme  $d_1$ , and coenzyme F<sub>430</sub> serve as essential metalloprosthetic components in metabolic processes in living organisms. The structural similarity of the tetrapyrrole derivatives underpins a similar, yet branched biosynthetic pathway involving the derivation of the macrocyclic progenitor uroporphyrinogen III from the metabolic precursor 5-aminolevulinic acid (Figure 90).<sup>387</sup> As mechanistic details to the biosynthesis of tetrapyrroles have been elucidated,

the oxygen-independent biosynthetic pathways share a common involvement of radical SAM enzymes. Radical SAM enzymes HemN, NirJ, AhbC, AhbD, and BchE/BchR are described in the following section.

### 11.1. HemN: An Oxygen-Independent Coproporphyrinogen Oxidase

Coproporphyrinogen III oxidases (CPOs) catalyze the conversion of coproporphyrinogen III to protoporphyrinogen IX, an essential step in the formation of heme from uroporphyrinogen III (Figure 90).<sup>387</sup> This step involves the oxidative decarboxylation of the propionate side chains of rings A and B to vinyl groups, producing 2 equiv of CO<sub>2</sub>. Two different enzymes in nature catalyze this reaction but are differentiated by their involvement of dioxygen. The oxygen-dependent enzyme HemF in eukaryotes catalyzes this reaction using dioxygen as an electron acceptor by a currently unknown mechanism;<sup>388</sup> HemN, in bacteria, catalyzes this reaction by an oxygen-independent mechanism involving SAM.<sup>100</sup> Early characterization of HemN-containing cell extracts, from *Rhodobacter sphaeroides*, *Chromatium* strain D, *Rhizobium japonicum*, and *S. cerevisiae* in the absence of oxygen, implicated a role for SAM as the L-Met, and ATP requirement could be replaced by SAM (in cell extracts, SAM synthetase could synthesize SAM from Met and ATP).<sup>389</sup> HemN was included in the original classification of the radical SAM enzymes,<sup>1</sup> thus pointing to the involvement of an oxygen-sensitive [4Fe–4S] cluster and SAM as requirements for activity.

**11.1.1. The Iron–Sulfur Cluster of HemN.** In the absence of oxygen, HemN was found to coordinate a single, site-differentiated [4Fe–4S]<sup>+</sup> cluster, as identified by UV-vis, EPR, and Mössbauer spectroscopic studies (Table 2).<sup>85,100</sup> EPR spectra were obtainable only in the absence of SAM, and had a large line width and substantial signal broadening, while samples in the presence of SAM were featureless.<sup>85</sup> However, the noted change in isomer shift in the obtained Mössbauer data suggested that SAM does bind to the site-differentiated site.<sup>85</sup> Interestingly, direct evidence for a radical mechanism for decarboxylation catalyzed by HemN was obtained when SAM and substrate coproporphyrinogen III were added to reduced HemN.<sup>390</sup> An organic radical EPR signal was observed at  $g_{\text{av}} = 2.0029$  with a complex pattern of hyperfine couplings from at least five different hydrogen atoms. Characterization of the substrate-derived signal (by using regiospecifically labeled <sup>15</sup>N or <sup>2</sup>H substrates) showed that the unpaired electron was delocalized over the  $\beta$ -carbon on the propionate side chain and the ring carbon atom between the methylene bridge and the pyrrole nitrogen via allylic radical stabilization.<sup>390</sup> The location of this substrate radical in the porphyrin ring is consistent with the proposed mechanism in which the dAdo<sup>•</sup> radical abstracts the pro-S hydrogen at the position of the propionate side chain to initiate the oxidative decarboxylation reaction.<sup>390</sup>

**11.1.2. Structural Characterization of HemN.** HemN was the first structurally characterized member of the radical SAM enzyme superfamily (Figure 91).<sup>241</sup> The structure of HemN is a  $(\beta\alpha)_6$  TIM barrel fold that binds a [4Fe–4S] cluster and two molecules of SAM.<sup>241</sup> While the structure was solved in the absence of substrate (coproporphyrinogen III) or product (protoporphyrinogen IX), the [4Fe–4S] cluster is bound in an amphipathic environment within the barrel; half of the cluster is surrounded by hydrophobic residues, and the other half of the cluster is surrounded by hydrophilic residues.<sup>241</sup> The first molecule of SAM (SAM #1) coordinates

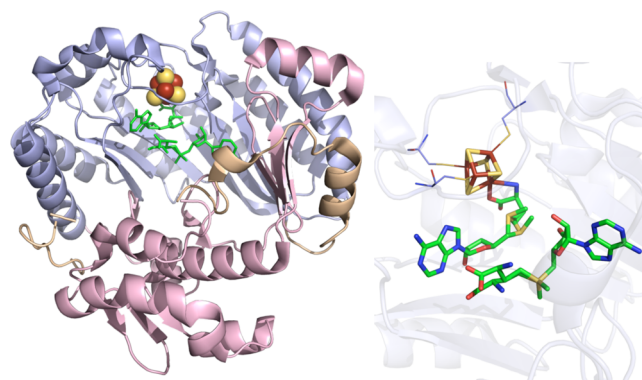


**Figure 91.** HemN crystal structure (PDB ID 1OLT). Left: N-terminal domain colored in wheat, radical SAM domain in light blue, C-terminal domain in light pink, [4Fe–4S] cluster in yellow and rust spheres, and SAM in green sticks. Right: Active site of HemN where the [4Fe–4S] cluster (yellow and rust) and SAM (green carbons) are depicted in sticks with oxygens colored red and nitrogens colored blue. Cysteines (light blue carbons) involved in ligating clusters are depicted in lines.

the unique iron atom of the [4Fe–4S] cluster as seen in other structures. Interestingly, the second molecule of SAM (SAM #2) binds in a position adjacent to the [4Fe–4S] coordinated SAM #1, and is held in place by five amino acids that are conserved to varying degrees among HemN sequences.<sup>241</sup> A hydrophilic pocket lined with charged residues sits symmetrically adjacent to the sulfonium of SAM #1 and SAM #2 and appears to be positioned near the propionate side chains in the substrate-bound model.<sup>241</sup> Interestingly, a stretch of N-terminal conserved residues (PRYTSYPTA) interfaces with the C-terminal domain, and is in proximity (9 Å) from the coordinated SAM molecule.<sup>241</sup> While the sequence corresponded to a poorly structured region of the crystal structure, this “trip-wire” loop has been proposed to help stabilize binding of substrate, as well as to possibly close the active site upon substrate binding.<sup>241</sup>

**11.1.3. Insight into the HemN Mechanism.** The mechanism of iterative decarboxylation events by HemN is intriguing, in that 2 equiv of SAM appear essential to the chemical reaction mechanism (Figure 92),<sup>100,241</sup> similar to BioB, LipA, and RlmN (sections 4.1, 4.2, 7.1). The overall HemN reaction involves a net four electron oxidation, probably involving two H-atom abstractions by dAdo<sup>•</sup> followed by two one-electron oxidations.<sup>100</sup> The specific role that SAM #2 serves in the HemN mechanism is unclear; however, it is apparent that direct reduction of SAM #2 by the [4Fe–4S] cluster is not feasible.<sup>85,100</sup> Mutagenesis studies of the amino acids responsible for binding SAM #2 provide strong evidence for the involvement of both SAM #1 and SAM #2 in the catalytic mechanism of protoporphyrinogen IX formation, invoking two active sites for decarboxylation of each propionate side chain relative to each SAM molecule.<sup>100,241</sup> It has been proposed that substrate coproporphyrinogen binding may induce rotation around the CS’–S bond of SAM #2, moving the sulfonium sulfur atom of SAM #2 closer to SAM #1. In this case, the first electron transfer event to SAM #1 might be immediately transferred to SAM #2, with the resulting SAM #2-derived dAdo<sup>•</sup> then abstracting a H-atom from the  $\beta$ -carbon of the substrate propionate side chain to produce an allylically stabilized coproporphyrinogen substrate radical.<sup>390</sup> Decarboxylation then would then result in electron transfer to the

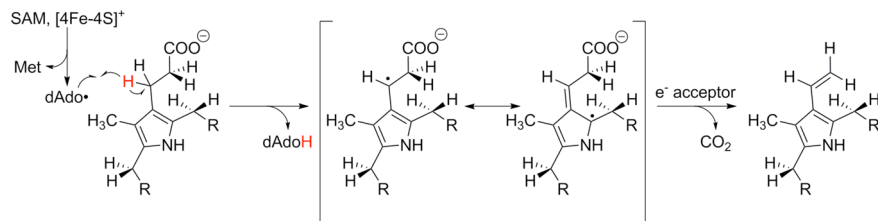


**Figure 92.** The mechanism of iterative decarboxylation events by HemN.

unknown oxidizing agent. Subsequent rereduction of the [4Fe–4S]<sup>2+</sup> cluster would result in cleavage of SAM #1 and the second decarboxylation of substrate, this time via the SAM #1-derived dAdo<sup>•</sup>.<sup>390</sup>

The net two decarboxylation events performed on 1 equiv of coproporphyrinogen is a complex reaction performed at a single [4Fe–4S] cluster (Figures 90 and 92). The proposed sequence of events above is consistent with the appearance of two molecules of SAM in the structure, and with the previously discussed biochemical evidence for the catalytic relevance of SAM #2.<sup>390</sup> If decarboxylation occurred only at the SAM #1 site, then following the first reductive cleavage of SAM #1 and subsequent oxidative decarboxylation of the first propionate side chain, another molecule of SAM would have to replace the methionine and dAdoH products of SAM cleavage. An alternative mechanism involves SAM #2 serving as the initial electron acceptor following the first decarboxylation reaction (initiated via the cleavage of SAM #1), thereby generating the second dAdo<sup>•</sup> radical.<sup>390</sup> The latter mechanism bypasses the need to transfer an electron from SAM #1 to SAM #2 for the initial cleavage event, although it still requires the presence of an unidentified electron acceptor molecule for the second decarboxylation reaction.<sup>390</sup>

While the sequential decarboxylation of the propionate side chains of ring A followed by ring B of coproporphyrinogen III has been well established in oxygen-dependent HemF catalysis,<sup>391</sup> this aspect of the mechanism in HemN catalysis remains uncertain. If the decarboxylation mechanism proceeds sequentially, one propionate side chain of either ring A or B will be decarboxylated first, forming either a harderoporphyrinogen (ring A) or an isoharderoporphyrinogen (ring B) intermediate; alternatively, both propionate side chains could be decarboxylated simultaneously (Figure 90). Incorporating HPLC and ESI–MS analysis, a HemN catalytic intermediate monovinyl-tripropionic acid porphyrin, containing one propionate side chain decarboxylated to the corresponding vinyl group, was observed that displayed properties similar to those of the intermediate harderoporphyrinogen (3-vinyl-8,13,17-tripropionic acid-2,7,12,18-tetramethylporphrin) in HemF catalysis; when synthesized, this harderoporphyrinogen intermediate yielded the protoporphyrin IX product in the presence of HemN, thus supporting a HemN mechanism involving sequential decarboxylation of the propionate side chains.<sup>392</sup> The similarity of the intermediates in HemN and HemF catalysis, in conjunction with HemN product (protoporphyrinogen IX) formation from this synthesized intermediate, implies the monovinyl intermediate from the decarboxylation of the ring A propionate side chain occurs first. It should be noted that the alternative possibility that the monovinyl intermediate is the 3-vinyl isoharderoporphyrinogen currently has not been tested, due to lack of an isolatable isoharderoporphyrinogen standard.<sup>392</sup>

## 11.2. NirJ and Related Enzymes in the Synthesis of Heme d<sub>1</sub>

The iron-containing cytochrome cd<sub>1</sub> (NirS) is a nitrite reductase that catalyzes the conversion of nitrite to nitric oxide and water at an iron-containing dioxo-isobacteriochlorin, called heme d<sub>1</sub>.<sup>393</sup> The macrocycle consists of addition of an unusual set of oxo, methyl, and acrylate substituents that branches from the traditional heme biosynthetic pathway at uroporphyrinogen III with formation of bis-methylated intermediates, making siroheme (Figure 90).<sup>394</sup> Gene nirJ from *Pseudomonas aeruginosa* (*orf393* from *Pseudomonas stutzeri*) is part of an identified gene cluster involved in heme d<sub>1</sub> biosynthesis that was found to have protein sequence homology to PqqE-related proteins<sup>395</sup> and later to NifB and MoaA proteins<sup>393c</sup> by the CX<sub>3</sub>CX<sub>2</sub>C motif.

As a putative radical SAM enzyme, NirJ has been proposed to be involved in the transformation of siroheme to heme d<sub>1</sub>; however, biochemical characterization of the other proteins involved to date remains largely uncharacterized, limiting mechanistic insight. NirJ from *Paracoccus pantotrophus* has been shown to coordinate a [4Fe–4S] cluster, likely site-differentiated, located at the N-terminal CX<sub>3</sub>CX<sub>2</sub>C motif (Table 2).<sup>110</sup> Addition of SAM resulted in an observable perturbation in an EPR signal consistent with SAM coordination. NirJ contains an additional C-terminal CX<sub>2</sub>CX<sub>5</sub>C motif that may coordinate an additional Fe–S cluster, but the role that this motif serves is currently unclear.<sup>110</sup>

Sulfate-reducing bacteria and archaea synthesize heme through oxidation of siroheme, involving the activity of two NirJ-like radical SAM enzymes, Ahb-NirJ1 (AhbC) and Ahb-NirJ2 (AhbD) (from *P. pantotrophus* and *Desulfovibrio vulgaris*, respectively) (Figure 90).<sup>396</sup> That a common precursor (siroheme) is used by NirJ and AhbC/AhbD enzymes suggested that a common intermediate serves as a branching point between the two pathways.<sup>396b</sup> Recently, didecarboxysiroheme was identified as the common intermediate for the NirD-L, G, and H complex lacking NirJ, as well as for *D. desulfuricans* AhbA–AhbB complex lacking AhbC and AhbD (Figure 90).<sup>396b</sup> For the Ahb system, incubation of anaerobically prepared cell lysates of *D. vulgaris* with siroheme resulted in formation of monodecarboxy-, didecarboxy-, monovinyl Fe-coproporphyrin III, as well as heme that required the involvement of AhbC and AhbD.<sup>396b</sup> Individual recombinant overexpression of *Methanoscincina barkeri* AhbC and *D. desulfuricans* AhbD has elucidated the likely reaction catalyzed by these radical SAM enzymes. Coincubation of AhbC cell extracts with didecarboxysiroheme resulted in production of Fe-coproporphyrin, while coincubation of AhbD cell extracts with Fe-coproporphyrin, SAM, and dithionite resulted in synthesis of predominantly heme product.<sup>396b</sup> Thus, it appears that AhbC catalyzes acetic acid side chain loss at C2 and C7 to synthesize Fe-coproporphyrin, while AhbD catalyzes a reaction

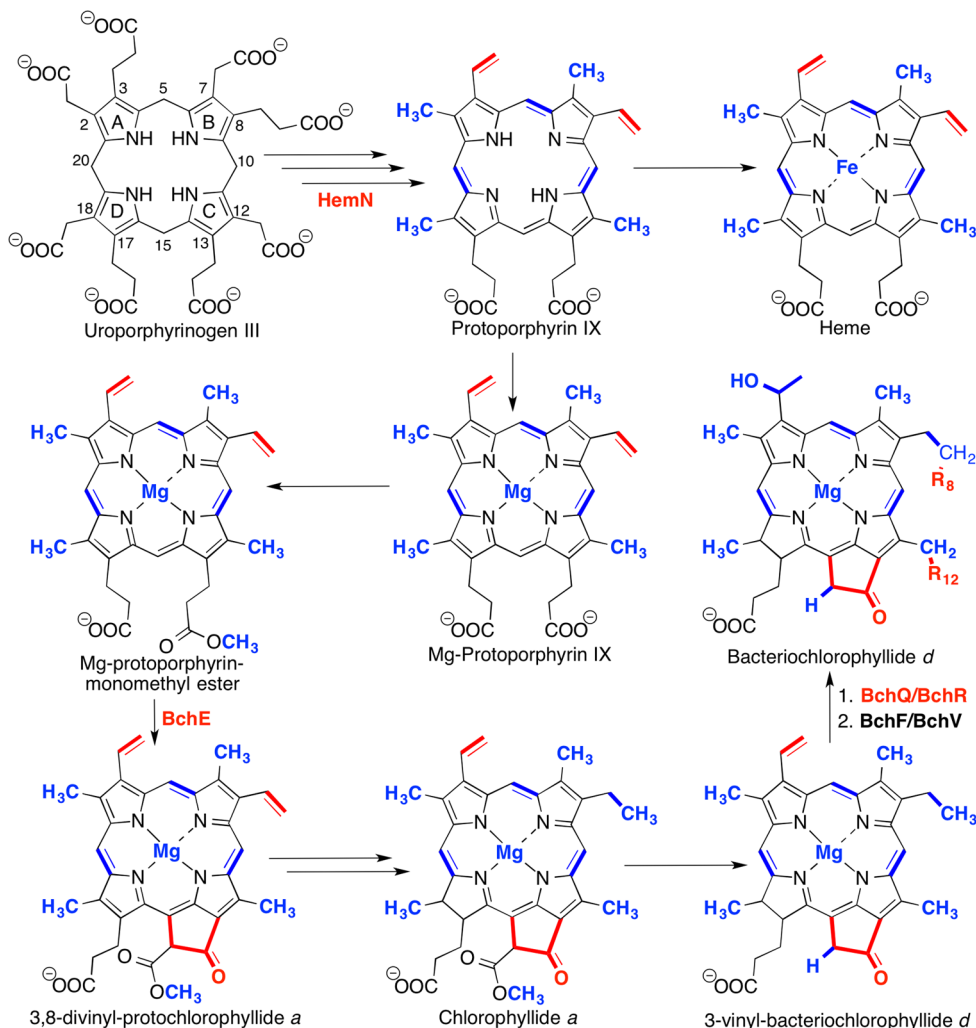


**Figure 93.** Chlorophyll and bacteriochlorophyll biosynthetic pathway. Involvement of radical SAM enzymes (and their respective transformation catalyzed) is bolded in red, while nonradical SAM enzyme involvement is bolded in blue.

similar to HemN, catalyzing CO<sub>2</sub> loss.<sup>396b</sup> In the case of NirJ, an additional enzyme (NirF) is involved and has been proposed to serve as a dehydrogenase; NirJ is therefore proposed to catalyze oxo group formation via propionate loss to synthesize a heme d<sub>1</sub> precursor.<sup>396b,397</sup>

### 11.3. BchE in Chlorophyll and Bacteriochlorophyll Biosynthesis

The conversion of light energy to chemical energy (chlorophototrophy) occurs in organisms that synthesize the pigment chlorophylls and bacteriochlorophylls or carotenoids.<sup>398</sup> The chlorophylls and bacteriochlorophylls are Mg-containing tetrapyrrole prosthetic groups that are synthesized through a coordinated biosynthetic pathway.<sup>399</sup> Interestingly, chlorophyll and bacteriochlorophyll biosyntheses follow biosynthetic routes similar to those of heme biosynthesis, up to protoporphyrin IX (Figures 90 and 93).<sup>399</sup> From here, the respective biosyntheses branch, as Mg chelation, ring modification, methylation, ring oxidation/reduction, and substituent modification result in a discrete family of chlorophyll and bacteriochlorophyll pigments.<sup>399</sup>

A particularly complex step in the synthesis of chlorophylls and bacteriochlorophylls is the formation of a five-membered isocyclic (E) ring from Mg-protoporphyrin-monomethyl ester, forming 3,8-divinyl-protoclorophyllide a (Figure 93).<sup>399</sup> Many

aspects of ring formation that are beyond the scope of this Review are reviewed elsewhere.<sup>400</sup> Chlorophyll biosynthesis can occur in organisms that live in aerobic and anaerobic environments, and redundant synthetic routes to catalyze ring cyclization have been identified in organisms adapted to either environment.<sup>401</sup> Oxygen isotope labeling and genetics studies have shown that the oxygen-dependent oxidase/cyclase AcsF and the oxygen-independent (radical SAM) oxidase/cyclase BchE catalyze isocyclic ring formation as chemically distinct reactions.<sup>402</sup> Of the latter, the only gene that appeared to be required for cyclase activity in *Rhodobacter capsulatus* was *bchE*.<sup>401a,403</sup>

Although the photosynthetic genes, including the *bchE* gene, were sequenced in 1995,<sup>404</sup> identification of BchE as a radical SAM enzyme was not made until the grouping of radical SAM enzymes as a superfamily in 2001.<sup>1</sup> BchE possesses a cobalamin-binding domain required for activity,<sup>405</sup> differentiating it from most other radical SAM enzymes. Its identification as both a radical SAM enzyme and a cobalamin-binding enzyme makes BchE structurally similar to the class B radical SAM methyltransferase enzymes discussed in section 7.1,<sup>285,296</sup> although at present, no *in vitro* characterization of the enzyme has been performed.

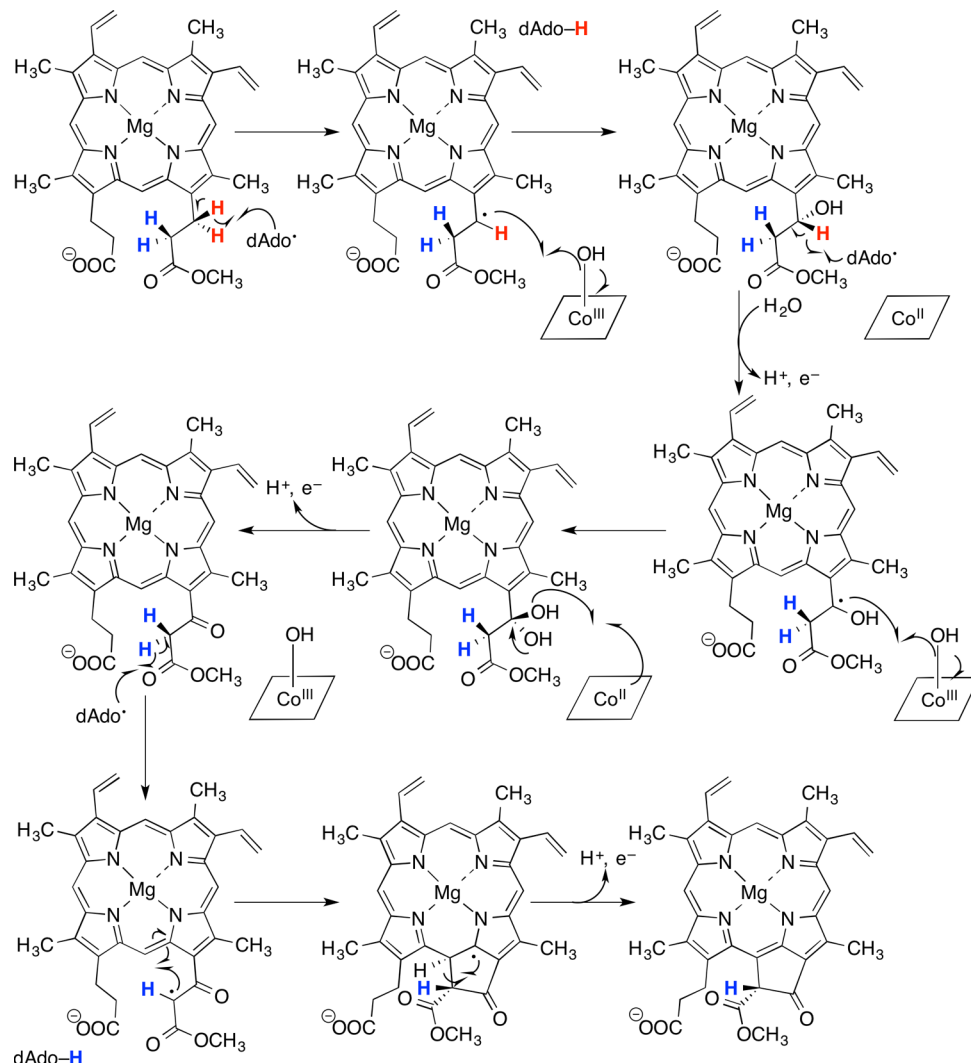


**Figure 94.** Putative mechanism of BchE-catalyzed ring cyclization, where both the radical SAM Fe–S cluster and the cobalamin-binding domains participate in the ring cyclization reaction.

A mechanism for ring cyclization<sup>400</sup> encompassing both dAdo<sup>•</sup> generation from the radical SAM Fe–S cluster and involvement of the cobalamin cofactor has been proposed (Figure 94).<sup>296</sup> The mechanism resembles the P-methylase mechanism proposed for class B methyltransferases (section 7.1; Figure 57).<sup>285,406</sup> In such a mechanism, the dAdo<sup>•</sup> (generated from reductive cleavage of SAM at the site-differentiated Fe–S cluster) abstracts an H-atom at the C13<sup>1</sup>-position of the Mg-protoporphyrin-monomethyl ester, forming a substrate radical.<sup>296</sup> The hydroxocobalamin cofactor then transfers a hydroxyl radical to the substrate, forming the C13<sup>1</sup>-hydroxo product that has been previously isolated, as well as cob(II)alamin.<sup>296,407</sup> The hydroxocobalamin cofactor is regenerated via one-electron oxidation and addition of a water molecule, thereby allowing it to transfer a second hydroxyl radical following a second abstraction of an H-atom at the C13<sup>1</sup>-position. The resulting C13<sup>1</sup>-geminal diol then collapses, forming the C13<sup>1</sup>-keto intermediate.<sup>296,407</sup> From here, subsequent H-atom abstraction at the C13<sup>2</sup>-position would result in ring cyclization. Protonation and oxidation of the pyrrole ring would result in formation of 3,8-divinylprotochlorophyllide *a* (Figure 94).

With the recent *in vitro* characterization of cobalamin-containing class B radical SAM methyltransferase enzymes (section 7.1), *in vitro* characterization of BchE should provide insight into the diversity that the cobalamin serves in the radical SAM-initiated mechanism expected by BchE. As noted above, BchE is expected to initiate a unique biotransformation relative to class B radical SAM methyltransferases, using structurally similar bound cofactors as part of the mechanism.

#### 11.4. BchQ/BchR: Methyl Transfer in Chlorophyll Biosynthesis

The biosyntheses of chlorophyll and bacteriochlorophyll photosynthetic pigments share a complex diversity of chemical modifications, including methylation, dehydration, oxidation, and esterification, around a central tetrapyrrole ring to convert light to chemical potential energy.<sup>399</sup> In addition to the rich radical SAM chemistry involved in tetrapyrrole biosynthesis and modifications described for AhbC, AhbD, BchE, HemN, and NirJ (sections 11.1–11.3), radical SAM enzymes are also involved in methyltransferase-type chemistry in chlorophyll-tetrapyrrole biosynthesis. Green sulfur bacteria have evolved unique, self-aggregating pigment structures (chlorosomes) to harvest solar energy. The chlorosome is composed of bacteriochlorophyll (BChl) *c*, *d*, or *e* pigments (Figure 93)

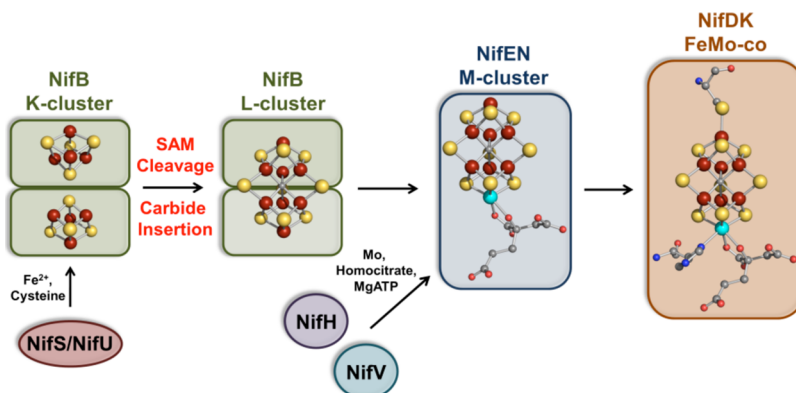


**Figure 95.** Nitrogenase FeMo-cofactor assembly.

that differ in the modifications around the central ring, as well as in the esterified product.<sup>399</sup> These central ring modifications help bacteria adapt to different levels of light. Approximately 200 000 BChl/Chl pigment molecules (in the green sulfur bacterium *Chlorobaculum tepidum*) comprise a chlorosome, and 97% of the total pigment content in the organism is BChl *c*<sub>F</sub> (BChl *c* esterified with farnesol).<sup>408</sup> This bacteriochlorophyll comprises a mixture of four homologues that carry different modifications at the C8<sup>2</sup> and C12<sup>1</sup> positions (ethyl, *n*-propyl, iso-butyl, or *neo*-pentyl at C8<sup>2</sup> and methyl or ethyl at C12<sup>1</sup>),<sup>409</sup> and it has been demonstrated that these side chains are derived from methylation reactions involving radical SAM chemistry.<sup>410</sup>

Relatively recent characterization of two gene products (BchQ and BchR) involved in chlorophyll biosynthesis demonstrate that they belong to the radical SAM superfamily and perform methyltransferase modifications on the BChl *c* pigments. BchQ modifies the C8<sup>2</sup> position with one or two methyls, while BchR modifies the C12<sup>1</sup> position with one methyl.<sup>409</sup> In *C. tepidum* mutant strains lacking the BchQ and/or BchR proteins, organism growth, especially at low light intensity, was impaired relative to wild-type as the amount of Bchl *c* produced could not be increased in low light.<sup>409</sup>

By amino acid sequence, BchQ and BchR are predicted to contain a cobalamin-binding domain, belonging to the class B radical SAM methyltransferase subfamily (section 7).<sup>285</sup> Therefore, methylations at the C8<sup>2</sup> and C12<sup>1</sup> positions likely require radical activation of the carbon atoms, possibly paralleling methyltransferase activities in enzymes such as GenK<sup>84</sup> and PhpK,<sup>116</sup> and TsrM<sup>89</sup> (section 7.1). Involvement of the cobalamin cofactor might mechanistically rationalize multiple methylation events occurring at the C8<sup>2</sup> position; however, a detailed investigation of the mechanism currently remains lacking. Regardless of the mechanism, the presence of these radical SAM methyltransferase enzymes is essential for reaching wild-type growth levels in *C. tepidum*.<sup>409</sup>

## 12. SYNTHESIS OF COMPLEX METAL CLUSTERS

The identification of radical SAM enzymes in the maturation pathways of complex metallocofactors like the FeMo-cofactor of nitrogenase and the H-cluster of [FeFe]-hydrogenase are relatively recent discoveries. Significant results over the past few years have provided great insight into the sophisticated reactions that are at the core of synthesizing these biological catalysts. New results related to the biosynthesis of these metallocofactors have shed light on the remarkable similarities between FeMo-co and H-cluster maturation; both synthesis pathways require standard iron sulfur cluster assembly

machinery to build the fundamental Fe–S cluster precursors, which then become modified throughout maturation. Moreover, biosynthesis exploits scaffold, carrier, and NTPase enzymes to foster cofactor assembly. Furthermore, the maturation events are distinctly merged through their common dependence on radical SAM chemistry, which is at the core of catalyzing the formation of the unique ligand sets that convey the essential reactivity to FeMo-co and the H-cluster. Last, maturation is completed by insertion of the modified cluster units into cofactorless forms of the target enzymes.<sup>411</sup>

### 12.1. NifB and the Biosynthesis of the FeMoCo of Nitrogenase

**12.1.1. Nitrogenase and the FeMoCo.** The majority of biological N<sub>2</sub> reduction to NH<sub>3</sub> on Earth is catalyzed by the Mo-nitrogenase enzyme, which houses a complex [MoFe<sub>7</sub>S<sub>9</sub>C] cluster known as FeMo-co; this cluster exists as [Fe<sub>4</sub>S<sub>3</sub>] and [MoFe<sub>3</sub>S<sub>3</sub>] subclusters bridged by three sulfide ions, with a carbon at the center of the cluster. The cofactor itself is coordinated to the nitrogenase protein through one cysteine thiolate ligand to the terminal Fe ion and a histidine and homocitrate molecule to the Mo ion. Importantly, at the core of the metal sulfur cluster unit is a μ<sub>6</sub>-light atom only recently characterized as a carbide ion.<sup>412</sup> The Mo-nitrogenase (Nif) is a two-component enzyme comprised of the Fe-protein (NifH) and the MoFe protein (NifDK), which together catalyze the reaction N<sub>2</sub> + 8e<sup>−</sup> + 16MgATP + 8H<sup>+</sup> → 2NH<sub>3</sub> + H<sub>2</sub> + 16MgADP + 16P<sub>i</sub>.<sup>413</sup> The FeMo-cofactor is responsible for N<sub>2</sub> reduction and is housed within the α-subunit of NifD. A second iron–sulfur cluster, referred to as the P-cluster, is bound at the α/β subunit interface of a single NifDK αβ dimer. Complex formation between NifH and NifDK positions the [4Fe–4S] cluster of the Fe-protein in proximity to the P-cluster, forming a conduit for ATP-dependent electron flow into the FeMo-co for N<sub>2</sub> reduction.<sup>414</sup> Biosynthesis of FeMo-co and its insertion into apoenzyme requires the participation of a multitude of gene products that include several scaffold and carrier proteins, the generalized Fe–S cluster assembly proteins NifS and NifU, and the radical SAM enzyme NifB.<sup>415</sup>

**12.1.2. Biogenesis of the FeMoCo and Nitrogenase Maturation.** Cofactor assembly begins with the synthesis of standard Fe–S clusters by the cysteine desulfurase NifS and the scaffold NifU, which then transfers these building block units to NifB where assembly of the core Fe–S unit of FeMo-co occurs (Figure 95). The identification from sequence annotation of NifB as a putative radical SAM protein based on the presence of an N-terminal CX<sub>3</sub>CX<sub>2</sub>C motif opened the exciting possibility

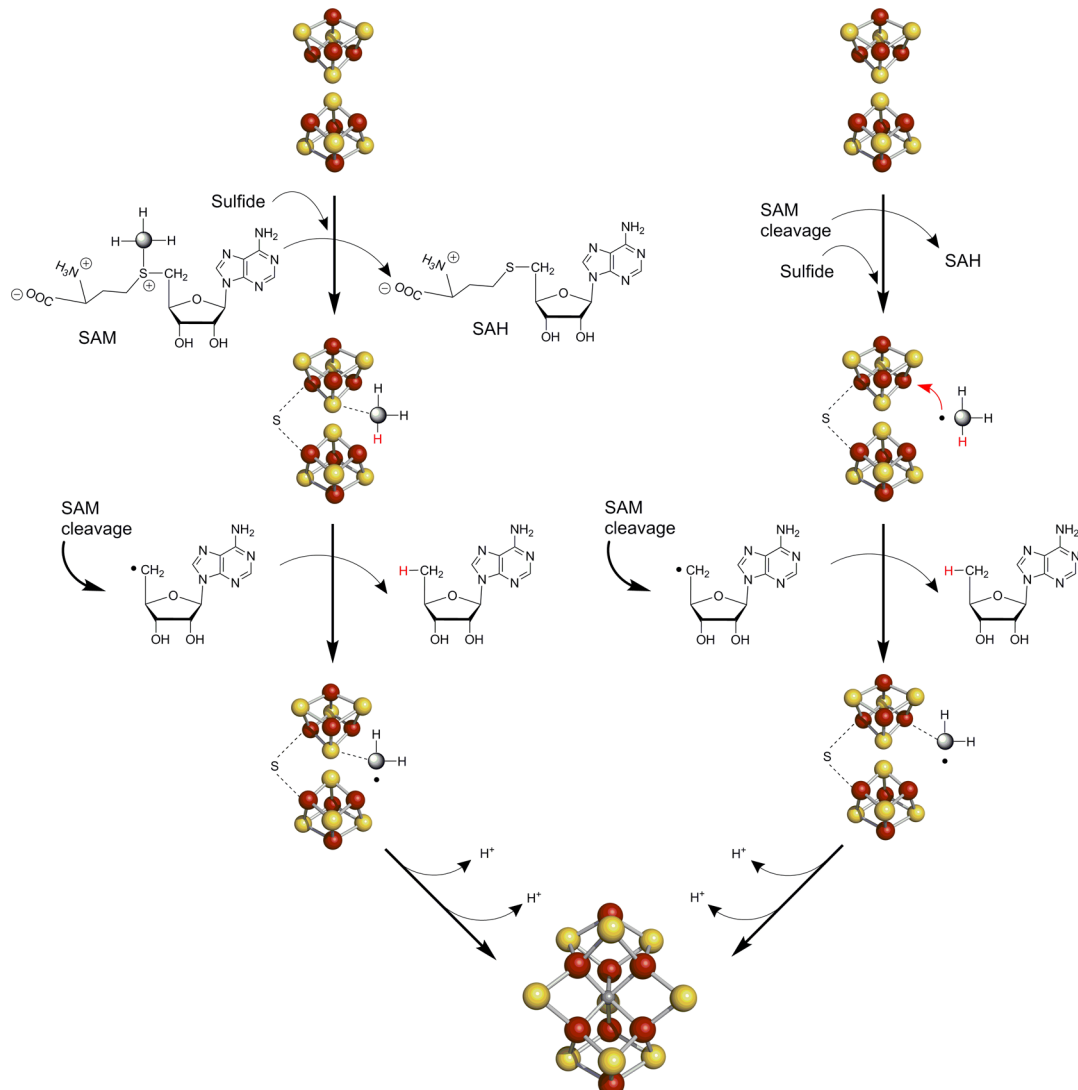


**Figure 96.** Radical SAM-based carbide insertion during FeMo-co biosynthesis. NifB is proposed to form the  $[\text{Fe}_8-\text{S}_9]$  L-cluster from the K-cluster, two  $[\text{4Fe}-4\text{S}]$  precursor units. The left pathway invokes methylation of a cluster sulfide followed by generation of a methylene radical upon hydrogen atom abstraction by the dAdo $^{\bullet}$ . The right pathway proposes methyl radical formation via SAM cleavage followed by addition to an Fe ion of the cluster where further processing to a methylene radical occurs.

that radical SAM chemistry was essential for FeMo-co biosynthesis, especially because deletion of *nifB* was shown to result in a MoFe protein that lacked the cofactor.<sup>132,415b,416</sup> Early work demonstrated the incorporation of  $^{55}\text{Fe}$  and  $^{35}\text{S}$  labeled NifB-cofactor (NifB-co) into apo-nitrogenase,<sup>417</sup> and subsequent analysis revealed the existence of six conserved cysteine residues (in addition to the radical SAM motif) and eight conserved histidine residues, indicating that NifB likely bound accessory Fe–S clusters.<sup>415b</sup> Purification and characterization of the *nifB* gene product revealed that the as-isolated protein bound 12 iron atoms per dimer and could be reconstituted to levels of 18 iron atoms per dimer. The protein displayed characteristic Fe–S cluster LMCT features in the UV-vis region, which bleached upon addition of sodium dithionite.<sup>132</sup> In vitro biosynthetic studies demonstrated that FeMo-co assembly and activation of apo-nitrogenase could be accomplished with a minimal set of components including NifB, SAM,  $\text{Fe}^{2+}$ ,  $\text{S}^{2-}$ , molybdate, homocitrate, NifEN, and NifH.<sup>418</sup> The activity of NifB was shown to be highly sensitive to  $\text{O}_2$ , and the addition of the SAM analogue S-

adenosylhomocysteine inhibited FeMo-co synthesis. Moreover, it was shown that NifB-co binds to NifX (see below), which then transfers the intermediate to NifEN where it is further modified via addition of iron, sulfide, molybdenum, and homocitrate.<sup>127b</sup>

Biochemical studies of NifX demonstrated that this small carrier protein binds NifB-co with a  $K_d \approx 1 \mu\text{M}$  (in many known diazotrophs NifB exists as a fusion protein with a NifX domain),<sup>419</sup> allowing for EXAFS and NRVS measurements to be performed on the NifX:NifB-co complex.<sup>420</sup> The Fe K-edge spectra of NifB-co are nearly superimposable with that of FeMo-co, indicating that the oxidation states and ligand environments of the Fe atoms between these two cofactors are nearly identical. Analysis of the Fourier transform of the Fe K-edge EXAFS region revealed a set of sulfur ligands at 2.3 Å, a set of Fe next nearest neighbors at 2.6 Å, and a set of long-range Fe–Fe interactions at 3.7 Å; these interactions are characteristic of FeMo-co itself and provide evidence for the existence of a “FeMo-co like” core in NifB-co.<sup>420</sup> Model fits to the experimental data showed that the Fe–S core best

describing the experimental distances was a  $[\text{Fe}_6\text{--S}_9]$  trigonal prismatic  $D_{3h}$  model that contained a single C, N, or O interstitial atom.<sup>420</sup> NRVS measurements showed the presence of a broad band between 183 and 198  $\text{cm}^{-1}$ , a feature only previously observed in NRVS of nitrogenase and isolated FeMo-co, thus providing additional support for the  $[\text{Fe}_6\text{--S}_9]$  model comprised of an interstitial atom.<sup>420</sup>

**12.1.3. Radical SAM Chemistry and the Insertion of the Interstitial Carbide.** One of the significant challenges related to the elucidation of NifB's role in FeMo-co maturation is the fact that the purified NifB from *Azotobacter vinelandii* is unstable.<sup>132</sup> By fusing the *nifB* and *nifN* genes, Ribbe and co-workers created a NifEN-B protein complex that was amenable to spectroscopic and kinetic analysis.<sup>133</sup> Metal analysis coupled with UV-vis and EPR studies of the NifEN-B complex show that the two precursor Fe–S clusters bound to NifB (referred to as the K-cluster) are  $[4\text{Fe}\text{--}4\text{S}]$  in nature; given the similar decrease in  $S = 1/2$  signal intensity for the K-cluster and the radical SAM cluster following addition of SAM, it was surmised that these Fe–S cluster moieties are in close proximity with one another (Table 2).<sup>133,421</sup> Importantly, the concomitant decrease in  $[4\text{Fe}\text{--}4\text{S}]^+$  signal intensity following addition of SAM is accompanied by the formation of a specific  $g = 1.94$  feature attributed to an  $[\text{Fe}_8\text{--S}_9]$  cluster referred to as the L-cluster. This observation implies that the redox perturbations at the SAM cluster (presumably caused by the reductive cleavage of SAM) have an immediate impact on the properties of the K-cluster, resulting in formation of the eight Fe intermediate L-cluster, calling into question the relevance of the  $[\text{Fe}_6\text{--S}_9]\text{--X}$  NifB-co cluster.<sup>133</sup> Several studies have demonstrated that the L-cluster bound to NifEN very much resembles FeMo-co itself, with the exception that an iron ion replaces the Mo and homocitrate groups.<sup>422</sup> Valence to core Fe K $\beta$  X-ray emission spectroscopic studies of NifEN established the presence of carbon in the  $[\text{Fe}_8\text{--S}_9]$  L-cluster, a result consistent with the NifB-based insertion of the carbide during K-cluster coupling.<sup>423</sup>

The observation made in 2007 by Rubio and co-workers that the minimal in vitro system to achieve FeMo-co biosynthesis and activation of apo-nitrogenase required only NifB, NifEN, NifH, SAM,  $\text{Fe}^{2+}$ ,  $\text{S}^{2-}$ , molybdate, homocitrate, and Mg-ATP suggested that SAM itself was a likely source for the interstitial carbide.<sup>418</sup> However, given the instability of NifB, this question could not be directly biochemically probed until the NifEN-B complex was prepared by Wiig and co-workers.<sup>133</sup> SAM cleavage assays in the presence of NifEN-B and reductant showed that SAM was converted into both S-adenosylhomocysteine (SAH) and dAdoH.<sup>424</sup> Experiments performed with deuterium labeled SAM ( $[\text{methyl-}d_3]\text{-SAM}$ ) showed the NifEN-B-based formation of SAH along with deuterium-enriched and natural abundance dAdoH. Intriguingly, the two radical SAM RNA methylases RlmN and Cfr (section 7.1), which utilize 2 equiv of SAM in the methylation of RNA, both display similar SAM cleavage and deuterium isotope patterns as NifEN-B.<sup>111b,c,295</sup> These observations therefore suggested that NifB also employed the methyl group of SAM as a carbon source. Radiolabeling experiments with  $[\text{methyl-}^{14}\text{C}]\text{-SAM}$  demonstrate that the  $^{14}\text{C}$  group is incorporated into the L-cluster during the NifB dependent coupling of the K-clusters and that the  $^{14}\text{C}$  isotope can ultimately be tracked to NifDK during the maturation process of the M-cluster.<sup>424</sup>

Two proposals have been put forth for the NifB-catalyzed formation of the L-cluster and are highlighted in Figure 96.<sup>424</sup>

The first invokes the  $\text{S}_{\text{N}}2$  based transfer of the methyl group of SAM to a sulfide ion of the K-cluster to yield a transient methanethiol ligand and SAH as products; the methanethiol group is then activated to form a methylene radical via H-atom abstraction from a 5'-deoxyadenosyl radical, which is formed upon the reductive cleavage of a second molecule of SAM. At this stage, the radical intermediate must undergo a ligand exchange event with the Fe ions of the cluster followed by removal of two additional hydrogen atoms to form the interstitial carbide moiety. An alternate mechanism suggests that the reductive cleavage of SAM results in formation of SAH and a methyl radical (Figure 96).<sup>424</sup> The methyl radical is thought to be captured by an  $\text{Fe}^{2+}$  ion of the K-cluster, generating an  $\text{Fe}\text{--C}$  bond.<sup>424</sup> Another molecule of SAM then undergoes reductive cleavage, and the resulting dAdo $\cdot$  radical is believed to abstract a H-atom from the intermediate, generating a methylene radical species. Regardless of the mechanism, formation of the eight iron L-cluster from the coupling of the two  $[4\text{Fe}\text{--}4\text{S}]$  K-clusters requires addition of a bridging sulfide ion from an unknown source, as well as the subsequent dehydrogenation or deprotonation events from the methylene radical intermediate that accompany  $\text{Fe}\text{--C}$  bond formation as the interstitial  $\mu_6$ -carbide is ultimately generated. Another outstanding question relates to the existence of carbide itself and why this central atom is required for the mechanism of  $\text{N}_2$  reduction by nitrogenase. A report monitoring the fate of either  $^{13}\text{C}$  or  $^{14}\text{C}$  labeled FeMo-co under substrate turnover conditions demonstrated that the interstitial carbide neither undergoes an exchange reaction nor can it be consumed as a substrate and incorporated into products.<sup>425</sup> These data suggest that the carbide acts to stabilize the structure of the cluster, although it certainly still remains possible that it could be involved in either binding substrate and/or tuning the electronic properties of the cofactor itself. Despite these outstanding issues, the progress made in recent years has provided a very clear picture as to how NifB and radical SAM chemistry are at the heart of synthesizing one of the most elegant metallocofactors in biology.

## 12.2. Biosynthesis of the H-Cluster of the [FeFe]-Hydrogenase

Hydrogenases are metalloenzymes that are integral components of metabolic pathways in a variety of microorganisms, either accepting electrons from reduced Fe–S carrier proteins like ferredoxin that accumulate during fermentation, or coupling the oxidation of  $\text{H}_2$  to energy yielding processes according to the reaction  $\text{H}_2 \rightleftharpoons 2\text{H}^+ + 2\text{e}^-$ .<sup>426</sup> Two classes of hydrogenase enzymes found in nature are the [NiFe]- and [FeFe]-hydrogenases; these enzymes are phylogenetically unrelated, with the [NiFe] enzymes routinely biased toward  $\text{H}_2$  oxidation and the [FeFe] enzymes biased toward  $\text{H}_2$  evolution.<sup>427</sup> [FeFe]-hydrogenases are found in bacteria and eukarya, and contain a complex metal center, referred to as the H-cluster, that is responsible for proton reduction. The composition of the H-cluster was determined by X-ray crystallographic analysis of the [FeFe]-hydrogenase (HydA) enzymes from *Clostridium pasteurianum* (CpI)<sup>428</sup> and *Desulfovibrio desulfuricans*,<sup>429</sup> complemented by FTIR spectroscopic studies.<sup>430</sup> The unique active site metal cluster consists of a  $[4\text{Fe}\text{--}4\text{S}]$  cubane that is bridged to a 2Fe subcluster through a cysteinyl thiolate linkage; the 2Fe subcluster contains three CO, two  $\text{CN}^-$ , and a bridging dithiolate moiety as ligands.<sup>428,429</sup> These  $\pi$ -acid ligands participate in back bonding with the metal ions, thereby

stabilizing lower oxidation states of the Fe and facilitating the rapid and reversible oxidation and reduction reactions associated with hydrogen catalysis.<sup>431</sup> The 2Fe subcluster in as-purified HydA is described as a low spin  $S = 1/2$  state with an Fe(II)/Fe(I) pair,<sup>432</sup> and the distal Fe atom is likely the site for proton binding and reduction.<sup>433</sup>

**12.2.1. H-Cluster Maturation Machinery.** Early efforts to heterologously express HydA in *Escherichia coli* (which lacks an endogenous [FeFe]-hydrogenase) yielded inactive enzyme,<sup>434</sup> demonstrating that *E. coli* is unable to properly assemble the active site H-cluster. A ground-breaking discovery came about through the work of Posewitz and King<sup>435</sup> who identified three hydrogenase accessory genes *hydE*, *hydF*, and *hydG* (*hydE* and *hydF* exist either as separate gene products or as a fused gene depending on the organism) that are absolutely conserved in all organisms containing [FeFe]-hydrogenases. They also demonstrated that active HydA is obtained when the hydrogenase gene is coexpressed with these accessory genes. Moreover, it was soon reported that inactive HydA overexpressed in *E. coli* alone (HydA<sup>ΔEFG</sup>) could be activated through the *in vitro* addition of an *E. coli* lysate containing overexpressed *hydE*, *hydF*, and *hydG* together, indicating that HydE, HydF, and HydG were the only unique components required to properly assemble the H-cluster.<sup>436</sup>

Analysis of the amino acid sequences of HydE and HydG revealed the presence of the canonical CX<sub>3</sub>CX<sub>2</sub>C motif characteristic of the radical SAM superfamily, while HydF contained several putative C-terminal Fe–S cluster binding ligands and was anticipated to be a GTPase given the presence of N-terminal Walker A P-loop and Walker B Mg<sup>2+</sup> binding motifs.<sup>129,435,437</sup> Importantly, site-directed mutagenesis studies have shown that the [4Fe–4S] cluster binding motifs in HydE and HydG, as well as both the GTPase and the Fe–S cluster binding regions of HydF, are all necessary to achieve proper H-cluster assembly and active hydrogenase.<sup>435b</sup> Collectively, these observations led to the development of a hypothetical pathway for H-cluster assembly that served as a platform for biochemical studies in the following years.<sup>438</sup> Peters and co-workers proposed that HydE and HydG were involved in synthesizing the 2Fe subcluster unit on the scaffold HydF through the modification of a [2Fe–2S] cluster moiety; alkylation of the sulfide groups was thought to be a first step followed by the decomposition of a glycyl radical into CO and CN<sup>−</sup>. It was proposed that HydE, HydF, and HydG were solely directed at 2Fe subcluster synthesis as standard Fe–S cluster assembly machinery could be expected to synthesize the [4Fe–4S] cubane of the H-cluster.<sup>438</sup>

**12.2.2. HydA Expressed in the Absence of HydE, HydF, and HydG Contains a [4Fe–4S] Cluster.** All [FeFe]-hydrogenases contain a common active site domain but have a variety of distinct arrangements of accessory cluster domains.<sup>439</sup> The simplest [FeFe]-hydrogenases from chlorophycean algae, such as *Chlamydomonas reinhardtii*, contain only the active site domain,<sup>440</sup> and accordingly have become attractive targets for H-cluster directed studies.<sup>441</sup> Characterization of the *C. reinhardtii* HydA enzyme expressed in *E. coli* in the absence of *hydE*, *hydF*, and *hydG* demonstrated that the purified protein contained UV-vis, EPR, and Mössbauer spectroscopic features characteristic of [4Fe–4S]<sup>2+/+</sup> clusters.<sup>441b</sup> Moreover, neither the as-purified nor metal free forms of HydA<sup>ΔEFG</sup> were active toward H<sub>2</sub> production, but activity could readily be restored through either addition of *E. coli* cellular extracts containing *C. acetobutylicum* HydE, HydF, and HydG or addition of this

extract following chemical reconstitution of the [4Fe–4S] cluster. The results provided a strong foundation for the requirement of the preassembled [4Fe–4S] cubane of the H-cluster (presumably synthesized by standard iron sulfur cluster assembly machinery) prior to activation by the hydrogenase maturation enzymes.<sup>441b</sup>

The nature of the immature [FeFe]-hydrogenase, as well as insights into its activation, were clarified by the X-ray crystal structure of *C. reinhardtii* HydA<sup>ΔEFG</sup> (PDB ID 3LX4).<sup>441e</sup> This structure shows the presence of the [4Fe–4S] cubane of the H-cluster and the absence of electron density associated with the 2Fe subcluster. Together with the spectroscopic data, the structure presents direct experimental evidence that HydE, HydF, and HydG are solely directed at 2Fe subcluster maturation. Moreover, the HydA<sup>ΔEFG</sup> structure shows the presence of an electropositive channel filled with H<sub>2</sub>O molecules leading to the active site; comparison with the *CpI* WT HydA structure suggests that the channel is formed by two conserved loop regions that are disordered.<sup>439,441e</sup> Collectively, the data advocate for the stepwise synthesis of the H-cluster, with 2Fe subcluster insertion into HydA<sup>ΔEFG</sup> and structural rearrangement of the disordered loop regions over the channel enclosing the active site, as is schematically represented in Figure 97 and discussed in further detail in the following

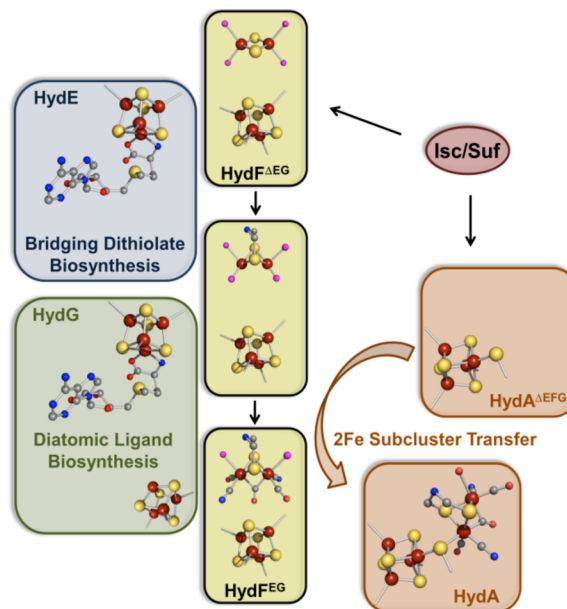


Figure 97. The proposed maturation pathway for the biosynthesis of the [FeFe]-hydrogenase H-cluster.

sections.<sup>439</sup> Additional support for this mechanism of assembly is provided by recent NRVS and EPR studies with *CpI* HydA.<sup>432c</sup> Kuchenreuther et al. showed that when <sup>56</sup>Fe containing *CpI* HydA<sup>ΔEFG</sup> is activated *in vitro* using <sup>57</sup>Fe labeled HydE, HydF, and HydG lysate mixtures enriched with exogenous <sup>57</sup>Fe, the <sup>57</sup>Fe isotope becomes associated with the 2Fe subcluster of the activated hydrogenase and not the [4Fe–4S] cubane of the H-cluster. This observation revealed that the cubane is not synthesized by the hydrogenase maturation machinery.

**12.2.3. HydF as an Assembly Scaffold or Carrier Protein for Radical SAM Chemistry.** In *in vitro* activation experiments of HydA<sup>ΔEFG</sup> demonstrated that H<sub>2</sub> evolution was

only observed when the immature hydrogenase was mixed with a strain of *E. coli* expressing HydE, HydF, and HydG in concert; activation of  $\text{HydA}^{\Delta\text{EF}}$  could not be attained when the maturation enzymes were either expressed individually or in varying combinations.<sup>436,441b</sup> Analysis of *C. acetobutylicum* HydE, HydF, and HydG proteins purified from *E. coli*-based coexpressions in which all three proteins were present ( $\text{HydE}^{\text{FG}}$ ,  $\text{HydF}^{\text{EG}}$ , and  $\text{HydG}^{\text{EF}}$ ) revealed that as-purified HydF from this genetic background activated  $\text{HydA}^{\Delta\text{EF}}$ , whereas HydF expressed in the absence of HydE and HydG ( $\text{HydF}^{\Delta\text{EG}}$ ) could not.<sup>442</sup> These data established that HydF acts as a scaffold or carrier protein transferring an H-cluster like species to HydA in the final step of hydrogenase maturation.

Given the presence of putative Fe–S cluster binding residues in HydF sequences and the requirement of these ligands in achieving hydrogenase maturation,<sup>435b</sup> it was postulated that this enzyme bound an Fe–S cluster that was somehow directly involved in the H-cluster assembly process. Several studies have now probed Fe–S cluster binding in both wild-type and variant forms of heterologously and homologously expressed HydF from *T. maritima*, *C. acetobutylicum*, *Thermotoga neopolitana*, and *Shewanella oneidensis*.<sup>437,443</sup> Low temperature EPR studies on *C. acetobutylicum*  $\text{HydF}^{\text{EG}}$  and  $\text{HydF}^{\Delta\text{EG}}$  proteins heterologously expressed in *E. coli* revealed two overlapping cluster signals in samples photoreduced using 5-deazariboflavin.<sup>443a</sup> On the basis of temperature dependence studies, the more prominent signal in samples of both  $\text{HydF}^{\text{EG}}$  and  $\text{HydF}^{\Delta\text{EG}}$  was assigned to a fast relaxing [4Fe–4S]<sup>+</sup> cluster ( $g = 1.89, 2.05$ ), while the overlapping feature was a slower relaxing signal attributed to a [2Fe–2S]<sup>+</sup> cluster ( $g = 2.00, 1.96$ ). FTIR studies on the  $\text{HydF}^{\text{EG}}$  and  $\text{HydF}^{\Delta\text{EG}}$  proteins revealed Fe–CO (1940 and 1881  $\text{cm}^{-1}$ ) and Fe–CN<sup>−</sup> (2046 and 2027  $\text{cm}^{-1}$ ) vibrations in as-purified  $\text{HydF}^{\text{EG}}$ , bands that were clearly absent in  $\text{HydF}^{\Delta\text{EG}}$ .<sup>443a</sup> Similarly, Czech and co-workers observed a high field component in the EPR spectrum of homologously expressed *C. acetobutylicum*  $\text{HydF}^{\text{EG}}$  that exhibited slower relaxation and was attributed to a Fe–S species belonging “to a cluster which contains three or less irons”; additionally, Fe–CN<sup>−</sup>, Fe–CO, and Fe–CO–Fe species were observed in FTIR spectra, fully consistent with a binuclear nature of the H-cluster intermediate bound to this enzyme.<sup>443b</sup> Interestingly, purified *S. oneidensis*  $\text{HydF}^{\text{EG}}$  displays very low hydrogen reduction/oxidation activity, behavior consistent with the presence of a 2Fe subcluster like moiety.<sup>444</sup> XAS studies of *C. acetobutylicum* HydF provided evidence for [4Fe–4S] and [2Fe–2S] clusters bound to  $\text{HydF}^{\Delta\text{EG}}$ , while the iron species on  $\text{HydF}^{\text{EG}}$  were highly similar to those in HydA, leading the authors to suggest that the 2Fe subcluster bound by HydF was directly bridged to the [4Fe–4S] cluster in a manner analogous to the H-cluster itself.<sup>443c</sup> Taken collectively, these results have helped to clarify the nature of the H-cluster like moiety bound to HydF and point to a role for HydE and HydG in modifying a [2Fe–2S] cluster precursor into the 2Fe subcluster.<sup>411</sup>

The nature of 2Fe subcluster binding to HydF is currently unresolved, although biomimetic studies using synthetic analogues of the 2Fe moiety have shown that these entities can be loaded into *T. maritima* HydF.<sup>445</sup> In addition, spectroscopic characterization provides evidence for the unique coordination of a CN<sup>−</sup> ligand where the carbon atom binds to an Fe ion of the [4Fe–4S] cubane while the nitrogen atom complexes the 2Fe unit;<sup>445</sup> further studies are warranted to determine if this unique bridging coordination exists in the natural enzyme. It is notable that EPR data collected on the *S.*

*oneidensis*  $\text{HydF}^{\Delta\text{EG}}$  protein show no evidence of [2Fe–2S]<sup>+</sup> cluster coordination.<sup>443e</sup> This result coupled with the observation that low levels of hydrogenase activation could be attained using *in vitro* cell lysate mixtures that lacked either HydE or HydF (but contained HydG) led to the proposal that HydG itself synthesizes the 2Fe subcluster (termed HydG-co), which is subsequently transferred to HydF and then  $\text{HydA}^{\Delta\text{EF}}$  to accomplish hydrogenase maturation.<sup>443e</sup> Additional experimental evidence is needed to demonstrate whether the 2Fe subcluster is first built on HydG or is directly synthesized on HydF.

#### 12.2.4. Radical SAM Chemistry and the Synthesis of Diatomic Ligands. 12.2.4.1. *HydG Preliminary Characterization and Substrate Identification.*

The involvement of radical SAM chemistry in [FeFe]-hydrogenase maturation was an exciting discovery, and insights from the work with both HydF and  $\text{HydA}^{\Delta\text{EF}}$  acted to clarify the importance of these enzymes in the synthesis of the H-cluster, underscoring the need to characterize the biochemical properties of HydE and HydG. Early analysis of *T. maritima* HydG demonstrated that the reconstituted enzyme bound up to 4 irons and 5 sulfides per protein, contained a  $S = 1/2$  [4Fe–4S]<sup>+</sup> cluster upon dithionite reduction (Table 2), and cleaved SAM non-productively.<sup>129</sup> HydG exhibited considerable (27%) amino acid sequence homology with ThiH, a radical SAM enzyme that forms *p*-cresol and dehydroglycine (DHG) from tyrosine during thiamine biosynthesis (section 10.1).<sup>284b,446</sup> Driven by this sequence similarity, Pilet and co-workers confirmed that in the presence of tyrosine, HydG exhibited enhanced rates of SAM cleavage, a hallmark attribute of SAM enzymes when assayed in the presence of their substrates.<sup>447</sup> Further, by using LC–MS techniques, the authors verified that *p*-cresol was formed during catalysis.<sup>447</sup> Independent support for the role of tyrosine in H-cluster biosynthesis came from *in vitro*  $\text{HydA}^{\Delta\text{EF}}$  activation experiments that monitored H<sub>2</sub> consumption levels following treatment with cell extracts containing HydE, HydF, and HydG; while either exogenously added tyrosine or 3,4-dihydroxy-L-phenylalanine resulted in stimulated levels of H<sub>2</sub> depletion, other tyrosine analogues lacking a *p*-hydroxyl group failed to provide any stimulation.<sup>448</sup> This observation led to the hypothesis that the initial H-atom abstraction event by the dAdo<sup>•</sup> radical occurred at the *para*-position on the phenyl ring, similar to the proposed mechanism for ThiH.<sup>77,352</sup>

**12.2.4.2. Diatomic Ligand Biosynthesis.** The identification of tyrosine as the substrate and *p*-cresol as a reaction product of HydG catalysis still left open the question as to the fate of the remaining products of tyrosine degradation.<sup>447</sup> Subsequent analysis demonstrated the formation of the fluorescent cyanide adduct 1-cyanobenz[f]isoindole (CBI) over time in assays performed with purified and chemically reconstituted HydG from *C. acetobutylicum*.<sup>78a</sup> CBI formation was shown to occur concomitantly with *p*-cresol and dAdoH production in near stoichiometric amounts. LC–MS analysis of assays performed with uniformly labeled [ $\text{U}-^{13}\text{C}, {^{15}\text{N}}$ ]-tyrosine resulted in a CBI adduct with a mass increase of two *m/z* units, reflecting incorporation of the <sup>15</sup>N-amino and <sup>13</sup>C- $\alpha$ -carbon of tyrosine.<sup>78a</sup> The fate of the final tyrosine fragment was soon discovered by performing HydG kinetic assays in the presence of SAM, tyrosine, dithionite, and deoxyhemoglobin (deoxyHb) (Figure 98).<sup>78b</sup> The time-based, isosbestic formation of carboxyhemoglobin (HbCO) with  $\lambda_{\text{max}} = 419 \text{ nm}$  was observed concurrent with the decrease in the deoxyHb Soret band ( $\lambda_{\text{max}} = 430 \text{ nm}$ ).<sup>78b</sup> Confirmation of the HydG-catalyzed formation

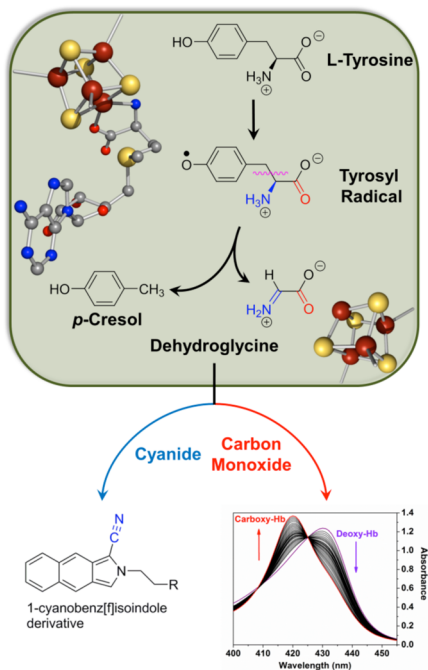


**Figure 98.** The mechanism of diatomic ligand biosynthesis as catalyzed by HydG.  $\alpha$ -C $\beta$  tyrosine bond cleavage has recently been demonstrated to occur through a heterolytic process (see text).<sup>130b,131</sup> Formation of the diatomics requires in some capacity the presence of the C-terminal [4Fe–4S] cluster where dehydroglycine is further processed into CN<sup>−</sup> and CO; the in vitro complexation/trapping of these diatomics are illustrated at the bottom. Bottom right reprinted with permission from ref 78b. Copyright 2010 American Chemical Society.

of CO was made by using uniformly labeled [ $U$ -<sup>13</sup>C,<sup>15</sup>N]-tyrosine in assays, which revealed the formation of a FTIR vibrational feature at 1907 cm<sup>−1</sup> characteristic of Hb<sup>13</sup>CO. Moreover, the rate constant for HbCO formation ( $k_{cat} = 11.4 \times 10^{-4}$  s<sup>−1</sup> at 30 °C) was similar to that of CN<sup>−</sup> formation ( $k_{cat} = 20 \times 10^{-4}$  s<sup>−1</sup> at 37 °C), suggesting these diatomics were derived from the same intermediate (Table 1).<sup>78a</sup>

It is important to note that the experiments monitoring carboxyHb formation showed substoichiometric CO amounts, whereas the experiments monitoring formation of CBI displayed near stoichiometric levels of CN<sup>−</sup>.<sup>78</sup> This difference was thought to arise as a direct consequence of the detection methods, because cyanide derivatization was initiated by acidification of HydG assay aliquots, whereas CO binding to deoxyHb precluded treatment of the samples with acid. The inability to correlate the amounts of CO formed to the amounts of CN<sup>−</sup> detected left open the issue as to whether or not the three CO and two CN<sup>−</sup> ligands of the H-cluster were all derived from tyrosine. Insight into this issue was provided by experiments that spectroscopically analyzed HydA<sup>ΔEFG</sup> following activation by cell extract mixtures containing HydE, HydF, and HydG that were supplemented with either tyrosine, [ $1$ -<sup>13</sup>C]-tyrosine, [ $2$ -<sup>13</sup>C]-tyrosine, or [ $U$ -<sup>13</sup>C,<sup>15</sup>N]-tyrosine analogues; FTIR bands associated with the repurified hydrogenase were traced and demonstrate that all five CO and CN<sup>−</sup> diatomic ligands of the H-cluster indeed originated from tyrosine.<sup>444</sup>

**12.2.4.3. HydG Iron–Sulfur Cluster States and Mechanism.** Beyond the conserved N-terminal radical SAM CX<sub>3</sub>CX<sub>2</sub>C motif, HydG contains a 90 amino acid extension on its C-

terminal end that contains a CX<sub>2</sub>CX<sub>22</sub>C accessory motif.<sup>435</sup> Cysteine to serine substitutions in this C-terminal motif nearly abolished H<sub>2</sub> production in whole cell extract mixtures containing HydA, HydE, HydF, and mutant HydG proteins,<sup>435b</sup> underscoring the results from the biochemical studies that diatomic ligand biosynthesis absolutely required the chemical reconstitution of as-purified HydG with iron and sulfide.<sup>78</sup> Characterization of *T. maritima* HydG demonstrated that the reconstituted enzyme displayed a [4Fe–4S]<sup>+</sup> cluster signal upon treatment with dithionite, and low and high field shoulders indicated an additional cluster was present.<sup>129</sup> Temperature relaxation studies of HydG from *C. acetobutylicum* indicated that a mixture of [4Fe–4S]<sup>+</sup> and [2Fe–2S]<sup>+</sup> clusters was present in photoreduced samples of the as-purified and inactive protein, while similar studies performed on the chemically reconstituted and active enzyme revealed only fast relaxing signals typical of [4Fe–4S]<sup>+</sup> clusters.<sup>78b</sup> Analysis of the experimental data suggested that the signal in reduced samples was adequately simulated by fast relaxing [4Fe–4S]<sup>+</sup> cluster signals. On the basis of the presence of the N- and C-terminal motifs, sequence analysis suggests that HydG could coordinate two site-differentiated [4Fe–4S] clusters, and EPR spectral simulations substantiated this concept by showing that distinct axial signals were present in the photoreduced enzyme state when SAM was present (Table 2).<sup>78b,130b</sup>

Fontecilla-Camps and co-workers first explored the role of the C-terminal [4Fe–4S] cluster via site-directed mutagenic studies in which they created two variant *C. acetobutylicum* HydG proteins, one in which two of the cysteine residues in the accessory CX<sub>2</sub>CX<sub>22</sub>C motif (C386 and C389) were mutated to serines, and the other in which 88 C-terminal amino acids were deleted (ΔCTD).<sup>130a</sup> The C386S/C389S protein did not produce CO but did generate significant amounts of CN<sup>−</sup>, with levels approximating 50% of wild-type enzyme. Conversely, the ΔCTD variant did not produce either CO or CN<sup>−</sup>. The authors assumed loss of the C-terminal [4Fe–4S] cluster in both variants based on a decrease in absorbance in the 400–420 nm region of UV-vis spectra. An additional study using *C. acetobutylicum* ΔCTD and *Thermoanaerobacter tengcongensis* ΔCTD HydG variants showed that these proteins could still cleave tyrosine into *p*-cresol in the absence of their C-terminal domains, although *p*-cresol amounts that were generated approximated only 2% of wild-type levels.<sup>449</sup>

Our own studies have recently expanded the spectroscopic and kinetic characterization of variant *C. acetobutylicum* HydG proteins.<sup>130b</sup> EPR spectroscopy unambiguously demonstrates the presence of [4Fe–4S]<sup>+</sup> clusters in ΔCTD and C96A/C100A/C103A (this variant is one in which the cysteines of the CX<sub>3</sub>CX<sub>2</sub>C motif have been mutated to alanines) HydG proteins. Simulations show that each of the axial signals in the respective variants displays similar g-values as exhibited in the WT enzyme. Addition of SAM to the ΔCTD protein resulted in a mixture of SAM bound and unbound states, allowing for accurate g-value assignment of each cluster form; the C96A/C100A/C103A protein containing only the accessory C-terminal [4Fe–4S] cluster was shown to not bind SAM, indicating that despite its site-differentiated nature it cannot substitute for the N-terminal cluster.<sup>130b</sup> Furthermore, only subtle spectral perturbations were seen in WT and C96A/C100A/C103A samples prepared in the presence of tyrosine, suggesting that either substrate does not coordinate the C-terminal cluster or coordination does not significantly alter cluster g-values.

Despite the lack of perturbation of the iron sulfur cluster EPR signals in the presence of tyrosine, there was a substantial loss in substrate binding affinity in the variant proteins. Even with the increased  $K_{M(\text{tyrosine})}$  values in C386S and ΔCTD proteins relative to the WT enzyme, substantial amounts of *p*-cresol were obtained in assays; the similar *p*-cresol formation rates for WT ( $4.4 \times 10^{-3} \text{ s}^{-1}$ ), C386S ( $4.3 \times 10^{-3} \text{ s}^{-1}$ ), and ΔCTD ( $3.0 \times 10^{-3} \text{ s}^{-1}$ ) proteins suggest that rates of radical formation and tyrosine cleavage are largely unaffected by mutations to residue(s) in the C-terminus.<sup>130b</sup> However, diatomic ligand production was altered in the variants, with the C386S protein generating 2.8 mol equiv of CN<sup>-</sup> but not forming CO, and ΔCTD HydG producing no appreciable amounts of either diatomic species. Both variant proteins additionally displayed enhanced levels of glyoxylate formation relative to amounts detected during wild-type turnover, suggesting that the tyrosine Cα–Cβ bond cleavage event is a heterolytic process (section 10.1). These results suggest that the degradation of tyrosine into *p*-cresol occurs within the TIM barrel core, as previously suggested by Fontecilla-Camps and co-workers,<sup>449</sup> and that the DHG product then migrates to the C-terminal domain where diatomic ligand production occurs. Cyanide formation does not appear to absolutely require the C-terminal [4Fe–4S] cluster, but does seem to require the C-terminal domain. Generation of CO, on the other hand, does require the C-terminal cluster, and this requirement may be related to the stoichiometric amounts of CO detected in the wild-type HydG, deoxyHb binding assays.<sup>78b,130</sup>

Further insights into diatomic ligand formation have been provided by Britt and co-workers, who have reported EPR signals at  $g \approx 9.5$  and 5, proposed to arise from a [3Fe–4S]<sup>+</sup> cluster bound to the C-terminal cluster site, in *S. oneidensis* HydG.<sup>131</sup> Tyrosine addition causes a large decrease in the high spin FeS cluster signal intensity concurrent with the emergence of a new axial signal with  $g = 2.06$ , 1.91, and 1.88 that is consistent with a [4Fe–4S]<sup>+</sup> species; this transformation in the EPR spectral properties is suggestive of cluster cannibalization upon substrate addition. EPR samples prepared by rapid freeze–quench show production of a  $g = 1.9$  FeS-based feature and a transient  $g = 2$  radical signal.<sup>131</sup> HYSCORE and ENDOR analysis recorded at the  $g = 1.9$  feature reveal <sup>15</sup>N and <sup>13</sup>C coupling interactions to the FeS cluster in reactions carried out with <sup>13</sup>C<sub>9</sub>, <sup>15</sup>N-tyrosine, confirming that either tyrosine or a tyrosine derived fragment coordinates the C-terminal cluster.<sup>131</sup> The  $g = 2$  radical signal was specifically probed through the use of various tyrosine isotopologues, and the observed hyperfine coupling constants, as analyzed through DFT simulations, are most consistent with a 4-oxidobenzyl radical intermediate that would be generated upon heterolytic Cα–Cβ tyrosine bond cleavage.<sup>131</sup> Last, stopped flow FTIR spectroscopy was used to examine diatomic ligand formation using both the wild-type enzyme and a C394S/C397S variant protein. Both of the diatomic ligands are observed to form quite rapidly during wild-type catalysis, whereas the C394S/C397S variant produced only CN<sup>-</sup> at longer time points, leading the authors to conclude that the CN<sup>-</sup> observed in the latter case was not mechanistically relevant and that the C-terminal [4Fe–4S]<sup>+</sup> cluster was essential for the on-pathway generation of both diatomics.<sup>131</sup>

Kuchenreuther et al. propose a mechanism for diatomic ligand production that invokes the N-terminal cluster binding SAM and the C-terminal cluster anchoring tyrosine.<sup>131</sup> SAM is first reductively cleaved with the resulting dAdo<sup>•</sup> radical

abstracting a H-atom from the *para* position of the phenyl ring of tyrosine, which is bound to the C-terminal cluster. Heterolytic tyrosine bond cleavage then occurs, yielding both the 4-oxidobenzyl radical and the dehydroglycine as intermediate products, with the latter tyrosine fragment remaining bound to the accessory cluster. Concomitant with the generation of *p*-cresol from the 4-oxidobenzyl radical species, scission of DHG would produce CO and CN<sup>-</sup> species coordinated to the site-differentiated Fe of the C-terminal cluster.<sup>131</sup>

While tyrosine may be able to coordinate the accessory cluster in HydG, however, our own analysis leads us to conclude that such binding is mechanistically irrelevant. Homology models indicate that the C-terminal cluster of HydG would be located outside the core TIM barrel at a distance that would be too great for H-atom abstraction by the dAdo<sup>•</sup> radical. Moreover, our results and those of others show that ΔCTD HydG resembles ThiH catalytically, and that tyrosine binding and degradation to *p*-cresol clearly occur independent of the C-terminal domain.<sup>130</sup> Accordingly, we propose that the <sup>15</sup>N and <sup>13</sup>C coupling interactions observed by Kuchenreuther et al. arise from a fragment of tyrosine, possibly DHG, bound to the C-terminal cluster, which is located adjacent to the TIM barrel; these concepts are addressed more fully in a recent review article.<sup>450</sup> Several outstanding issues still remain in regards to the catalytic formation of CN<sup>-</sup> in the variant proteins and to the specific requirement of the [4Fe–4S] cluster for CO formation. Elucidation of the mechanism of ligand transfer to HydF is also necessary, specifically whether the ligands are delivered as free diatomics to a [2Fe–2S] cluster bound to HydF (Figure 97),<sup>443a</sup> or whether the diatomics are delivered to HydF as bound mononuclear Fe species, or whether the 2Fe subcluster is synthesized through the cannibalization of the accessory [4Fe–4S] cluster on HydG before being transferred to HydF (section 12.2.4.2).<sup>443e</sup>

**12.2.5. Radical SAM Chemistry and the Synthesis of the Bridging Dithiolate.** **12.2.5.1. HydE and the Search for a Substrate.** The demonstration that both diatomics were derived from HydG-based catalysis of tyrosine suggested that HydE's role may be in the synthesis of the remaining component of the H-cluster, the nonprotein, bridging dithiolate ligand. While some biochemical studies have been reported on HydE, little is resolved about its role in maturation, and at the date of this writing, the carbon-based substrate for this enzyme still remains to be identified. It is very likely that the substrate is a common metabolite, as [FeFe]-hydrogenase activation is readily accomplished in *E. coli* cell lysate mixtures coexpressing the three maturation genes.<sup>436,441b,448</sup> A report exploring the effect of exogenous additives on *in vitro* HydA<sup>ΔEFG</sup> activation levels discovered that both tyrosine and cysteine individually and cooperatively enhanced H<sub>2</sub> consumption levels.<sup>448</sup> While the effects of tyrosine can be attributed to the activity of HydG, the stimulation obtained from cysteine addition may either be a consequence of HydE's activity or is an artifact of more efficient cluster assembly due to the generalized Fe–S machinery present in the cell lysate.

One of the outstanding issues in H-cluster structure over the past decade has been the identity of the bridgehead atom in the dithiolate ligand, an especially important question when attempting to define the origin of this molecule. Initially modeled as 1,3-propanedithiolate,<sup>429</sup> the assignment was quickly revised to dithiomethylamine given the ability of the amine functionality to act as a proton donor/acceptor.<sup>430a</sup>

While computational studies suggested that the dithiolate ligand could be dithiomethyleneether,<sup>432b</sup> spectroscopic, computational, and functional biomimetic studies have now demonstrated that it is unequivocally dithiomethylamine.<sup>445,451</sup> This assignment will undoubtedly clarify the reaction mechanism HydE catalyzes, once a putative substrate is identified. Along these lines, it is plausible that HydE generates a carbon-based radical species upon H-atom abstraction by the dAdo<sup>•</sup> radical that then reacts with the sulfide groups of a [2Fe–2S] cluster; it is also possible that the sulfur atoms of the bridging dithiolate are derived from the substrate molecule itself.<sup>438,452</sup>

**12.2.5.2. HydE Iron–Sulfur Cluster States and Structure.** Reconstituted HydE from *T. maritima* binds up to eight iron and eight sulfides per protein, contains two  $S = 1/2$  [4Fe–4S]<sup>+</sup> clusters upon treatment with dithionite (Table 2), and cleaves SAM nonproductively at a rate of one mole of dAdoH per mole of protein per hour.<sup>129</sup> Structural characterization shows that HydE belongs to a subset of radical SAM enzymes having a full  $(\alpha/\beta)_8$  TIM barrel fold (Figure 99).<sup>42</sup> Structure determination

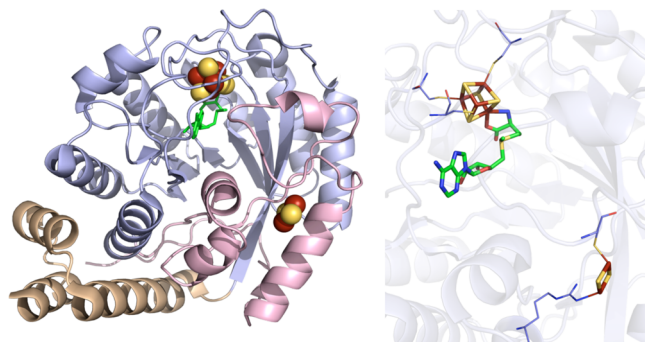


**Figure 99.** HydE crystal structure (PDB ID 3IIZ). Left: N-terminal domain colored in wheat, radical SAM domain in light blue, C-terminal domain in light pink, [4Fe–4S] and [2Fe–2S] clusters in yellow and rust spheres, and SAM in green sticks. Right: Active site of HydE where the [4Fe–4S] and [2Fe–2S] clusters (yellow and rust) and SAM (green carbons) are depicted in sticks with oxygens colored red and nitrogens colored blue. Cysteines (light blue carbons) involved in ligating clusters are depicted in lines.

in both SAM and methionine/dAdoH bound states provides a clear picture of the active site in two states, and the high affinity of the enzyme for the products indicates that SAM might be utilized as a cofactor.<sup>27a</sup> HydE shares significant sequence similarity with BioB and PylB, and contains an accessory cluster binding site near the protein surface located 20 Å away from the radical SAM cluster (Figure 99). Three cysteine residues and a water molecule act as ligands to this second Fe–S cluster, although occupancy of this site is quite variable depending on protein preparation.<sup>42</sup> Notably, the cysteines used to coordinate this cluster (Cys311, Cys319, and Cys322) are only conserved in ~48% of available HydE sequences, and despite the similar positioning of the two Fe–S clusters in HydE to those observed in MoaA, the accessory cluster in HydE directs its unique Fe site toward solvent, not the center of the active site cavity as is observed in MoaA (section 6.1.3). Moreover, variant HydE proteins where these cysteines were mutated to alanines showed no adverse effects toward hydrogenase activation in whole cell extracts, suggesting that this auxiliary cluster plays no role in the H-cluster maturation process.<sup>42</sup>

Intriguingly, the HydE structure reveals a large internal electropositive cavity that spans the full length of the  $(\beta\alpha)_8$

barrel and is the site of three distinct anion binding sites.<sup>42</sup> Thiocyanate was discovered to bind with high affinity in the third anion-binding site at the bottom of the barrel. It still remains unclear as to why HydE would have such high affinity for thiocyanate, although this observation may define a pathway wherein substrate reacts at the top of barrel near the radical SAM cluster and the product molecule then migrates to the bottom of the barrel for transfer to either HydF or HydG.<sup>42,453</sup>

Even before the revelation of HydF binding the 2Fe subcluster and diatomic ligand biosynthesis by HydG, it was surmised that the hydrogenase maturation enzymes interacted with one another in an intimate fashion. A reaction sequence was proposed where the alkylation of the sulfide ions of a [2Fe–2S] cluster was suggested to precede CO and CN<sup>−</sup> ligand addition, as modification of the sulfides would protect these groups against further alteration and shift chemical reactivity toward the Fe ions.<sup>438</sup> Experimental evidence for protein–protein interactions was first observed during affinity tag purifications where the maturases were observed to coelute with one another.<sup>442</sup> Subsequent work showed that HydE and HydG both independently stimulate the rate at which HydF hydrolyzes GTP, suggesting that GTP binding and/or hydrolysis may act to gate the interactions between the other maturation proteins during 2Fe subcluster assembly.<sup>443a</sup> Recent studies using surface plasmon resonance demonstrate that HydE binds to HydF with a  $K_D$  value of  $9.19 \times 10^{-8}$  M, displaying an order of magnitude lower value than the  $K_D$  for HydG binding to HydF ( $1.31 \times 10^{-6}$  M).<sup>454</sup> Additional results suggest that HydG is unable to displace HydE when it is bound to HydF and that HydG and HydE do not appear to interact with one another. Experiments aimed at probing the GTPase functionality of HydF show that GTP addition to either the HydF–HydE or HydF–HydG complexes during dissociative phases result in an increase in the rates of dissociation, suggesting that the GTPase activity of HydF promotes displacement of the interacting partners.<sup>454</sup> These data certainly speak toward the tightly controlled stepwise reaction between HydE and HydG with HydF,<sup>411a</sup> and the observation of the high binding affinity between HydE and HydF is certainly not surprising given the existence of fused *hydEF* genes in certain organisms.<sup>54b</sup>

Recent sequence and structure analysis of HydE has revealed remarkable resemblance to PylB, the radical SAM enzyme that catalyzes the isomerization of L-lysine to L-methylornithine in the biosynthetic pathway of pyrrolysine (section 5.2). Superpositioning of the HydE and PylB crystal structures (PylB 3T7V, HydE 3CIW) shows comparable SAM and putative substrate binding pockets, with a root mean square deviation value of only 1.3 Å.<sup>43</sup> Given what is known about the mechanism catalyzed by PylB, it is likely time to reconsider the potential chemical reactivity of HydE during H-cluster maturation. We propose that the results summarized herein argue against the idea that HydE acts simply as a chaperone for HydF during cluster translocation from HydG to HydA<sup>ΔEFG</sup>,<sup>443e</sup> because if this hypothesis were correct it would be challenging to rationalize the results of Vallese and co-workers.<sup>454</sup> Instead, these findings appear to support the action of HydE in a specific role during H-cluster biosynthesis, and we propose this is in some first step relating to the synthesis of the dithiomethylamine ligand.

### 13. RADICAL SAM ENZYMES OF UNKNOWN FUNCTION

#### 13.1. Radical SAM Chemistry in the Antiviral Response: Viperin

Human Viperin, also known as RSAD2 or Cig5, plays a key role in the host immune response system in response to a wide variety of dsRNA and DNA viruses, microbial infection, and other immune stimuli such as atherosclerotic lesions and pregnancy.<sup>455</sup> Initially, the immune system triggers release of both type I ( $\alpha/\beta$ ) and type II ( $\gamma$ ) interferons, which stimulates a multitude of signaling cascades, including expression of interferon stimulated genes (ISGs). Viperin, classified among the family ISGs, was initially discovered as an antiviral using differential display analysis by Zhu et al. in response to fibroblasts infected with human cytomegalovirus.<sup>455b</sup> Since then, several other groups including Boudinot, Grewal, and Chin and Cresswell have expanded this subset of ISGs to include additional *cig5* viperin analogues such as *vig1* (trout), *best5* (rat), and *mvig* (mouse).<sup>455c,d,456</sup> In every case, these genes were stimulated in reaction to either viral or bacterial infection via the immune response pathway.

Based upon sequence alignments of Vig1 and Cig5, this family of enzymes was proposed to belong to the radical SAM superfamily, hence the alternative name RSAD2 or radical SAM containing domain 2, due to the presence of four conserved motifs commonly observed in other radical SAM enzymes.<sup>219,455d</sup> These sequences include the CX<sub>3</sub>CX<sub>2</sub>C motif, known to bind a [4Fe–4S] cluster, as well as the GGE, SNG, and ISCDS motifs interact with SAM in known structures. Homology models utilizing the Phyre<sup>279</sup> server program demonstrated that human viperin (hVip) most likely bears an ( $\alpha/\beta$ )<sub>6</sub> TIM barrel with structural similarities to MoaA, HydE, and PFL-AE.<sup>113c,455a</sup> The protein is predicted to contain three domains: the amphipathic N-terminal domain, a middle domain (which includes both a leucine zipper motif in all sequences except lower vertebrates as well as the strictly conserved CX<sub>3</sub>CX<sub>2</sub>C motif), and the highly conserved C-terminal domain. Results from Hinson and Cresswell have shown that the amphipathic N-terminal  $\alpha$ -helical region is capable of associating the protein to the cytosolic face of the ER membrane as well as functioning to inhibit protein secretion and protein transport.<sup>457</sup> While the N-terminal domain did not appear necessary for antiviral activity, either mutation of the CX<sub>3</sub>CX<sub>2</sub>C motif or deletion of the C-terminal domain completely abrogate viperin's antiviral properties.<sup>458</sup> Although the function of the highly conserved C-terminus remains unclear, it possibly functions in substrate recognition and/or binding.

Computational modeling predicted a low-resolution viperin structure with an Fe–S cluster bound to the CX<sub>3</sub>CX<sub>2</sub>C motif at the center of a hydrophobic core surrounded by a partial TIM barrel. It is hypothesized that removal of the Fe–S cluster likely leads to instability in the core, thereby making the TIM barrel “collapse” into itself.<sup>113c</sup> To substantiate this idea, mutational analysis of the CX<sub>3</sub>CX<sub>2</sub>C motif using CD and steady state fluorescence spectroscopy demonstrated the requirement for a bound Fe–S cluster for proper folding. Protein lacking the Fe–S cluster was less stable and more prone to unfolding, as demonstrated by a large decrease in secondary and tertiary content, and easily aggregated as it was found primarily in inclusion bodies. Such self-association may lead to dimerization

of the protein and inhibition of the interaction with the ER membrane.<sup>113c</sup>

Additional evidence that viperin indeed binds a [4Fe–4S] cluster came in 2010 by two different groups. Shaveta et al. performed NMR and CD spectroscopy on full-length and fragmented viperin, and their results showed that deletion of the N-terminal 1–44 amino acids led to increased solubility of the protein.<sup>113a</sup> Following chemical reconstitution, the stability of the protein was enhanced, as the  $T_m$  increased from 30 to 45 °C and the protein adopted a more ordered secondary structure relative to the isolated fragments, suggesting that a bound Fe–S cluster enables proper folding of the protein.<sup>113a</sup> Duschene and Broderick further categorized viperin as a member of the radical SAM superfamily through their work with N-terminally deleted viperin.<sup>113b</sup> The protein was shown to bind [3Fe–4S]<sup>+</sup> and possibly [4Fe–4S]<sup>2+</sup> clusters in the reconstituted state and [4Fe–4S]<sup>+</sup> in the reconstituted and reduced state, as demonstrated by EPR and UV-vis spectroscopies (Table 2). HPLC analysis showed that reconstituted viperin catalyzes the nonproductive cleavage of SAM in vitro resulting in the production of dAdoH.<sup>113b</sup> While the substrate(s) involved in viperin's catalytic antiviral activity remains a mystery, based upon its known interaction with farnesyl pyrophosphate, an enzyme involved in lipid metabolism, viperin may act on FPPS or another related enzyme. It is also possible that viperin utilizes a metabolite in the cholesterol biosynthesis pathway as substrate, thereby leading to eventual alteration of downstream lipids, lipid droplets, or lipid raft domains.<sup>459</sup>

#### 13.2. Radical SAM Chemistry in the Synthesis of the Iron-Guanylylpyridinol Cofactor in [Fe]-Hydrogenase?

The Hmd-hydrogenase, also referred to as the [Fe]-hydrogenase, is expressed in methanogens that do not contain cytochromes and, along with the F<sub>420</sub>-dependent methylenetetrahydromenopterin dehydrogenase, acts to reduce F<sub>420</sub>.<sup>460</sup> The [Fe]-hydrogenase itself heterolytically cleaves H<sub>2</sub> and reversibly transfers a hydride to methylenetetrahydromenopterin (H<sub>4</sub>MPT<sup>+</sup>), yielding methylenetetrahydromenopterin (H<sub>4</sub>MPT) according to the reaction CH=H<sub>4</sub>MPT<sup>+</sup> + H<sub>2</sub> ⇌ CH<sub>2</sub>—H<sub>4</sub>MPT + H<sup>+</sup>.<sup>460,461</sup> Hydrogen is cleaved at the iron-guanylylpyridinol cofactor (FeGP-co) site, a moiety comprised of a single low spin Fe(II) ion ligated in bidentate fashion by an acyl carbon and a nitrogen of a pyridinol ring, as well as by two CO molecules and a protein-based cysteine thiolate (Figure 100).<sup>462</sup>

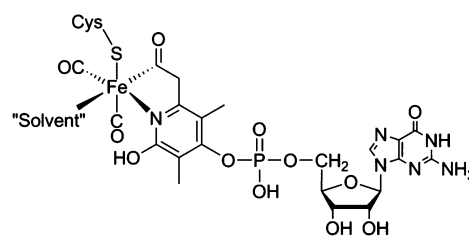


**Figure 100.** The iron-guanylylpyridinol cofactor (FeGP-co) of [Fe]-hydrogenase.

All methanogens with the *hmd* gene also contain a suite of seven co-occurring genes denoted *hmdA-G* that are often clustered adjacent to *hmd* and are critical for attaining active enzyme.<sup>460,463</sup> Two of these genes appear to encode proteins that have been proposed to perform SAM-dependent reactions. The colocalized *hcgG* gene is annotated as a fibrillarin-like

protein with homology to enzymes involved in RNA maturation and nucleoside modification, including methylation and methoxycarboxylation reactions.<sup>109</sup> Moreover, the crystal structure of a fibrillarin homologue from *Methanocaldococcus janaschii* contains a catalytic domain common to SAM-dependent methyltransferases,<sup>269,464</sup> and it was subsequently proposed that HcgG (or HmdC) was responsible for the methylation of the pyridinol ring of the GP cofactor.<sup>109</sup> The second SAM-associated gene is *hcgA* (or *hmdB*). Sequence annotation indicated that *hcgA* encoded for a radical SAM-like binding protein that comprised a CX<sub>5</sub>CX<sub>2</sub>C consensus sequence, distinct from the typical CX<sub>3</sub>CX<sub>2</sub>C motif, suggesting that HcgA was a new member of the radical SAM superfamily, joining a subclass of enzymes that contain variants of the characteristic SAM binding motif (ThiC and Elp3, sections 6.2 and 10.5).<sup>32,103,108,258</sup> Amino acid sequence homology modeling of HcgA shows that it is predicted to have a complete ( $\beta\alpha$ )<sub>8</sub> TIM barrel with analogous SAM binding motifs as observed in other superfamily members (Figure 101) (section 2.6).<sup>34,279</sup>

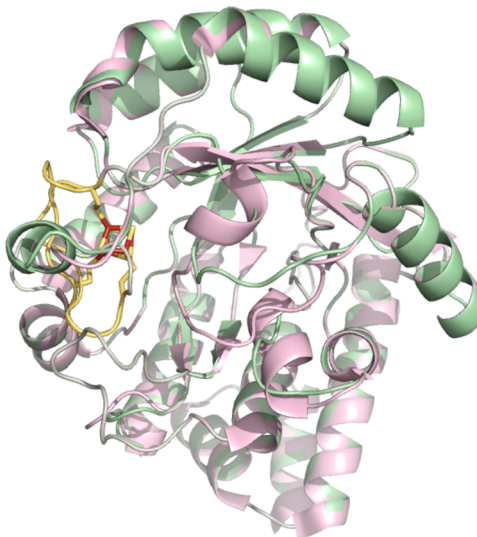


**Figure 101.** Structure homology model of the amino acid sequence of HcgA (*M. maripaludis*) (green), aligned to the HydE crystal structure (PDB ID 3CIX) (pink) (section 12.2.5.2). Radical SAM motif is colored in yellow, cysteines involved in ligating the [4Fe–4S] are shown as yellow sticks, while the [4Fe–4S] cluster is depicted as yellow and rust sticks. For clarity, the [2Fe–2S] cluster of HydE has been omitted. MqNE structural model was generated using the protein structure prediction server Phyre2,<sup>279</sup> where the HydE template model yielded the top hit.

Preliminary biochemical characterization of HcgA demonstrated that the heterologously expressed *Methanococcus maripaludis* protein contained a [4Fe–4S]<sup>+</sup> cluster that interacted with and reductively cleaved SAM into dAdOH (Table 2).<sup>109</sup> However, no substrate was identified, complicating the assignment of the role of radical SAM chemistry in FeGP biosynthesis. Nonetheless, a putative role for HcgA was surmised on the basis of the observation that it clusters within a sequence lineage comprising ThiH, HydE, and HydG. The role of HydE and HydG in the synthesis of the diatomic and nonprotein ligands of the H-cluster (sections 12.2.4 and 12.2.5) suggested that HcgA was responsible for the SAM-initiated synthesis of the CO ligands of FeGP;<sup>109</sup> an alternate proposal

suggested that this enzyme was responsible for the methylation of the pyridinol ring.<sup>460</sup> Insights into the biosynthesis of the FeGP cofactor were recently obtained via supplementing media with various isotopic precursors during growth of *Methanothermobacter marburgensis* and *Methanobrevibacter smithii*; NMR and MS techniques were utilized to identify positions of <sup>13</sup>C and <sup>2</sup>H incorporation into the extracted cofactor.<sup>465</sup> Importantly, these *in vivo* labeling studies reveal that the CO ligands are derived from CO<sub>2</sub>, demonstrating that HcgA does not function in an analogous manner to HydG in diatomic ligand synthesis. Integration of the intact methyl group of L-[methyl-<sup>2</sup>H<sub>3</sub>]methionine into the pyridinol moiety suggests that methyl transfer from methionine is catalyzed by a SAM-dependent methyltransferase, as opposed to a radical SAM enzyme.<sup>465</sup> While these results help to clarify how the FeGP cofactor is synthesized, little evidence currently exists in terms of defining the requirement of HcgA in this process.

### 13.3. A Radical SAM Epimerase? AviX12 in Avilamycin A Biosynthesis

The antibiotic avilamycin A is an oligosaccharide antibiotic of the orthosomycin subclass with known activity against many Gram-positive bacteria.<sup>466</sup> Sequencing of the avilamycin biosynthetic gene cluster identified the proteins involved in its biosynthetic pathway. Gene knockout studies have elucidated several details of the biosynthetic steps; however, gene characterization has been limited by enzymes of no known function.<sup>466,467</sup> Sequence annotation of the gene *aviX12* (positioned between methyltransferase and sugar biosynthetic genes) revealed that it would yield a protein containing the CX<sub>3</sub>CX<sub>2</sub>C motif, and was proposed to be involved in an oxidation-type reaction during biosynthesis via its postulated site-differentiated [4Fe–4S] cluster.<sup>467b</sup> Metabolite analysis of a *Streptomyces viridochromogenes* culture with the *aviX12* gene inactivated resulted in accumulation of gavibamycin N1, containing an epimerized heptasaccharide glucose moiety in place of the expected mannose; this led to a proposed reaction for AviX12 in which it acts as an epimerase (Figure 102).<sup>104</sup>



**Figure 102.** Proposed AviX12 reaction catalyzing the epimerization reaction to convert gavibamycin N1 to avilamycin A.

AviX12 overexpression and aerobic purification resulted in the isolation of an enzyme that was found to bind [3Fe–4S] clusters in the oxidized state (as gauged by EPR spectroscopy) with an isotropic signal of *g* = 2.01 (Table 2).<sup>104</sup> However, in these studies, the enzyme was not chemically reconstituted with Fe and S and thus had no observable activity.

While preliminary experiments concerning AviX12 function have been initiated, the nature of the epimerization reaction proposed for AviX12 is currently unknown. Given the recent characterization of radical SAM enzymes involved in sugar modifications, it is possible that AviX12 may exhibit similarities to BtrN or DesII (sections 8.2 and 10.3). Interestingly, similar to the BtrN dehydrogenase enzyme, AviX12 contains several accessory cysteine residues that could plausibly coordinate a second Fe–S cluster. However, further biochemical and spectroscopic investigation is needed to better clarify the

putative epimerization reaction catalyzed by this presumed radical SAM enzyme (Figure 102).

#### 14. RADICAL SAM CHEMISTRY OUTSIDE THE SUPERFAMILY: DPH2

Diphthamide is a rare amino acid synthesized by posttranslational modification of a histidine residue on translational elongation factor 2 (EF2) that serves an essential role in ribosomal protein synthesis.<sup>468</sup> Since the elucidation of its structure in 1980 as 2-[3-carboxyamido-3-(trimethylammonio)-propyl]-histidine (diphthamide), it is now known to help prevent −1 frame shift mutations during protein synthesis, as it serves as the site of ADP-ribosylation by diphtheria toxin and *Pseudomonas aeruginosa* exotoxin A in eukaryotes and archaea.<sup>469</sup> Biosynthesis of diphthamide is associated with five genes (*dph1–dph5* in yeast) that participate in a three-step biosynthesis generally summarized as involving C–C bond formation between the histidine imidazole ring and a 3-amino-3-carboxypropyl (ACP) group, methyl transfer, and carboxyl amidation.<sup>470</sup>

Synthesis and insertion of the ACP group involves a rare type of translational modification (C–C bond formation) involving activation of the poorly nucleophilic  $\varepsilon$  carbon of histidine. Initial radiolabeling studies showed that [ $\alpha$ -<sup>3</sup>H]-methionine and [Me-<sup>3</sup>H]-methionine were incorporated into diphthine, suggesting that both the backbone and the methyl groups of diphthamide originated from methionine.<sup>471</sup> Considering that methionine is a metabolic component of SAM,<sup>472</sup> that the known nucleoside 3-(3-carboxy-3-aminopropyl)-uridine is synthesized through nucleophilic attack of the  $\gamma$ -methylene carbon of SAM,<sup>473</sup> and that discrete portions of methionine were incorporated into diphthine suggested that backbone and methyl label incorporation likely involved different enzymes.<sup>470a,471</sup> Following characterization of Dph5 as a SAM-dependent methyltransferase<sup>470a</sup> and association of Dph1–Dph4 with the initial C–C bond formation event, Dph2 stood out as an initial target.<sup>474</sup> Because archaeal species have only a Dph2 protein (relative to Dph1 and Dph2 in eukaryotic species) and no Dph3 and Dph4 orthologues, Dph2 could be anticipated to perform the C–C bond insertion reaction.<sup>32</sup>

Crystallographic structure determination of *Pyrococcus horikoshii* Dph2 purified aerobically resulted in a cofactorless protein that was found to have no activity.<sup>32</sup> Interestingly, the aerobically purified enzyme contained a pocket of three cysteines (Cys59, Cys163, and Cys287) that originated from different structural domains and came together in the center of the Dph2 monomer in close enough proximity for putative Fe–S cluster coordination (Figure 103).<sup>32</sup> Anaerobic preparation of the enzyme resulted in an active enzyme with a coordinated Fe–S cluster. Upon reduction, the EPR spectroscopic *g*-values (2.03, 1.92, and 1.86) and Mössbauer parameters were consistent with a [4Fe–4S] cluster (Table 2).<sup>32</sup> The crystal structure with the bound [4Fe–4S] cluster (PDB ID 3LZD; 2.10 Å resolution) revealed a homodimer with a structure that was distinct from the traditional TIM barrel radical SAM enzymes: each monomer was composed of three domains in a triangular orientation with each domain consisting of a four-stranded parallel  $\beta$ -sheet with three flanking  $\alpha$ -helices, and an additional antiparallel  $\beta$ -strand in domains 1 and 2, and two additional  $\alpha$ -helices in domains 2 and 3.<sup>32</sup> Overall, the structure was similar to quinolate synthase<sup>475</sup> and had a structural

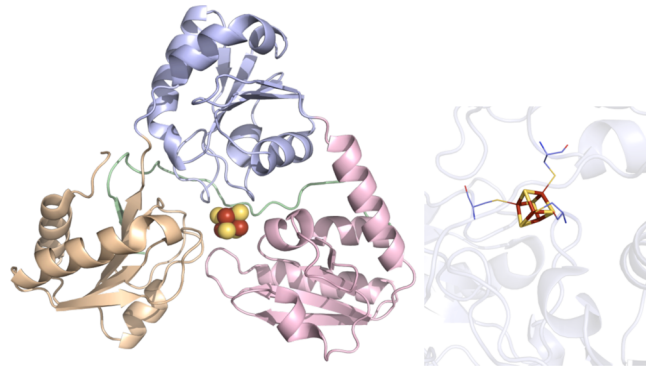


**Figure 103.** Dph2 crystal structure (PDB ID 3LZD). Left: Domain 1 colored in wheat, domain 2 in light blue, domain 3 in light pink, C-terminal domain in light green, and [4Fe–4S] cluster in yellow and rust spheres. Right: Active site of Dph2 where the [4Fe–4S] cluster (yellow and rust) is depicted in sticks. Cysteines (light blue carbons) involved in ligating clusters are depicted in lines.

arrangement comparable to that of the IspH enzyme in isoprenoid biosynthesis.<sup>476</sup>

In vitro assays containing Dph2, SAM, reductant, and EF2 resulted in production of MTA but no dAdoH, indicating bond cleavage had occurred between the sulfonium sulfur and the  $\gamma$ -C of the methionine portion of SAM.<sup>32</sup> In the absence of EF2, dansylated 2-aminobutyric acid and homocysteine sulfinic acid, suggested to be products of a quenched SAM-derived 3-amino-3-carboxypropyl (ACP) radical, were detected by LC–MS.<sup>32</sup> The proposed Dph2 reaction mechanism thus involves SAM coordination to the site-differentiated Fe of the [4Fe–4S] cluster, where electron transfer from the cluster results in homolytic cleavage of the S–C( $\gamma$ ) bond of SAM, producing the ACP radical and MTA (Figure 104).<sup>108</sup> The ACP radical then

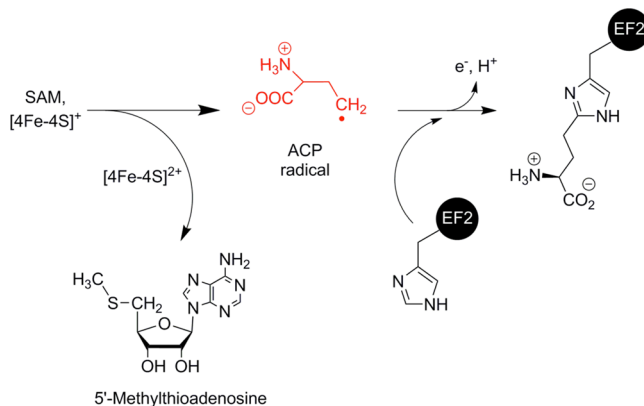


**Figure 104.** Proposed reaction mechanism for Dph2 catalyzing the modification of EF2-His600 during the first step of diphthamide biosynthesis.

undergoes electrophilic attack on the  $\pi$  orbitals of the  $\varepsilon$  carbon of the imidazole ring on EF, forming an imidazole-based radical that may be quenched via electron transfer back to the [4Fe–4S] cluster upon deprotonation.<sup>32,108</sup>

This mechanism would appear then to place Dph2 within the radical SAM superfamily, as it uses a site-differentiated [4Fe–4S] cluster and SAM to generate a SAM-derived radical intermediate. Dph2 is not, however, a member of the radical SAM superfamily, as it has none of the sequence features that are conserved among superfamily members that are used as

indicators of their divergent evolution from a common ancestor; Dph2 also lacks the conserved TIM barrel fold found in the radical SAM superfamily members (Figure 103). This suggests that the Dph2-catalyzed reaction utilizing a [4Fe–4S] cluster and SAM is a case of convergent evolution, with Dph2 carrying out a similar type of catalytic mechanism but doing so in a manner that utilizes a distinct structural design from radical SAM enzymes. What is particularly exciting about this discovery of an enzyme that has through convergent evolution adopted radical SAM chemistry is the prospect that there are perhaps many other enzymes that do not belong to this superfamily but that utilize its amazingly versatile chemistry in catalysis.

## 15. CONCLUDING REMARKS

In the 13 years since Heidi Sofia first identified the radical SAM superfamily with its ~600 original members,<sup>1</sup> there has been a veritable explosion of new radical SAM enzymes identified with the size of the superfamily currently estimated at nearly 50 000 members.<sup>14</sup> Moreover, our understanding of the chemical transformations catalyzed by these enzymes has grown considerably; it is now clear that radical SAM enzymatic reactions are remarkably diverse, ranging from simple H-atom abstractions to generate product radicals, to H-atom abstractions that initiate a cascade of extraordinary chemical transformations. There are now even cases of radical SAM enzymes that couple radical SAM chemistry to other types of chemistry in a single active site, an example being the class A methyltransferases that carry out nucleophilic methylation together with H-atom abstraction. Radical SAM chemistry plays critical roles in numerous biosynthetic pathways including antibiotic production, posttranslational modifications, synthesis of protein cofactors, and catalyzing the synthesis of the nonprotein ligands that impart chemical reactivity to some of the most complex biological metal clusters known. The utilization of a universal protein fold with one of the most ubiquitous metal cofactors in biology, the [4Fe–4S] cluster, together with a simple organic molecule, SAM, is apparently a quite remarkable and adaptable method to carry out a wide variety of difficult transformations. This chemical recipe is so pervasive in biology that it is not surprising that it is also now being detected in enzymes that are not superfamily members but whose mechanistic chemistry has converged with the radical SAM superfamily. Given that the study of radical SAM enzymes is in its infancy, with only a small fraction of recognized superfamily members biochemically characterized in any detail, it is probable that the next few years will bring with it a wealth of novel reactions that will undoubtedly enhance our understanding and appreciation of the fascinating chemical transformations that these enzymes carry out in biology.

## AUTHOR INFORMATION

### Corresponding Author

\*E-mail: jbroderick@chemistry.montana.edu.

### Notes

The authors declare no competing financial interest.

## Biographies



Joan B. Broderick received her undergraduate education at Washington State University, where she did research in both inorganic chemistry (with Roger Willett) and biochemistry (with Tom Okita) while earning a B.S. in Chemistry. She earned a Ph.D. in Chemistry in 1992 in the lab of Tom O'Halloran at Northwestern University as an N.S.F. Predoctoral Fellow, carrying out spectroscopic and mechanistic studies of chlorocatechol dioxygenase. She then worked with JoAnne Stubbe at MIT as an American Cancer Society Postdoctoral Fellow, where she carried out biochemical and mechanistic studies on the B<sub>12</sub>-dependent ribonucleotide reductase, and developed a keen interest in bioinorganic radical reactions. As an Assistant Professor at Amherst College in 1993, she began her work on the radical SAM enzyme pyruvate formate-lyase activating enzyme. She moved to Michigan State University in 1998, and to Montana State University in 2005, where she is the Women in Science Distinguished Professor of Chemistry and Biochemistry. She enjoys spending time with her family, husband Will and twin sons Jerry and James, skiing and hiking in the mountains around Bozeman.



Benjamin R. Duffus was born in Owatonna, MN in 1983, and was raised in south central Minnesota. In 2005, he earned his B.A. degree in Chemistry (*cum laude*) from Concordia College (Moorhead, MN), and at Texas A&M University developed an appreciation of the importance of metals in biological systems with Professor Kim R. Dunbar working on synthesis of Ru polypyridyl photocisplatin analogs. Since 2008, Benjamin is a Ph.D. candidate in Professor Joan Broderick's laboratory at Montana State University where he is examining the role of radical SAM enzymes in the biosynthesis of complex Fe–S metallocofactors in [FeFe]-hydrogenase along with Professor John Peters. Outside of the lab, Benjamin enjoys peakbagging, downhill skiing, and international travel.



Kaitlin Duschene was born in 1978. She received her B.S. and M.S. degrees in biochemistry from Furman University where she studied the effects of potential anticancer drugs synthesized in the lab of Dr. Moses Lee in both *in vitro* and *in vivo* models. Prior to coming to Montana State University, she studied the activity of HIF1 $\alpha$  in prostate cancer with Dr. Jonathan Simons, president of Winship Cancer Institute, Emory University. Since 2006, she has been working under Dr. Joan Broderick where her research interests are the biochemistry involved in elucidating the characteristics of iron–sulfur cluster-containing enzymes.



Eric M. Shepard was born in Kittanning, PA, in 1977. He earned his B.S. in Chemistry from Rocky Mountain College (*summa cum laude*) in 1999. His dissertation work at Montana State University under Professor David Dooley contributed to understanding the molecular factors controlling substrate analogue binding and the role of copper in dioxygen activation in copper amine oxidases, awarding him a N.S.F. IGERT fellowship. Upon completion of his Ph.D. in Biochemistry in 2006, he began postdoctoral research in Professor Joan Broderick's laboratory where, in close collaboration with Professor John Peters, he investigated the [FeFe]-hydrogenase maturation enzymes HydE, HydF, and HydG that are responsible for H-cluster biosynthesis. He is currently a Senior Research Scientist in the Broderick lab where he helps lead the Broderick Hydrogenase Team investigating radical SAM maturases and simple [Fe–S]-based peptide catalysts. When not in the lab he is often found either digging for smoky and amethyst quartz ( $\text{SiO}_2$ ) crystals alongside his wife or chasing bull elk in the mountains of Montana.

## ACKNOWLEDGMENTS

We would like to thank Will Broderick for helpful discussions, and Jeremiah Betz, Amanda Byer, and Krista Shisler for careful reading and editing of the manuscript. We are grateful to funding agencies NIH (2R01GM054608-14) and DOE (DE-

FG02-10ER16194) for support of our work on radical SAM enzymes.

## ABBREVIATIONS

ACP	acyl carrier protein
AE	activating enzyme
AdoCbl or B <sub>12</sub>	adenosylcobalamin
AHQ <sub>Q</sub>	3 $\alpha$ -(2-amino-2-carboxyethyl)-4,5-dioxo-4,5,6,7,8,9-hexahydroquinoline-7,9-dicarboxylic acid
AIR	4-aminoimidazole ribonucleotide
anAdo $\bullet$	5'-deoxy-3',4'-anhydroadenosine-5'-yl radical
anSAM	S-3',4'-anhydroadenosyl-L-methionine
anSME	anaerobic sulfatase maturing enzyme
aRNR	anaerobic ribonucleotide reductase
BSS	benzylsuccinate synthase
cPMP	1,1'-dihydroxy-2',4'-cyclic pyranopterin monophosphate or precursor Z
dAdoH	5'-deoxyadenosine
dAdo $\bullet$	5'-deoxyadenos-5'-yl radical
CAP	cytosylarabinopyranose
CBI	1-cyanobenz[f]isoindole
CDG	7-carboxy-7-deazaguanine
CH <sub>3</sub> Cbl	methylcobalamin
CPO	coproporphyrinogen III oxidase
DHG	dehydroglycine
DOIA	2-deoxy- <i>scyllo</i> -inosamine
DTT	dithiothreitol
ENDOR	electron–nuclear double resonance
EPR	electron paramagnetic resonance
ESEEM	electron spin–echo envelope modulation
EXAFS	X-ray absorption fine structure
FeGP-co	iron-guanylylpyridinol cofactor
F <sub>0</sub>	8-hydroxy-7-desmethyl-5-deazariboflavin
FGly	formylglycine
GD	glycerol dehydratase
GRE	glycyl radical enzyme
HAT	histone acetyltransferase
HbCO	carbonmonoxyhemoglobin
HMP	4-amino-5-hydroxymethyl-2-methylpyrimidine
HMP-PP	4-amino-5-hydroxymethyl-2-methylpyrimidine pyrophosphate
H4MPT	methylenetetrahydromethanopterin
HPD	4-hydroxyphenylacetate decarboxylase
ISG	interferon stimulated gene
LAM	lysine 2,3-aminomutase
MIA	3-methyl-2-indolic acid
MDTB	9-mercaptodethiobiotin
Moco	molybdopterin cofactor
MTA	5'-methylthioadenosine
MTAN	5'-methylthioadenosine/S-adenosylhomocysteine nucleosidase
MTTase	methyltransferase
NAcDMPT	N-acetyldeimethylphosphinothricin
NAcPT	N-acetylphosphinothricin
NRVS	nuclear resonant vibrational spectroscopy
PDC	pyruvate dehydrogenase complex
PFL	pyruvate-formate lyase
PLP	pyridoxal-L-phosphate
PQQ	pyrroloquinoline quinone
Pre-Q <sub>0</sub>	7-cyano-7-deazaguanine
PrCp	$\alpha$ -D-ribose-1,2-cyclic-phosphate-5-phosphate
PRPn	$\alpha$ -D-ribose-1-methylphosphonate-5-phosphate

RNR	ribonucleotide reductase
RSMTs	radical SAM methyltransferases
SAH	S-adenosyl-L-homocysteine
SAM	S-adenosyl-L-methionine
SASP	small acid-soluble protein
Se-SAM	S-adenosyl-L-selenomethionine
SKF	sporulation killing factor
SP	spore photoproduct
SPL	spore photoproduct lyase
THZ-P	4-methyl-5-( $\beta$ -hydroxyethyl)thiazole phosphate carboxylate
TIM	triose phosphate isomerase
WT	wild-type
XAS	X-ray absorption spectroscopy
YTM	yatakemycin
yW	wybutosine

## REFERENCES

- (1) Sofia, H. J.; Chen, G.; Hetzler, B. G.; Reyes-Spindola, J. F.; Miller, N. E. *Nucleic Acids Res.* **2001**, *29*, 1097.
- (2) Knappe, J.; Neugebauer, F. A.; Blaschkowski, H. P.; Gänzler, M. *Proc. Natl. Acad. Sci. U.S.A.* **1984**, *81*, 1332.
- (3) Knappe, J.; Schacht, J.; Mockel, W.; Hopner, T.; Vetter, H. J.; Edenharder, R. *Eur. J. Biochem.* **1969**, *11*, 316.
- (4) Wagner, A. F. V.; Frey, M.; Neugebauer, F. A.; Schäfer, W.; Knappe, J. *Proc. Natl. Acad. Sci. U.S.A.* **1992**, *89*, 996.
- (5) Broderick, J. B.; Duderstadt, R. E.; Fernandez, D. C.; Wojtuszewski, K.; Henshaw, T. F.; Johnson, M. K. *J. Am. Chem. Soc.* **1997**, *119*, 7396.
- (6) Knappe, J.; Schmitt, T. *Biochem. Biophys. Res. Commun.* **1976**, *71*, 1110.
- (7) (a) Mulliez, E.; Fontecave, M.; Gaillard, J.; Reichard, P. *J. Biol. Chem.* **1993**, *268*, 2296. (b) Sun, X.; Harder, J.; Krook, M.; Jörnvall, H.; Sjöberg, B.-M.; Reichard, P. *Proc. Natl. Acad. Sci. U.S.A.* **1993**, *90*, 577.
- (8) Chirpich, T. P.; Zappia, V.; Costilow, R. N.; Barker, H. A. *J. Biol. Chem.* **1970**, *245*, 1778.
- (9) Petrovich, R. M.; Ruzicka, F. J.; Reed, G. H.; Frey, P. A. *J. Biol. Chem.* **1991**, *266*, 7656.
- (10) Moss, M.; Frey, P. A. *J. Biol. Chem.* **1987**, *262*, 14859.
- (11) Birch, O. M.; Fuhrmann, M.; Shaw, N. M. *J. Biol. Chem.* **1995**, *270*, 19158.
- (12) (a) Sanyal, I.; Cohen, G.; Flint, D. H. *Biochemistry* **1994**, *33*, 3625. (b) Guianvarc'h, D.; Florentin, D.; Bui, B. T. S.; Nunzi, F.; Marquet, A. *Biochem. Biophys. Res. Commun.* **1997**, *236*, 402. (c) Escalettes, F.; Florentin, D.; Bui, B. T. S.; Lesage, D.; Marquet, A. *J. Am. Chem. Soc.* **1999**, *121*, 3571.
- (13) Cheek, J.; Broderick, J. B. *J. Biol. Inorg. Chem.* **2001**, *6*, 209.
- (14) Babbitt, P.; Gerlt, J. *The Regents of the University of California; 2013; Vol. 2013*, <http://sfld.rvbi.ucsf.edu/django/>.
- (15) Hinckley, G. T.; Frey, P. A. *Biochemistry* **2006**, *45*, 3219.
- (16) (a) Walsby, C. J.; Ortillo, D.; Broderick, W. E.; Broderick, J. B.; Hoffman, B. M. *J. Am. Chem. Soc.* **2002**, *124*, 11270. (b) Chen, D.; Walsby, C.; Hoffman, B. M.; Frey, P. A. *J. Am. Chem. Soc.* **2003**, *125*, 11788.
- (17) Walsby, C. J.; Hong, W.; Broderick, W. E.; Cheek, J.; Ortillo, D.; Broderick, J. B.; Hoffman, B. M. *J. Am. Chem. Soc.* **2002**, *124*, 3143.
- (18) (a) Frey, P. A. *FASEB J.* **1993**, *7*, 662. (b) Jordan, A.; Reichard, P. *Annu. Rev. Biochem.* **1998**, *67*, 71.
- (19) (a) Magnusson, O. T.; Frey, P. A. *J. Am. Chem. Soc.* **2000**, *122*, 8807. (b) Magnusson, O. T.; Frey, P. A. *Biochemistry* **2002**, *41*, 1695. (c) Mansoorabadi, S. O.; Magnusson, O. T.; Poyner, R. R.; Frey, P. A.; Reed, G. H. *Biochemistry* **2006**, *45*, 14362.
- (20) (a) Magnusson, O. T.; Reed, G. H.; Frey, P. A. *J. Am. Chem. Soc.* **1999**, *121*, 9764. (b) Magnusson, O. T.; Reed, G. H.; Frey, P. A. *Biochemistry* **2001**, *40*, 7773.
- (21) Henshaw, T. F.; Cheek, J.; Broderick, J. B. *J. Am. Chem. Soc.* **2000**, *122*, 8331.
- (22) Lieder, K. W.; Booker, S.; Ruzicka, F. J.; Beinert, H.; Reed, G. H.; Frey, P. A. *Biochemistry* **1998**, *37*, 2578.
- (23) (a) Colichman, E. L.; Love, D. L. *J. Org. Chem.* **1953**, *18*, 40. (b) Grimshaw, J. In *Chemistry of the Sulphonium Group*; Stirling, C. J. M., Ed.; Wiley: Chichester, 1981.
- (24) (a) Ugulava, N. B.; Gibney, B. R.; Jarrett, J. T. *Biochemistry* **2001**, *40*, 8343. (b) Pierrel, F.; Hernandez, H. L.; Johnson, M. K.; Fontecave, M.; Atta, M. *J. Biol. Chem.* **2003**, *278*, 29515.
- (25) (a) Daley, C. J. A.; Holm, R. H. *Inorg. Chem.* **2001**, *40*, 2785. (b) Daley, C. J. A.; Holm, R. H. *J. Inorg. Biochem.* **2003**, *97*, 287.
- (26) Wang, S. C.; Frey, P. A. *Biochemistry* **2007**, *46*, 12889.
- (27) (a) Nicolet, Y.; Amara, P.; Mouesca, J.-M.; Fontecilla-Camps, J. C. *Proc. Natl. Acad. Sci. U.S.A.* **2009**, *106*, 14867. (b) Challand, M. R.; Ziegert, T.; Douglas, P.; Wood, R. J.; Kriek, M.; Shaw, N. M.; Roach, P. L. *FEBS Lett.* **2009**, *583*, 1358.
- (28) Dey, A.; Peng, Y.; Broderick, W. E.; Hodgson, K. O.; Broderick, J. B.; Solomon, E. I. *J. Am. Chem. Soc.* **2011**, *133*, 18656.
- (29) Vey, J. L.; Yang, J.; Li, M.; Broderick, W. E.; Broderick, J. B.; Drennan, C. L. *Proc. Natl. Acad. Sci. U.S.A.* **2008**, *105*, 16137.
- (30) Markham, G. D. *Nature Encyclopedia of Life Sciences*; Nature Publishing Group: London, 2002.
- (31) Demick, J. M.; Lanzilotta, W. N. *Biochemistry* **2011**, *50*, 440.
- (32) Zhang, Y.; Zhu, X.; Torelli, A. T.; Lee, M.; Dzikovski, B.; Koralewski, R. M.; Wang, E.; Freed, J.; Krebs, C.; Ealick, S. E.; Lin, H. *Nature* **2010**, *465*, 891.
- (33) (a) Broderick, J. B. *Nature* **2010**, *465*, 877. (b) Kampmeier, J. A. *Biochemistry* **2010**, *49*, 10770.
- (34) Vey, J. L.; Drennan, C. L. *Chem. Rev.* **2011**, *111*, 2487.
- (35) Silver, S. C.; Gardenghi, D. J.; Shepard, E. M.; Naik, S. G.; Huynh, B. H.; Szilagyi, R. K.; Broderick, J. B. *J. Biol. Inorg. Chem.* **2014**, in press.
- (36) Noddleman, L.; Case, D. A. In *Advances in Inorganic Chemistry*; Sykes, A. G., Ed.; Academic Press: New York, 1992; Vol. 38.
- (37) Kamachi, T.; Kouno, T.; Doitomi, K.; Yoshizawa, K. *J. Inorg. Biochem.* **2011**, *105*, 850.
- (38) Lees, N. S.; Chen, D.; Walsby, C.; Behshad, E.; Frey, P. A.; Hoffman, B. M. *J. Am. Chem. Soc.* **2006**, *128*, 10145.
- (39) Lepore, B. W.; Ruzicka, F. J.; Frey, P. A.; Ringe, D. *Proc. Natl. Acad. Sci. U.S.A.* **2005**, *102*, 13819.
- (40) Berkovitch, F.; Nicolet, Y.; Wan, J. T.; Jarrett, J. T.; Drennan, C. L. *Science* **2004**, *303*, 76.
- (41) Chatterjee, A.; Li, Y.; Zhang, Y.; Grove, T. L.; Lee, M.; Krebs, C.; Booker, S. J.; Begley, T. P.; Ealick, S. E. *Nat. Chem. Biol.* **2008**, *4*, 758.
- (42) Nicolet, Y.; Rubach, J. K.; Posewitz, M. C.; Amara, P.; Mathevou, C.; Atta, M.; Fontecave, M.; Fontecilla-Camps, J. C. *J. Biol. Chem.* **2008**, *283*, 18861.
- (43) Quitterer, F.; List, A.; Eisenreich, W.; Bacher, A.; Groll, M. *Angew. Chem., Int. Ed.* **2012**, *51*, 1339.
- (44) Akanuma, S.; Yamagishi, A. *J. Mol. Biol.* **2008**, *382*, 458.
- (45) (a) Nagano, N.; Orengo, C. A.; Thornton, J. A. *J. Mol. Biol.* **2002**, *321*, 741. (b) Nicolet, Y.; Drennan, C. L. *Nucleic Acids Res.* **2004**, *32*, 4015.
- (46) Farrar, C. E.; Jarrett, J. T. *Biochemistry* **2009**, *48*, 2448.
- (47) Baker, J. J.; Stadtman, T. C. In *B12. Biochemistry and Medicine*; Dolphin, D., Ed.; Wiley-Interscience: New York, 1982; Vol. 2.
- (48) Marsh, E. N. G.; Meléndez, G. D. R. *Biochim. Biophys. Acta, Proteins* **2012**, *1824*, 1154.
- (49) Frey, P. A.; Magnusson, O. T. *Chem. Rev.* **2003**, *103*, 2129.
- (50) Halpern, J. *Science* **1985**, *227*, 869.
- (51) *B12. Chemistry*; Dolphin, D.; Ed.; Wiley-Interscience: New York, 1982; Vol. 1.
- (52) Halpern, J.; Kim, S.-H.; Leung, T. W. *J. Am. Chem. Soc.* **1984**, *106*, 8317.
- (53) (a) Frey, P. A.; Reed, G. H. In *Advances in Enzymology and Related Areas of Molecular Biology*; John Wiley & Sons, Inc.: New York, 1993. (b) Beinert, H. *J. Biol. Inorg. Chem.* **2000**, *5*, 2.

- (54) (a) Kozbial, P. Z.; Mushegian, A. R. *BMC Struct. Biol.* **2005**, 5. (b) Duffus, B. R.; Hamilton, T. L.; Shepard, E. M.; Boyd, E. S.; Peters, J. W.; Broderick, J. B. *Biochim. Biophys. Acta* **2012**, 1824, 1254.
- (55) Stubbe, J. *Curr. Opin. Struct. Biol.* **2000**, 10, 731.
- (56) Eklund, H.; Fontecave, M. *Structure* **1999**, 7, R257.
- (57) Buckel, W.; Golding, B. T. *Annu. Rev. Microbiol.* **2006**, 60, 27.
- (58) (a) Stadtman, E. R.; Novelli, G. D.; Lipmann, F. *J. Biol. Chem.* **1951**, 191, 365. (b) Utter, M. F.; Lipmann, F.; Werkman, C. H. *J. Biol. Chem.* **1945**, 158, 521.
- (59) Chase, T., Jr.; Rabinowitz, J. C. *J. Bacteriol.* **1968**, 96, 1065.
- (60) Knappe, J.; Bohnert, E.; Brummer, W. *Biochim. Biophys. Acta* **1965**, 107, 603.
- (61) Rödel, W.; Plaga, W.; Frank, R.; Knappe, J. *Eur. J. Biochem.* **1988**, 177, 153.
- (62) Frey, M.; Rothe, M.; Wagner, A. F. V.; Knappe, J. *J. Biol. Chem.* **1994**, 269, 12432.
- (63) Conradt, H.; Hohmann-Berger, M.; Hohmann, H.-P.; Blaschkowski, H. P.; Knappe, J. *Arch. Biochem. Biophys.* **1984**, 228, 133.
- (64) Wong, K. K.; Murray, B. W.; Lewis, S. A.; Baxter, M. K.; Ridky, T. W.; Ulissi-DeMario, L.; Kozarich, J. W. *Biochemistry* **1993**, 32, 14102.
- (65) Broderick, J. B.; Henshaw, T. F.; Cheek, J.; Wojtuszewski, K.; Smith, S. R.; Trojan, M. R.; McGhan, R. M.; Kopf, A.; Kibbey, M.; Broderick, W. E. *Biochem. Biophys. Res. Commun.* **2000**, 269, 451.
- (66) Krebs, C.; Henshaw, T. F.; Cheek, J.; Huynh, B.-H.; Broderick, J. B. *J. Am. Chem. Soc.* **2000**, 122, 12497.
- (67) Walsby, C. J.; Ortillo, D.; Yang, J.; Nyepi, M.; Broderick, W. E.; Hoffman, B. M.; Broderick, J. B. *Inorg. Chem.* **2005**, 44, 727.
- (68) Farrar, C. E.; Siu, K. K.; Howell, P. L.; Jarrett, J. T. *Biochemistry* **2010**, 49, 9985.
- (69) Cicchillo, R. M.; Iwig, D. F.; Jones, A. D.; Nesbitt, N. M.; Baleanu-Gogonea, C.; Souder, M. G.; Tu, L.; Booker, S. J. *Biochemistry* **2004**, 43, 6378.
- (70) Palmer, L. D.; Downs, D. M. *J. Biol. Chem.* **2013**, 288, 30693.
- (71) Zhang, Q.; Chen, D.; Lin, J.; Liao, R.; Tong, W.; Xu, Z.; Liu, W. *J. Biol. Chem.* **2011**, 286, 21287.
- (72) Miller, J.; Bandarian, V.; Reed, G. H.; Frey, P. A. *Arch. Biochem. Biophys.* **2001**, 387, 281.
- (73) Ruzicka, F. J.; Frey, P. A. *Biochim. Biophys. Acta* **2007**, 1774, 286.
- (74) (a) Chandra, T.; Silver, S. C.; Zilinskas, E.; Shepard, E. M.; Broderick, W. E.; Broderick, J. B. *J. Am. Chem. Soc.* **2009**, 131, 2420. (b) Silver, S. C.; Chandra, T.; Zilinskas, E.; Ghose, S.; Broderick, W. E.; Broderick, J. B. *J. Biol. Inorg. Chem.* **2010**, 15, 943.
- (75) Selvaraj, B.; Pierik, A. J.; Bill, E.; Martins, B. M. *J. Biol. Inorg. Chem.* **2013**, 18, 633.
- (76) (a) Yokoyama, K.; Numakura, M.; Kudo, F.; Ohmori, D.; Eguchi, T. *J. Am. Chem. Soc.* **2007**, 129, 15147. (b) Yokoyama, K.; Ohmori, D.; Kudo, F.; Eguchi, T. *Biochemistry* **2008**, 47, 8950.
- (77) Challand, M. R.; Martins, F. T.; Roach, P. L. *J. Biol. Chem.* **2010**, 285, 5240.
- (78) (a) Driesener, R. C.; Challand, M. R.; McGlynn, S. E.; Shepard, E. M.; Boyd, E. S.; Broderick, J. B.; Peters, J. W.; Roach, P. L. *Angew. Chem., Int. Ed.* **2010**, 49, 1687. (b) Shepard, E. M.; Duffus, B. R.; George, S. J.; McGlynn, S. E.; Challand, M. R.; Swanson, K. D.; Roach, P. L.; Cramer, S. P.; Peters, J. W.; Broderick, J. B. *J. Am. Chem. Soc.* **2010**, 132, 9247.
- (79) Grove, T. L.; Lee, K.-h.; Clair, J.; Krebs, C.; Booker, S. J. *Biochemistry* **2008**, 47, 7523.
- (80) (a) Benjdia, A.; Leprince, J.; Sandström, C.; Vaudry, H.; Berteau, O. *J. Am. Chem. Soc.* **2009**, 131, 8348. (b) Grove, T. L.; Ahlum, J. H.; Qin, R. M.; Lanz, N. D.; Radle, M. I.; Krebs, C.; Booker, S. J. *Biochemistry* **2013**, 52, 2874.
- (81) Feng, J.; Wu, J.; Dai, N.; Lin, S.; Xu, H. H.; Deng, Z.; He, X. *PLoS One* **2013**, 8, e68545.
- (82) Hover, B. M.; Loksztejn, A.; Ribeiro, A. A.; Yokoyama, K. *J. Am. Chem. Soc.* **2013**, 135, 7019.
- (83) Landgraf, B. J.; Arcinas, A. J.; Lee, K.-H.; Booker, S. J. *J. Am. Chem. Soc.* **2013**, 135, 15404.
- (84) Kim, H. J.; McCarty, R. M.; Ogasawara, Y.; Liu, Y. N.; Mansoorabadi, S. O.; LeVieux, J.; Liu, H. W. *J. Am. Chem. Soc.* **2013**, 135, 8093.
- (85) Layer, G.; Grage, K.; Teschner, T.; Schünemann, V.; Breckau, D.; Masoumi, A.; Jahn, M.; Heathcote, P.; Trautwein, A. X.; Jahn, D. *J. Biol. Chem.* **2005**, 280, 29038.
- (86) Flühe, L.; Knappe, T. A.; Gattner, M. J.; Schaefer, A.; Burghaus, O.; Linne, U.; Marahiel, M. A. *Nat. Chem. Biol.* **2012**, 8, 350.
- (87) Szu, P.-H.; Ruszczycky, M. W.; Choi, S.-h.; Yan, F.; Liu, H.-w. *J. Am. Chem. Soc.* **2009**, 131, 14030.
- (88) McCarty, R. M.; Krebs, C.; Bandarian, V. *Biochemistry* **2013**, 52, 188.
- (89) Pierre, S.; Guillot, A.; Benjdia, A.; Sandstrom, C.; Langella, P.; Berteau, O. *Nat. Chem. Biol.* **2012**, 8, 957.
- (90) Petrovich, R. M.; Ruzicka, F. J.; Reed, G. H.; Frey, P. A. *Biochemistry* **1992**, 31, 10774.
- (91) (a) Ollagnier, S.; Mulliez, E.; Schmidt, P. P.; Eliasson, R.; Gaillard, J.; Deronzier, C.; Bergman, T.; Gräslund, A.; Reichard, P.; Fontecave, M. *J. Biol. Chem.* **1997**, 272, 24216. (b) Tamarit, J.; Mulliez, E.; Meier, C.; Trautwein, A.; Fontecave, M. *J. Biol. Chem.* **1999**, 274, 31291. (c) Padovani, D.; Thomas, F.; Trautwein, A. X.; Mulliez, E.; Fontecave, M. *Biochemistry* **2001**, 40, 6713.
- (92) (a) Torrents, E.; Buist, G.; Liu, A.; Eliasson, R.; Kok, J.; Gibert, I.; Gräslund, A.; Reichard, P. *J. Biol. Chem.* **2000**, 275, 2463. (b) Liu, A.; Gräslund, A. *J. Biol. Chem.* **2000**, 275, 12367.
- (93) (a) Krebs, C.; Broderick, W. E.; Henshaw, T. F.; Broderick, J. B.; Huynh, B. H. *J. Am. Chem. Soc.* **2002**, 124, 912. (b) Yang, J.; Naik, S. G.; Ortillo, D. O.; Garcia-Serres, R.; Li, M.; Broderick, W. E.; Huynh, B. H.; Broderick, J. B. *Biochemistry* **2009**, 48, 9234.
- (94) Küller, R.; Pils, T.; Kappl, R.; Hüttermann, J.; Knappe, J. *J. Biol. Chem.* **1998**, 273, 4897.
- (95) Rebeil, R.; Sun, Y.; Chooback, L.; Pedraza-Reyes, M.; Kinsland, C.; Begley, T. P.; Nicholson, W. L. *J. Bacteriol.* **1998**, 180, 4879.
- (96) (a) Rebeil, R.; Nicholson, W. L. *Proc. Natl. Acad. Sci. U.S.A.* **2001**, 98, 9038. (b) Chandor, A.; Berteau, O.; Douki, T.; Gasparutto, D.; Sanakis, Y.; Ollagnier-de-Choudens, S.; Atta, M.; Fontecave, M. *J. Biol. Chem.* **2006**, 281, 26922.
- (97) (a) Buis, J. M.; Cheek, J.; Kalliri, E.; Broderick, J. B. *J. Biol. Chem.* **2006**, 281, 25994. (b) Yang, L.; Lin, G.; Liu, D.; Dria, K. J.; Telser, J.; Li, L. *J. Am. Chem. Soc.* **2011**, 133, 10434. (c) Yang, L.; Lin, G.; Nelson, R. S.; Jian, Y.; Telser, J.; Li, L. *Biochemistry* **2012**, 51, 7173. (d) Yang, L.; Nelson, R. S.; Benjdia, A.; Lin, G.; Telser, J.; Stoll, S.; Schlichting, I.; Li, L. *Biochemistry* **2013**, 52, 3041.
- (98) Chandor, A.; Douki, T.; Gasparutto, D.; Gambarelli, S.; Sanakis, Y.; Nicolet, Y.; Ollagnier-de-Choudens, S.; Atta, M.; Fontecave, M. C. *R. Chim.* **2007**, 10, 756.
- (99) Pieck, J. C.; Hennecke, U.; Pierik, A. J.; Friedel, M. G.; Carell, T. *J. Biol. Chem.* **2006**, 281, 36317.
- (100) Layer, G.; Verfürth, K.; Mahlitz, E. *J. Biol. Chem.* **2002**, 277, 34136.
- (101) (a) Leonardi, R.; Fairhurst, S. A.; Kriek, M.; Lowe, D. J.; Roach, P. L. *FEBS Lett.* **2003**, 539, 95. (b) Kriek, M.; Martins, F.; Leonardi, R.; Fairhurst, S. A.; Lowe, D. J.; Roach, P. L. *J. Biol. Chem.* **2007**, 282, 17413.
- (102) Szu, P.-H.; He, X.; Zhao, L.; Liu, H.-w. *Angew. Chem., Int. Ed.* **2005**, 44, 6742.
- (103) Paraskevopoulou, C.; Fairhurst, S. A.; Lowe, D. J.; Brick, P.; Onesti, S. *Mol. Microbiol.* **2006**, 59, 795.
- (104) Boll, R.; Hofmann, C.; Heitmann, B.; Hauser, G.; Glaser, S.; Koslowski, T.; Friedrich, T.; Bechthold, A. *J. Biol. Chem.* **2006**, 281, 14756.
- (105) (a) Raschke, M.; Bürkle, L.; Müller, N.; Nunes-Nesi, A.; Fernie, A. R.; Arigoni, D.; Amrhein, N.; Fitzpatrick, T. B. *Proc. Natl. Acad. Sci. U.S.A.* **2007**, 104, 19637. (b) Coquille, S.; Roux, C.; Mehta, A.; Begley, T. P.; Fitzpatrick, T. B.; Thore, S. *J. Struct. Biol.* **2013**, 184, 438.
- (106) Martinez-Gomez, N. C.; Downs, D. M. *Biochemistry* **2008**, 47, 9054.

- (107) (a) Li, L.; Patterson, D. P.; Fox, C. C.; Lin, B.; Coschigano, P. W.; Marsh, E. N. G. *Biochemistry* **2009**, *48*, 1284. (b) Hilberg, M.; Pierik, A. J.; Bill, E.; Friedrich, T.; Lippert, M.-L.; Heider, J. *J. Biol. Inorg. Chem.* **2012**, *17*, 49.
- (108) Zhu, X.; Dzikovski, B.; Su, X.; Torelli, A. T.; Zhang, Y.; Ealick, S. E.; Freed, J. H.; Lin, H. *Mol. BioSyst.* **2011**, *7*, 74.
- (109) McGlynn, S. E.; Boyd, E. S.; Shepard, E. M.; Lange, R. K.; Gerlach, R.; Broderick, J. B.; Peters, J. W. *J. Bacteriol.* **2010**, *192*, 595.
- (110) Brindley, A. A.; Zajicek, R.; Warren, M. J.; Ferguson, S. J.; Rigby, S. E. *J. FEBS Lett.* **2010**, *584*, 2461.
- (111) (a) Yan, F.; LaMarre, J. M.; Rohrich, R.; Wiesner, J.; Jomaa, H.; Mankin, A. S.; Fujimori, D. G. *J. Am. Chem. Soc.* **2010**, *132*, 3953. (b) Grove, T. L.; Benner, J. S.; Radle, M. I.; Ahlum, J. H.; Landgraf, B. J.; Krebs, C.; Booker, S. J. *Science* **2011**, *332*, 604. (c) Grove, T. L.; Radle, M. I.; Krebs, C.; Booker, S. J. *J. Am. Chem. Soc.* **2011**, *133*, 19586.
- (112) (a) Booth, M. P. S.; Challand, M. R.; Emery, D. C.; Roach, P. L.; Spencer, J. *Protein Expression Purif.* **2010**, *74*, 204. (b) Challand, M. R.; Salvadori, E.; Driesener, R. C.; Kay, C. W. M.; Roach, P. L.; Spencer, J. *PLoS One* **2013**, *8*, e67979.
- (113) (a) Shaveta, G.; Shi, J.; Chow, V. T. K.; Song, J. *Biochem. Biophys. Res. Commun.* **2010**, *391*, 1390. (b) Duschene, K. S.; Broderick, J. B. *FEBS Lett.* **2010**, *584*, 1263. (c) Haldar, S.; Paul, S.; Joshi, N.; Dasgupta, A.; Chattopadhyay, K. *PLoS One* **2012**, *7*, e31797.
- (114) Zhang, Q.; Li, Y.; Chen, D.; Yu, Y.; Duan, L.; Shen, B.; Liu, W. *Nat. Chem. Biol.* **2011**, *7*, 154.
- (115) (a) Kamat, S. S.; Williams, H. J.; Raushel, F. M. *Nature* **2011**, *480*, 570. (b) Kamat, S. S.; Williams, H. J.; Dangott, L. J.; Chakrabarti, M.; Raushel, F. M. *Nature* **2013**, *497*, 132.
- (116) Werner, W. J.; Allen, K. D.; Hu, K.; Helms, G. L.; Chen, B. S.; Wang, S. C. *Biochemistry* **2011**, *50*, 8986.
- (117) Decamps, L.; Philmus, B.; Benjdia, A.; White, R. H.; Begley, T. P.; Berteau, O. *J. Am. Chem. Soc.* **2012**, *134*, 18173.
- (118) Huang, W.; Xu, H.; Li, Y.; Zhang, F.; Chen, X.-Y.; He, Q.-L.; Igarashi, Y.; Tang, G.-L. *J. Am. Chem. Soc.* **2012**, *134*, 8831.
- (119) Mahanta, N.; Fedoseyenko, D.; Dairi, T.; Begley, T. P. *J. Am. Chem. Soc.* **2013**, *135*, 15318.
- (120) Duin, E. C.; Lafferty, M. E.; Crouse, B. R.; Allen, R. M.; Sanyal, I.; Flint, D. H.; Johnson, M. K. *Biochemistry* **1997**, *36*, 11811.
- (121) (a) Tse Sum Bui, B.; Florentin, D.; Marquet, A.; Benda, R.; Trautwein, A. X. *FEBS Lett.* **1999**, *459*, 411. (b) Ollagnier-de Choudens, S.; Sanakis, Y.; Hewitson, K. S.; Roach, P.; Baldwin, J. E.; Münck, E.; Fontecave, M. *Biochemistry* **2000**, *39*, 4165. (c) Ollagnier-de Choudens, S.; Sanakis, Y.; Hewitson, K. S.; Roach, P.; Münck, E.; Fontecave, M. *J. Biol. Chem.* **2002**, *277*, 13449.
- (122) Cosper, M. M.; Jameson, G. N. L.; Davydov, R.; Eidsness, M. K.; Hoffman, B. M.; Huynh, B. H.; Johnson, M. K. *J. Am. Chem. Soc.* **2002**, *124*, 14006.
- (123) Ollagnier-de Choudens, S.; Fontecave, M. *FEBS Lett.* **1999**, *453*, 25.
- (124) (a) Busby, R. W.; Schelvis, J. P. M.; Yu, D. S.; Babcock, G. T.; Marletta, M. A. *J. Am. Chem. Soc.* **1999**, *121*, 4706. (b) Miller, J. R.; Busby, R. W.; Jordan, S. W.; Cheek, J.; Henshaw, T. F.; Ashley, G. W.; Broderick, J. B.; Cronan, J. E., Jr.; Marletta, M. A. *Biochemistry* **2000**, *39*, 15166. (c) Kriek, M.; Peters, L.; Takahashi, Y.; Roach, P. L. *Protein Expression Purif.* **2003**, *28*, 241.
- (125) Cicchillo, R. M.; Lee, K.-H.; Baleanu-Gogonea, C.; Nesbitt, N. M.; Krebs, C.; Booker, S. J. *Biochemistry* **2004**, *43*, 11770.
- (126) Pierrel, F.; Björk, G. R.; Fontecave, M.; Atta, M. *J. Biol. Chem.* **2002**, *277*, 13367.
- (127) (a) Pierrel, F.; Douki, T.; Fontecave, M.; Atta, M. *J. Biol. Chem.* **2004**, *279*, 47555. (b) Hernandez, H. L.; Pierrel, F.; Elleingand, E.; Garcia-Serres, R.; Huynh, B. H.; Johnson, M. K.; Fontecave, M.; Atta, M. *Biochemistry* **2007**, *46*, 5140.
- (128) Hänelmann, P.; Hernández, H. L.; Menzel, C.; García-Serres, R.; Huynh, B. H.; Johnson, M. K.; Mendel, R. R.; Schindelin, H. *J. Biol. Chem.* **2004**, *279*, 34721.
- (129) Rubach, J. K.; Brazzolotto, X.; Gaillard, J.; Fontecave, M. *FEBS Lett.* **2005**, *579*, 5055.
- (130) (a) Nicolet, Y.; Martin, L.; Tron, C.; Fontecilla-Camps, J. C. *FEBS Lett.* **2010**, *584*, 4197. (b) Driesener, R. C.; Duffus, B. R.; Shepard, E. M.; Bruzas, I. R.; Duschene, K. S.; Coleman, N. J.-R.; Morrison, A. P. G.; Salvadori, E.; Kay, C. W. M.; Peters, J. W.; Broderick, J. B.; Roach, P. L. *Biochemistry* **2013**, *52*, 8696.
- (131) Kuchenreuther, J. M.; Myers, W. K.; Stich, T. A.; George, S. J.; Nejatyjahromy, Y.; Swartz, J. R.; Britt, R. D. *Science* **2013**, *342*, 472.
- (132) Curatti, L.; Ludden, P. W.; Rubio, L. M. *Proc. Natl. Acad. Sci. U.S.A.* **2006**, *103*, 5297.
- (133) Wiig, J. A.; Hu, Y.; Ribbe, M. W. *Proc. Natl. Acad. Sci. U.S.A.* **2011**, *108*, 8623.
- (134) Yu, L.; Blaser, M.; Andrei, P. I.; Pierik, A. J.; Selmer, T. *Biochemistry* **2006**, *45*, 9584.
- (135) (a) Benjdia, A.; Leprince, J.; Guillot, A.; Vaudry, H.; Rabot, S.; Berteau, O. *J. Am. Chem. Soc.* **2007**, *129*, 3462. (b) Benjdia, A.; Subramanian, S.; Leprince, J.; Vaudry, H.; Johnson, M. K.; Berteau, O. *J. Biol. Chem.* **2008**, *283*, 17815.
- (136) Benjdia, A.; Subramanian, S.; Leprince, J.; Vaudry, H.; Johnson, M. K.; Berteau, O. *FEBS J.* **2010**, *277*, 1906.
- (137) Grove, T. L.; Ahlum, J. H.; Sharma, P.; Krebs, C.; Booker, S. J. *Biochemistry* **2010**, *49*, 3783.
- (138) Lee, K.-H.; Saleh, L.; Anton, B. P.; Madinger, C. L.; Benner, J. S.; Iwig, D. F.; Roberts, R. J.; Krebs, C.; Booker, S. J. *Biochemistry* **2009**, *48*, 10162.
- (139) Arragain, S.; Garcia-Serres, R.; Blondin, G.; Douki, T.; Clemancey, M.; Latour, J.-M.; Forouhar, F.; Neely, H.; Montelione, G. T.; Hunt, J. F.; Mulliez, E.; Fontecave, M.; Atta, M. *J. Biol. Chem.* **2010**, *285*, 5792.
- (140) (a) Wecksler, S. R.; Stoll, S.; Tran, H.; Magnusson, O. T.; Wu, S.-p.; King, D.; Britt, R. D.; Klinman, J. P. *Biochemistry* **2009**, *48*, 10151. (b) Wecksler, S. R.; Stoll, S.; Iavarone, A. T.; Imsand, E. M.; Tran, H.; Britt, R. D.; Klinman, J. P. *Chem. Commun.* **2010**, *46*, 7031.
- (141) Arragain, S.; Handelman, S. K.; Forouhar, F.; Wei, F.-Y.; Tomizawa, K.; Hunt, J. F.; Douki, T.; Fontecave, M.; Mulliez, E.; Atta, M. *J. Biol. Chem.* **2010**, *285*, 28425.
- (142) Perche-Letuvée, P.; Kathirvelu, V.; Berggren, G.; Clemancey, M.; Latour, J.-M.; Maurel, V.; Douki, T.; Armengaud, J.; Mulliez, E.; Fontecave, M.; Garcia-Serres, R.; Gambarelli, S.; Atta, M. *J. Biol. Chem.* **2012**, *287*, 41174.
- (143) Flühe, L.; Burghaus, O.; Wieckowski, B. M.; Giessen, T. W.; Linne, U.; Marahiel, M. A. *J. Am. Chem. Soc.* **2013**, *135*, 959.
- (144) Beinert, H.; Thomson, A. J. *Arch. Biochem. Biophys.* **1983**, *222*, 333.
- (145) (a) Jameson, G. N. L.; Walters, E. M.; Manieri, W.; Schürmann, P.; Johnson, M. K.; Huynh, B. H. *J. Am. Chem. Soc.* **2003**, *125*, 1146. (b) Walters, E. M.; Garcia-Serres, R.; Jameson, G. N. L.; Glauser, D. A.; Bourquin, F.; Manieri, W.; Schürmann, P.; Johnson, M. K.; Huynh, B. H. *J. Am. Chem. Soc.* **2005**, *127*, 9612.
- (146) Crain, A. V.; Broderick, J. B. *Biochim. Biophys. Acta* **2013**, *1834*, 2512.
- (147) (a) Becker, A.; Fritz-Wolf, K.; Kabsch, W.; Knappe, J.; Schultz, S.; Wagner, A. F. V. *Nat. Struct. Biol.* **1999**, *6*, 969. (b) Becker, A.; Kabsch, W. *J. Biol. Chem.* **2002**, *277*, 40036.
- (148) Nnyepi, M. R.; Peng, Y.; Broderick, J. B. *Arch. Biochem. Biophys.* **2007**, *459*, 1.
- (149) Peng, Y.; Veneziano, S. E.; Gillispie, G. D.; Broderick, J. B. *J. Biol. Chem.* **2010**, *285*, 27224.
- (150) Crain, A. V.; Broderick, J. B. *J. Biol. Chem.* **2013**, online December 2013.
- (151) Thelander, L.; Reichard, P. *Annu. Rev. Biochem.* **1979**, *48*, 133.
- (152) Barlow, T. *Biochem. Biophys. Res. Commun.* **1988**, *155*, 747.
- (153) Fontecave, M.; Eliasson, R.; Reichard, P. *Proc. Natl. Acad. Sci. U.S.A.* **1989**, *86*, 2147.
- (154) Eliasson, R.; Fontecave, M.; Jörnvall, H.; Krook, M.; Pontis, E.; Reichard, P. *Proc. Natl. Acad. Sci. U.S.A.* **1990**, *87*, 3314.
- (155) Sun, X.; Ollagnier, S.; Schmidt, P. P.; Atta, M.; Mulliez, E.; Lepape, L.; Eliasson, R.; Gräslund, A.; Fontecave, M.; Reichard, P.; Sjöberg, B.-M. *J. Biol. Chem.* **1996**, *271*, 6827.

- (156) Sun, X.; Eliasson, R.; Pontis, E.; Andersson, J.; Buist, G.; Sjöberg, B.-M.; Reichard, P. *J. Biol. Chem.* **1995**, *270*, 2443.
- (157) (a) Ollagnier, S.; Mulliez, E.; Gaillard, J.; Eliasson, R.; Fontecave, M.; Reichard, P. *J. Biol. Chem.* **1996**, *271*, 9410. (b) Torrents, E.; Eliasson, R.; Wolpher, H.; Gräslund, A.; Reichard, P. *J. Biol. Chem.* **2001**, *276*, 33488.
- (158) Ollagnier, S.; Meier, C.; Mulliez, E.; Gaillard, J.; Schuenemann, V.; Trautwein, A.; Mattioli, T.; Lutz, M.; Fontecave, M. *J. Am. Chem. Soc.* **1999**, *121*, 6344.
- (159) Tamarit, J.; Gerez, C.; Meier, C.; Mulliez, E.; Trautwein, A.; Fontecave, M. *J. Biol. Chem.* **2000**, *275*, 15669.
- (160) Mulliez, E.; Padovani, D.; Atta, M.; Alcouffe, C.; Fontecave, M. *Biochemistry* **2001**, *40*, 3730.
- (161) Raynaud, C.; Sarcabal, P.; Meynial-Salles, I.; Croux, C.; Souaille, P. *Proc. Natl. Acad. Sci. U.S.A.* **2003**, *100*, 5010.
- (162) O'Brien, J. R.; Raynaud, C.; Croux, C.; Girbal, L.; Souaille, P.; Lanzilotta, W. N. *Biochemistry* **2004**, *43*, 4635.
- (163) Logan, D. T.; Andersson, J.; Sjöberg, B.-M.; Nordlund, P. *Science* **1999**, *283*, 1499.
- (164) Leuthner, B.; Leutwein, C.; Schulz, H.; Hörrth, P.; Haehnel, W.; Schiltz, E.; Schägger, H.; Heider, J. *Mol. Microbiol.* **1998**, *28*, 615.
- (165) Andrei, P. I.; Pierik, A. J.; Zauner, S.; Andrei-Selmer, L.; Selmer, T. *Eur. J. Biochem.* **2004**, *271*, 2225.
- (166) Feliks, M.; Martins, B. M.; Ullmann, G. M. *J. Am. Chem. Soc.* **2013**, *135*, 14574.
- (167) Martins, B. M.; Blaser, M.; Feliks, M.; Ullmann, G. M.; Buckel, W.; Selmer, T. *J. Am. Chem. Soc.* **2011**, *133*, 14666.
- (168) (a) Craciun, S.; Balskus, E. P. *Proc. Natl. Acad. Sci. U.S.A.* **2012**, *109*, 21307. (b) Thibodeaux, C. J.; van der Donk, W. A. *Proc. Natl. Acad. Sci. U.S.A.* **2012**, *109*, 21184.
- (169) Ifuku, O.; Kishimoto, J.; Haze, S.; Yanagi, M.; Fukushima, S. *Biosci., Biotechnol., Biochem.* **1992**, *56*, 1780.
- (170) Ohshiro, T.; Yamamoto, M.; Izumi, Y.; Bui, B. T.; Florentin, D.; Marquet, A. *Biosci., Biotechnol., Biochem.* **1994**, *58*, 1738.
- (171) Sanyal, I.; Gibson, K. J.; Flint, D. H. *Arch. Biochem. Biophys.* **1996**, *326*, 48.
- (172) Méjean, A.; Bui, B. T. S.; Florentin, D.; Ploux, O.; Izumi, Y.; Marquet, A. *Biochem. Biophys. Res. Commun.* **1995**, *217*, 1231.
- (173) Ugulava, N. B.; Gibney, B. R.; Jarrett, J. T. *Biochemistry* **2000**, *39*, 5206.
- (174) Hewitson, K. S.; Baldwin, J. E.; Shaw, N. M.; Roach, P. L. *FEBS Lett.* **2000**, *466*, 372.
- (175) Hewitson, K. S.; Ollagnier-de-Choudens, S.; Sanakis, Y.; Shaw, N. M.; Baldwin, J. E.; Münck, E.; Roach, P. L.; Fontecave, M. *J. Biol. Inorg. Chem.* **2002**, *7*, 83.
- (176) Ugulava, N. B.; Surerus, K. K.; Jarrett, J. T. *J. Am. Chem. Soc.* **2002**, *124*, 9050.
- (177) Cosper, M. M.; Jameson, G. N. L.; Hernandez, H. L.; Krebs, C.; Huynh, B. H.; Johnson, M. K. *Biochemistry* **2004**, *43*, 2007.
- (178) Ugulava, N. B.; Sacanell, C. J.; Jarrett, J. T. *Biochemistry* **2001**, *40*, 8352.
- (179) Jameson, G. N. L.; Cosper, M. M.; Hernandez, H. L.; Johnson, M. K.; Huynh, B. H. *Biochemistry* **2004**, *43*, 2022.
- (180) Broach, R.; Jarrett, J. *Biochemistry* **2006**, *45*, 14166.
- (181) Tse Sum Bui, B.; Florentin, D.; Fournier, F.; Ploux, O.; Méjean, A.; Marquet, A. *FEBS Lett.* **1998**, *440*, 226.
- (182) Tse Sum Bui, B.; Benda, R.; Schünemann, V.; Florentin, D.; Trautwein, A. X.; Marquet, A. *Biochemistry* **2003**, *42*, 8791.
- (183) (a) Ollagnier-de-Choudens, S.; Mulliez, E.; Hewitson, K. S.; Fontecave, M. *Biochemistry* **2002**, *41*, 9145. (b) Ollagnier-de-Choudens, S.; Mulliez, E.; Fontecave, M. *FEBS Lett.* **2002**, *532*, 465.
- (184) Tse Sum Bui, B.; Mattioli, T. A.; Florentin, D.; Bolbach, G.; Marquet, A. *Biochemistry* **2006**, *45*, 3824.
- (185) Taylor, A. M.; Farrar, C.; Jarrett, J. T. *Biochemistry* **2008**, *47*, 9309.
- (186) Taylor, A. M.; Stoll, S.; Britt, R. D.; Jarrett, J. T. *Biochemistry* **2011**, *50*, 7953.
- (187) Fugate, C. J.; Stich, T. A.; Kim, E. G.; Myers, W. K.; Britt, R. D.; Jarrett, J. T. *J. Am. Chem. Soc.* **2012**, *134*, 9042.
- (188) Lotierzo, M.; Raux, E.; Tse Sum Bui, B.; Goasdoue, N.; Libot, F.; Florentin, D.; Warren, M. J.; Marquet, A. *Biochemistry* **2006**, *45*, 12274.
- (189) Reed, L. J.; Okaichi, T.; Nakanishi, I. *Abstr. Int. Symp. Chem. Nat. Prod. (Kyoto)* **1964**, *218*.
- (190) Parry, R. J. *J. Am. Chem. Soc.* **1977**, *99*, 6464.
- (191) (a) Parry, R. J.; Kunitani, M. G. *J. Am. Chem. Soc.* **1976**, *98*, 4024. (b) Guillerm, G.; Frappier, F.; Gaudry, M.; Marquet, A. *Biochimie* **1977**, *59*, 119.
- (192) Parry, R. J.; Trainor, D. A. *J. Am. Chem. Soc.* **1978**, *100*, 5243.
- (193) White, R. H. *Biochemistry* **1980**, *19*, 15.
- (194) White, R. H. *J. Am. Chem. Soc.* **1980**, *102*, 6605.
- (195) (a) Vanden Boom, T. J.; Reed, K. E.; Cronan, J. E., Jr. *J. Bacteriol.* **1991**, *173*, 6411. (b) Hayden, M. A.; Huang, I.; Bussiere, D. E.; Ashley, G. W. *J. Biol. Chem.* **1992**, *267*, 9512.
- (196) (a) Hayden, M. A.; Huang, I. Y.; Iliopoulos, G.; Orozco, M.; Ashley, G. W. *Biochemistry* **1993**, *32*, 3778. (b) Reed, K. E.; Cronan, J. E., Jr. *J. Bacteriol.* **1993**, *175*, 1325.
- (197) Morris, T. W.; Reed, K. E.; Cronan, J. E., Jr. *J. Bacteriol.* **1995**, *177*, 1.
- (198) Zhao, X.; Miller, J. R.; Jiang, Y.; Marletta, M. A.; Cronan, J. E., Jr. *Chem. Biol.* **2003**, *10*, 1293.
- (199) Douglas, P.; Krieg, M.; Bryant, P.; Roach, P. L. *Angew. Chem., Int. Ed.* **2006**, *45*, 5197.
- (200) Aberhart, D. J.; Lin, H.-J.; Weiller, B. H. *J. Am. Chem. Soc.* **1981**, *103*.
- (201) Aberhart, D. J.; Gould, S. J.; Lin, H.-J.; Thiruvengadam, T. K.; Weiller, B. H. *J. Am. Chem. Soc.* **1983**, *105*, 5461.
- (202) Aberhart, D. J. *J. Chem. Soc., Perkin Trans.* **1988**, *1*, 343.
- (203) Baraniak, J.; Moss, M. L.; Frey, P. A. *J. Biol. Chem.* **1989**, *264*, 1357.
- (204) Kilgore, J. L.; Aberhart, D. J. *J. Chem. Soc., Perkin Trans.* **1991**, *1*, 79.
- (205) Moss, M. L.; Frey, P. A. *J. Biol. Chem.* **1990**, *265*, 18112.
- (206) Han, O.; Frey, P. A. *J. Am. Chem. Soc.* **1990**, *112*, 8982.
- (207) Chen, D.; Frey, P. A. *Biochemistry* **2001**, *40*, 596.
- (208) Hinckley, G. T.; Ruzicka, F. J.; Thompson, M. J.; Blackburn, G. M.; Frey, P. A. *Arch. Biochem. Biophys.* **2003**, *414*, 34.
- (209) Cosper, N. J.; Booker, S. J.; Ruzicka, F.; Frey, P. A.; Scott, R. A. *Biochemistry* **2000**, *39*, 15668.
- (210) Song, K. B.; Frey, P. A. *J. Biol. Chem.* **1991**, *266*, 7651.
- (211) Ruzicka, F. J.; Lieder, K. W.; Frey, P. A. *J. Bacteriol.* **2000**, *182*, 469.
- (212) Wu, W.; Lieder, K. W.; Reed, G. H.; Frey, P. A. *Biochemistry* **1995**, *34*, 10532.
- (213) Wu, W.; Booker, S.; Lieder, K. W.; Bandarian, V.; Reed, G. H.; Frey, P. A. *Biochemistry* **2000**, *39*, 9561.
- (214) Ballinger, M. D.; Reed, G. H.; Frey, P. A. *Biochemistry* **1992**, *31*, 949.
- (215) Ballinger, M. D.; Frey, P. A.; Reed, G. H. *Biochemistry* **1992**, *31*, 10782.
- (216) Ballinger, M. D.; Frey, P. A.; Reed, G. H.; LoBrott, R. *Biochemistry* **1995**, *34*, 10086.
- (217) Chang, C. H.; Ballinger, M. D.; Reed, G. H.; Frey, P. A. *Biochemistry* **1996**, *35*, 11081.
- (218) Chen, D.; Ruzicka, F. J.; Frey, P. A. *Biochem. J.* **2000**, *348*, 539.
- (219) Frey, P. A.; Hegeman, A. D.; Ruzicka, F. J. *Crit. Rev. Biochem. Mol. Biol.* **2008**, *43*, 63.
- (220) (a) Srinivasan, G.; James, C. M.; Krzycki, J. A. *Science* **2002**, *296*, 1459. (b) Hao, B.; Gong, W.; Ferguson, T. K.; James, C. M.; Krzycki, J. A.; Chan, M. K. *Science* **2002**, *296*, 1462.
- (221) (a) Ferguson, D. J., Jr.; Krzycki, J. A. *J. Bacteriol.* **1997**, *179*, 846. (b) Burke, S. A.; Krzycki, J. A. *J. Biol. Chem.* **1997**, *272*, 16570. (c) Ferguson, D. J., Jr.; Gorlatova, N.; Grahame, D. A.; Krzycki, J. A. *J. Biol. Chem.* **2000**, *275*, 29053.
- (222) (a) Ferguson, D. J., Jr.; Krzycki, J. A.; Grahame, D. A. *J. Biol. Chem.* **1996**, *271*, 5189. (b) Bose, A.; Pritchett, M. A.; Metcalf, W. W. *J. Bacteriol.* **2008**, *190*, 4017. (c) Gaston, M. A.; Jiang, R.; Krzycki, J. A. *Curr. Opin. Microbiol.* **2011**, *14*, 342.

- (223) (a) Soares, J. A.; Zhang, L.; Pitsch, R. L.; Kleinholtz, N. M.; Jones, R. B.; Wolff, J. J.; Amster, J.; Green-Church, K. B.; Krzycki, J. A. *J. Biol. Chem.* **2005**, *280*, 36962. (b) Hao, B.; Zhao, G.; Kang, P. T.; Soares, J. A.; Ferguson, T. K.; Gallucci, J.; Krzycki, J. A.; Chan, M. K. *Chem. Biol.* **2004**, *11*, 1317.
- (224) Cellitti, S. E.; Ou, W.; Chiu, H. P.; Grunewald, J.; Jones, D. H.; Hao, X.; Fan, Q.; Quinn, L. L.; Ng, K.; Anfora, A. T.; Lesley, S. A.; Uno, T.; Brock, A.; Geierstanger, B. H. *Nat. Chem. Biol.* **2011**, *7*, 528.
- (225) Quitterer, F.; List, A.; Beck, P.; Bacher, A.; Groll, M. *J. Mol. Biol.* **2012**, *424*, 270.
- (226) Gaston, M. A.; Zhang, L.; Green-Church, K. B.; Krzycki, J. A. *Nature* **2011**, *471*, 647.
- (227) (a) Buckel, W.; Kratky, C.; Golding, B. T. *Chemistry* **2005**, *12*, 352. (b) Banerjee, R. *Chem. Rev.* **2003**, *103*, 2083.
- (228) Krzycki, J. A. *Curr. Opin. Chem. Biol.* **2013**, *17*, 619.
- (229) Zhu, W.; Liu, Y.; Zhang, R. *Theor. Chem. Acc.* **2013**, *132*, 1385.
- (230) (a) Rajagopalan, K. V. In *Advances in Enzymology and Related Areas of Molecular Biology*; Meister, A., Ed.; Wiley Interscience: New York, 1991; Vol. 64. (b) Rajagopalan, K. V.; Johnson, J. L. *J. Biol. Chem.* **1992**, *267*, 10199. (c) Schwarz, G.; Mendel, R. R. *Annu. Rev. Plant Biol.* **2006**, *57*, 623. (d) Leimkuhler, S.; Wuebbens, M. M.; Rajagopalan, K. V. *Coord. Chem. Rev.* **2011**, *255*, 1129.
- (231) (a) Stewart, V. *Microbiol. Rev.* **1988**, *52*, 190. (b) Shanmugam, K. T.; Stewart, V.; Gunsalus, R. P.; Boxer, D. H.; Cole, J. A.; Chippaux, M.; Demoss, J. A.; Giordano, G.; Lin, E. C. C.; Rajagopalan, K. V. *Mol. Microbiol.* **1992**, *6*, 3452.
- (232) (a) Wuebbens, M. M.; Rajagopalan, K. V. *J. Biol. Chem.* **1993**, *268*, 13493. (b) Santamaria-Araujo, J. A.; Fischer, B.; Otte, T.; Nimtz, M.; Mendel, R. R.; Wray, V.; Schwarz, G. N. *J. Biol. Chem.* **2004**, *279*, 15994.
- (233) (a) Wuebbens, M. M.; Rajagopalan, K. V. *J. Biol. Chem.* **1995**, *270*, 1082. (b) Rieder, C.; Eisenreich, W.; O'Brien, J.; Richter, G.; Gotze, E.; Boyle, P.; Blanchard, S.; Bacher, A.; Simon, H. *Eur. J. Biochem./FEBS* **1998**, *255*, 24.
- (234) Rivers, S. L.; McNairn, E.; Blasco, F.; Giordano, G.; Boxer, D. H. *Mol. Microbiol.* **1993**, *8*, 1071.
- (235) St. John, R. T.; Johnston, H. M.; Seidman, C.; Garfinkel, D.; Gordon, J. K.; Shah, V. K.; Brill, W. J. *J. Bacteriol.* **1975**, *121*, 759.
- (236) Rossen, L.; Ma, Q. S.; Mudd, E. A.; Johnston, A. W. B.; Downie, J. A. *Nucleic Acids Res.* **1984**, *12*, 7123.
- (237) Goosen, N.; Horsman, H. P. A.; Huinen, R. G. M.; van de Putte, P. *J. Bacteriol.* **1989**, *171*, 447.
- (238) (a) Menendez, C.; Siebert, D.; Brandsch, R. *FEBS Lett.* **1996**, *391*, 101. (b) Menendez, C.; Igloi, G.; Henninger, H.; Brandsch, R. *Arch. Microbiol.* **1995**, *164*, 142. (c) Solomon, P. S.; Shaw, A. L.; Lane, I.; Hanson, G. R.; Palmer, T.; McEwan, A. G. *Microbiology (Reading, U.K.)* **1999**, *145*, 1421.
- (239) Hänelmann, P.; Schwarz, G.; Mendel, R. R. *J. Biol. Chem.* **2002**, *277*, 18303.
- (240) Hänelmann, P.; Schindelin, H. *Proc. Natl. Acad. Sci. U.S.A.* **2004**, *101*, 12870.
- (241) Layer, G.; Moser, J.; Heinz, D. W.; Jahn, D.; Schubert, W.-D. *EMBO J.* **2003**, *22*, 6214.
- (242) Hänelmann, P.; Schindelin, H. *Proc. Natl. Acad. Sci. U.S.A.* **2006**, *103*, 6829.
- (243) Beinert, H.; Kennedy, M. C.; Stout, C. D. *Chem. Rev.* **1996**, *96*, 2335.
- (244) Lees, N. S.; Hänelmann, P.; Hernandez, H. L.; Subramanian, S.; Schindelin, H.; Johnson, M. K.; Hoffman, B. M. *J. Am. Chem. Soc.* **2009**, *131*, 9184.
- (245) Mehta, A. P.; Hanes, J. W.; Abdelwahed, S. H.; Hilmey, D. G.; Hänelmann, P.; Begley, T. P. *Biochemistry* **2013**, *52*, 1134.
- (246) Mehta, A. P.; Abdelwahed, S. H.; Begley, T. P. *J. Am. Chem. Soc.* **2013**, *135*, 10883.
- (247) Schellenberger, A. *Biochim. Biophys. Acta* **1998**, *1385*, 177.
- (248) Hong, J.; Sun, S.; Derrick, T.; Larive, C.; Schowen, K. B.; Schowen, R. L. *Biochim. Biophys. Acta* **1998**, *1385*, 187.
- (249) Peapus, D. H.; Chiu, H.-J.; Campobasso, N.; Reddick, J. J.; Begley, T. P.; Ealick, S. E. *Biochemistry* **2001**, *40*, 10103.
- (250) Jurgenson, C. T.; Begley, T. P.; Ealick, S. E. *Annu. Rev. Biochem.* **2009**, *78*, 569.
- (251) Brown, G. M., Williamson, J. M., In *Advances in Enzymology and Related Areas of Molecular Biology*; Meister, A., Ed.; Wiley Interscience: New York, 1982; Vol. 53.
- (252) Newell, P. C.; Tucker, R. G. *Biochem. J.* **1968**, *106*, 279.
- (253) (a) Frodyma, M.; Rubio, A.; Downs, D. M. *J. Bacteriol.* **2000**, *182*, 236. (b) Allen, S.; Zilles, J. L.; Downs, D. M. *J. Bacteriol.* **2002**, *184*, 6130. (c) Dougherty, M. J.; Downs, D. M. *Microbiology* **2006**, *152*, 2345. (d) Palmer, L. D.; Dougherty, M. J.; Downs, D. M. *J. Bacteriol.* **2012**, *194*, 6088.
- (254) Himmeldirk, K.; Sayer, B. G.; Spenser, I. D. *J. Am. Chem. Soc.* **1998**, *120*, 3581.
- (255) (a) Vander Horn, P. B.; Backstrom, A. D.; Stewart, V.; Begley, T. P. *J. Bacteriol.* **1993**, *175*, 982. (b) Zhang, Y.; Begley, T. P. *Gene* **1997**, *198*, 73.
- (256) Lawhorn, B. G.; Mehl, R. A.; Begley, T. P. *Org. Biomol. Chem.* **2004**, *2*, 2538.
- (257) Chatterjee, A.; Hazra, A. B.; Abdelwahed, S.; Hilmey, D. G.; Begley, T. P. *Angew. Chem., Int. Ed.* **2010**, *49*, 8653.
- (258) Martinez-Gomez, N. C.; Poyner, R. R.; Mansoorabadi, S. O.; Reed, G. H.; Downs, D. M. *Biochemistry* **2009**, *48*, 217.
- (259) Dowling, D. P.; Vey, J. L.; Croft, A. K.; Drennan, C. L. *Biochim. Biophys. Acta* **2012**, *1764*, 773.
- (260) (a) Suhadolnik, R. J. *Nucleoside Antibiotics*; Wiley-Interscience: New York, 1970. (b) McCarty, R. M.; Bandarian, V. *Bioorg. Chem.* **2012**, *43*, 15. (c) McCarty, R. M.; Somogyi, A.; Lin, G.; Jacobsen, N. E.; Bandarian, V. *Biochemistry* **2009**, *48*, 3847.
- (261) Nishimura, H.; Katagiri, K.; Sato, K.; Mayama, M.; Shimaoka, N. *J. Antibiot.* **1956**, *9*, 60.
- (262) (a) Kasai, H.; Ohashi, Z.; Harada, F.; Nishimura, S.; Oppenheimer, N. J.; Crain, P. F.; Liehr, J. G.; Minden, D. L. V.; McCloskey, J. A. *Biochemistry* **1975**, *14*, 4198. (b) Harada, F.; Nishimura, S. *Biochemistry* **1972**, *11*, 301. (c) RajBhandary, U.; Chang, S. H.; Gross, H. J.; Harada, F.; Kimura, F.; Nishimura, S. *Fed. Proc.* **1969**, *28*, 409.
- (263) (a) McCarty, R. M.; Bandarian, V. *Chem. Biol.* **2008**, *15*, 790. (b) Phillips, G.; El Yacoubi, B.; Lyons, B.; Alvarez, S.; Iwata-Reuy, D.; de Crecy-Lagard, V. *J. Bacteriol.* **2008**, *190*, 7876. (c) McCarty, R. M.; Somogyi, A.; Bandarian, V. *Biochemistry* **2009**, *48*, 2301. (d) Kuchino, Y.; Kasai, H.; Nihei, K.; Nishimura, S. *Nucleic Acids Res.* **1976**, *3*, 393. (e) Uematsu, T.; Suhadolnik, R. J. *Biochemistry* **1970**, *9*, 1260. (f) Suhadolnik, R. J.; Uematsu, T. *J. Biol. Chem.* **1970**, *245*, 4365. (g) Reader, J. S.; Metzgar, D.; Schimmel, P.; de Crecy-Lagard, V. *J. Biol. Chem.* **2003**, *279*, 6280.
- (264) Kersten, H. *BioFactors* **1988**, *1*, 27.
- (265) Walsh, C. *Acc. Chem. Res.* **1986**, *19*, 216.
- (266) Cousins, F. B. *Biochim. Biophys. Acta* **1960**, *40*, 532.
- (267) Cheeseman, P.; Toms-Wood, A.; Wolfe, R. S. *J. Bacteriol.* **1972**, *112*, 527.
- (268) Eirich, L. D.; Vogels, G. D.; Wolfe, R. S. *Biochemistry* **1978**, *17*, 4583.
- (269) Bult, C. J.; White, O.; Olsen, G. J.; Zhou, L.; Fleischmann, R. D.; Sutton, G. G.; Blake, J. A.; Fitzgerald, L. M.; Clayton, R. A.; Gocayne, J. D.; Kerlavage, A. R.; Dougherty, B. A.; Tomb, J.-F.; Adams, M. D.; Reich, C. I.; Overbeek, R.; Kirkness, E. F.; Weinstock, K. G.; Merrick, J. M.; Glodek, A.; Scott, J. L.; Geoghegan, N. S. M.; Weidman, J. F.; Fuhrmann, J. L.; Nguyen, D.; Utterback, T. R.; Kelley, J. M.; Peterson, J. D.; Sadow, P. W.; Hanna, M. C.; Cotton, M. D.; Roberts, K. M.; Hurst, M. A.; Kaine, B. P.; MBorodovsky, M.; Klenk, H.-P.; Fraser, C. M.; Smith, H. O.; Woese, C. R.; Venter, J. C. *Science* **1996**, *273*, 1058.
- (270) Choi, K.-P.; Kendrick, N.; Daniels, L. *J. Bacteriol.* **2002**, *184*, 2420.
- (271) Graham, D. E.; Xu, H.; White, R. H. *Arch. Microbiol.* **2003**, *180*, 455.
- (272) Isabelle, D.; Simpson, D. R.; Daniels, L. *Appl. Environ. Microbiol.* **2002**, *68*, 5750.

- (273) Nowicka, B.; Kruk, J. *Biochim. Biophys. Acta, Bioenerg.* **2010**, *1797*, 1587.
- (274) Bentley, R.; Meganathan, R. *Microbiol. Rev.* **1982**, *46*, 241.
- (275) (a) Marcelli, S. W.; Chang, H.-T.; Chapman, T.; Chalk, P. A.; Miles, R. J.; Poole, R. K. *FEMS Microbiol. Lett.* **1996**, *138*, 59. (b) Parkhill, J.; Wren, B. W.; Mungall, K.; Ketley, J. M.; Churcher, C.; Basham, D.; Chillingworth, T.; Davies, R. M.; Feltwell, T.; Holroyd, S.; Jagels, K.; Karlyshev, A. V.; Moule, S.; Pallen, M. J.; Penn, C. W.; Quail, M. A.; Rajandream, M.-A.; Rutherford, K. M.; van Vliet, A. H. M.; Whitehead, S.; Barrell, B. G. *Nature* **2000**, *403*, 665. (c) Bentley, S. D.; Chater, K. F.; Cerdeño-Tárraga, A.-M.; Challis, G. L.; Thomson, N. R.; James, K. D.; Harris, D. E.; Quail, M. A.; Kieser, H.; Harper, D.; Bateman, A.; Brown, S.; Chandra, G.; Chen, C. W.; Collins, M.; Cronin, A.; Fraser, A.; Goble, A.; Hidalgo, J.; Hornsby, T.; Howarth, S.; Huang, C.-H.; Kieser, T.; Larke, L.; Murphy, L.; Oliver, K.; O'Neil, S.; Rabbinowitsch, E.; Rajandream, M.-A.; Rutherford, K.; Rutter, S.; Seeger, K.; Saunders, D.; Sharp, S.; Squares, R.; Squares, S.; Taylor, K.; Warren, T.; Wietzorek, A.; Woodward, J.; Barrell, B. G.; Hopwood, D. A. *Nature* **2002**, *417*, 141.
- (276) Hiratsuka, T.; Furihata, K.; Ishikawa, J.; Yamashita, H.; Itoh, N.; Seto, H.; Dairi, T. *Science* **2008**, *321*, 1670.
- (277) Cooper, L. E.; Fedoseyenko, D.; Abdelwahed, S. H.; Kim, S.-H.; Dairi, T.; Begley, T. P. *Biochemistry* **2013**, *52*, 4592.
- (278) (a) Seto, H.; Jinnai, Y.; Hiratsuka, T.; Fukawa, M.; Furihata, K.; Itoh, N.; Dairi, T. *J. Am. Chem. Soc.* **2008**, *130*, 5614. (b) Dairi, T. *Methods Enzymol.* **2012**, *515*, 107.
- (279) Kelley, L. A.; Sternberg, M. J. E. *Nat. Protoc.* **2009**, *4*, 363.
- (280) (a) Bagley, M. C.; Dale, J. W.; Merritt, E. A.; Xiong, X. *Chem. Rev.* **2005**, *105*, 685. (b) Li, C.; Kelly, W. L. *Nat. Prod. Rep.* **2010**, *27*, 153.
- (281) Yu, Y.; Duan, L.; Zhang, Q.; Liao, R.; Ding, Y.; Pan, H.; Wendt-Pienkowski, E.; Tang, G.; Shen, B.; Liu, W. *ACS Chem. Biol.* **2009**, *4*, 855.
- (282) Ding, Y.; Yu, Y.; Pan, H.; Guo, H.; Li, Y.; Liu, W. *Mol. BioSyst.* **2010**, *6*, 1180.
- (283) Tao, M.; Wang, L.; Wendt-Pienkowski, E.; George, N. P.; Galm, U.; Zhang, G.; Coughlin, J. M.; Shen, B. *Mol. BioSyst.* **2007**, *3*, 60.
- (284) (a) Zhang, Q.; Liu, W. *J. Biol. Chem.* **2011**, *286*, 30245. (b) Kriek, M.; Martins, F.; Challand, M. R.; Croft, A.; Roach, P. L. *Angew. Chem., Int. Ed.* **2007**, *46*, 9223.
- (285) Zhang, Q.; van der Donk, W. A.; Liu, W. *Acc. Chem. Res.* **2012**, *45*, 555.
- (286) Schwarz, S.; Werckenthin, C.; Kehrenberg, C. *Antimicrob. Agents Chemother.* **2000**, *44*, 2530.
- (287) Giessing, A. M. B.; Jensen, S. S.; Rasmussen, A.; Hansen, L. H.; Gondela, A.; Long, K.; Vester, B.; Kirpekar, F. *RNA* **2009**, *15*, 327.
- (288) Kehrenberg, C.; Ojo, K. K.; Schwarz, S. *J. Antimicrob. Chemother.* **2004**, *54*, 936.
- (289) Toh, S.-M.; Xiong, L.; Bae, T.; Mankin, A. S. *RNA* **2008**, *14*, 98.
- (290) (a) Kehrenberg, C.; Schwarz, S.; Jacobsen, L.; Hansen, L. H.; Vester, B. *Mol. Microbiol.* **2005**, *57*, 1064. (b) Long, K. S.; Poehlsgaard, J.; Kehrenberg, C.; Schwarz, S.; Vester, B. *Antimicrob. Agents Chemother.* **2006**, *50*, 2500. (c) Toh, S.-M.; Xiong, L.; Arias, C. A.; Villegas, M. V.; Lolans, K.; Quinn, J.; Mankin, A. S. *Mol. Microbiol.* **2007**, *64*, 1506.
- (291) Yan, F.; Fujimori, D. G. *Proc. Natl. Acad. Sci. U.S.A.* **2011**, *108*, 3930.
- (292) Kaminska, K. H.; Purta, E.; Hansen, L. H.; Bujnicki, J.; Vester, B.; Long, K. S. *Nucleic Acids Res.* **2010**, *38*, 1652.
- (293) McCusker, K. P.; Medzihradzky, K. F.; Shiver, A. L.; Nichols, R. J.; Yan, F.; Maltby, D. A.; Gross, C. A.; Fujimori, D. G. *J. Am. Chem. Soc.* **2012**, *134*, 18074.
- (294) Shao, X.; Grishin, N. V. *Nucleic Acids Res.* **2000**, *28*, 2643.
- (295) Boal, A. K.; Grove, T. L.; McLaughlin, M. I.; Yennawar, N. H.; Booker, S. J.; Rosenzweig, A. C. *Science* **2011**, *332*, 1089.
- (296) Booker, S. J. *Curr. Opin. Chem. Biol.* **2009**, *13*, 58.
- (297) Kelly, W. L.; Pan, L.; Li, C. *J. Am. Chem. Soc.* **2009**, *131*, 4327.
- (298) Dutcher, J. D.; Vandeputte, J. *Antibiot. Annu.* **1955**, *3*, 560.
- (299) (a) Kwok, J. M.-M.; Peck, B.; Monteiro, L. J.; Schwenen, H. D. C.; Millour, J.; Coomes, R. C.; Myatt, S. S.; Lam, E. W.-F. *Mol. Cancer Res.* **2010**, *8*, 24. (b) Hegde, N. S.; Sanders, D. A.; Rodriguez, R.; Balasubramanian, S. *Nat. Chem.* **2011**, *3*, 725.
- (300) (a) Hong, W.; Yan, L. *J. Gen. Appl. Microbiol.* **2012**, *58*, 349. (b) Kim, J. Y.; Suh, J. W.; Kang, S. H.; Phan, T. H.; Park, S. H.; Kwon, H. J. *Biochem. Biophys. Res. Commun.* **2008**, *372*, 730.
- (301) (a) Mills, J. S.; Werner, A. E. *A. J. Chem. Soc.* **1955**, 3132. (b) *Brock Biology of Microorganisms*, 11th ed.; Madigan, M., Martinko, J., Eds.; Benjamin Cummings: San Francisco, CA, 2005.
- (302) Welander, P. V.; Coleman, M. L.; Sessions, A. L.; Summons, R. E.; Newman, D. K. *Proc. Natl. Acad. Sci. U.S.A.* **2010**, *107*, 8537.
- (303) (a) Rashby, S. E.; Sessions, A. L.; Summons, R. E.; Newman, D. K. *Proc. Natl. Acad. Sci. U.S.A.* **2007**, *104*, 15099. (b) Zundel, M.; Rohmer, M. *FEBS J.* **2005**, *150*, 23.
- (304) Morris, R. P.; Leeds, J. A.; Naegeli, H. U.; Oberer, L.; Memmert, K.; Weber, E.; LaMarche, M. J.; Parker, C. N.; Burrer, N.; Esterow, S.; Hein, A. E.; Schmitt, E. K.; Krastel, P. *J. Am. Chem. Soc.* **2009**, *131*, 5946.
- (305) (a) Du, L. C.; Sanchez, C.; Chen, M.; Edwards, D. J.; Shen, B. *Chem. Biol.* **2000**, *7*, 623. (b) Tao, M. F.; Wang, L.; Wendt-Pienkowski, E.; Zhang, N. N.; Yang, D.; Galm, U.; Coughlin, J. M.; Xu, Z. N.; Shen, B. *Mol. BioSyst.* **2010**, *6*, 349. (c) Galm, U.; Wendt-Pienkowski, E.; Wang, L. Y.; George, N. P.; Oh, T. J.; Yi, F.; Tao, M. F.; Coughlin, J. M.; Shen, B. *Mol. BioSyst.* **2009**, *5*, 77.
- (306) (a) Mocek, U.; Zeng, Z. P.; Ohagan, D.; Zhou, P.; Fan, L. D. G.; Beale, J. M.; Floss, H. G. *J. Am. Chem. Soc.* **1993**, *115*, 7992. (b) Mocek, U.; Knaggs, A. R.; Tsuchiya, R.; Nguyen, T.; Beale, J. M.; Floss, H. G. *J. Am. Chem. Soc.* **1993**, *115*, 7557. (c) Houck, D. R.; Chen, L. C.; Keller, P. J.; Beale, J. M.; Floss, H. G. *J. Am. Chem. Soc.* **1988**, *110*, 5800.
- (307) Grosjean, H.; Nicoghosian, K.; Haumont, E.; Soll, D.; Cedergren, R. *Nucleic Acids Res.* **1985**, *13*, 5697.
- (308) (a) Diaz, I.; Ehrenberg, M. *J. Mol. Biol.* **1991**, *222*, 1161. (b) Gustilo, E. M.; Vendeix, F. A.; Agris, P. F. *Curr. Opin. Microbiol.* **2008**, *11*, 134. (c) Kaczanowska, M.; Ryden-Aulin, M. *Microbiol. Mol. Biol. Rev.* **2007**, *71*, 477. (d) Kurland, C. G. *The Ribosome: Structure, Function, and Evolution*; American Society for Microbiology: Washington, DC, 1990.
- (309) Ozaki, M.; Mizushima, S.; Nomura, M. *Nature* **1969**, *222*, 333.
- (310) (a) Leung, H. C.; Chen, Y.; Winkler, M. E. *J. Biol. Chem.* **1997**, *272*, 13073. (b) Moore, J. A.; Poulter, C. D. *Biochemistry* **1997**, *36*, 604. (c) Soderberg, T.; Poulter, C. D. *Biochemistry* **2000**, *39*, 6546.
- (311) (a) Agris, P. F.; Armstrong, D. J.; Schafer, K. P.; Soll, D. *Nucleic Acids Res.* **1975**, *2*, 691. (b) Gefter, M. L. *Biochem. Biophys. Res. Commun.* **1969**, *36*, 435. (c) Rosenberg, A. H.; Gefter, M. L. *J. Mol. Biol.* **1969**, *46*, 581.
- (312) Esberg, B.; Leung, H. C.; Tsui, H. C.; Bjork, G. R.; Winkler, M. E. *J. Bacteriol.* **1999**, *181*, 7256.
- (313) (a) Anton, B. P.; Saleh, L.; Benner, J. S.; Raleigh, E. A.; Kasif, S.; Roberts, R. J. *Proc. Natl. Acad. Sci. U.S.A.* **2008**, *105*, 1826. (b) Kowalak, J. A.; Walsh, K. A. *Protein Sci.* **1996**, *5*, 1625.
- (314) Booker, S. J.; Cicchillo, R. M.; Grove, T. L. *Curr. Opin. Chem. Biol.* **2007**, *11*, 543.
- (315) Kaminska, K. H.; Baraniak, U.; Boniecki, M.; Nowaczyk, K.; Czerwoniec, A.; Bujnicki, J. M. *Proteins* **2008**, *70*, 1.
- (316) Lee, T. T.; Agarwalla, S.; Stroud, R. M. *Structure* **2004**, *12*, 397.
- (317) Anantharaman, V.; Koonin, E. V.; Aravind, L. *FEMS Microbiol. Lett.* **2001**, *197*, 215.
- (318) Forouhar, F.; Arragain, S.; Atta, M.; Gambarelli, S.; Mouesa, J. M.; Hussain, M.; Xiao, R.; Kieffer-Jaquinod, S.; Seetharaman, J.; Acton, T. B.; Montelione, G. T.; Mulliez, E.; Hunt, J. F.; Fontecave, M. *Nat. Chem. Biol.* **2013**, *9*, 333.
- (319) El Yacoubi, B.; Lyons, B.; Cruz, Y.; Reddy, R.; Nordin, B.; Agnelli, F.; Williamson, J. R.; Schimmel, P.; Swairjo, M. A.; de Crecy-Lagard, V. *Nucleic Acids Res.* **2009**, *37*, 2894.
- (320) Anton, B. P.; Russell, S. P.; Vertrees, J.; Kasif, S.; Raleigh, E. A.; Limbach, P. A.; Roberts, R. J. *Nucleic Acids Res.* **2010**, *38*, 6195.

- (321) Wei, F.-Y.; Suzuki, T.; Watanabe, S.; Kimura, S.; Kaitksuka, T.; Fujimura, A.; Matsui, H.; Atta, M.; Michiue, H.; Fontecave, M.; Yamagata, K.; Suzuki, T.; Tomizawa, K. *J. Clin. Invest.* **2011**, *121*, 3598.
- (322) Jenner, L.; Demeshkina, N.; Yusupova, G.; Yusupov, M. *Nat. Struct. Mol. Biol.* **2010**, *17*, 1072.
- (323) Watanabe, S.; Wei, F. Y.; Tomizawa, K. *Drug Discovery Today: Dis. Models* **2013**, *10*, e65.
- (324) Parenti, G.; Meroni, G.; Ballabio, A. *Curr. Opin. Genet. Dev.* **1997**, *7*, 386.
- (325) (a) Schmidt, B.; Selmer, T.; Ingendoh, A.; von Figura, K. *Cell* **1995**, *82*, 271. (b) Bojarova, P.; Williams, S. J. *Curr. Opin. Chem. Biol.* **2008**, *12*, 573. (c) Berteau, O.; Guillot, A.; Benjdia, A.; Rabot, S. J. *Biol. Chem.* **2006**, *281*, 22464. (d) Ghosh, D. *Cell. Mol. Life Sci.* **2007**, *64*, 2013. (e) Dierks, T.; Dickmanns, A.; Preusser-Kunze, A.; Schmidt, B.; Mariappan, M.; von Figura, K.; Ficner, R.; Rudolph, M. G. *Cell* **2005**, *121*, S41.
- (326) (a) Marquardt, C.; Fang, Q.; Will, E.; Peng, J.; von Figura, K.; Dierks, T. *J. Biol. Chem.* **2003**, *278*, 2212. (b) Szameit, C.; Miech, C.; Balleininger, M.; Schmidt, B.; von Figura, K.; Dierks, T. *J. Biol. Chem.* **1999**, *274*, 15375.
- (327) Fang, Q.; Peng, J.; Dierks, T. *J. Biol. Chem.* **2004**, *279*, 14570.
- (328) Goldman, P. J.; Grove, T. L.; Sites, L. A.; McLaughlin, M. I.; Booker, S. J.; Drennan, C. L. *Proc. Natl. Acad. Sci. U.S.A.* **2013**, *110*, 8519.
- (329) (a) Toyama, H.; Chistoserdova, L.; Lidstrom, M. E. *Microbiology* **1997**, *143*, 595. (b) Velterop, J. S.; Sellink, E.; Meulenbergh, J. J. M.; David, S.; Bulder, I.; Postma, P. W. *J. Bacteriol.* **1995**, *177*, 5088.
- (330) (a) Houck, D. R.; Hanners, J. L.; Unkefer, C. J. *J. Am. Chem. Soc.* **1988**, *110*, 6920. (b) Houck, D. R.; Hanners, J. L.; Unkefer, C. J. *J. Am. Chem. Soc.* **1991**, *113*, 3162.
- (331) (a) Magnusson, O. T.; Toyama, H.; Saeki, M.; Schwarzenbacher, R.; Klinman, J. P. *J. Am. Chem. Soc.* **2004**, *126*, 5342. (b) Toyama, H.; Fukumoto, H.; Saeki, M.; Matsushita, K.; Adachi, O.; Lidstrom, M. E. *Biochem. Biophys. Res. Commun.* **2002**, *299*, 268.
- (332) Meulenbergh, J. J. M.; Sellink, E.; Riegman, N. H.; Postma, P. W. *Mol. Gen. Genet.* **1992**, *232*, 284.
- (333) Noma, A.; Kirino, Y.; Ikeuchi, Y.; Suzuki, T. *EMBO J.* **2006**, *25*, 2142.
- (334) Waas, W. F.; Crécy-Lagard, V. d.; Schimmel, P. *J. Biol. Chem.* **2005**, *280*, 37616.
- (335) Young, A. P.; Bandarian, V. *Biochemistry* **2011**, *50*, 10573.
- (336) Suzuki, Y.; Noma, A.; Suzuki, T.; Senda, M.; Senda, T.; Ishitani, R.; Nureki, O. *J. Mol. Biol.* **2007**, *372*, 1204.
- (337) Young, A. P.; Bandarian, V. *Curr. Opin. Chem. Biol.* **2013**, *17*, 613.
- (338) Arnison, P. G.; et al. *Nat. Prod. Rep.* **2013**, *30*, 108.
- (339) (a) Babasaki, K.; Takao, T.; Shimonishi, Y.; Kurahashi, K. J. *Biochem.* **1985**, *98*, 585. (b) Shelburne, C. E.; An, F. Y.; Dhople, V.; Ramamoorthy, A.; Lopatin, D. E.; Lantz, M. S. *J. Antimicrob. Chemother.* **2007**, *59*, 297. (c) Sutyak, K. E.; Anderson, R. A.; Dover, S. E.; Feathergill, K. A.; Aroutcheva, A. A.; Faro, S.; Chikindas, M. L. *Infect. Dis. Obstet. Gynecol.* **2008**, *S40758*. (d) Silkin, L.; Hamza, S.; Kaufman, S.; Cobb, S. L.; Vedera, J. C. *Bior. Med. Chem. Lett.* **2008**, *18*, 3103.
- (340) (a) Kawulka, K.; Sprules, T.; McKay, R. T.; Mercier, P.; Diaper, C. M.; Zuber, P.; Vedera, J. C. *J. Am. Chem. Soc.* **2003**, *125*, 4726. (b) Kawulka, K.; Sprules, T.; Diaper, C. M.; Whittal, R. M.; McKay, R. T.; Mercier, P.; Zuber, P.; Vedera, J. C. *Biochemistry* **2004**, *43*, 3385.
- (341) (a) Zheng, G.; Yan, L. Z.; Vedera, J. C.; Zuber, P. *J. Bacteriol.* **1999**, *181*, 7346. (b) Zheng, G.; Hehn, R.; Zuber, P. *J. Bacteriol.* **2000**, *182*, 3266.
- (342) Rea, M. C.; Sit, C. S.; Clayton, E.; O'Connor, P. M.; Whittal, R. M.; Zheng, J.; Vedera, J. C.; Ross, R. P.; Hill, C. *Proc. Natl. Acad. Sci. U.S.A.* **2010**, *107*, 9352.
- (343) Sit, C. S.; McKay, R. T.; Hill, C.; Ross, R. P.; Vedera, J. C. *J. Am. Chem. Soc.* **2011**, *133*, 7680.
- (344) Murphy, K.; O'Sullivan, O.; Rea, M. C.; Cotter, P. D.; Ross, R. P.; Hill, C. *PLoS One* **2011**, *6*, e20852.
- (345) Sit, C. S.; van Belkum, M. J.; McKay, R. T.; Worobo, R. W.; Vedera, J. C. *Angew. Chem., Int. Ed.* **2011**, *50*, 8718.
- (346) Lee, H.; Churey, J. J.; Worobo, R. W. *FEMS Microbiol. Lett.* **2009**, *299*, 205.
- (347) González-Pastor, J. E.; Hobbs, E. C.; Losick, R. *Science* **2003**, *301*, 510.
- (348) Liu, W.-T.; Yang, Y.-L.; Xu, Y.; Lamsa, A.; Haste, N. M.; Yang, J. Y.; Ng, J.; Gonzalez, D.; Ellermeier, C. D.; Straight, P. D.; Pevzner, P. A.; Pogliano, J.; Nizet, V.; Pogliano, K.; Dorrestein, P. C. *Proc. Natl. Acad. Sci. U.S.A.* **2010**, *107*, 16286.
- (349) Settembre, E. C.; Dorrestein, P. C.; Park, J. H.; Augustine, A. M.; Begley, T. P.; Ealick, S. E. *Biochemistry* **2003**, *42*, 2971.
- (350) Gralnick, J.; Webb, E.; Beck, B.; Downs, D. *J. Bacteriol.* **2000**, *182*, 5180.
- (351) Martinez-Gomez, N. C.; Robers, M.; Downs, D. M. *J. Biol. Chem.* **2004**, *279*, 40505.
- (352) Leonardi, R.; Roach, P. L. *J. Biol. Chem.* **2004**, *279*, 17054.
- (353) (a) Munakata, N. *Mol. Gen. Genet.* **1969**, *104*, 258. (b) Munakata, N.; Rupert, C. S. *J. Bacteriol.* **1972**, *111*, 192. (c) Munakata, N.; Rupert, C. S. *Mol. Gen. Genet.* **1974**, *130*, 239. (d) Wang, T. C.; Rupert, C. S. *Photochem. Photobiol.* **1977**, *25*, 123. (354) Sancar, A. *Chem. Rev.* **2003**, *103*, 2203.
- (355) Fajardo-Cavazos, P.; Salazar, C.; Nicholson, W. L. *J. Bacteriol.* **1993**, *175*, 1735.
- (356) Slieman, T. A.; Rebeil, R.; Nicholson, W. L. *J. Bacteriol.* **2000**, *182*, 6412.
- (357) Nicholson, W. L.; Chooback, L.; Fajardo-Cavazos, P. *Mol. Gen. Genet.* **1997**, *255*, 587.
- (358) Cheek, J.; Broderick, J. B. *J. Am. Chem. Soc.* **2002**, *124*, 2860.
- (359) (a) Setlow, B.; Setlow, P. *Proc. Natl. Acad. Sci. U.S.A.* **1987**, *84*, 421. (b) Nicholson, W. L.; Setlow, B.; Setlow, P. *Proc. Natl. Acad. Sci. U.S.A.* **1991**, *88*, 8288. (c) Douki, T.; Cadet, J. *Photochem. Photobiol.* **2003**, *2*, 433. (d) Douki, T.; Setlow, B.; Setlow, P. *Photochem. Photobiol.* **2005**, *81*, 163. (e) Sun, Y.; Palasingam, K.; Nicholson, W. L. *Anal. Biochem.* **1994**, *221*, 61.
- (360) (a) Setlow, P. *Annu. Rev. Microbiol.* **1988**, *42*, 319. (b) Nicholson, W. L.; Setlow, B.; Setlow, P. *J. Bacteriol.* **1990**, *172*, 6900. (c) Mohr, S. C.; Sokolov, N. V. H. A.; He, C.; Setlow, P. *Proc. Natl. Acad. Sci. U.S.A.* **1991**, *88*, 77. (d) Setlow, B.; Sun, D.; Setlow, P. *J. Bacteriol.* **1992**, *174*, 2312. (e) Lee, K. S.; Bumbaca, D.; Kosman, J.; Setlow, P.; Jedrzejas, M. J. *Proc. Natl. Acad. Sci. U.S.A.* **2008**, *105*, 2806.
- (361) Kim, S. J.; Lester, C.; Begley, T. P. *J. Org. Chem.* **1995**, *60*, 6256.
- (362) (a) Friedel, M. G.; Berteau, O.; Pieck, J. C.; Atta, M.; Ollagnier-de-Choudens, S.; Fontecave, M.; Carell, T. *Chem. Commun.* **2006**, *445*. (b) Friedel, M. G.; Pieck, J. C.; Klages, J.; Dauth, C.; Kessler, H.; Carell, T. *Chem.—Eur. J.* **2006**, *12*, 6081.
- (363) Nicewonger, R.; Begley, T. P. *Tetrahedron Lett.* **1997**, *38*, 935.
- (364) Mantel, C.; Chandor, A.; Gasparutto, D.; Douki, T.; Atta, M.; Fontecave, M.; Bayle, P.-A.; Mouesa, J.-M.; Bardet, M. *J. Am. Chem. Soc.* **2008**, *130*, 16978.
- (365) Heil, K.; Kneuttinger, A. C.; Schneider, S.; Lischke, U.; Carell, T. *Chem.—Eur. J.* **2011**, *17*, 9651.
- (366) Lin, G.; Chen, C.-H.; Pink, M.; Pu, J.; Li, L. *Chem.—Eur. J.* **2011**, *17*, 9658.
- (367) Mehl, R. A.; Begley, T. P. *Org. Lett.* **1999**, *1*, 1065.
- (368) Chandor-Proust, A.; Berteau, O.; Douki, T.; Gasparutto, D.; Ollagnier-de-Choudens, S.; Fontecave, M.; Atta, M. *J. Biol. Chem.* **2008**, *283*, 36361.
- (369) Benjdia, A.; Heil, K.; Barends, T. R. M.; Carell, T.; Schlichting, I. *Nucleic Acids Res.* **2012**, *40*, 9308.
- (370) (a) Guo, J.-D.; Luo, Y.; Himo, F. *J. Phys. Chem. B* **2003**, *107*, 11188. (b) Himo, F. *Biochim. Biophys. Acta* **2005**, *1707*, 24.
- (371) Fajardo-Cavazos, P.; Rebeil, R.; Nicholson, W. L. *Curr. Microbiol.* **2005**, *51*, 331.
- (372) Kneuttinger, A. C.; Heil, K.; Kashiwazaki, G.; Carell, T. *Chem. Commun.* **2012**, *49*, 722.

- (373) Thibodeaux, C. J.; Melancon, C. E.; Liu, H.-w. *Nature* **2007**, 446, 1008.
- (374) He, X. M.; Agnihotri, G.; Liu, H.-w. *Chem. Rev.* **2000**, 100, 4615.
- (375) (a) Zhao, L. S.; Que, N. L. S.; Xue, Y. Q.; Sherman, D. H.; Liu, H.-w. *J. Am. Chem. Soc.* **1998**, 120, 12159. (b) Zhao, L.; Borisova, S.; Yeung, S.-M.; Liu, H.-w. *J. Am. Chem. Soc.* **2001**, 123, 7909.
- (376) Xue, Y.; Zhao, L.; Liu, H.-w.; Sherman, D. H. *Proc. Natl. Acad. Sci. U.S.A.* **1998**, 95, 12111.
- (377) Ruszczycky, M. W.; Choi, S.-h.; Liu, H.-w. *J. Am. Chem. Soc.* **2010**, 132, 2359.
- (378) Ruszczycky, M. W.; Choi, S.-h.; Mansoorabadi, S. O.; Liu, H.-w. *J. Am. Chem. Soc.* **2011**, 133, 7292.
- (379) Ruszczycky, M. W.; Ogawara, Y.; Liu, H.-w. *Biochim. Biophys. Acta, Proteins Proteomics* **2012**, 1824, 1231.
- (380) Ruszczycky, M. W.; Choi, S.-h.; Liu, H.-w. *Proc. Natl. Acad. Sci. U.S.A.* **2013**, 110, 2088.
- (381) Metcalf, W. W.; Wanner, B. L. *Gene* **1993**, 129, 27.
- (382) Parker, G. F.; Higgins, T. P.; Hawkes, T.; Robson, R. L. *J. Bacteriol.* **1999**, 181, 389.
- (383) Chinenov, Y. *Trends Biol. Sci.* **2002**, 27, 115.
- (384) Stilger, K. L.; Sullivan, W. J. *J. Biol. Chem.* **2013**, 288, 25318.
- (385) (a) Okada, Y.; Yamagata, K.; Hong, K.; Wakayama, T.; Zhang, Y. *Nature* **2010**, 463, 554. (b) Wu, S. C.; Zhang, Y. *Nat. Rev. Mol. Cell Biol.* **2010**, 11, 607.
- (386) Yamaguchi, H.; Yamamoto, C.; Tanaka, N. *J. Biochem.* **1965**, 57, 667.
- (387) Heinemann, I. U.; Jahn, M.; Jahn, D. *Arch. Biochem. Biophys.* **2008**, 474, 238.
- (388) (a) Yoshinaga, T.; Sano, S. *J. Biol. Chem.* **1980**, 255, 4722. (b) Medlock, A. E.; Dailey, H. A. *J. Biol. Chem.* **1996**, 271, 32507. (c) Labbe, P. *Methods Enzymol.* **1997**, 281, 367.
- (389) (a) Tait, G. H. *Biochem. Biophys. Res. Commun.* **1969**, 37, 116. (b) Sehra, J. S.; Jordan, P. M.; Akhtar, M. *Biochem. J.* **1983**, 209, 709. (c) Tait, G. H. *Biochem. J.* **1972**, 128, 1159. (d) Keithly, J. H.; Nadler, K. D. *J. Bacteriol.* **1983**, 154, 838. (e) Poulsom, R.; Polglase, W. *J. Biol. Chem.* **1974**, 249, 6367.
- (390) Layer, G.; Pierik, A. J.; Trost, M.; Rigby, S. E.; Leech, H. K.; Grage, K.; Breckau, D.; Astner, I.; Jänsch, L.; Heathcote, P.; Warren, M. J.; Heinz, D. W.; Jahn, D. *J. Biol. Chem.* **2006**, 15727.
- (391) Jackson, A. H.; Lash, T. D.; Ryder, D. J.; Smith, S. G. *Intl. J. Biochem.* **1980**, 12, 775.
- (392) Rand, K.; Noll, C.; Schiebel, H. M.; Kemken, D.; Dülcks, T.; Kalesse, M.; Heinz, D. W.; Layer, G. *Biol. Chem.* **2010**, 391, 55.
- (393) (a) Rinaldo, S.; Cutruzzola, F. In *Biology of the Nitrogen Cycle*; Bothe, E., Ferguson, S. J., Newton, W. E., Eds.; Elsevier: Amsterdam, 2007. (b) Zajicek, R. S.; Cartron, M. L.; Ferguson, S. J. *Biochemistry* **2006**, 45, 11208. (c) Zumft, W. G. *Microbiol. Mol. Biol. Rev.* **1997**, 61, 533.
- (394) Yap-Bondoc, F.; Bondoc, L. L.; Timkovich, R.; Baker, D. C.; Hebbler, A. *J. Biol. Chem.* **1990**, 265, 13498.
- (395) (a) Glockner, A. B.; Zumft, W. G. *Biochim. Biophys. Acta, Bioenerg.* **1996**, 1277, 6. (b) Kawasaki, S.; Arai, H.; Kodama, T. *J. Bacteriol.* **1997**, 179, 235.
- (396) (a) Storbeck, S.; Rolfs, S.; Raux-Deery, E.; Warren, M. J. *Archaea* **2010**, 175050. (b) Bali, S.; Lawrence, A. D.; Lobo, S. A.; Saraiva, L. M.; Golding, B. T.; Palmer, D. J.; Howard, M. J.; Ferguson, S. J.; Warren, M. J. *Proc. Natl. Acad. Sci. U.S.A.* **2011**, 108, 18260.
- (397) Bali, S.; Warren, M. J.; Ferguson, S. J. *FEBS J.* **2010**, 277, 4944.
- (398) Bryant, D. A.; Frigaard, N. U. *Trends Microbiol.* **2006**, 14, 488.
- (399) Chew, A. G. M.; Bryant, D. A. *Annu. Rev. Microbiol.* **2007**, 61, 113.
- (400) Beale, S. I.; Weinstein, J. D. In *Biosynthesis of Tetrapyrroles*; Jordan, P. M., Ed.; Elsevier: Amsterdam, 1991.
- (401) (a) Bollivar, D. W.; Suzuki, J. Y.; Beatty, J. T.; Dobrowolski, J. M.; Bauer, C. E. *J. Mol. Biol.* **1994**, 237, 622. (b) Bollivar, D. W. *Photosynth. Res.* **2006**, 90, 173.
- (402) (a) Porra, R. J.; Urzinger, M.; Winkler, J.; Bubenzier, C.; Scheer, H. *Eur. J. Biochem.* **1998**, 257, 185. (b) Porra, R. J.; Schafer, W.; Katheder, I.; Scheer, H. *FEBS Lett.* **1995**, 371, 21. (c) Ouchane, S.; Steunou, A. S.; Picaud, M.; Astier, C. *J. Biol. Chem.* **2004**, 279, 6385.
- (403) Yang, Z. M.; Bauer, C. E. *J. Bacteriol.* **1990**, 172, 5001.
- (404) Alberti, M.; Burke, D. H.; Hearst, J. E. In *Anoxygenic Photosynthetic Bacteria*; Blankenship, R. E., Madigan, M. T., Bauer, C. E., Eds.; Kluwer: Dordrecht, Netherlands, 1995; Vol. 2.
- (405) Gough, S. P.; Petersen, B. O.; Duus, J. O. *Proc. Natl. Acad. Sci. U.S.A.* **2000**, 97, 6908.
- (406) van der Donk, W. A. *J. Org. Chem.* **2006**, 71, 9561.
- (407) (a) Ellsworth, R. K.; Aronoff, S. *Arch. Biochem. Biophys.* **1969**, 130, 374. (b) Ellsworth, R. K.; Aronoff, S. *Arch. Biochem. Biophys.* **1968**, 125, 269.
- (408) Montano, G. A.; Bowen, B. P.; LaBelle, J. T.; Woodbury, N. W.; Pizziconi, V. B.; Blankenship, R. E. *Biophys. J.* **2003**, 85, 2560.
- (409) Chew, A. G. M.; Frigaard, N.-U.; Bryant, D. A. *J. Bacteriol.* **2007**, 189, 6176.
- (410) Huster, M.; Smith, K. *Biochemistry* **1990**, 29, 4348.
- (411) (a) Shepard, E. M.; Boyd, E. S.; Broderick, J. B.; Peters, J. W. *Curr. Opin. Chem. Biol.* **2011**, 15, 319. (b) Peters, J. W.; Broderick, J. B. *Annu. Rev. Biochem.* **2012**, 81, 429.
- (412) (a) Spatzal, T.; Aksoyoglu, M.; Zhang, L.; Andrade, S. L. A.; Schleicher, E.; Weber, S.; Rees, D. C.; Einsle, O. *Science* **2011**, 334, 940. (b) Lancaster, K. M.; Roemelt, M.; Ettenhuber, P.; Hu, Y.; Ribbe, M. W.; Neese, F.; Bergmann, U.; DeBeer, S. *Science* **2011**, 334, 974.
- (413) Igarashi, R. Y.; Seefeldt, L. C. *Crit. Rev. Biochem. Mol. Biol.* **2003**, 38, 351.
- (414) Seefeldt, L. C.; Hoffman, B. M.; Dean, D. R. *Curr. Opin. Chem. Biol.* **2012**, 16, 19.
- (415) (a) Hu, Y.; Fay, A. W.; Lee, C. C.; Yoshizawa, J.; Ribbe, M. W. *Biochemistry* **2008**, 47, 3973. (b) Dos Santos, P. C.; Dean, D. R.; Hu, Y.; Ribbe, M. W. *Chem. Rev.* **2004**, 104, 1159. (c) Rubio, L. M.; Ludden, P. W. *J. Bacteriol.* **2005**, 187, 405.
- (416) (a) Tal, S.; Chun, T. W.; Gavini, N.; Burgess, B. K. *J. Biol. Chem.* **1991**, 266, 10654. (b) Schmid, B.; Ribbe, M. W.; Einsle, O.; Yoshida, M.; Thomas, L. M.; Dean, D. R.; Rees, D. C.; Burgess, B. K. *Science* **2002**, 296, 352.
- (417) Allen, R. M.; Chatterjee, R.; Ludden, P. W.; Shah, V. K. *J. Biol. Chem.* **1995**, 270, 26890.
- (418) Curatti, L.; Hernandez, J. A.; Igarashi, R. Y.; Soboh, B.; Zhao, D.; Rubio, L. M. *Proc. Natl. Acad. Sci. U.S.A.* **2007**, 104, 17626.
- (419) (a) Hernandez, J. A.; Igarashi, R. Y.; Soboh, B.; Curatti, L.; Dean, D. R.; Ludden, P. W.; Rubio, L. M. *Mol. Microbiol.* **2007**, 63, 177. (b) Rubio, L. M.; Ludden, P. W. *Annu. Rev. Microbiol.* **2008**, 62, 93. (c) Boyd, E. S.; Anbar, A. D.; Miller, S.; Hamilton, T. L.; Lavin, M.; Peters, J. W. *Geobiology* **2011**, 9, 221.
- (420) George, S. J.; Igarashi, R. Y.; Xiao, Y.; Hernandez, J. A.; Demuez, M.; Zhao, D.; Yoda, Y.; Ludden, P. W.; Rubio, L. M.; Cramer, S. P. *J. Am. Chem. Soc.* **2008**, 130, 5673.
- (421) Schwarz, G.; Mendel, R. R.; Ribbe, M. W. *Nature* **2009**, 460, 839.
- (422) (a) Hu, Y.; Fay, A. W.; Ribbe, M. W. *Proc. Natl. Acad. Sci. U.S.A.* **2005**, 102, 3236. (b) Corbett, M. C.; Hu, Y.; Fay, A. W.; Ribbe, M. W.; Hedman, B.; Hodgson, K. O. *Proc. Natl. Acad. Sci. U.S.A.* **2006**, 103, 1238. (c) Fay, A. W.; Blank, M. A.; Lee, C. C.; Hu, Y.; Hodgson, K. O.; Hedman, B.; Ribbe, M. W. *Angew. Chem., Int. Ed.* **2011**, 50, 7787. (d) Kaiser, J. T.; Hu, Y.; Wiig, J. A.; Rees, D. C.; Ribbe, M. W. *Science* **2011**, 331, 91.
- (423) Lancaster, K. M.; Hu, Y.; Bergmann, U.; Ribbe, M. W.; DeBeer, S. *J. Am. Chem. Soc.* **2013**, 135, 610.
- (424) Wiig, J. A.; Hu, Y.; Lee, C. C.; Ribbe, M. W. *Science* **2012**, 337, 1672.
- (425) Wiig, J. A.; Lee, C. C.; Hu, Y.; Ribbe, M. W. *J. Am. Chem. Soc.* **2013**, 135, 4982.
- (426) (a) Peters, J. W. *Curr. Opin. Struct. Biol.* **1999**, 9, 670. (b) Adams, M. W. W. *Biochim. Biophys. Acta* **1990**, 1020, 115.
- (427) (a) Böck, A.; King, P. W.; Blokesch, M.; Posewitz, M. C. In *Advances in Microbial Physiology*; Poole, R. K., Ed.; Elsevier/Academic Press: New York, 2006; Vol. 51. (b) Swanson, K. D.; Duffus, B. R.

- Beard, T. E.; Peters, J. W.; Broderick, J. B. *Eur. J. Inorg. Chem.* **2011**, 935.
- (428) Peters, J. W.; Lanzilotta, W. N.; Lemon, B. J.; Seefeldt, L. C. *Science* **1998**, 282, 1853.
- (429) Nicolet, Y.; Piras, C.; Legrand, P.; Hatchikian, C. E.; Fontecilla-Camps, J. C. *Structure* **1999**, 7, 13.
- (430) (a) Nicolet, Y.; de Lacey, A. L.; Vernède, X.; Fernandez, V. M.; Hatchikian, E. C.; Fontecilla-Camps, J. C. *J. Am. Chem. Soc.* **2001**, 123, 1596. (b) Chen, Z.; Lemon, B. J.; Huang, S.; Swartz, D. J.; Peters, J. W.; Bagley, K. A. *Biochemistry* **2002**, 41, 2036.
- (431) Kubas, G. J. *Chem. Rev.* **2007**, 107, 4152.
- (432) (a) Silakov, A.; Reijerse, E. J.; Albracht, S. P.; Hatchikian, E. C.; Lubitz, W. *J. Am. Chem. Soc.* **2007**, 129, 11447. (b) Pandey, A. S.; Harris, T. V.; Giles, L. J.; Peters, J. W.; Szilagyi, R. K. *J. Am. Chem. Soc.* **2008**, 130, 4533. (c) Kuchenreuther, J. M.; Guo, Y.; Wang, H.; Myers, W. K.; George, S. J.; Boyke, C. A.; Yoda, Y.; Alp, E. E.; Zhao, J.; Britt, R. D.; Swartz, J. R.; Cramer, S. P. *Biochemistry* **2013**, 52, 818.
- (433) Lemon, B. J.; Peters, J. W. *Biochemistry* **1999**, 38, 12969.
- (434) (a) Voordouw, G.; Hagen, W. R.; Kruse-Wolters, K. M.; van Berkelaars, A.; Veeger, C. *Eur. J. Biochem.* **1987**, 162, 31. (b) Atta, M.; Meyer, J. *Biochim. Biophys. Acta, Protein Struct.* **2000**, 1476, 368.
- (435) (a) Posewitz, M. C.; King, P. W.; Smolinski, S. L.; Zhang, L.; Seibert, M.; Ghirardi, M. L. *J. Biol. Chem.* **2004**, 279, 25711. (b) King, P. W.; Posewitz, M. C.; Ghirardi, M. L.; Seibert, M. *J. Bacteriol.* **2006**, 188, 2163.
- (436) McGlynn, S. E.; Ruebush, S. S.; Naumov, A.; Nagy, L. E.; Dubini, A.; King, P. W.; Broderick, J. B.; Posewitz, M. C.; Peters, J. W. *J. Biol. Inorg. Chem.* **2007**, 12, 443.
- (437) Brazzolotto, X.; Rubach, J. K.; Gaillard, J.; Gambarelli, S.; Atta, M.; Fontecave, M. *J. Biol. Chem.* **2006**, 281, 769.
- (438) Peters, J. W.; Szilagyi, R. K.; Naumov, A.; Douglas, T. *FEBS Lett.* **2006**, 580, 363.
- (439) Mulder, D. W.; Shepard, E. M.; Meuser, J. E.; Joshi, N.; King, P. W.; Posewitz, M. C.; Broderick, J. B.; Peters, J. W. *Structure* **2011**, 19, 1038.
- (440) (a) Florin, L.; Tsokoglou, A.; Happe, T. *J. Biol. Chem.* **2001**, 276, 6125. (b) Happe, T.; Kaminski, A. *Eur. J. Biochem.* **2002**, 269, 1022. (c) Forestier, M.; King, P.; Zhang, L.; Posewitz, M.; Schwarzer, S.; Happe, T.; Ghirardi, M.; Seibert, M. *Eur. J. Biochem.* **2003**, 270, 2750.
- (441) (a) Kamp, C.; Silakov, A.; Winkler, M.; Reijerse, E. J.; Lubitz, W.; Happe, T. *Biochim. Biophys. Acta, Bioenerg.* **2008**, 1777, 410. (b) Mulder, D. W.; Ortillo, D. O.; Gardenghi, D. J.; Naumov, A.; Ruebush, S. S.; Szilagyi, R. K.; Huynh, B. H.; Broderick, J. B.; Peters, J. W. *Biochemistry* **2009**, 48, 6240. (c) Silakov, A.; Kamp, C.; Reijerse, E.; Happe, T.; Lubitz, W. *Biochemistry* **2009**, 48, 7780. (d) Stripp, S.; Sanganas, O.; Happe, T.; Haumann, M. *Biochemistry* **2009**, 48, 5042. (e) Mulder, D. W.; Boyd, E. S.; Sarma, R.; Lange, R. K.; Endrizzi, J. A.; Broderick, J. B.; Peters, J. W. *Nature* **2010**, 465, 248.
- (442) McGlynn, S. E.; Shepard, E. M.; Winslow, M. A.; Naumov, A. V.; Duschene, K. S.; Posewitz, M. C.; Broderick, W. E.; Broderick, J. B.; Peters, J. W. *FEBS Lett.* **2008**, 582, 2183.
- (443) (a) Shepard, E. M.; McGlynn, S. E.; Bueling, A. L.; Grady-Smith, C.; George, S. J.; Winslow, M. A.; Cramer, S. P.; Peters, J. W.; Broderick, J. B. *Proc. Natl. Acad. Sci. U.S.A.* **2010**, 107, 10448. (b) Czech, I.; Silakov, A.; Lubitz, W.; Happe, T. *FEBS Lett.* **2010**, 584, 638. (c) Czech, I.; Stripp, S.; Sanganas, O.; Leidel, N.; Happe, T.; Haumann, M. *FEBS Lett.* **2011**, 585, 225. (d) Joshi, N.; Shepard, E. M.; Byer, A. S.; Swanson, K. D.; Broderick, J. B.; Peters, J. W. *FEBS Lett.* **2012**, 586, 3939. (e) Kuchenreuther, J. M.; Britt, R. D.; Swartz, J. R. *PLoS One* **2012**, 7, e45850. (f) Berto, P.; Di Valentin, M.; Cendron, L.; Vallese, F.; Albertini, M.; Salvadori, E.; Giacometti, G. M.; Carbonera, D.; Costantini, P. *Biochim. Biophys. Acta* **2012**, 1817, 2149. (g) Berggren, G.; Garcia-Serres, R.; Brazzolotto, X.; Clemancey, M.; Gambarelli, S.; Atta, M.; Latour, J.-M.; Hernández, H. L.; Subramanian, S.; Johnson, M. K.; Fontecave, M. *J. Biol. Inorg. Chem.* **2013**.
- (444) Kuchenreuther, J. M.; George, S. J.; Grady-Smith, C. S.; Cramer, S. P.; Swartz, J. R. *PLoS One* **2011**, 6, e20346.
- (445) Berggren, G.; Adamska, A.; Lambertz, C.; Simmons, T. R.; Esselborn, J.; Atta, M.; Gambarelli, S.; Mouesa, J. M.; Reijerse, E.; Lubitz, W.; Happe, T.; Artero, V.; Fontecave, M. *Nature* **2013**, 499, 66.
- (446) (a) Begley, T. P.; Downs, D. M.; Ealick, S. E.; McLafferty, F. W.; Van Loon, A. P. G. M.; Taylor, S.; Campobasso, N.; Chiu, H.-J.; Kinsland, C.; Reddick, J. J.; Xi, J. *Arch. Microbiol.* **1999**, 171, 293. (b) Begley, T. P. *Nat. Prod. Rep.* **2006**, 23, 15.
- (447) Pilet, E.; Nicolet, Y.; Mathevon, C.; Douki, T.; Fontecilla-Camps, J. C.; Fontecave, M. *FEBS Lett.* **2009**, 583, 506.
- (448) Kuchenreuther, J. M.; Stapleton, J. A.; Swartz, J. R. *PLoS One* **2009**, 4, e7565.
- (449) Tron, C.; Cherrier, M. V.; Amara, P.; Lydie, M.; Fauth, F.; Fraga, E.; Corread, M.; Fontecave, M.; Nicolet, Y.; Fontecilla-Camps, J. C. *Eur. J. Inorg. Chem.* **2011**, 1121.
- (450) Shepard, E. M.; Mus, F.; Betz, J. N.; Duffus, B. R.; Byer, A. S.; Peters, J. W.; Broderick, J. B. *Biochemistry* **2014**, in review.
- (451) (a) Silakov, A.; Wenk, B.; Reijerse, E.; Lubitz, W. *Phys. Chem. Chem. Phys.* **2009**, 11, 6592. (b) Ryde, U.; Greco, C.; DeGioia, L. J. *Am. Chem. Soc.* **2010**, 132, 4512. (c) Erdem, Ö. F.; Schwartz, L.; Stein, M.; Silakov, A.; Kaur-Ghumaaan, S.; Huang, P.; Ott, S.; Reijerse, E. J.; Lubitz, W. *Angew. Chem., Int. Ed.* **2011**, 50, 1439.
- (452) (a) Grigoropoulos, A.; Szilagyi, R. K. *J. Biol. Inorg. Chem.* **2010**, 15, 1177. (b) Grigoropoulos, A.; Szilagyi, R. K. *Comput. Chem.* **2011**, 32, 3194.
- (453) Nicolet, Y.; Fontecilla-Camps, J. C. *J. Biol. Chem.* **2012**, 287, 13532.
- (454) Valles, F.; Berto, P.; Ruzzene, M.; Cendron, L.; Sarno, S.; De Rosa, E.; Giacometti, G. M.; Costantini, P. *J. Biol. Chem.* **2012**, 276, 36544.
- (455) (a) Duschene, K. S.; Broderick, J. B. *Biomol. Concepts* **2012**, 3, 255. (b) Zhu, H.; Cong, J.-P.; Shenk, T. *Proc. Natl. Acad. Sci. U.S.A.* **1997**, 94, 13985. (c) Grewal, T. S.; Genever, P. G.; Brabbs, A. C.; Birch, M.; Skerry, T. M. *FASEB J.* **2000**, 14, 523. (d) Boudinot, P.; Riffault, S.; Salhi, S.; Carrat, C.; Sedlik, C.; Mahmoudi, N.; Charley, B.; Benmansour, A. *J. Gen. Virol.* **2000**, 81, 2675. (e) Olofsson, P. S.; Jatta, K.; Wagsater, D.; Gredmark, S.; Hedin, U.; Paulsson-Berne, G.; Soderberg-Naucler, C.; Hansson, G. K.; Sirsjo, A. *Arterioscler., Thromb., Vasc. Biol.* **2005**, 25, e113. (f) Song, G.; Bazer, F. W.; Spencer, T. E. *Reproduction* **2007**, 133, 285.
- (456) (a) Chin, K.-C.; Cresswell, P. *Proc. Natl. Acad. Sci. U.S.A.* **2001**, 98, 15125. (b) Boudinot, P.; Massin, P.; Blanco, M.; Riffault, S.; Benmansour, A. *J. Virol.* **1999**, 73, 1846.
- (457) Hinson, E.; Cresswell, P. *J. Biol. Chem.* **2009**, 284, 4705.
- (458) (a) Jiang, D.; Guo, H. T.; Xu, C. X.; Chang, J. H.; Gu, B. H.; Wang, L. J.; Block, T. M.; Guo, J.-T. *J. Virol.* **2008**, 82, 1665. (b) Helbig, K. J.; Eyre, N. S.; Yip, E.; Narayana, S.; Li, K.; Fiches, G.; McCartney, E. M.; Jangra, R. K.; Lemon, S. M.; Beard, M. R. *Hepatology* **2011**, 54, 1506. (c) Wang, S.; Wu, X.; Pan, T.; Song, W.; Wang, Y.; Zhang, F.; Yuan, Z. *J. Gen. Virol.* **2012**, 93, 83.
- (459) Wang, X.; Hinson, E. R.; Cresswell, P. *Cell Host Microbe* **2007**, 2, 96.
- (460) Thauer, R. K.; Kaster, A.-K.; Goenrich, M.; Schick, M.; Hiromoto, T.; Shima, S. *Annu. Rev. Biochem.* **2010**, 79, 507.
- (461) Shima, S.; Thauer, R. K. *Chem. Rec.* **2007**, 7, 37.
- (462) (a) Shima, S.; Pilak, O.; Vogt, S.; Schick, M.; Stagni, M. S.; Meyer-Klaucke, W.; Warkentin, E.; Thauer, R. K.; Ermler, U. *Science* **2008**, 321, 572. (b) Hiromoto, T.; Warkentin, E.; Moll, J.; Ermler, U.; Shima, S. *Angew. Chem., Int. Ed.* **2009**, 48, 6457. (c) Hiromoto, T.; Ataka, K.; Pilak, O.; Vogt, S.; Stagni, M. S.; Meyer-Klaucke, W.; Warkentin, E.; Thauer, R. K.; Shima, S.; Ermler, U. *FEBS Lett.* **2009**, 583, 585. (d) Shima, S.; Schick, M.; Kahnt, J.; Ataka, K.; Steinbach, K.; Linne, U. *Dalton Trans.* **2012**, 41, 767.
- (463) (a) Afting, C.; Kremmer, E.; Brucker, C.; Hochheimer, A.; Thauer, R. K. *Arch. Microbiol.* **2000**, 174, 225. (b) Lie, T. J.; Costa, K. C.; Pak, D.; Sakesan, V.; Leigh, J. A. *FEMS Microbiol. Lett.* **2013**, 343, 156.
- (464) Wang, H.; Boisvert, D.; Kim, K. K.; Kim, R.; Kim, S. H. *EMBO J.* **2000**, 19, 317.

- (465) Schick, M.; Xie, X.; Ataka, K.; Kahnt, J.; Linne, U.; Shima, S. *J. Am. Chem. Soc.* **2012**, *134*, 3271.
- (466) Weitnauer, G.; Hauser, G.; Hofmann, C.; Linder, U.; Boll, R.; Pelz, K.; Glaser, S. J.; Bechthold, A. *Chem. Biol.* **2004**, *11*, 1403.
- (467) (a) Treede, I.; Hauser, G.; Muhlenweg, A.; Hofmann, C.; Schmidt, M.; Weitnauer, G.; Glaser, S.; Bechthold, A. *Appl. Environ. Microbiol.* **2005**, *71*, 400. (b) Weitnauer, G.; Muhlenweg, A.; Trefzer, A.; Hoffmeister, D.; Sussmuth, R. D.; Jung, G.; Welzel, K.; Vente, A.; Girreser, U.; Bechthold, A. *Chem. Biol.* **2001**, *8*, 569.
- (468) (a) Robinson, E. A.; Henrikse, O.; Maxwell, E. S. *J. Biol. Chem.* **1974**, *249*, 5088. (b) Van Ness, B. G.; Howard, J. B.; Bodley, J. W. *J. Biol. Chem.* **1980**, *255*, 10710.
- (469) (a) Van Ness, B. G.; Howard, J. B.; Bodley, J. W. *J. Biol. Chem.* **1978**, *253*, 8687. (b) Brown, B. A.; Bodley, J. W. *FEBS Lett.* **1979**, *103*, 253. (c) Van Ness, B. G.; Howard, J. B.; Bodley, J. W. *J. Biol. Chem.* **1980**, *255*, 10717.
- (470) (a) Chen, J. Y. C.; Bodley, J. W. *J. Biol. Chem.* **1988**, *263*, 11692. (b) Chen, J. Y. C.; Bodley, J. W.; Livingston, D. M. *Mol. Cell. Biol.* **1985**, *5*, 3357. (c) Mattheakis, L. C.; Shen, W. H.; Collier, R. J. *Mol. Cell. Biol.* **1992**, *12*, 4026. (d) Moehring, T. J.; Danley, D. E. *Mol. Cell. Biol.* **1984**, *4*, 642.
- (471) Dunlop, P. C.; Bodley, J. W. *J. Biol. Chem.* **1983**, *258*, 4754.
- (472) Cantoni, G. L. *J. Biol. Chem.* **1953**, *204*, 403.
- (473) Ohashi, Z.; Maeda, M.; McCloskey, J. A.; Nishimura, S. *Biochemistry* **1974**, *13*, 2620.
- (474) Liu, S.; Milne, G. T.; Kuremsky, J. G.; Fink, G. R.; Leppla, S. H. *Mol. Cell. Biol.* **2004**, *24*, 9487.
- (475) Sakuraba, H.; Tsuge, H.; Yoneda, K.; Katunuma, N.; Ohshima, T. *J. Biol. Chem.* **2005**, *280*, 26645.
- (476) Rekittke, I.; Wiesner, J.; Rohrich, R.; Demmer, U.; Warkentin, E.; Xu, W. Y.; Troschke, K.; Hintz, M.; No, J. H.; Duin, E. C.; Oldfield, E.; Jomaa, H.; Ermler, U. *J. Am. Chem. Soc.* **2008**, *130*, 17206.
- (477) Dowling, D. P.; Bruender, N. A.; Young, A. P.; McCarty, R. M.; Bandarian, V.; Drennan, C. L. *Nat. Chem. Biol.* **2014**, *10*, 106–112.
- (478) Hioe, J.; Zipse, H. *Chem. Eur. J.* **2012**, *18*, 16463–16472.
- (479) Hioe, J.; Zipse, H. *Faraday Discuss.* **2010**, *145*, 301–313.

#### NOTE ADDED AFTER ASAP PUBLICATION

This paper was published ASAP on January 29, 2014, without references 477, 478, and 479 and the associated text citing these references. The corrected version was reposted on March 4, 2014.